

Chris Velzel

A Course in Lens Design



Springer

Springer Series in Optical Sciences

Volume 183

Founded by

H. K. V. Lotsch

Editor-in-Chief

William T. Rhodes, Georgia Institute of Technology, Atlanta, USA

Editorial Board

Ali Adibi, Georgia Institute of Technology, Atlanta, USA

Toshimitsu Asakura, Hokkai-Gakuen University, Sapporo, Japan

Theodor W. Hänsch, Max-Planck-Institut für Quantenoptik, Garching, Germany

Takeshi Kamiya, National Institution for Academic Degrees, Tokyo, Japan

Ferenc Krausz, Ludwig-Maximilians-Universität München, Garching, Germany

Bo A. J. Monemar, Linköping University, Linköping, Sweden

Herbert Venghaus, Fraunhofer Institut für Nachrichtentechnik, Berlin, Germany

Horst Weber, Technische Universität Berlin, Berlin, Germany

Harald Weinfurter, Ludwig-Maximilians-Universität München, München,
Germany

For further volumes:
<http://www.springer.com/series/624>

Springer Series in Optical Sciences

The Springer Series in Optical Sciences, under the leadership of Editor-in-Chief William T. Rhodes, Georgia Institute of Technology, USA, provides an expanding selection of research monographs in all major areas of optics: lasers and quantum optics, ultrafast phenomena, optical spectroscopy techniques, optoelectronics, quantum information, information optics, applied laser technology, industrial applications, and other topics of contemporary interest.

With this broad coverage of topics, the series is of use to all research scientists and engineers who need up-to-date reference books.

The editors encourage prospective authors to correspond with them in advance of submitting a manuscript. Submission of manuscripts should be made to the Editor-in-Chief or one of the Editors. See also www.springer.com/series/624

Editor-in-Chief

William T. Rhodes

School of Electrical and Computer Engineering
Georgia Institute of Technology
Atlanta, GA 30332-0250
USA

e-mail: bill.rhodes@ece.gatech.edu

Editorial Board

Ali Adibi
School of Electrical and Computer Engineering
Georgia Institute of Technology
Atlanta, GA 30332-0250
USA
e-mail: adibi@ee.gatech.edu

Toshimitsu Asakura
Faculty of Engineering
Hokkai-Gakuen University
1-1, Minami-26, Nishi 11, Chuo-ku
Sapporo, Hokkaido 064-0926, Japan
e-mail: asakura@eli.hokkai-s-u.ac.jp

Theodor W. Hänsch
Max-Planck-Institut für Quantenoptik
Hans-Kopfermann-Straße 1
85748 Garching, Germany
e-mail: t.w.haensch@physik.uni-muenchen.de

Takeshi Kamiya
Ministry of Education, Culture, Sports
Science and Technology
National Institution for Academic Degrees
3-29-1 Otsuka Bunkyo-ku
Tokyo 112-0012, Japan
e-mail: kamiyatk@niad.ac.jp

Ferenc Krausz
Ludwig-Maximilians-Universität München
Lehrstuhl für Experimentelle Physik
Am Coulombwall 1
85748 Garching, Germany *and*
Max-Planck-Institut für Quantenoptik
Hans-Kopfermann-Straße 1
85748 Garching, Germany
e-mail: ferenc.krausz@mpq.mpg.de

Bo A. J. Monemar

Department of Physics and Measurement Technology
Materials Science Division
Linköping University
58183 Linköping, Sweden
e-mail: bom@ifm.liu.se

Herbert Venghaus

Fraunhofer Institut für Nachrichtentechnik
Heinrich-Hertz-Institut
Einsteinufer 37
10587 Berlin, Germany
e-mail: venghaus@hhi.de

Horst Weber

Optisches Institut
Technische Universität Berlin
Straße des 17. Juni 135
10623 Berlin, Germany
e-mail: weber@physik.tu-berlin.de

Harald Weinfurter

Sektion Physik
Ludwig-Maximilians-Universität München
Schellingstraße 4/III
80799 München, Germany
e-mail: harald.weinfurter@physik.uni-muenchen.de

Chris Velzel

A Course in Lens Design

Chris Velzel
Deurne
The Netherlands

ISSN 0342-4111 ISSN 1556-1534 (electronic)
ISBN 978-94-017-8684-3 ISBN 978-94-017-8685-0 (eBook)
DOI 10.1007/978-94-017-8685-0
Springer Dordrecht Heidelberg New York London

Library of Congress Control Number: 2014932214

© Springer Science+Business Media Dordrecht 2014

This work is subject to copyright. All rights are reserved by the Publisher, whether the whole or part of the material is concerned, specifically the rights of translation, reprinting, reuse of illustrations, recitation, broadcasting, reproduction on microfilms or in any other physical way, and transmission or information storage and retrieval, electronic adaptation, computer software, or by similar or dissimilar methodology now known or hereafter developed. Exempted from this legal reservation are brief excerpts in connection with reviews or scholarly analysis or material supplied specifically for the purpose of being entered and executed on a computer system, for exclusive use by the purchaser of the work. Duplication of this publication or parts thereof is permitted only under the provisions of the Copyright Law of the Publisher's location, in its current version, and permission for use must always be obtained from Springer. Permissions for use may be obtained through RightsLink at the Copyright Clearance Center. Violations are liable to prosecution under the respective Copyright Law. The use of general descriptive names, registered names, trademarks, service marks, etc. in this publication does not imply, even in the absence of a specific statement, that such names are exempt from the relevant protective laws and regulations and therefore free for general use.

While the advice and information in this book are believed to be true and accurate at the date of publication, neither the authors nor the editors nor the publisher can accept any legal responsibility for any errors or omissions that may be made. The publisher makes no warranty, express or implied, with respect to the material contained herein.

Printed on acid-free paper

Springer is part of Springer Science+Business Media (www.springer.com)

Preface

Lenses play an important role in our life. Our eyes make images of the world around us and are sometimes aided by spectacle glasses or contact lenses.

In daily life we use lenses in CD-drives, in webcams and cellphones, in cameras for photography and observation, in film projectors and search lights, in binoculars for looking at birds, or other far-away objects. Scientific applications of lenses (and mirrors) are found in microscopes and astronomical telescopes. And machines for the production of integrated circuits use huge lens (or mirror) systems to project very tiny details. Lenses are everywhere.

The book presented here has the title “A Course in Lens Design.” This title should be understood as follows: the design of lenses is a complicated activity, because it comprises the design of an *optical system* that performs a desired function, but also the design of the *mechanical* parts in which the optics are mounted (and sometimes also electronics and software). Moreover, the design must result in a product that can be manufactured by existing *technology*.

Because optical system design is the first in this chain of activities, the success of later stages depends on its performance. This book is limited to lens design in the sense of design of a suitable optical system for a given application.

As “A Course in Lens Design” is aimed at users who have little knowledge of the subject (an elementary optics course would be helpful, but is not strictly required), it is limited in treatment to the essentials, as will be seen from the description of its contents below.

As in many research and development activities (and in society as a whole) in the second half of the twentieth-century, the “art and science” of lens design was revolutionized by the coming of the computer.

In the past it took an accomplished optical designer several minutes to calculate the path of a ray through a spherical surface. With the computer this “ray-surface time interval” was reduced to parts of microseconds. In the beginning there was the hope that the design of lenses could be automated completely with the aid of computers. After some time it became clear that this was an illusion; the design of lenses makes in many of its stages decisions of the designer necessary. Nevertheless, the use of design software on the computer saves the designer a lot of time and effort.

It remains true that one needs a certain level of expertise to profit from the expertise stored in lens design software programs. This course is intended to build

up this expertise; it brings the beginner to a point where he/she can design a variety of lenses and will be able to use a software program with success.

Coming from a career as an optical scientist, I taught myself the subject of lens design; with this book I want to share this experience with the reader.

I found that most books on lens design either gave more attention to the results than to the process of lens design, or drowned the design process in a sea of details on physics, mechanics, and production technology. That does not mean that these books are not useful; when you have mastered the process of lens design, they can provide a wider and/or more detailed view of the subject. With this book I offer a complete method of lens design that is neither too simple nor too detailed. For a wider perspective the book refers to the literature. As one of my professors said: we want to spare the wolf, the goat, and the cabbage.

The book is divided in six chapters.

[Chapter 1](#) contains a short introduction to geometrical optics. The image formation by spherical mirrors, refractive surfaces, and lenses is described. The thin lens is introduced as a useful and simple model of a real lens. An algorithm is given for tracing rays through optical systems in the paraxial approximation. Finally, definition and function of stops and pupils are discussed. The concepts and tools prepared in this chapter are used continuously in the rest of the book.

[Chapter 2](#) gives a description of important categories of optical instruments: cameras, magnifiers, microscopes, telescopes, and of the optics of the human eye. This is useful to understand the function of lenses used in optical instruments.

In [Chaps. 1](#) and [2](#), the paraxial approximation of geometrical optics is used throughout. It is a simple, but very useful method to describe centered optical systems. In this book, we do not treat the design of noncentered systems.

In [Chap. 3](#), the description of optical systems is made more accurate by considering third-order aberrations. The relation between wavefront errors in the exit pupil and aberrations in the image plane is shown. The formulas for the calculation of aberration coefficients are given and discussed. The aberration coefficients depend on the position of the stop; stop shift equations are given that quantify these effects.

[Chapter 4](#) describes the processes of lens design.

In [Sect. 4.1](#), system specification is treated; also a review of existing lens types is given.

In [Sect. 4.2](#), the paraxial lay out of the systems to be designed is described. The number, powers, and positions of components are determined. The primary chromatic aberrations are corrected. The components are described by thin lenses.

In [Sect. 4.3](#), the formulas for the aberrations of a thin lens at the stop are given. The stop shift equations are used to determine the coefficients of system components. A procedure for the correction of the aberrations of the thin lens model is described that, with some variations, is used in the design examples of [Chap. 6](#).

In [Sect. 4.4](#), a procedure is given to convert the thin lens predesign to a “surface model” by giving thickness. After this the third-order aberrations of the surface model can be calculated.

In [Sect. 4.5](#), the optimization of the design is discussed. Topics of this section are: construction of merit functions, aberration balancing and fifth order aberrations, the mathematics of optimization and the analysis of the optimized design.

In [Sect. 4.6](#), the sensitivity of the design to fabrication errors is considered; a method of calculation of the system tolerances is presented.

In [Sect. 4.7](#), we derive some results from diffraction theory that can be used in lens design, viz. point spread function (PSF), modulation transfer function (MTF), Strehl's number, and Airy radius.

In [Chap. 5](#), the strategies of lens design are reviewed. We consider five fields of application: color correction (with a section on optical materials), degrees of freedom, symmetries, stops and pupils, and correction of field aberrations.

[Chapter 6](#) contains the detailed descriptions of the design of a variety of lenses. This begins with the design of thin systems (singlets and doublets), followed by the design of a telescope, asymmetric two-component systems, triplets and triplet variants, symmetric four-component systems, micro-objectives, and a section on the application of aspheric surfaces with a postscript on diffractive optics.

The book is addressed primarily to beginners in lens design; for instance, people with an education in applied physics or engineering, or students of technical optics.

When you want to learn lens design, it is not enough to read this book. You should begin to design lenses yourself. The book contains 21 exercises that are meant for that purpose. By completing these you will find that, step-by-step, you will become able to make your own designs. In the beginning this will take some time, because you have to do calculations with pen and paper (and a calculator). By using the spreadsheet facility on your computer you can speed up these calculations. When you have mastered the first stages of the lens design process, you can use lens design software to optimize the design. With the designs of [Chap. 6](#), the Zemax® software was used for this purpose.

In most of this book the mathematics is limited to algebra. In some sections mathematics of a higher level is used. These sections provide background material and can be skipped if necessary. Part of [Sect. 4.5](#) and all of [Sect. 4.7](#) belong to this category, marked by an asterisk.

Deurne, 2013

Chris Velzel

Acknowledgments

Many people helped me to produce this book.

From the beginning, Bogusia Dubik supported me by typing the manuscript. In a later stage, Ariadne Tenner took care of the lay-out, the figures, and the version management.

The photograph on page 329 (About the Author) was made by Paul Keizer.

Harry Kessels, Michiel van Rijnbach, and Jørgen van der Veen helped to formulate the contents of the course by discussions.

Abdel Boujname and Elena Sokolova gave their support by checking the calculations and exercises.

An early version of the manuscript was read by Leo Beckmann, Peter Nuyens, Beate Mitchunas, and Wolfgang Vollrath. The final manuscript profited from their criticism.

I am most thankful to Leonoor, who supported me during the 3 years in which the book grew.

November 2013

Chris Velzel

Contents

1 Geometrical Optics	1
1.1 Principles of Geometrical Optics	1
1.2 Paraxial Optics	5
1.2.1 The Concave Mirror	5
1.2.2 The Spherical Refractive Surface.	7
1.2.3 Prisms and Plates	8
1.3 Optical Systems.	9
1.3.1 The Single Lens	12
1.3.2 Thin Lenses	13
1.4 Paraxial Raytracing	14
1.4.1 The Optical Invariant.	16
1.4.2 Ray Tracing with Thin Lenses	18
1.5 Stops and Pupils	19
1.5.1 Telecentric Stop	22
1.5.2 Adding Rays.	24
References	24
2 Optical Instruments (Paraxial Approximation)	25
2.1 Camera.	25
2.1.1 Camera Obscura	26
2.2 Human Eye.	27
2.2.1 Nodal Points.	29
2.2.2 Exercise 4, Nodal Points of the Eye.	29
2.3 Magnifier and Microscope	30
2.3.1 Maximum Magnification	31
2.4 Telescopes	32
2.5 Illumination	35
References	38
3 Aberrations	39
3.1 Wavefronts and Aberrations	39
3.1.1 First Order Errors	41
3.1.2 The Third Order Aberrations.	43
3.1.3 Spherical	43

3.1.4	Coma	43
3.1.5	Field Curvature	45
3.1.6	Astigmatism	45
3.1.7	Distortion	47
3.2	Chromatic Aberration	47
3.3	Calculation of Aberration Coefficients	49
3.3.1	Calculation Scheme	52
3.4	Stop Shift Equations	54
3.5	Zero Seidel Conditions	55
	References	57
4	Lens Design Process	59
4.1	Specification	60
4.1.1	Transmission of Lenses	63
4.1.2	Lens Types	63
4.1.3	Camera Lenses	64
4.1.4	Telescope Objectives	68
4.1.5	Micro-Objectives	72
4.1.6	Oculars	74
4.2	Lay-out	75
4.2.1	Scale Factor	76
4.2.2	Field Curvature	77
4.2.3	Distortion	78
4.2.4	Axial Colour Correction	78
4.2.5	Lateral Colour Correction	80
4.2.6	Degrees of Freedom	80
4.2.7	Lay-out of a Zoom Lens	82
4.3	Thin Lens Predesign	84
4.3.1	Spherical and Coma as Functions of B and G	87
4.3.2	Coma-Free Lens	88
4.3.3	Correction of Thin Lens Systems	88
4.3.4	Exercise 6, Predesign of a Triplet	89
4.4	Surface Model	90
4.4.1	Effect of Thickness on Aberrations	91
4.5	Optimization	92
4.5.1	Weight Factors	93
4.5.2	Variables and Constraints	94
4.5.3	Merit Functions	95
4.5.4	Aberration Balancing	96
4.5.5	Fifth Order Aberrations	97
4.5.6	*Mathematics of Optimization	99
4.5.7	Damped Least Squares Algorithm	101
4.5.8	After Optimization	103
4.5.9	Spot Diagrams	103

4.5.10	Aberration Plots	103
4.5.11	Wavefront Error Plots	105
4.5.12	Modulation Transfer Function	105
4.5.13	Point Spread Function	106
4.6	Tolerancing.	106
4.6.1	Third Order Analysis of Decentring Errors	108
4.6.2	Tolerances, Optimization and Strain	112
4.6.3	Fabrication Errors	113
4.7	*Diffraction Theory for Lens Design	114
4.7.1	Strehl Ratio	118
4.7.2	Modulation Transfer	119
	References	122
5	Design Strategies	125
5.1	Colour Correction	126
5.1.1	Optical Materials	126
5.1.2	Colour Correction of Thin Systems	128
5.1.3	Apochromatic Thin Systems	129
5.1.4	Colour Correction in Two-Component Systems	130
5.1.5	Buried Surface	131
5.1.6	Glass Selection	132
5.2	Changing the Number of Variables	133
5.2.1	Splitting or Adding Lenses	133
5.2.2	Adding System Properties	134
5.2.3	Adding an Airspace	136
5.2.4	Aspherizing	136
5.3	Symmetries.	138
5.3.1	Mirror Symmetry.	138
5.3.2	Concentric Systems	139
5.3.3	Aplanatic Surfaces.	140
5.4	Stops and Diaphragms	141
5.4.1	Stop Position.	141
5.4.2	Vignetting.	142
5.5	Field Correction	142
5.5.1	Field Curvature	142
5.5.2	Astigmatism	145
5.5.3	Distortion	146
	References	147
6	Design Examples	149
6.1	Thin Systems	149
6.1.1	Single Lens.	150
6.1.2	Doublets.	152
6.1.3	Aplanatic Doublets	156

6.1.4	Cemented Doublets	158
6.1.5	Surface Model of a Doublet	160
6.1.6	Exercise 7, Predesign of a Chevalier Lens	161
6.2	Design of a Telescope	163
6.2.1	Design of a Kellner Ocular	164
6.2.2	Inverting System	167
6.2.3	Optimization of the Telescope Design	169
6.2.4	Exercise 8, Predesign of a Plossl Ocular	170
6.3	Two-Component Systems	175
6.3.1	The Retinascope (Fundus Camera)	179
6.3.2	Exercise 9, Design of an Eye Lens	180
6.3.3	Exercise 10a, Thin Lens Design of a Retinascope Objective	184
6.3.4	Exercise 10b, Surface Model of a Retinascope Objective	186
6.3.5	Exercise 11, Linear Optimization of a Retinascope Objective	189
6.3.6	The Petzval Lens	195
6.3.7	Exercise 12, Aberrations of a Petzval Lens	198
6.3.8	Exercise 13, Air Space of the Petzval Lens	204
6.3.9	Tele-Objectives	208
6.3.10	The Split Tele-Objective	219
6.3.11	The Reversed Tele-Objective	225
6.3.12	Exercise 14, Design of a Reversed Tele-Objective	227
6.3.13	The Galilei Telescope	228
6.3.14	Exercise 15, Design of a Galilei Telescope	228
6.4	Three Component Lenses	228
6.4.1	The Cooke Triplet	229
6.4.2	Exercise 16, Design of a High Resolution Triplet	236
6.4.3	The Tessar	240
6.4.4	The Heliar	247
6.4.5	Exercise 17, Predesign of a Heliar	253
6.5	Symmetric Four-Component Lenses	253
6.5.1	Conjugate Shift Equations	254
6.5.2	The Celor	258
6.5.3	The Planar	267
6.5.4	The Double Gauss	282
6.5.5	Exercise 18, Matsui's Double Gauss	286
6.5.6	The Symmetric Wide-Angle Quadruplet	287
6.5.7	The Hologon	293

6.6	Microscope Objectives	297
6.6.1	The Lister Type	298
6.6.2	A 40 \times Apochromatic Objective	302
6.6.3	Exercise 19, Aberrations of the 40 \times Apochromat	307
6.6.4	Tudorovsky's Objective	308
6.6.5	Centring Tolerance Calculations	310
6.6.6	Exercise 20, Centring Tolerances of the 40 \times Apochromat	311
6.6.7	A Flat Field Objective	311
6.7	Applications of Aspheric Surfaces	318
6.7.1	Design of a CD Objective	318
6.7.2	Mirror Objectives	319
6.7.3	Newton's Objective	320
6.7.4	Cassegrain-Type Objectives	321
6.7.5	The Schmidt Camera	323
6.7.6	Exercise 21, Aspherization of a Double Gauss Objective	325
6.7.7	Diffractive Optics	325
	References	328
	About the Author	329
	Index	331

Chapter 1

Geometrical Optics

1.1 Principles of Geometrical Optics

In modern physics, light is described as waves of the electro-magnetic field. In geometrical optics, a science much older than modern physics, light is a form of energy that propagates along trajectories in space that are called light rays.

A single ray, having no thickness, can only carry an infinitesimal amount of energy.

A finite amount of energy is carried by a bundle of rays; a ray bundle can be seen as a tube through which the energy streams.

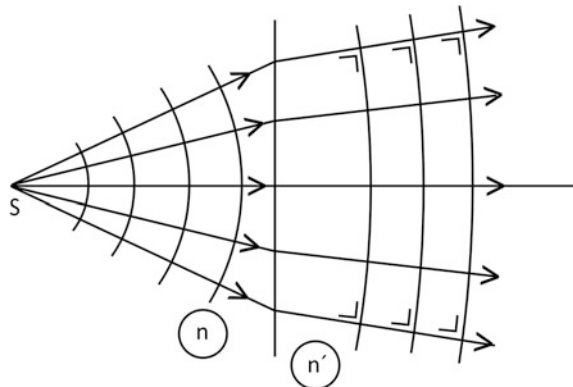
In homogeneous media the rays are straight lines. When we have a point source of light in a homogeneous medium, from which straight rays can be drawn in all directions, we can draw spheres around the source that have the rays as normals (see Fig. 1.1). Such surfaces are called wavefronts in the wave theory of light.

It was shown by Etienne Malus in 1808 that a concentric bundle of rays that is reflected or refracted at a smooth boundary between two media still has a normal surface after passing the boundary. In general the resulting wavefronts will be no longer spherical. Later, in 1916, C. Dupin showed that further reflections or refractions conserve this property that the wavefronts intersect the rays in a bundle at right angles.

The wavefronts of a bundle can be considered as surfaces of constant optical distance from the source. The time necessary for light to propagate from the source to a wavefront is equal for all points on the same wavefront. Geometrical optics is the science of rays and wavefronts.

Geometrical optics can be derived from the wave theory of light under the assumption that changes of the wave amplitude over a distance of the order of the wavelength are very small. That means that it is no longer valid near a focus and near obstacles such as the edges of diaphragms. In such situations we must take recourse to the wave theory. In a later chapter ([Chap. 4](#)) we will treat some of the consequences of the wave theory for lens design.

Fig. 1.1 The wavefronts are spherical up to the boundary; after refraction the wavefronts are no longer spherical



A fundamental principle of geometrical optics was formulated by Pierre de Fermat (1601–1665), who stated that light propagates between two points A and B along a trajectory for which the *optical path length*, defined as

$$\overline{AB} \equiv \int_A^B n ds \quad (1.1)$$

is shortest. (A proof of this principle is given by Born and Wolf [1, Sect. 3.3.2].) Here ds is the element of geometrical pathlength along the ray and n is the *refractive index* of the medium or media of propagation, defined as

$$n = c/v \quad (1.2)$$

where c is the velocity of light in free space, and v is the velocity of light in a (transparent) medium. Knowing this we can write

$$\overline{AB} = c \int_A^B dt = c(t_B - t_A) \quad (1.3)$$

where t stands for time of propagation.

The geometrical optics calculations in this course are based on the laws of reflection and refraction.

A ray that meets the boundary of two transparent media, for instance air and glass, is reflected in such a way that (see Fig. 1.2)

$$i'' = -i \quad (1.4)$$

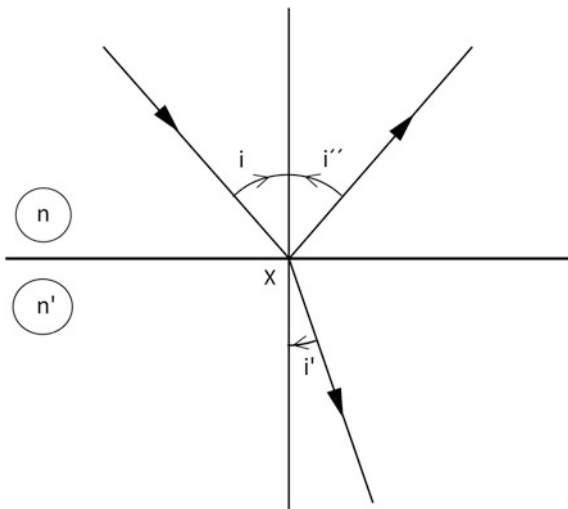
where i is the *angle of incidence*, and i'' is the *angle of reflection*. The reference of these angles is the normal to the boundary.

For the *angle of refraction* i' we have the law

$$n \sin i = n' \sin i' \quad (1.5)$$

where n and n' are the indices of refraction on both sides of the boundary.

Fig. 1.2 Reflection and refraction ($n' > n$)



The reflection law was known to Euclid (300 BC), the law of refraction was found empirically by Willebrord Snell (1591–1626) and is known as Snell's law.

The two laws can be derived from Fermat's Principle. Fermat himself showed this for the reflection law.

In Fig. 1.2 the incoming, reflected and refracted rays all lie in one plane; this is also the case in three dimensions and is a consequence of Fermat's principle.

We do not give a formal derivation here, but we show that the geometrical derivation given by Christiaan Huygens (1629–1695) is in agreement with Fermat's principle.

In Fig. 1.3a the incoming wavefront is AB. For CD to be the reflected wavefront we must have $\overline{AC} = \overline{BD}$. For both optical paths the refractive index is equal. The ray AC must be perpendicular to the outgoing wavefront CD, and the distance from A to CD is the shortest when that is the case. This proves the reflection law, (1.4).

In Fig. 1.3b we also must have $\overline{AC} = \overline{BD}$, but now the indices are unequal. This gives

$$\frac{AC}{BD} = \frac{n}{n'} = \frac{AC}{AD} \cdot \frac{AD}{BD} = \frac{\sin i'}{\sin i}$$

Also in this case AC is shortest when AC is perpendicular to CD. This proves the refraction law, (1.5).

Now we can start with our practical work.

In this course we consider mainly image forming optical instruments. In Fig. 1.4 we give a schematic picture of image formation by a lens.

In this picture we draw the rays and the wavefronts. The optical pathlength between two wavefronts is everywhere the same. In the lens the distance between wavefronts is smaller than in the surrounding air. Light travels slower in glass than in air.

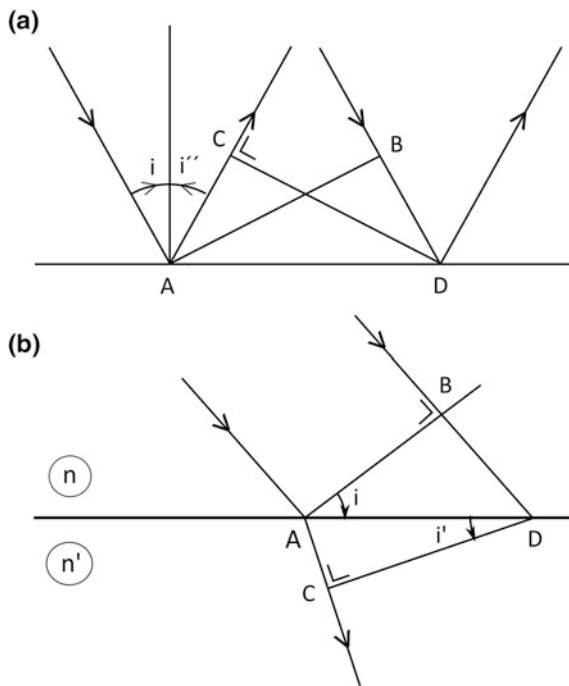


Fig. 1.3 **a** Reflection. **b** Refraction

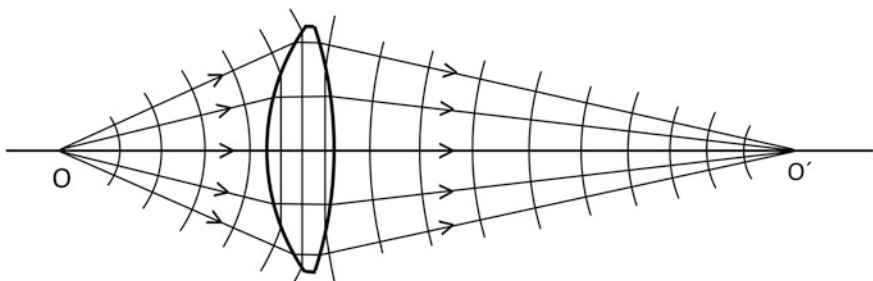


Fig. 1.4 Image formation by a lens: rays and wavefronts

The wavefronts coming from the object point O are spherical. When a point image is perfect, the wavefronts in image space must be spherical as well. Usually this is not the case and the rays do not meet exactly in O'. We then have *aberrations*, deviations of rays from the desired meeting point.

A great part of this book is devoted to the description, calculation and correction of aberrations.

1.2 Paraxial Optics

When the angles i and i' are small, Snell's law can be written

$$n'i' = ni \quad (1.6)$$

We point out the consequences of this for a centered system, that is an optical system in which all components have a common axis of symmetry.

To make sure that i and i' are small always, all rays in a centered system must remain in the neighborhood of the optical axis. In this course we do not consider non-centered systems (examples are: prism and grating spectrometers, anamorphic imaging systems). The above approximation is called the *paraxial approximation*. It is very useful because it gives, without much effort, essential information about optical systems, such as the position and size of images.

We treat first two examples of image formation in the paraxial approximation: the concave spherical mirror and the spherical refractive surface.

1.2.1 The Concave Mirror

In Fig. 1.5 the center of curvature of the mirror is in C. We take a point V on the mirror and use VC as an axis. The radius of curvature $r = VC$. A ray parallel to the axis is reflected by the mirror and intersects the axis at the point F, halfway between V and C. F is called the *focal point*.

When we have an *object* PQ on the left of C we can find its image in the following way. From P we draw a ray through C; this ray meets the mirror perpendicularly. Where the rays through C and F meet we find the *image* P' of P. A point Q on the perpendicular from P to the axis is imaged in Q' on the perpendicular from P'.

When we would draw more rays from P they would meet, after reflection by the mirror, in the point P'. This is a property of the paraxial approximation.

Now let us draw a ray from P to V; this ray is reflected to P'. The angles with the axis of the incoming and reflected rays at V are equal, according to the reflection law, with opposite signs.

When we use the notation $VQ = s$, $VQ' = s'$, where s is called the *object distance* and s' the *image distance*, we state without proof that

$$-\frac{1}{s'} = \frac{1}{s} - \frac{2}{r} \quad (1.7)$$

This is called an *image equation*.

We use the *convention for distances* depicted in Fig. 1.6. Axial distances to the right are positive, to the left negative. The same for radii of curvature. For distances perpendicular to the axis we have: up is positive, down is negative.

From the image equation follows that, when s is infinite, $\frac{1}{s} = 0$, $s' = \frac{r}{2}$.

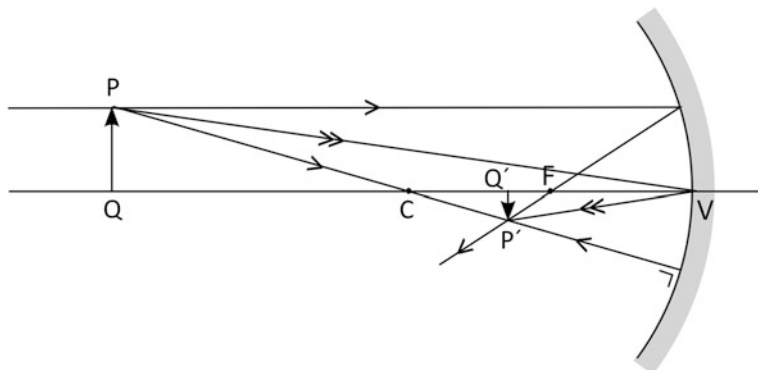
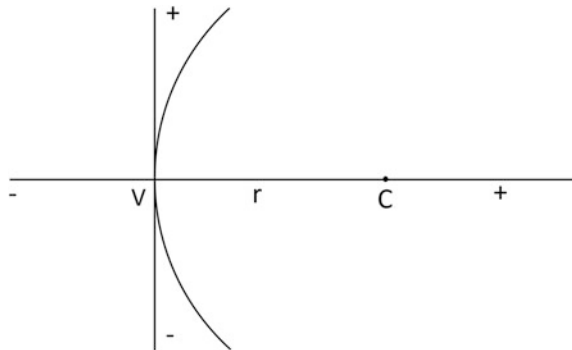


Fig. 1.5 Concave mirror

Fig. 1.6 Convention for distances



Due to our convention, s' and r are both negative. This particular s' is called the focal distance, notation f' . So we have $VF \equiv f' = \frac{r}{2}$. We now can write the imaging equation as

$$-\frac{1}{s'} = \frac{1}{s} - \frac{1}{f'} = \frac{1}{s} + K \quad (1.8)$$

where $K = -\frac{1}{f'}$ is called the *power* of the mirror. With a concave mirror, f' is negative and K is positive.

Exercise 1, Image equations

Check the image equation of the concave mirror for the following cases: object in C, object in V, image at infinity.

When we turn the mirror around, we have a *convex mirror*. Find the imaging equation for the convex mirror, its focal distance and its power. The light should come from the left.

From $VQ = s$, $VQ' = s'$ and Fig. 1.5 we see that the magnification M is given by

$$M \equiv \frac{P'Q'}{PQ} = -\frac{s'}{s} \quad (1.9)$$

Note the minus sign.

What is the value of M when the object is in C, in V, in F?

We worked out the example of the concave mirror in detail, to introduce a notation, several concepts (image equation, magnification, power etc.) and a convention for distances.

1.2.2 The Spherical Refractive Surface

Spherical surfaces are used almost exclusively in technical optics. The reason is that the fabrication of spherical (and planar) surfaces is much easier than the production of other types of surfaces (cylindrical, aspherical or “free-form”). We will consider the use of aspherical surfaces in a later Sect. 6.7.

The imaging equation of a spherical refracting surface is

$$\frac{n'}{s'} = \frac{n}{s} + K, \quad \text{with } K = \frac{n' - n}{r} \quad (1.10)$$

K is called the *power* of the surface.

The notation was explained in the previous example. Here n' , n are the refractive indices behind and in front of the surface, respectively. See Fig. 1.7.

From Fig. 1.8 we find that the magnification M is given by

$$M \equiv \frac{y'}{y} = \frac{ns'}{n's} \quad (1.11)$$

because $n'w' = nw$ (Snell).

We use Figs. 1.7 and 1.8 to explain our *convention for angles*.

When the rotation of a ray towards its reference is clockwise, the angle between the two is positive; when the rotation is anticlockwise, the angle is negative.

A reference may be a surface normal (i and i' in Fig. 1.7), the optical axis (u' in Fig. 1.7) or another ray (not in these figures).

Exercise 2, Spherical refractive surface

There are now two focal points on different sides of the surface. Calculate the focal distances for the following data:

$$n = 1, n' = 1.5, r = 20 \text{ mm.}$$

Fig. 1.7 Spherical refracting surface

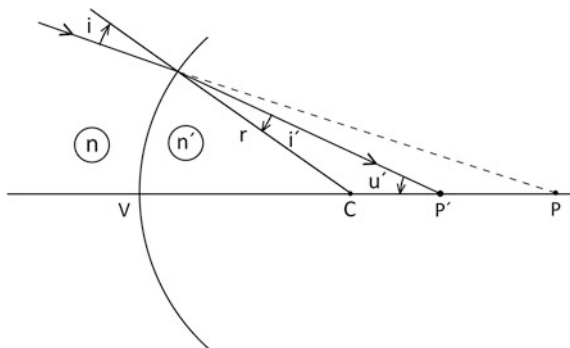
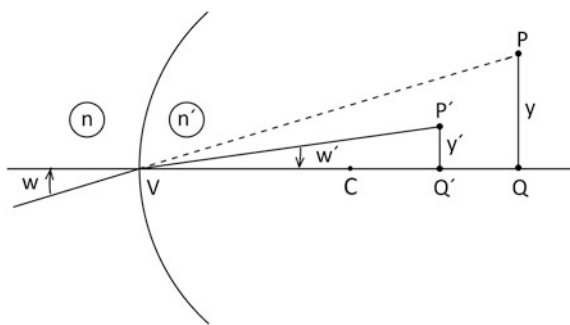


Fig. 1.8 Magnification



What is the value of M for an object at infinity, in the focal points F and F' , in V and in C ? Check first the image equation in these points.

The image equation for a refracting surface can be written in invariant form as

$$n' \left(\frac{1}{s'} - \frac{1}{r} \right) = n \left(\frac{1}{s} - \frac{1}{r} \right).$$

The quantity on the right (or that on the left) of this equation is known as Abbe's invariant. Can you write the image equation of the concave mirror in invariant form?

1.2.3 Prisms and Plates

The use of prisms in image-forming systems is based on *total internal reflection*. A wave that meets the boundary between glass and air, coming from the glass (see Fig. 1.9) is reflected totally when the incident angle is larger than i_c , the critical angle, that is given by $n \sin i_c = 1$.

With a glass prism, as shown in the figure and a refractive index $n = 1.5$, the critical angle is 41.8° , smaller than $i = 45^\circ$ in the figure.

Fig. 1.9 Total internal reflection when $i > i_c$

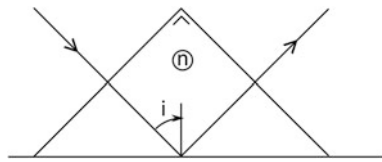


Fig. 1.10 Retrodirection prism

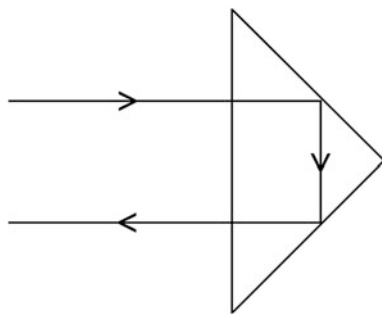
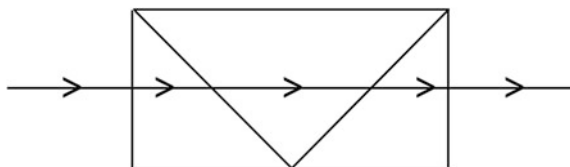


Fig. 1.11 Tunnel diagram



The prism in the figure can be used to send a beam back in the direction from which it came, as is shown in Fig. 1.10. The incident angles are still 45° , so total reflection works here too.

Ray tracing through such a prism is a bit clumsy (for the computer this is no problem); the remedy is to unfold the rays. In the case of Fig. 1.10 the unfolded prism is shown in Fig. 1.11. A picture such as Fig. 1.11 is called a tunnel diagram.

We will apply the method of unfolding in the design of a binocular telescope in Sect. 6.2. The unfolded prism will be considered as a thick glass plate. Thin glass plates are frequently used as cover glasses in microscopy; we will have to do with these in Sect. 6.6.

1.3 Optical Systems

For a general centered system the imaging equation

$$\frac{n'}{s'} = \frac{n}{s} + K, \quad K = \frac{n'}{f'} = -\frac{n}{f} \quad (1.12)$$

is valid when we measure s' , s and f' , f from the *principal planes*.

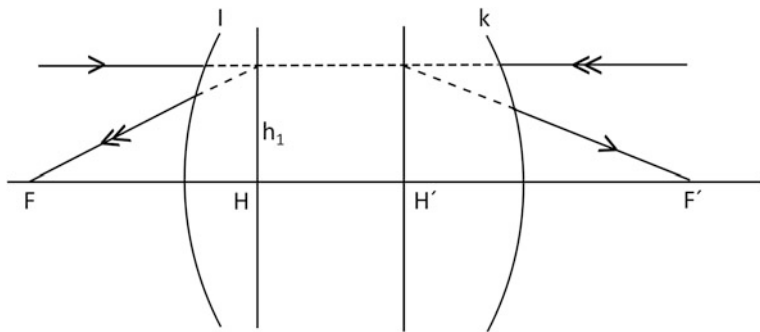


Fig. 1.12 Principal planes

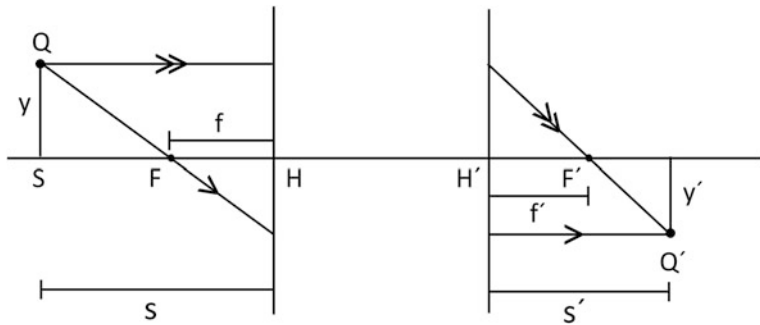


Fig. 1.13 Image construction

The principal planes are defined as those planes that have a magnification $M = +1$ between them. They can be found by ray-tracing (see Sect. 1.4). In Fig. 1.12 we show the first and last surface of a centered system. We trace a ray that is parallel to the optical axis on the object (left) side. After passage through the system this ray intersects the axis in the focal point F' . When from F' we prolong the ray backward until the ray height is the same (h_1) as in object space we find the image side principal plane, denoted by H' . We have $H'F' = f'$.

By tracing a ray from the image side, parallel to the axis, we find F and H , with $HF = f$.

We see from the figure that $M = 1$ between H and H' .

When the position of the focal points and principal planes is known, one can construct the image as in Fig. 1.13. A ray from Q parallel to the axis and one through F are enough to find Q' . The imaging equation follows from Fig. 1.13, provided that we take $s = HS$, $s' = H'S'$, $f = HF$ and $f' = H'F'$.

From Fig. 1.13 we obtain

$$(s - f)(s' - f') = ff'$$

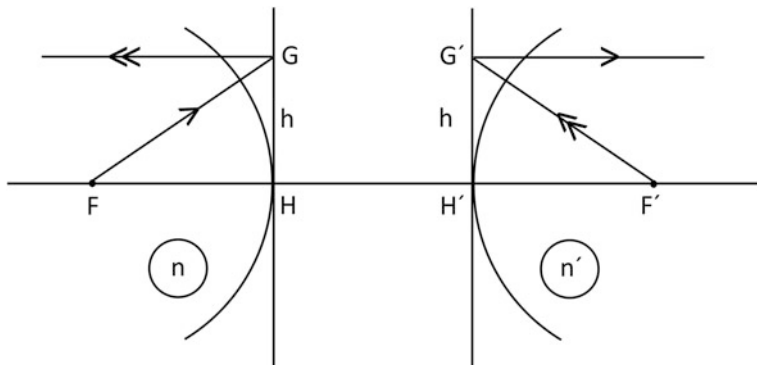


Fig. 1.14 Proof of $n'/f' = -n/f = K$

because

$$M = \frac{-f}{s-f} = \frac{s'-f'}{-f'}.$$

With

$$\frac{n'}{f'} = -\frac{n}{f} = K$$

we have

$$\frac{n'}{s'} = \frac{n}{s} + K$$

as before (with the spherical refractive surface).

We prove that $\frac{n'}{f'} = -\frac{n}{f}$ as follows.

A spherical wave from F becomes a plane wave in image space. Between conjugate points on the principal planes the system must have an optical path that compensates for the curvature of the wave at the object side. See Fig. 1.14.

The optical path between points G and G' at height h must be of the form (in paraxial approximation)

$$l(h) = l(0) + \frac{nh^2}{2f} = l(0) - \frac{n'h^2}{2f'}$$

because the same is true for a wave from F'.

From this $\frac{n}{f} = -\frac{n'}{f'}$ follows.

The principal planes of a single refracting or reflecting surface are found in the top of the surface, where it intersects the optical axis. In Figs. 1.5, 1.7 and 1.8 these are the points marked by V.

For all centered systems that have focal points the principal planes can be found by the procedure described in this section. But for telescopic systems, where an incoming ray parallel to the optical axis leaves the system parallel to the axis, the principal planes and the focal points do not exist.

We discuss the design of such a system in Sect. 6.2. It will be seen that in such a case the system will be split up in two parts that are designed separately.

1.3.1 The Single Lens

As a practical example of an optical system we find the principal points of a single lens in air (Fig. 1.15).

From Sect. 1.2 we have the imaging equations

$$\frac{n}{s_1'} = \frac{1}{s_1} + K_1, \quad \frac{1}{s_2'} = \frac{n}{s_2} + K_2$$

with $K_1 = (n - 1)/r_1$, $K_2 = (1 - n)/r_2$ and the magnifications $M_1 = s_1'/ns_1$, $M_2 = ns_2'/s_2$.

With thickness d we have the *transfer equation*:

$$s_2 = s_1' - d$$

The total magnification is given by:

$$M = M_1 M_2 = s_1' s_2' / s_1 s_2$$

The principal points H, H' (see Fig. 1.15) are found from setting $M = 1$. The position of the principal point H is now found by eliminating first s_2' , then s_2 and finally s_1' , using the imaging equations. We find

$$s_p = dK_2/nK \tag{1.13}$$

In the same way we find the position of H' with

$$s'_p = -dK_1/nK \tag{1.14}$$

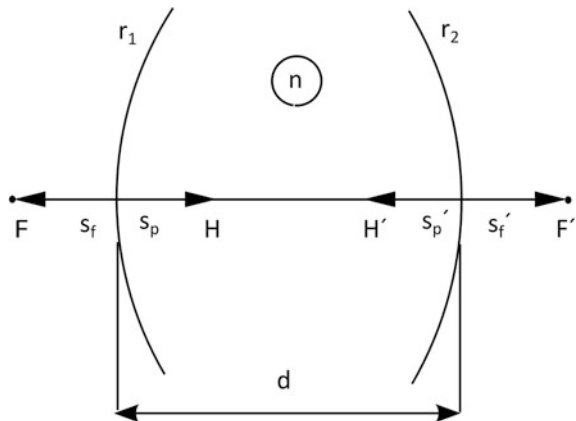
where $K = K_1 + K_2 - dK_1 K_2 / n$,

We find the position of F', the image-side focal point, by taking $1/s_1 = 0$. This gives

$$s_f' = \left(1 - \frac{d}{n} K_1 \right) / K \tag{1.15}$$

the *back focal length*. By definition we have

Fig. 1.15 Single lens in air; notation



$$s_f' - s_p' = f'$$

the focal length of the lens, so that we find

$$f' = 1/K$$

The *power* of the lens is therefore given by

$$K = K_1 + K_2 - dK_1K_2/n \quad (1.16)$$

It follows that $f = -1/K$ (lens in air) and that the *front focal length* s_f is given by

$$s_f = f' + s_p = \left(-1 + \frac{d}{n} K_2 \right) / K \quad (1.17)$$

Example

With $r_1 = 1$, $r_2 = -2$, $d = 0.1$ and $n = 1.5$ we find

$$\begin{aligned} K_1 &= 0.5, \quad K_2 = 0.25, \quad K = 0.7375, \quad f' = -f = 1.356, \\ s_p' &= -0.0452, \quad s_p = 0.0226, \quad s_f' = 1.311, \quad s_f = -1.333. \end{aligned}$$

Check this.

1.3.2 Thin Lenses

A thin lens is a lens of which we take the thickness equal to zero. Such a lens cannot exist in practice, but the thin lens is a concept that is very useful in lens design.

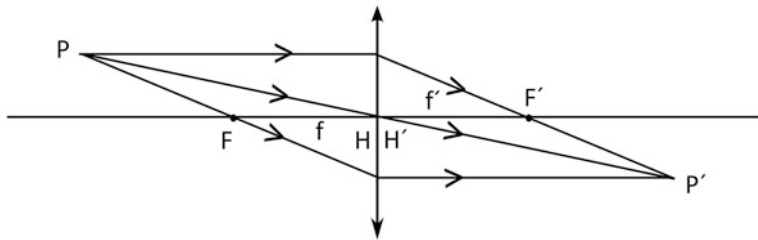


Fig. 1.16 Paraxial image formation by a thin lens in air

In this course we conceive a thin lens predesign before calculating the surface contributions to aberrations of the real system. By approximating a real system by a system of thin lenses, that is paraxially equivalent to the real system, we can obtain an insight in the dependency of paraxial and third order properties of the system from its construction data (radii, distances, materials).

(In practice spectacle lenses can be treated like thin lenses, when we do not expect very accurate results of our calculations.)

Because the thin lens has no thickness, its power is given as the sum of the powers of its surfaces. See (1.16) with $d = 0$.

Therefore we have, for a thin lens in air

$$K = (n - 1) \left(\frac{1}{r_1} - \frac{1}{r_2} \right). \quad (1.18)$$

The image formation by a thin lens can be constructed in the same way as in Fig. 1.13.

The principal planes are now situated in the plane of the lens. See Fig. 1.16.

1.4 Paraxial Raytracing

We consider again refraction at the spherical surface. See Fig. 1.17.

In triangle ACP we have, in the paraxial approximation,

$$i = u + \frac{h}{r}.$$

In triangle ACP' we have

$$i' = u' + \frac{h}{r}.$$

Since $n_i = n'i'$ (Snell) we obtain

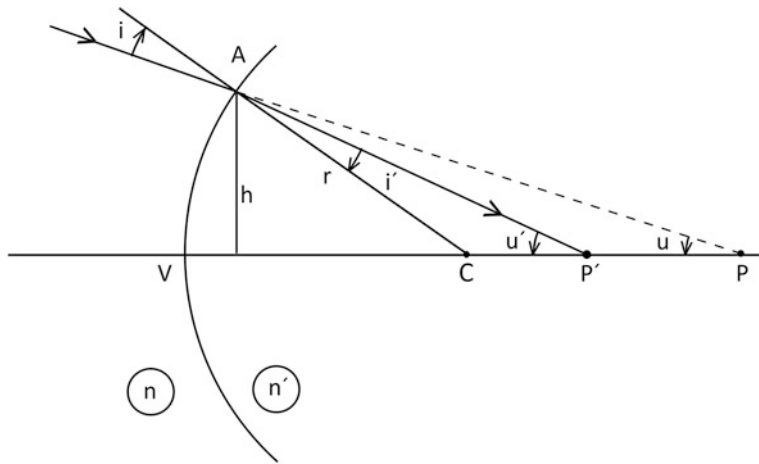


Fig. 1.17 Refraction equation

$$\begin{aligned} nu + \frac{nh}{r} &= n'u' + n'\frac{h}{r}, \text{ or} \\ n'u' &= nu - Kh, \quad K = \frac{n' - n}{r} \end{aligned} \quad (1.19)$$

With $u = -\frac{h}{s}$, $u' = -\frac{h}{s'}$ we find the imaging equation again.

The above derivation uses our *convention* for angles: when the rotation from ray to reference (normal, axis) is clockwise, the angle is positive.

We show the rotations in Fig. 1.17.

The equation $n'u' = nu - Kh$ is called the *refraction equation*.

To describe the transfer to the next surface we use the *transfer equation*

$$h' = h + n'u' \frac{d}{n'} \quad (1.20)$$

that is illustrated by Fig. 1.18.

The (1.19) and (1.20) can be used in an algorithm for paraxial tracing, as follows

$$\begin{aligned} n_{i+1}u_{i+1} &= n_iu_i - K_ih_i \\ h_{i+1} &= h_i + \frac{n_{i+1}u_{i+1}d_i}{n_{i+1}} \end{aligned} \quad (1.21)$$

where we have used $n_{i+1}u_{i+1} \equiv n'_iu'_i$.

This algorithm can be used for

- finding focal points and principal planes and other paraxial data of centered systems,
- calculating third-order aberration coefficients.

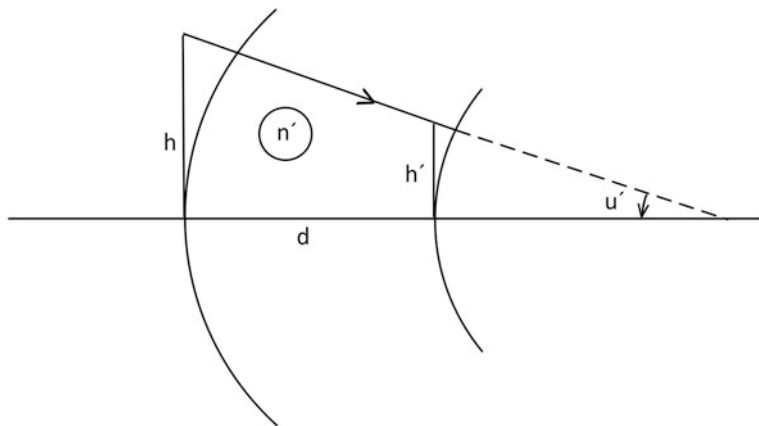


Fig. 1.18 Transfer equation

1.4.1 The Optical Invariant

The algorithm (1.16) can also be used to prove that the expression

$$H = n(\bar{h}u - \bar{u}h) \quad (1.22)$$

where (h, u) and (\bar{h}, \bar{u}) are the ray parameters of two rays, has the same value for all planes in an optical system. In other words, it is a paraxial invariant.

The passage of a ray from one plane to another can be described by the linear equations

$$\begin{aligned} n'u' &= a.nu + b.h \\ h' &= c.nu + d.h \end{aligned}$$

where a, b, c, d are constants, so that

$$H' = \{(cn\bar{u} + d\bar{h})(a.nu + b.h) - (c.nu + d.h)(a.n\bar{u} + b.\bar{h})\} = (ad - bc).n(\bar{h}u - \bar{u}h) = H$$

because from (1.21) follows that $ad - bc = 1$.

With $A = nh/r + nu = ni$, $\bar{A} = n\bar{h}/r + n\bar{u} = n\bar{i}$, where i, \bar{i} are the angles of incidence and r is the surface radius we can also write

$$H = n(\bar{h}i - \bar{i}h) = \bar{h}A - h\bar{A} \quad (1.23)$$

This expression will be used in the derivation of the stop shift equations in Sect. 3.4.

Example

With a single lens we can find the principal points H , H' , F , F' by using the formulas (1.13)–(1.16) given in Sect. 1.3. This is not so with more complicated systems; in principle the image (1.12) can be used, but this leads to a proliferation of formulas. A numerical approach as given in this section is more efficient.

As an example we show how to find the principal points of a doublet. We use the calculation scheme found also in the books of Kingslake and Johnson [2] and O’Shea [3].

It is easy to transform this into a spread sheet calculation on your computer.

	1	2	3	4
r	68.9	-68.9	-61.3	-134.1
n	1	1.589	1	1.805
n'	1.589	1	1.805	1
d	2	0.2	1	98.702
K	0.00855	0.00855	-0.01313	0.00600
d/n'	1.259	0.2	0.554	
nu	0	-0.00855	-0.01701	-0.00406
h	1	0.9892	0.9858	0.9836
nu_	0.009961	0.001448	-0.00709	0.00600
h_	0.9963	0.9981	0.9967	1

The length units are mm, as everywhere in this book.

In this scheme first the radii, indices and distances for the surfaces of the doublet are inserted. The distance d_4 is still not known, this is the back focal length.

Then K and d/n' are calculated.

Starting values $u_1 = 0$, $h_1 = 1$ are inserted, and with (1.20) nu and h are calculated for all surfaces, and finally u'_4 .

The focal length f' is found from $f' = -h_1/u'_4 = 100.361$, the back focal length as $d_4 = -h_4/u'_4 = 98.702$.

The position of the image-side principal point is given by:

$$V_4H' = (h_1 - h_4)/u'_4 = -1.659$$

The values of the front focal length, the focal length f and the position of the object-side principal point are found by tracing a ray backwards through the system, with starting values $u'_4 = 0$, $h_4 = 1$.

The (1.20) are used in the form

$$(nu)_k = (nu)_{k+1} + h_k K_k$$

$$h_k = h_{k+1} - (nu)_{k+1} (d/n')_k$$

We find $f = -100.391$, $ffl = -100.017$, $V_1H = 0.284$.

As a check on this calculation we should find $f = -f'$. There is a difference of -0.03 mm between the two values found; certainly due to rounding.

This procedure can be applied with all centered systems. We will use it repeatedly in the design examples of [Chap. 6](#).

Exercise 3, Paraxial ray tracing

Kingslake and Johnson [2, p. 355] describes a symmetric dialyte lens (like the Celor of [Sect. 6.5](#)) of which the prescription is as follows.

	Radius	Distance	Index
1	1.473	0.2	1.6053
2	-4.418	0.0756	Air
3	-2.043	0.06	1.6109
4	3.065	0.12	Air
STO 5	Plane	0.12	Air
6	-3.065	0.06	1.6109
7	2.043	0.0756	Air
8	4.418	0.2	1.6053
9	-1.473		Air
IMA 10	Plane		

The units are given in inches in this table, by exception.

The object plane of this lens is at infinity. We will trace two rays through this system. One ray is parallel to the axis in object space ($n_{u_1} = 0$). It comes from the center of the object.

We will take the ray height at the first surface $h_1 = 1$.

Calculate the focal length and the back focal length of this system.

The other ray goes through the center of the stop (STO) that is a diaphragm at the position 5. This ray must be traced from the stop in two directions.

Its initial data are $n_5 \bar{u}_5 = 1$, $\bar{h}_5 = 0$.

The ray data of the two rays can be used in the calculation of the aberration coefficients of this system in [Sect. 3.3](#), Exercise 5. For this purpose the data (n_{u_i} and h_i) of the first ray must be multiplied by $f/12$, with f in inches; the data of the second ray ($n_{\bar{u}_i}$, \bar{h}_i) must be multiplied by 0.3893. With the object at infinity $h_1 = f/12$ gives an aperture angle $u_k' = 1/12$ or $F/6$. The field angle is $\tan w = 0.3893$.

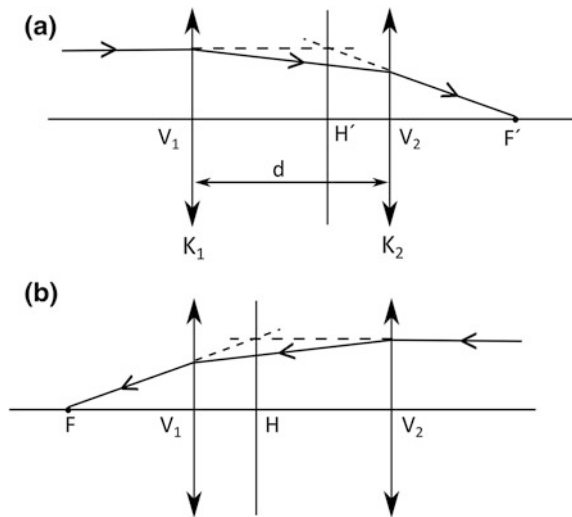
1.4.2 Ray Tracing with Thin Lenses

The preceding treatment of paraxial ray-tracing can be applied to thin lenses as well. The ray-tracing formulas become, for thin lenses in air, which is most frequently the case,

$$u' = u - Kh \quad (1.24)$$

$$h' = h + u'd \quad (1.25)$$

Fig. 1.19 Principal points for a system of two thin lenses in air. Note that $H'F' = FH$ **a** image side, **b** object side principal plane



For a system of thin lenses, the position of focal points and principal planes can be determined with the aid of these formulas. Readymade formulas for a system of two thin lenses are (see Fig. 1.19 for the notation):

$$K = K_1 + K_2 - dK_1 K_2 \quad (1.26)$$

$$V_1 H = \frac{K_2 d}{K} \quad (1.27)$$

$$V_2 H' = -\frac{K_1 d}{K} \quad (1.28)$$

where V_1 , V_2 are the vertices of the lenses and H , H' the axial points of the principal planes.

The power of a system of thin lenses is given by

$$h_l K = \sum_1^k h_i K_i \quad (1.29)$$

The equations in this section will be used in the lay-out and thin lens predesign.

1.5 Stops and Pupils

The local energy density in the image plane of an optical system is proportional to the angular extent (solid angle) of the bundle of rays that reaches the image plane (see also Sect. 1.6). This solid angle is limited by the size of the lenses and diaphragms in the system. We suppose that all lenses and diaphragms have circular edges, centered on the optical axis of the system.

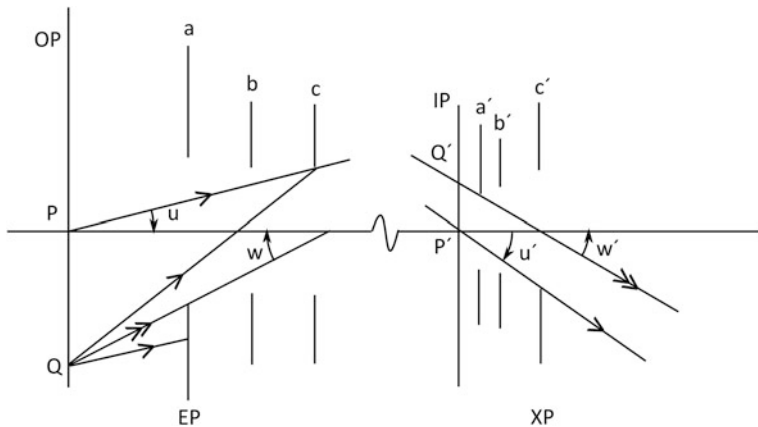


Fig. 1.20 Diaphragm images in object space (a, b, c) and image space (a', b', c'). OP is the object plane, IP the image plane; c, c' are entrance and exit pupil, a, a' are entrance and exit window

Following Van Heel [4] we show how to find which rays will be transmitted for axial and off-axis points of the object.

We make an image of *all* lens and diaphragm edges in the object space of the system and also in image space. It is sufficient in most cases to do a paraxial calculation of the position and size of these images (with wide-field camera lenses the paraxial approximation may be not accurate enough).

We can now study the limitations of the ray bundles using the two sets of edge images; the system itself can be ignored.

For an axial object point P , consider Fig. 1.20. In this figure a, b, c , denote the edge images in object space, and a', b', c' those in image space. It follows that a', b', c' are the paraxial images of a, b, c .

We find the limiting ray from P through the system by looking which of the edge images spans up the smallest angle. In the figure this is c . The diaphragm that corresponds to c is called the *aperture stop*. The ray from P through the edge of edge-image c , and also through the edge of the aperture stop and through the edge of c' is called *marginal ray*. This ray ends in P' , the paraxial image of P .

The edge image c is now called *entrance pupil* (EP); the edge image c' is called *exit pupil* (XP). In the figure u is the *object aperture angle* and u' is the *image aperture angle*.

For off-axis points the picture does not change much, as long as the marginal rays are not cut off by the other edges (a, b). When this is the case (see the point Q in Fig. 1.20) the solid angle of the beam is limited further (in the figure by a). This situation is called *vignetting* in lens design terminology. Because vignetting can lead to a complicated dependence of the illumination in the image field, we find an

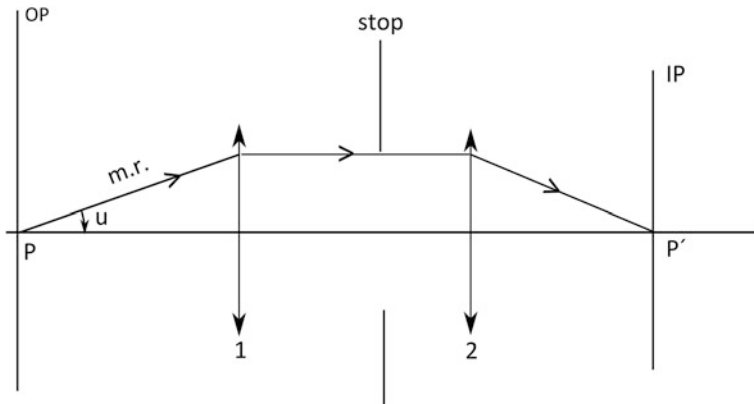


Fig. 1.21 Aperture stop

off-axis position for which about half of the ray bundle is cut off by the vignetting edge. We draw in Fig. 1.20 a ray from the center of the entrance pupil EP through the edge of the vignetting diaphragm image a. Such a ray is called a *chief ray*. The vignetting diaphragm itself (not in the figure) is called the *field stop*, and its images a and a' *entrance* and *exit windows*, respectively.

The angle of the principal ray with the axis is called the field angle, we have an *object field angle* w and an *image field angle* w' (see Fig. 1.20). The off-axis points Q and Q' are taken as field limits in object and image space.

Example (adapted from O'Shea [3])

In Fig. 1.21 we show a simple optical system with a stop between its two components.

The aperture angle u of the marginal ray (through the edge of the stop) is limited by the stop.

The image of the aperture stop in object space is the entrance pupil (EP).

The image of the stop in image space is the exit pupil (XP), see Fig. 1.22.

The *field stop* is the edge that limits the angle w of the *chief ray* that is drawn through the centre of the aperture stop, see Fig. 1.23.

In this system the first lens is the field stop. The chief ray in object space points to the centre of the entrance pupil (marked by an E).

In image space it seems to come from the centre of the exit pupil (marked by an X).

Rays from the object point Q above the chief ray do not pass the system. Only part of the beam from Q reaches the image plane; this effect is called vignetting. We take Q as the edge of the usable field.

Vignetting can be prevented when the field stop is in the object plane or a plane conjugated with it. This is the case in microscopes and telescopes (see Chap. 2).

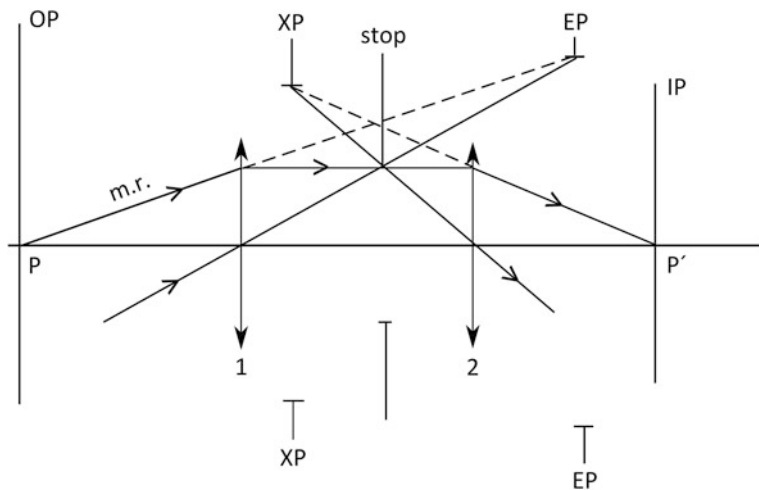


Fig. 1.22 Entrance pupil and exit pupil

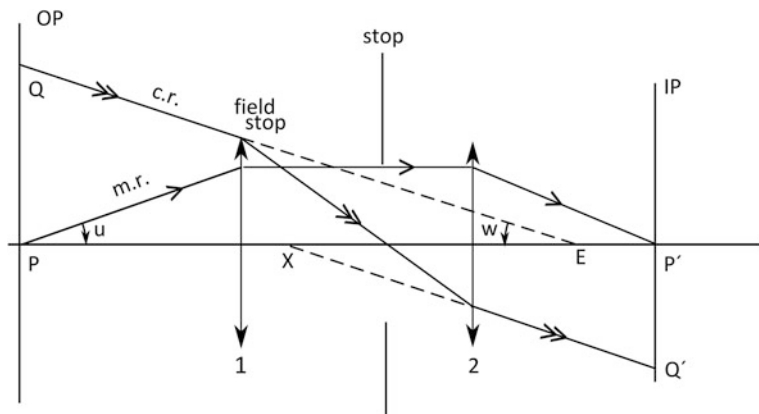


Fig. 1.23 Field stop

1.5.1 Telecentric Stop

When the stop is in the focal plane, as shown in the figures, the size of either object or image, or both, is independent of the distance from the lens.

We have three types of telecentricity: object telecentricity (Fig. 1.24a), image telecentricity (Fig. 1.24b), and doublesided telecentricity (Fig. 1.25).

Defocusing will cause a blurring of the image, but the chief ray, at the centre of the point image, will land at the same position in the image plane.

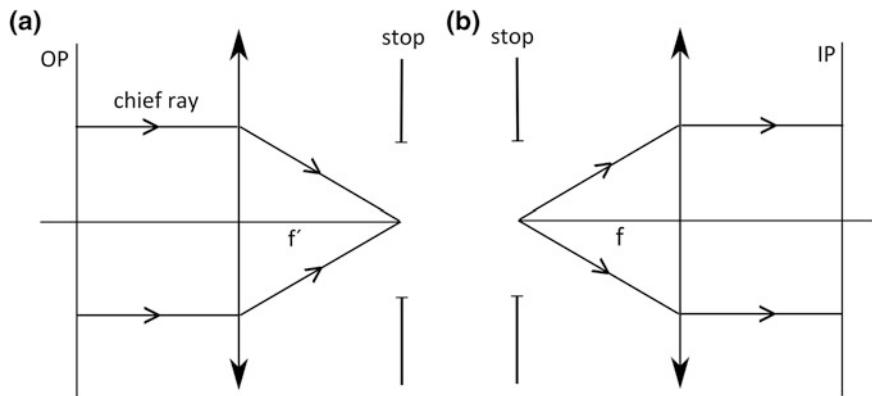


Fig. 1.24 **a** Object telecentricity. **b** Image telecentricity

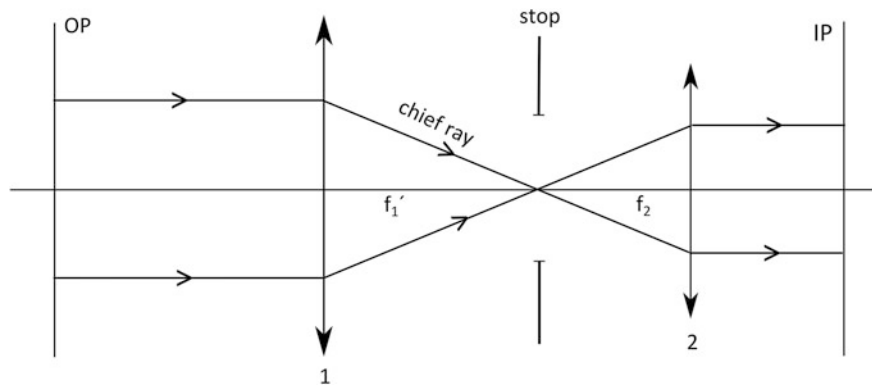


Fig. 1.25 Double-sided telecentricity, we have drawn here chief rays only

In Fig. 1.24a it is clear that the size of the image made of an object at a finite distance from the lens is independent of the object distance. In photography this is called a telecentric perspective. It is understood that the image distance is constant, so that again the image will be sharp only for one value of the object distance.

In Fig. 1.25 the magnification is independent of the axial position of object and its conjugate image plane.

Telecentricity is applied in measuring objectives, sometimes in microscopes (for instance confocal microscopes), profile projectors and stepper lenses.

1.5.2 Adding Rays

When we have traced two rays through a system, we can find the ray data for any other paraxial ray by adding the *ray vectors*

$$\begin{vmatrix} n_i u_i \\ h_i \end{vmatrix} \quad \text{and} \quad \begin{vmatrix} n_i \bar{u}_i \\ \bar{h}_i \end{vmatrix}$$

multiplied by suitable constants.

This is a valid procedure because the (1.21) are linear in the angle and ray height variables.

It can be used in finding focal points and principal planes, to do reverse ray tracing, and to find entrance and exit pupil when the stop is given. In each of these cases it is only necessary to trace two rays, and use the data of these to find the data of every other paraxial ray.

Example

We give an example of this procedure.

Suppose that we know the position of the stop and that we have traced a marginal ray from the axial object point, so that we know n_u and h at the stop (as in Fig. 1.20).

We also need, to calculate the aberration coefficients, a chief ray through the axial point of the stop (as in Fig. 1.23).

The coordinates of the chief ray can be found as follows. First we trace a test ray, not proportional to the marginal ray, through the entire system. The coordinates of this ray at the stop be $(n_u)_t$ and h_t .

We construct a chief ray by adding the marginal ray and the test ray in such a way that the resulting ray has zero height at the stop. We must have

$$\alpha h + h_t = 0$$

The ray that we have found has ray coordinates $\bar{h}_i = \alpha h_i + h_{ti}$, $(n\bar{u})_i = \alpha(nu)_i + (nu)_{ti}$ at each surface i ($1 \leq i \leq k$) of the system. When we find that $(n\bar{u})_1$ does not have the value $\tan(w)$ that we specified in the lay-out, this must be corrected at the entrance pupil.

In this chapter we have described the basics of geometrical optics. A more extensive description is given in the book of Mouroulis and Macdonald [5].

References

1. M. Born, E. Wolf, *Principles of Optics*, 7th edn. (Cambridge University Press, Cambridge, 1999)
2. R. Kingslake, R.B. Johnson, *Lens Design Fundamentals*, 2nd edn. (SPIE Press/Academic Press, 2010)
3. D. O'Shea, *Elements of Modern Optical Design*. (Wiley, 1985)
4. A.C.S. van Heel, *Inleiding in de Optica*. (M. Nijhoff, 1950)
5. P. Mouroulis, J. Macdonald, *Geometrical Optics and Optical Design* (Oxford University Press, Oxford, 1997)

Chapter 2

Optical Instruments (Paraxial Approximation)

We give only a short description of the most important optical instruments. For more details see the textbooks, e.g. Hecht [1] or Longhurst [2].

2.1 Camera

The simplest camera has a lens, shutter, an iris diaphragm and a box in which the back wall contains the film plane. Axial movement of the lens makes focusing on the object plane possible, see Fig. 2.1.

The F-number, defined as $F\# = \frac{f'}{2a}$, where f' is the focal length of the lens and $2a$ the diameter of the iris, controls exposure time and the depth of focus. A $\sqrt{2}$ times smaller F-number gives a 2 times smaller exposure time.

The depth of focus Δz is given by

$$\Delta z = \pm \Delta y F\#,$$

where Δy is the acceptable unsharpness, for instance the smallest detail discussed above.

With a diffraction limited lens the depth of focus is given by $\pm 4\lambda(F\#)^2$. This is called the Rayleigh DOF and constitutes a minimum of Δz .

The distance from lens to film plane s' is given by the imaging equation

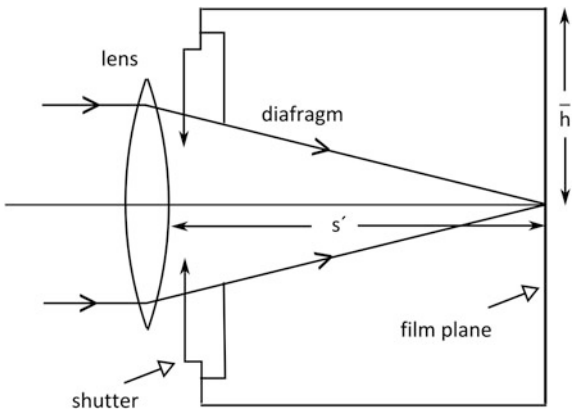
$$\frac{1}{s'} = \frac{1}{s} + \frac{1}{f}$$

where s is the object distance.

With a height \bar{h} of the film plane, the field angle w is given by $\tan w = \bar{h}/s'$.

The resolution of lenses used in cameras depends on the application of the camera.

The human eye can resolve details of 0.1 mm at a distance of 250 mm. When a negative with a format of 24×36 mm is enlarged by a factor 4, its smallest details should have a size of 0.025 mm.

Fig. 2.1 A simple camera

The lens of a film camera (and also a film projection lens) should have a better resolution over a smaller field (8 or 16 mm).

With a CCD as target in a camera, the pixel size is related to the required resolution. With pixels of 5 μm and arguing that 4 pixels per period are necessary for a good contrast, a resolution of 0.010 mm should be sufficient.

In our review of camera lenses in Sect. 4.1 we will see that a resolution of 30 periods per mm is standard for modern camera lenses.

2.1.1 Camera Obscura

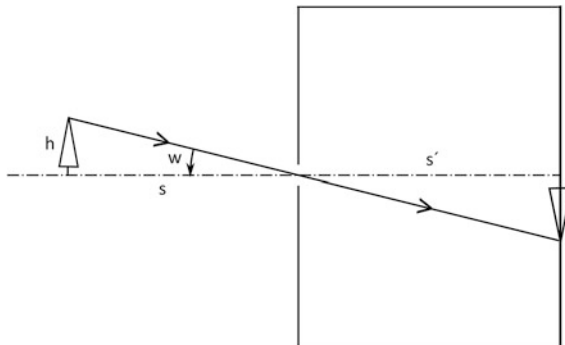
The camera obscura, or pinhole camera, is a predecessor of our modern photocamera. It was used in the renaissance era to record the contours of landscapes and played an essential role in the discovery of the laws of *perspective*, see Fig. 2.2.

The image on the backside (film or ground glass) is a projection with the entrance diaphragm as a center. It is clear that the size of the image is given by $w s'$, where w is the field angle. We have $w = -\frac{h}{s}$, where h is the object height. With s' constant we see that a more distant object makes a smaller image. This is called *homocentric perspective*.

By imaging the diaphragm with a lens to the left we can make the perspective so that a more distant object gives a larger image. This is called *hypercentric perspective*.

In Sect. 1.5 (Fig. 1.24a) we saw that a telecentric perspective can be obtained when the diaphragm is in the focal plane of the imaging lens.

To make a sharp image the diaphragm must be made small. Diffraction at a small pinhole gives a blur with the size $\frac{\lambda s'}{d}$, where λ is the wavelength; equating this with the diameter d of the pinhole we get as optimum $d = \sqrt{\lambda s'}$. With $\lambda = 0.5 \mu\text{m}$ and $s' = 125 \text{ mm}$ we find $d_{\text{opt}} = 0.25 \text{ mm}$. This is also the optimum of resolution.

Fig. 2.2 Camera obscura

2.2 Human Eye

In optics the following components of the eye (and their properties) are important. See Fig. 2.3.

- The cornea, the eye's first surface, is covered with a tear layer of about $50 \mu\text{m}$ thickness. The cornea is transparent and approximately spherical with a radius of curvature of 7.8 mm (average).
- Between the cornea and the eye lens there is a watery fluid with index $n = 1.336$.
- The eye lens is situated about 7 mm behind the cornea and has a refractive index that varies in the axial direction between 1.386 (outside) and 1.406 (center). Its axial thickness and curvature are controlled by the ciliary muscle, so that its power can vary between 17 and 25 dioptres (accommodation) in persons under the age of 45.
- The iris diaphragm is in front of the eye lens and can vary its diameter from 2 to 8 mm to adapt to the light level.
- Between the lens and the retina there is a watery gel with index 1.336.
- The retina is situated at an axial distance of about 25 mm behind the cornea; it is curved with a radius of about 12 mm.

At the backside of the retinal tissue we find the sensitive elements, “cones” and “rods”. The cones are concentrated in the macula, the cone density is greatest in the fovea with distances between their centres from 2.5 to 5 μm . The cones are used for seeing with high resolution (about 0.5 mrad) in daylight.

The rods are distributed over the peripheral retina; they are connected by nerve patterns and serve for pattern recognition and movement detection. The resolution in the periphery is considerably lower than in the macula; the sensitivity of the rods is highest at low light levels.

In Fig. 2.4 we give a model of the eye based on work of Gullstrand [2, p. 425].

In this figure, 1 is the cornea, 2 and 3 are surfaces of the eye lens, 4 is the retina. The iris (pupil) is just in front of the eye lens. The refractive indices behind cornea

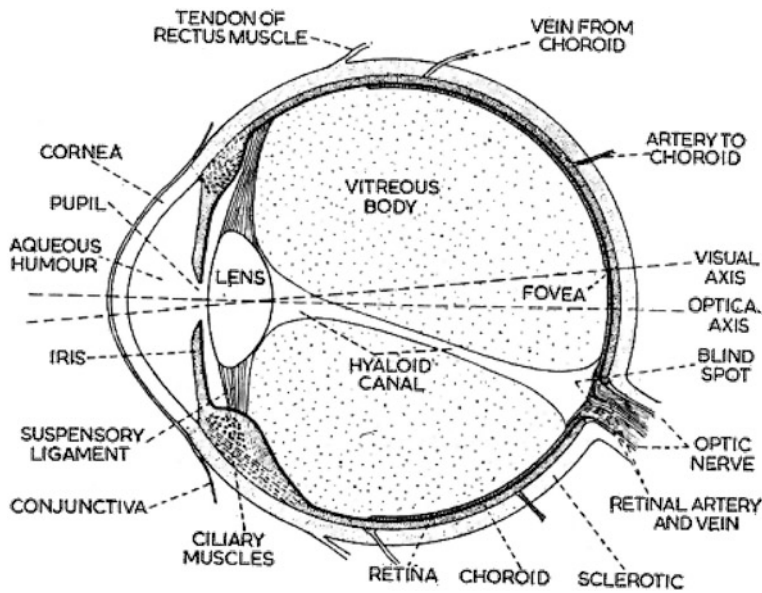
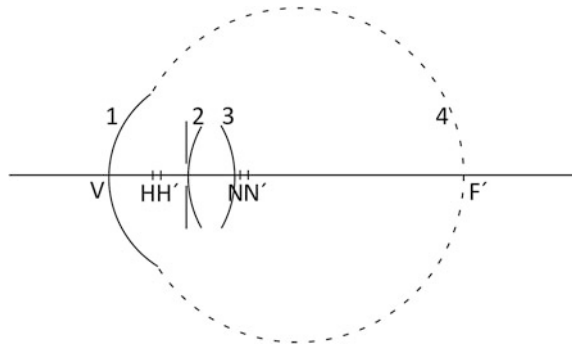


Fig. 2.3 The human eye, horizontal cross-section of the eye. Nose is *below*, so it is the *right* eye

Fig. 2.4 Gullstrand's eye model



and lens are those of aqueous and vitreous bodies. The refractive index of the lens in this model is an average value.

The data of this eye model are

	#	Radius	Distance	Index
OBJ	0	—	∞	1
	1	7.8	7	1.336
	2	10.0	3.6	1.413
	3	-6.0	13.4	1.336
IMA	4	-12.0	—	—

The stop (iris) is in front of the first lens surface. The principal planes lie at distances $VH = 1.47$ mm and $VH' = 1.50$ mm from the cornea. The distance VF' is 24 mm. The radius of curvature of the image surface is 12 mm. The power is 60 diopters. See [2, Sect. 17.2].

2.2.1 Nodal Points

The *nodal points* of an optical system are defined as axial points with an angular magnification of +1, so that $u' = u$. In Fig. 2.4 N and N' are the nodal points and H and H' the principal points.

With $n'u' = nu - Kh$ (1.19) and $u' = u$ we have

$$HN = H'N' = h/u - u = (n' - n)/K = f'/f$$

Note that $HN = H'N' = 0$ when $n' = n$.

2.2.2 Exercise 4, Nodal Points of the Eye

When the eye is rotated around the second nodal point (N' in Fig. 2.4) the image on the retina of a far object will not move (check this with your own eye).

Calculate the position of the nodal points in Gullstrand's eye model.

Tip: first find the position of the principal planes.

A few words about eye corrections:

- cornea too steep gives *nearsightedness*, to be corrected by a negative glass,
- cornea too shallow *farsightedness*, to be corrected by a positive glass,
- at old age accommodation fails, one needs reading spectacles then,
- when the cornea has different curvature in two perpendicular directions (with arbitrary orientation) we have *astigmatism*, to be corrected by "cylinder power",
- the eye lens can become opaque by cataract; then a plastic "intra-ocular lens" can be inserted.

In this course we do not consider

- color vision
- binocular vision
- eye movements.

Cones can discriminate between red, green and blue accurately, so that many different shades of color can be perceived. The cones are more sensitive for green than for red and blue, with maximum sensitivity of 680 lumen/watt at 555 nm.

By comparing the images of both eyes, the brain can see depth.

The eye can be rotated in two dimensions by two sets of muscles (see Fig. 2.3) to direct the eye axis to objects of interest.

2.3 Magnifier and Microscope

With the unaided eye we can resolve details of the order of 0.1 mm at a distance of 250 mm.

When we use a magnifier lens in front of the eye, with focal length f' , we have an *angular magnification*

$$M = \frac{250}{f'} \quad (1)$$

compared to the original situation, when we put the object in the focal plane. See Fig. 2.5.

One could expect that with a magnification M , details of the order of magnitude of $100/M \mu\text{m}$ could be resolved. This was confirmed in the work of Anthoni van Leeuwenhoek.

Anthoni van Leeuwenhoek (1632–1723) used lenses in the form of small glass spheres, where

$$K = \frac{2(n - 1)}{nr}$$

With $r = 4 \text{ mm}$ and $n = 1.6$ we have $f' = 5.3 \text{ mm}$ and $M = 48$. It turned out that the observable details were of the order of $2 \mu\text{m}$.

The *compound microscope* consists of an objective lens that makes a magnified image of the object, and an ocular that projects an image at infinity, so that the eye has a focused image on its retina (see Fig. 2.6).

The angular magnification of the compound microscope is given by

$$M = M_{ob} \frac{250}{f_{oc}}, \quad (2)$$

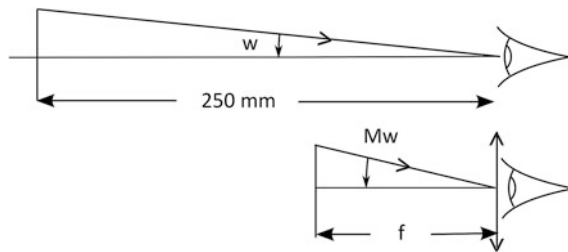
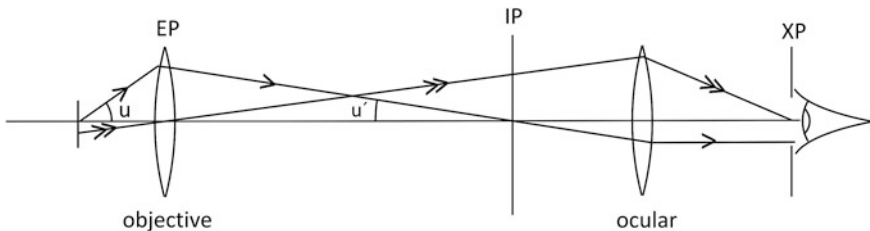
where M_{ob} is the (linear) magnification of the objective and f_{oc} the focal length of the ocular. With $M_{ob} = 20$ and $f_{oc} = 25$ we have a magnification of $200\times$ and we expect to see details of $0.5 \mu\text{m}$.

This is of the order of the wavelength of light, so we should consider the effect of diffraction.

According to the theory of diffraction the smallest detail that can be resolved by an objective with aperture angle u is given by [see Sect. 4.7, (4.53)]

$$\Delta y = 0.6 \frac{\lambda}{n \sin u},$$

where n is the index in object space, λ is the wavelength in vacuo; $n \sin u$ is called the *numerical aperture*. With $\lambda = 0.5 \mu\text{m}$ (green light) and $\sin u = 0.5$ (quite normal for a $20\times$ objective), $n = 1$, we have $\Delta y = 0.6 \mu\text{m}$. With such an objective details of $0.5 \mu\text{m}$ cannot be observed.

**Fig. 2.5** Magnifier**Fig. 2.6** Compound microscope

By making the refractive index higher than 1 in object space we can improve the resolution. Microscopy in a transparent medium, for which water and other fluids are being used in practice, is called *immersion microscopy*.

With a water *immersion* we have $n = 1.33$, and the diffraction limit becomes, with the same values of u and λ as before, equal to $0.45 \mu\text{m}$; smaller than $0.5 \mu\text{m}$.

2.3.1 Maximum Magnification

We calculate the maximum magnification as function of the diameter of the eye pupil. This is important for visual microscopy (and also for observation with a telescope).

According to *Abbe's sine rule* we have, for a well corrected objective (see Fig. 2.6)

$$n' \sin u' = \frac{n \sin u}{M_{ob}}$$

Abbe's sine rule and its consequences are explained in Sect. 14-3 of Longhurst [2]. Usually $n = 1$, $M_{ob} \gg 1$, so that $n' \sin u'$ is small and

$$n' \sin u' = \frac{\Phi}{2f_{oc}},$$

where Φ is the diameter of the eye pupil, is a good approximation.

The ocular magnification is $M_{oc} = \frac{250}{f_{oc}}$, so that we find for the total magnification

$$M = M_{ob}M_{oc} = 500 \frac{n \sin u}{\Phi}. \quad (3)$$

Because the smallest pupil diameter is $\Phi = 2$, the maximum magnification is

$$M_{max} = 250 n \sin u \quad (4)$$

when the eye pupil is the limiting diameter.

When we make the exit pupil of the ocular narrower, we can take a somewhat higher value for M ; but beware of diffraction (a Φ_{oc} of 1 mm gives a spot of 5 μm on the retina). Van Heel recommends to take the maximum magnification as 1,000 $n \sin u$ [3].

2.4 Telescopes

Kepler's (astronomical) telescope consist of an objective and a positive ocular, see Fig. 2.7.

It gives an inverted image; the inversion can be corrected by inserting a prism arrangement (for instance that of Porro) or an inverting system between objective and ocular. Here we will not consider this any further, but in the design of telescopes of this type it is an important issue (see Sect. 6.2).

In this arrangement, with a single lens ocular, we take the aperture stop at the objective. Then the exit pupil is at a distance behind the ocular given by

$$\frac{1}{s'_2} = \frac{-1}{f_1 + f_2} + \frac{1}{f_2}$$

Because $f_1 + f_2 \gg f_2$, we have $s'_2 \cong f_2$; s'_2 is called the *eye relief*. The *linear magnification*, defined as the ratio between the ray heights in the exit and entrance pupils, is $M_L = -\frac{f_2}{f_1}$.

The *angular magnification*, defined as the ratio $\frac{W'}{W}$ (see Fig. 2.8) is given by $M_A = -\frac{f_1}{f_2}$.

($M_L = \frac{1}{M_A}$ is an example of a more general relationship, known as Lagrange's invariant, see Sect. 2.5.)

Usually we designate a hand-held telescope by a product like 8 × 30, where the first figure denotes M_A and the second the diameter of the entrance pupil.

The diameter of the exit pupil is now $\frac{30}{8} = 3.75$ mm.

The system of Fig. 2.9 suffers from *vignetting*: a chief ray from the centre of the entrance stop (at the objective) misses the ocular when its angle w with the axis (the *field angle*) is larger than

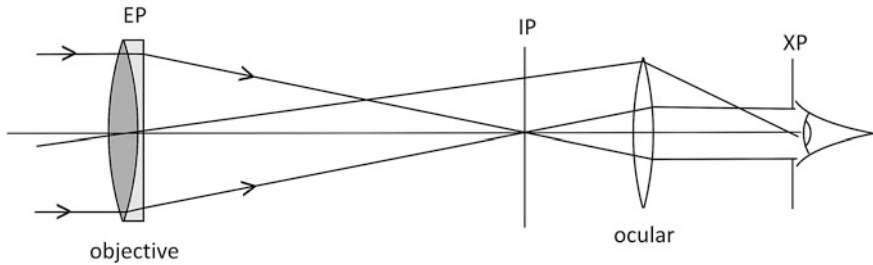


Fig. 2.7 Kepler's telescope

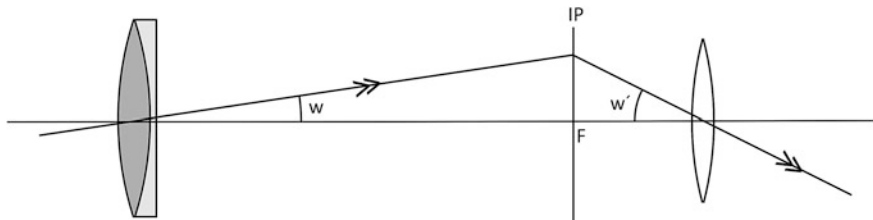


Fig. 2.8 Magnification

$$w = \frac{1}{2} \frac{\Phi_{oc}}{(f_1 + f_2)}$$

where Φ_{oc} is the diameter of the ocular. With our 8×30 telescope and $f_1 = 200$ mm we have $f_1 + f_2 = 225$ mm. With $\Phi_{oc} = 4.5$ mm we could have $w = 0.01$. The full field would be $2w = 0.02$ or 20 mrad.

Van Heel [3] points out that with the exit pupil XP rather far from the eye lens and partial illumination of this pupil due to vignetting, the observer has to move his head to see objects at the edge of the field. This is shown in Fig. 2.9.

An improvement of this situation can be obtained by the use of a *field lens*, see Fig. 2.10.

When we put a lens in (or near) the point F where intermediate image is, and take the power of this lens so that the objective is imaged by it on the eye lens, we can take the diameter of the field lens Fig. 2.16, so that the field angle $\frac{\Phi_F}{f_1}$ is what we want.

In our example $\Phi_F = 4$ mm would give $2w = 0.02$. Because, as we will see later, a lens near the image plane does not contribute much to the aberrations, we can make its diameter easily larger to obtain a larger field angle.

With telescope and microscope objectives $\Phi_F = 20$ mm is frequently used.

Now the eye lens acts as aperture stop, with a minimum diameter of 3.75 mm, and the field lens acts as a field stop. Over the whole field we have (nearly) no vignetting.

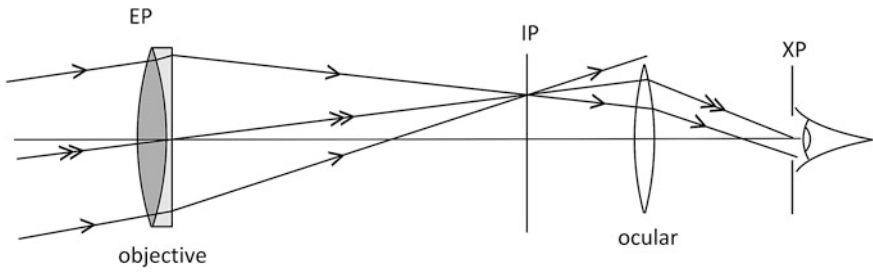
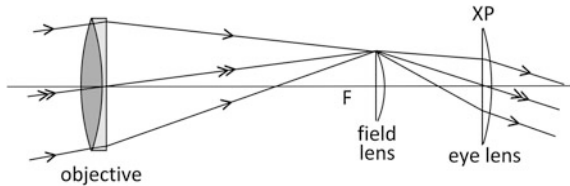


Fig. 2.9 Vignetting in a simple telescope

Fig. 2.10 Telescope with field lens



In this set-up the eye of the observer should be immediately behind the eye lens; in many situations this is not practical, an eye relief of a few centimeters is usually required. This leads to a compromise, by taking a slightly larger Φ_{oc} and increasing the focal length of the field lens, we obtain the final lay-out. See Fig. 2.11.

The parameters of this lay-out are given in the following table:

		Focal length	Distance	Diameter
Objective	1	300	300	30
Field lens	2	81.8	37.5	20
Eye lens	3	37.5	25	17.2
Stop	4			3.75

Galilei's telescope consists of a positive objective and a negative eye lens. With the stop at the objective its exit pupil lies between the lenses, and therefore far from the eye, so that vignetting cannot be avoided.

This telescope has no inversion, so that it can be used directly for terrestrial applications; it is applied (at low magnifications) in the theatre and in sports. See Fig. 2.12.

A modern application of the telescope, in reverted order, as a beam expander for laser beams. Between the lenses (in F) a pinhole filter takes away stray light. See Fig. 2.13.

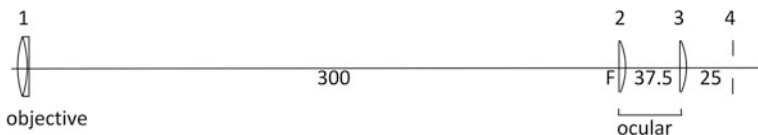


Fig. 2.11 Lay-out of a telescope, scale 2:1

Fig. 2.12 Galilei's telescope, $M_A = 2$

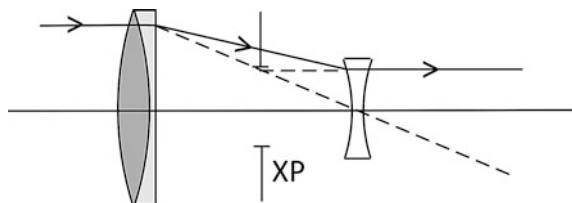
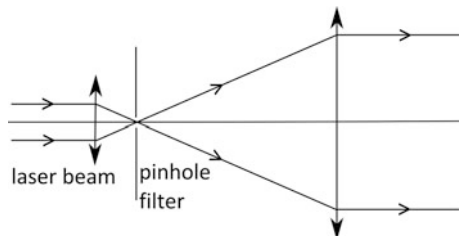


Fig. 2.13 Beam expander



2.5 Illumination

Some instruments, such as the microscope and the projector, need artificial illumination. Others, like the camera and the telescope (and also the human eye) have objects that send out light themselves, or light reflected by light sources already present.

A simplified illumination system for a microscope contains a light source, a condenser lens, a transparent object, the objective and the stop. See Fig. 2.14.

In the figure the object size is greatly exaggerated; the full field of a 10 \times microscope objective has a diameter of about 2 mm.

The condenser and the objective image the source in the aperture stop. It can be shown that with a flat source, the light flux (Watt/m^2) through the object is given by

$$\Phi = \pi B S \sin^2 u_c \quad (5)$$

where S is the area of the source and u_c is the aperture angle of the condenser.

Fig. 2.14 Illumination system

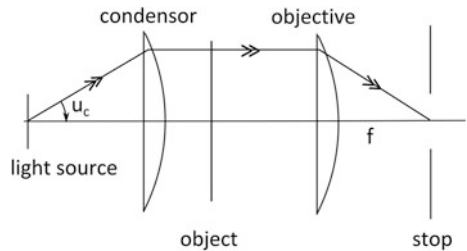
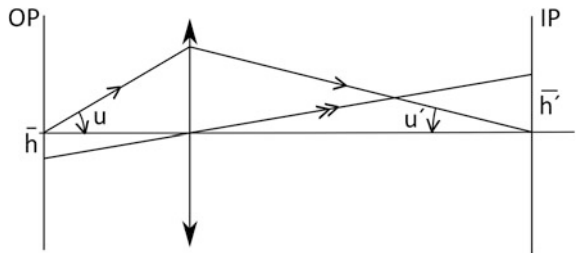


Fig. 2.15 Lagrange invariant



The constant B , called *radiance*, is a property of the source. With a thermal light source it is a function of the temperature of the source.

In paraxial optics we have the invariant

$$S'u'^2 = Su^2. \quad (6)$$

This equation is a special case of the optical invariant.

$$H = n(h\bar{u} - \bar{h}u),$$

where (h, u) and (\bar{h}, \bar{u}) are two paraxial rays. See Sect. 1.4, (1.22).

H is equal in all planes of the system. Here we consider object and image plane. See Fig. 2.15.

In the above object plane, when we take $h = 0$, we have $H = -n\bar{u}$. This is equal to $H' = -n'\bar{h}'u'$ in the image plane, so that, with $n' = n$, we have $Su^2 = S'u'^2$. This is called Lagrange's invariant or Helmholtz-Lagrange invariant in the literature.

Ernst Abbe showed that for well corrected optical systems

$$S' \sin^2 u' = S \sin^2 u \quad (7)$$

Without loss of light (by absorption or scattering) in the system therefore the radiance of the source is equal to that of its image $B = B'$.

This is in agreement with the second law of thermodynamics (Clausius): the temperature in the image cannot be higher than in the source itself.

The quantity $S \sin^2 u$ is called the *throughput* of the system. It is proportional to H^2 ; we have seen that the throughput determines the transport of energy through the system.

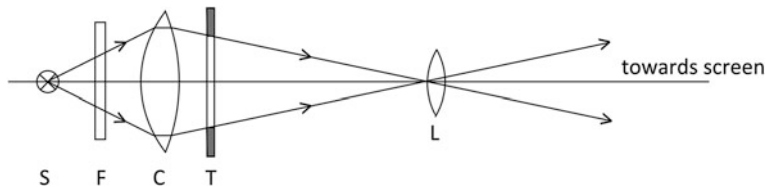


Fig. 2.16 Slide projector

Throughput is also important in the description of the *channel capacity*; according to Shannon [4] this is the number of bits that can be transported per second through the system.

The channel capacity is proportional to the number of degrees of freedom N , defined as

$$N = \frac{S_0}{S_D}$$

where S_0 is the area of the object and S_D is the area of the object-side diffraction spot,

$$S_D = \frac{\lambda^2}{n^2 \sin^2 u} \frac{\pi}{4}$$

so that we have

$$N = S_0 \sin^2 u \frac{4n^2}{\pi \lambda^2}$$

Because throughput is an invariant ($\sim H^2$) also N is invariant (the “pixel theorem”).

With a field radius of 1 mm and $\frac{\lambda}{n \sin u} = 1 \mu\text{m}$ we have $N = 4 \cdot 10^6$. This is typical for a $20\times$ microscope objective. With a stepper lens N can be of the order of 5×10^{10} .

Example

As an example of an illumination system we discuss a simple projection device: the slide projector. Slide projectors are not in frequent use anymore, but their modern successors operate according to the same principle. See Fig. 2.16 for a scheme of a slide projector.

A light source S is imaged by a condenser lens C in the pupil of the projection lens L . Between the source and the condenser there is a filter F that transmits only the visible part of the source spectrum, so as to prevent heating of the transparency (slide) T that follows the condenser. The slide is imaged on a screen (not in the figure) that is far from L , typically a few meters (at home) or some tens of meters (in a lecture room).

Let us assume that the projector source is a 100 W halogen lamp, that will produce about 3,000 lumen.

How much of this light will reach the screen depends on the aperture of the condenser and the transmission of the components between the source and screen.

Assuming that the lamp sends an equal amount of light in all directions (it is a uniform source, not Lambertian) the condenser will receive a portion $u^2/4$, where u is the condenser aperture. With $u = \pi/6$, or 30° this factor is equal to 0.0685. Let the filter F have a transmission coefficient of 0.8 and let us assume that we have reflection losses of 2 % for each optical surface and there are 10 of these; the transmission coefficient without transparency then becomes 0.64.

A blank slide does not contain useful information; let us assume that the average transparency transmits 50 % of the light. Then the luminous flux that hits the screen is given approximately by

$$\Phi = 3000 \times 0.0685 \times 0.64 \times 0.5 \approx 66 \text{ lm}$$

When we assume that the screen is a diffuse scatterer that absorbs 30 % of the light impinging on it and the spectator is at a distance of 4 m from the screen in an otherwise dark room, his two eyes will receive a portion of u_e^2 of the light reflected from the screen, where u_e is the aperture angle of the eye measured from the screen. With a pupil diameter of the eye of 8 mm we have $u_e = 0.001$.

The luminous flux received by the eye pupil is therefore given by

$$\Phi = 66 \times 0.7 \times (0.001)^2 = 0.46 \times 10^{-4} \text{ lm}$$

When we estimate that the screen image on the retina occupies an area of about 100 mm^2 , the illuminance on the retina will be of the order of $0.5 \text{ lm/m}^2 = 0.5 \text{ lux}$.

This is enough for a well-adapted eye to perceive a clear screen image.

More on the subject of illumination is found in Mouroulis and Macdonald [5].

References

1. E. Hecht, *Optics*, 4th ed. (Addison-Wesley, Boston, 2002)
2. R.S. Longhurst, *Geometrical and Physical Optics*, 2nd ed. (Longman, London, 1973)
3. A.C.S. van Heel, *Inleiding in de Optica* (M. Nijhoff, Boston, 1950)
4. C. Shannon, W. Weaver, *The Mathematical Theory of Communication* (University of Illinois Press, Urbana, 1964)
5. P. Mouroulis, J. McDonald, *Geometrical Optics and Optical Design* (Oxford University Press, New York, 1997)

Chapter 3

Aberrations

3.1 Wavefronts and Aberrations

The centered system has only aberrations of uneven order. There are five aberrations of the third order; we will derive these from the function $E(x,y;\eta')$, *the wavefront error*. See Fig. 3.1. In the figure x, y are the coordinates of the exit pupil. A chief ray meets the image plane in P , with coordinates ξ', η' . We draw a reference wavefront (spherical) with P as centre through the axial point of the exit pupil (S_0 with radius R). The wavefront S , also through the axial point of the exit pupil, deviates by an amount $E(x, y; \eta')$ from S_0 , as measured from P ; $E(x, y; \eta')$ is the optical path difference along a reference ray through P .

A ray perpendicular to S has deviations $\delta\eta'$ and $\delta\xi'$ from P given by

$$\delta\eta' = \frac{R}{n'} \frac{\partial E}{\partial y}, \quad \delta\xi' = \frac{R}{n'} \frac{\partial E}{\partial x} \quad (3.1)$$

to a good approximation.

We introduce relative pupil coordinates x_r, y_r by

$$x = x_r a, \quad y = y_r a \quad (3.2)$$

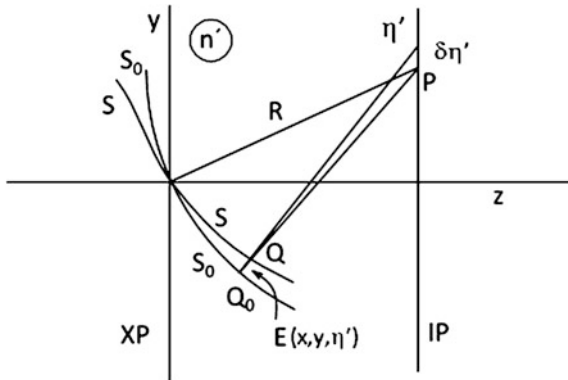
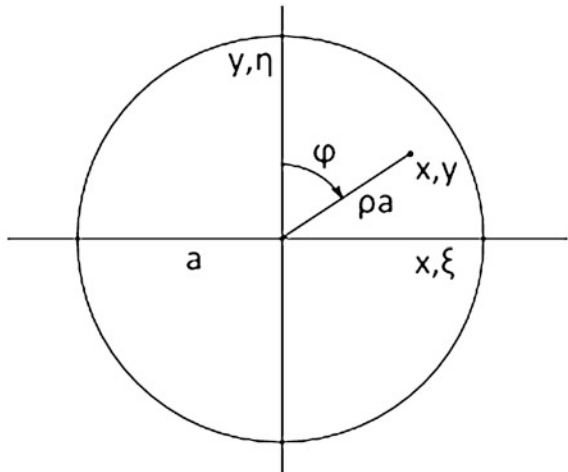
where a is the radius of the exit pupil.

With $\frac{a}{R} = \sin u'$ we have

$$\delta\eta' = \frac{1}{n' \sin u'} \frac{\partial E}{\partial y_r}, \quad \delta\xi' = \frac{1}{n' \sin u'} \frac{\partial E}{\partial x_r}. \quad (3.3)$$

The equations for $\delta\eta', \delta\xi'$ are derived by Welford [1, Sect. 7.3].

We also define relative field coordinates $\eta' = \bar{a}\eta_r$, where \bar{a} is the image field radius.

Fig. 3.1 Wavefront error**Fig. 3.2** Polar pupil coordinates

Because of the axial symmetry of the system, E can be written as a function of the coordinates

$$\begin{aligned} U &= x_r^2 + y_r^2, \\ V &= \xi'_r x_r + \eta'_r y_r, \\ W &= \xi'_r + \eta'^2_r. \end{aligned} \quad (3.4)$$

Taking $\xi = 0$, which is allowed because of axial symmetry, and introducing polar coordinates in the pupil gives (see Fig. 3.2)

$$\begin{aligned} U &= x_r^2 + y_r^2 = \rho^2, \\ V &= \eta'_r y_r = \eta'_r \rho \cos \varphi, \\ W &= \eta'^2_r. \end{aligned} \quad (3.5)$$

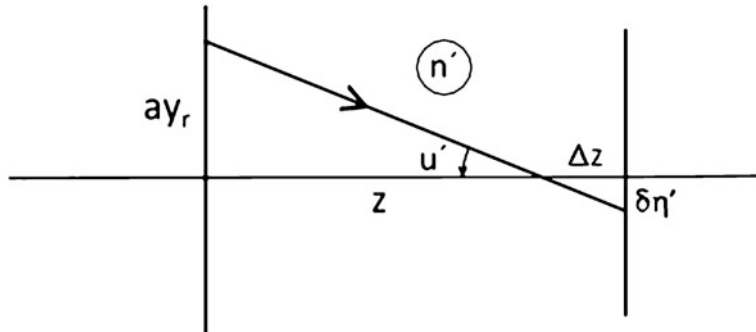


Fig. 3.3 Defocusing, $\delta\eta' = ay_r \cdot \Delta z / z$, where z is the distance between exit pupil and the image plane. With $\Delta z = 2a_1$ and $u' = a/z$ we have (3.7)

A series development of E up to the sixth order gives

$$\begin{aligned} E = & a_1 U + a_2 V + a_3 W \\ & + b_1 U^2 + b_2 UV + b_3 UW + b_4 V^2 + b_5 VW + b_6 W^2 + O(6). \end{aligned} \quad (3.6)$$

3.1.1 First Order Errors

We treat first the second order terms

$$\begin{aligned} E^{(2)} = & a_1 U + a_2 V + a_3 W. \\ -E = a_1 U \text{ gives } \delta\eta' = & \frac{2a_1 y_r}{n'u'}, \quad \delta\xi' = \frac{2a_1 x_r}{n'u'}. \end{aligned} \quad (3.7)$$

The wavefront error is quadratic in x_r and y_r , the aberrations are proportional to x_r and y_r : this is defocusing, as can be seen in Fig. 3.3.

The *zonal image* is the locus in the image plane of the ray intersections from rays that come from points in the pupil with a constant value ρ of the distance to the axis (pupil zone).

In Fig. 3.4 we show the zonal image of defocusing, its radius depends linearly on the relative pupil radius ρ .

$$-E = a_2 V \text{ gives } \delta\eta' = \frac{a_2 \eta'_r}{n'u'}, \quad \delta\xi' = 0. \quad (3.8)$$

The wavefront error is linear in η'_r and y_r (tilt), see Fig. 3.5.

The aberration is a magnification error, $\frac{\delta\eta'}{\eta'_r} = a_2/n'u'$

$$-E = a_3 W \text{ gives } \delta y' = \delta\xi' = 0 \quad (3.9)$$

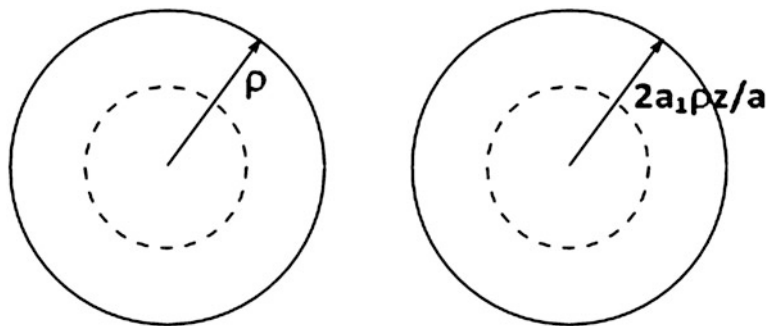


Fig. 3.4 Pupil zone. Zonal image of defocusing

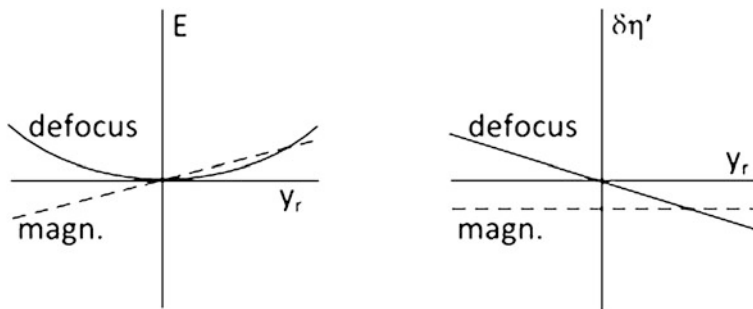
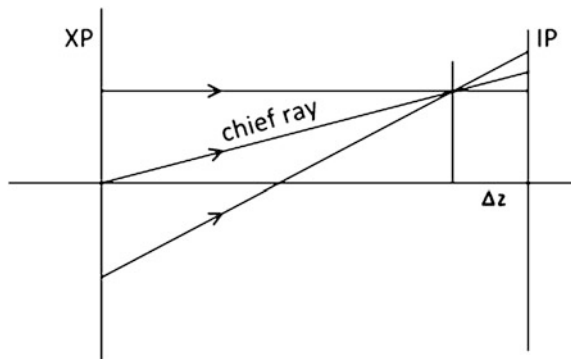


Fig. 3.5 Wavefront error $E(0, y_r, \eta')$ and aberration $\delta\eta'$ for defocusing and magnification error (magn.) as a function of y_r for a fixed value of η'

Fig. 3.6 Ray picture of defocus and magnification error



The two first order aberrations can be compensated by a change in paraxial parameters.

With the exit pupil at a finite distance from the image plane a focus shift Δz leads to both defocus and magnification error. See Fig. 3.6.

3.1.2 The Third Order Aberrations

We now consider the fourth order terms of the wavefront error

$$E^{(4)} = b_1 U^2 + b_2 UV + b_3 UW + b_4 V^2 + b_5 VW + b_6 W^2$$

3.1.3 Spherical

$$\begin{aligned} -E = b_1 U^2 \text{ gives } \delta\eta' &= 4 \frac{b_1 \rho^3 \cos \varphi}{n'u'} \\ \delta\xi' &= 4 \frac{b_1 \rho^3 \sin \varphi}{n'u'} \end{aligned} \quad (3.10)$$

The wavefront error is proportional to ρ^4 . The zonal image is a circle around P with radius $4 \frac{b_1 \rho^3}{n'u'}$.

This aberration is called *spherical aberration*. The ray picture is given below (Figs. 3.7 and 3.8).

Spherical aberration is independent of the field radius η' . It is the only aberration of the axial image point.

3.1.4 Coma

$$\begin{aligned} -E = b_2 UV \text{ gives } \delta\xi' &= b_2 \eta'_r \rho^2 \frac{\sin 2\varphi}{n'u'} \\ \delta\eta' &= b_2 \eta'_r \rho^2 \frac{(2 + \cos 2\varphi)}{n'u'}. \end{aligned} \quad (3.11)$$

The cross-section $x_r = 0$ of the wavefront is given by

$$E(0, y_r) = b_2 \eta'_r y_r^3.$$

The cross-section $y_r = 0$ is $E(x_r, 0) = 0$.

The zonal image is a circle with radius $b_2 \eta'_r \rho^2$ centered on the y' -axis at a distance of $2b_2 \eta'_r \rho^2$ from P.

This circle is completed twice for one run through the pupil zone (radius ρ). That means that the two meridional rays (M, M in the figure) for which $\varphi = 0$ or 180° are focused at $\delta\eta' = \frac{3b_2 \eta'_r \rho^2}{n'u'}$, $\delta\xi' = 0$ (meridional coma). The two sagittal rays are focused at $\delta\eta' = \frac{b_2 \eta'_r \rho^2}{n'u'}$, $\delta\xi' = 0$ (sagittal coma). This is also clear from the ray diagrams of Figs. 3.9 and 3.10.

This aberration is called *coma*.

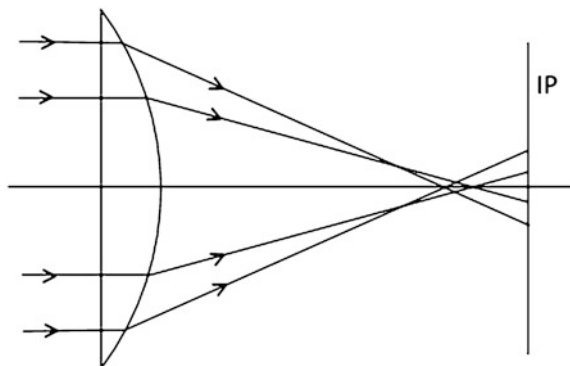


Fig. 3.7 A ray picture of spherical aberration

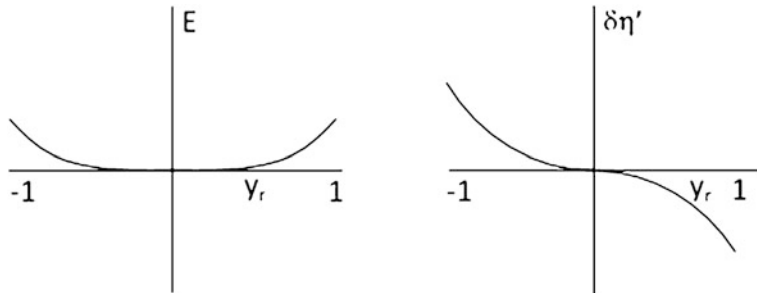


Fig. 3.8 Wavefront error and aberration plot for spherical aberration

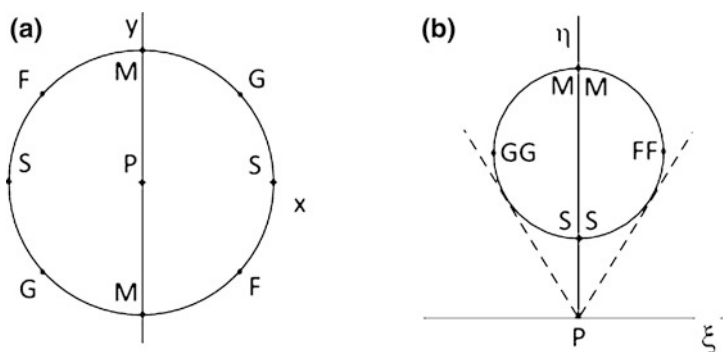
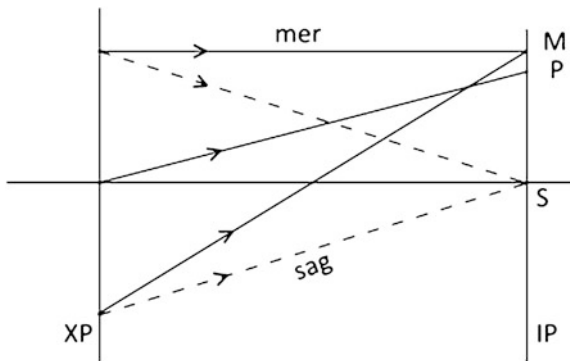


Fig. 3.9 Zonal image of coma. **a** Pupil, **b** image plane

Fig. 3.10 Meridional and sagittal ray diagrams of coma (in perpendicular planes)



Linearly dependent on field height η' , quadratically dependent on pupil height ρ . The zonal images lie between two asymptotes (see Fig. 3.9) at an angle of 60°.

3.1.5 Field Curvature

$$-E = b_3 UW \text{ gives } \delta\eta' = 2 \frac{b_3 \eta_r'^2 y_r}{n'u'}, \quad \delta\xi' = 2 \frac{b_3 \eta_r'^2 x_r}{n'u'}. \quad (3.12)$$

The wavefront error can be written $E = b_3 \rho^2 \eta_r'^2$.

The aberration is defocus, proportional to $\eta_r'^2$.

This aberration is called *field curvature*.

3.1.6 Astigmatism

$$-E = b_4 V^2 \text{ gives } \delta\eta' = 2 \frac{b_4 \eta_r'^2 y_r}{n'u'} \cdot \delta\xi' = 0. \quad (3.13)$$

The wavefront error is proportional to $\rho^2 y_r^2$, curvature only in the meridional cross-section. The aberration is a defocus of the meridional rays, proportional to $\eta_r'^2$.

This aberration is called *astigmatism*.

Wavefront error and aberration plots for field curvature (f.c.) and astigmatism (ast.) are equal in form to those for defocus shown in Fig. 3.5.

When both b_3 and b_4 are $\neq 0$, we have meridional field curvature $\frac{1}{R_m} = 4(b_3 + b_4)$.

Sagittal field curvature $\frac{1}{R_s} = 4b_3$, where again we have taken $n'u' = \frac{a}{z}$.

Fig. 3.11 Ray diagram for meridional field curvature

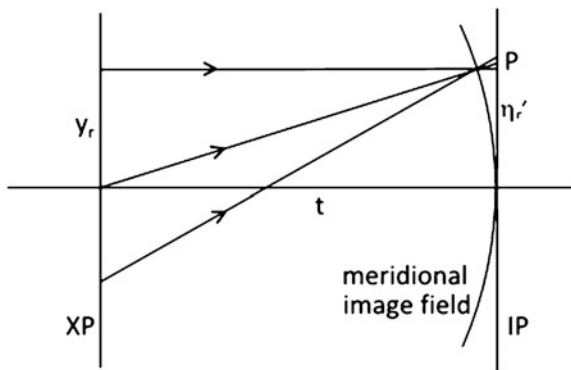
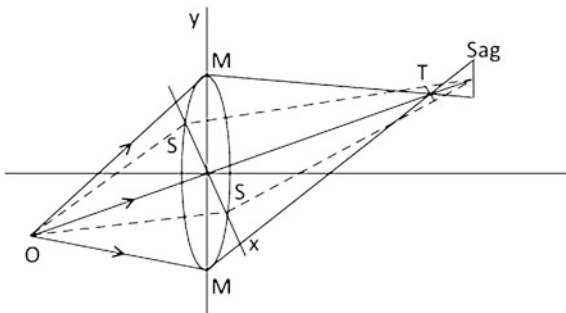


Fig. 3.12 Astigmatism, OM meridional (tangential) rays, OS sagittal rays, T tangential focal line, Sag sagittal focal line



In many cases $n' = 1$ will be valid. In third order it is permitted to take the paraxial value $\frac{a}{z}$ of $\sin u'$; this introduces an error of higher order.

See also the ray diagram in Fig. 3.11 and the perspective drawing in Fig. 3.12.

In Fig. 3.12 the sagittal rays OS lie in the *sagittal plane* through the chief ray and perpendicular to the meridional plane.

It is seen that astigmatism and field curvature are closely related.

The quantity $UW - V^2 = \rho^2 \eta_r'^2 \sin^2 \varphi$ is a measure of the deviation of a ray from the meridional plane ("skewness").

The rays for which $\varphi = \pm \frac{\pi}{2}$ are called sagittal rays.

Rays for values of $\sin^2 \varphi$ between 0 and 1 are called skew rays.

It can be shown from the paraxial raytracing equations that $UW - V^2$ is invariant (paraxially) through a centered system. It is related to the "skew invariant" (see Welford [1, p. 84]).

3.1.7 Distortion

$$-E = b_5 V W = b_5 y_r \eta_r'^3 \text{ gives } \delta\eta' = \frac{b_5 \eta_r'^3}{n' u'}, \quad \delta\xi' = 0. \quad (3.14)$$

The wavefront is tilted, compared to the reference, over an angle $b_5 \eta_r'^3$.

This aberration is called *distortion* (of 3^d order).

The wavefront error and aberration plots for distortion are equal in form to those for magnification error shown in Fig. 3.5.

Summary (geometrical properties of aberrations)

Aberration	Wavefront error Proportional to	$\delta\eta'$	$\delta\xi'$
Spherical	ρ^4	$\rho^3 \cos \varphi$	$\rho^3 \sin \varphi$
Coma	$\rho^2 y_r \eta_r'$	$\rho^2 \eta_r' (2 + \cos 2\varphi)$	$\rho^2 \eta_r' \sin 2\varphi$
Field curvature	$\rho^2 \eta_r'^2$	$\rho \eta_r'^2 \cos \varphi$	$\rho \eta_r'^2 \sin \varphi$
Astigmatism	$y_r^2 \eta_r'^2$	$\rho \eta_r'^2 \cos \varphi$	0
Distortion	$y_r \eta_r'^3$	$\eta_r'^3$	0

The term $b_6 W^2$ does not contribute to the aberrations in the image plane. By interchanging object and entrance pupil it turns out that b_6 is the coefficient of pupil spherical. See Sect. 6.5.

The summary can be used as a guide for the interpretation of aberration plots. Take $\varphi = 0$ for the meridional plot ($\delta\eta'$ vs. y_r) and $\varphi = \frac{\pi}{2}$ for the sagittal plot ($\delta\xi'$ vs. x_r).

3.2 Chromatic Aberration

The refractive index of optical glass (and plastics) depends on the wavelength of light (dispersion).

In such a way that the index is higher for blue than for red light.

The value of $\frac{\delta n}{(n-1)}$ varies between 0.01 and 0.04. Consequently, we have already in the first order (paraxial) two aberrations. We give two examples where these aberrations are shown in isolation.

With a thin lens, with the stop at the lens, we have *longitudinal Chromatic aberration* (LCA).

The marginal ray for blue intersects the axis nearer to the lens (see Fig. 3.13). LCA is defocus.

With the stop away from the lens, we have also *transverse chromatic aberration* (TCA).

Fig. 3.13 Longitudinal chromatic aberration
 $\frac{\delta s'}{s'} = \frac{-\delta n}{n-1}$

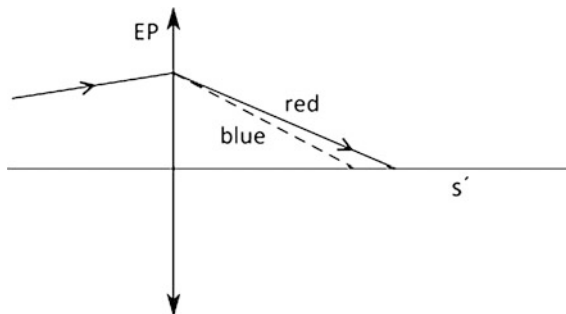


Fig. 3.14 Transverse chromatic aberration
 $\frac{\delta M}{M} = \frac{-\delta n}{n-1}$

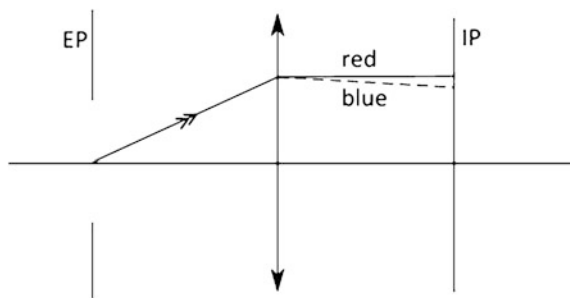
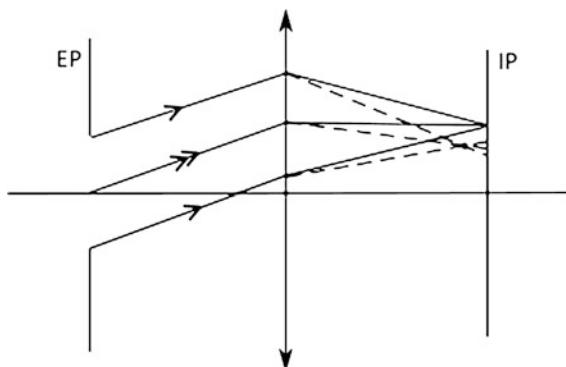


Fig. 3.15 Longitudinal and transverse chromatic aberration, "blue rays" are denoted by broken lines



The chief ray for blue intersects the image plane nearer to the axis (see Fig. 3.14) TCA is a magnification error.

In Fig. 3.14 we did not draw other rays than the chief ray. When we add more rays it will become clear that in general LCA and TCA occur together. See Fig. 3.15. Only for the axial object point LCA is the only primary Chromatic aberration.

Note that also the aberrations of the third order and of higher orders depend on the wavelength. The dependence of spherical aberration on the wavelength is called *spherochromatism*.

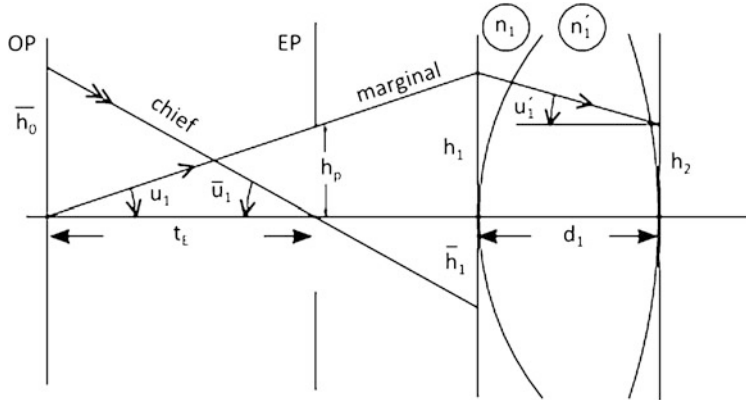


Fig. 3.16 Calculation of aberration coefficients; notation

3.3 Calculation of Aberration Coefficients

The aberration coefficients of the third order are obtained as follows.

We trace a marginal ray (from the axial object point through the edge of the entrance pupil) and a chief ray (from the edge of the object field through the center of the entrance pupil) through the system, using the paraxial ray tracing equations of Sect. 1.4. See also Fig. 3.16.

At each surface we obtain

$n_i u_i, h_i$ for the marginal ray, and

$n_i \bar{u}_i, \bar{h}_i$ for the chief ray.

At each surface we calculate

$$A_i = n_i \left(u_i + \frac{h_i}{r_i} \right), \quad \bar{A}_i = n_i \left(\bar{u}_i + \frac{\bar{h}_i}{r_i} \right),$$

$$\Delta_i \left(\frac{u}{n} \right) = \frac{u'}{n'_i} - \frac{u_i}{n_i}, \quad \Delta_i \left(\frac{1}{n} \right) = \frac{1}{n'_i} - \frac{1}{n_i}.$$

Note that $A_i = n_i i_i = n'_i \bar{i}_i$, $\bar{A}_i = n_i \bar{i}_i = n'_i \bar{i}'_i$, where i, i' are incident and refractive angle of the marginal ray, and \bar{i}_i, \bar{i}'_i for the chief ray.

Now the surface coefficients of third order are

$$\begin{aligned} \text{Spherical: } S_{1,i} &= -A_i^2 h_i \Delta_i \left(\frac{u}{n} \right), \\ \text{Coma: } S_{2,i} &= -A_i \bar{A}_i h_i \Delta_i \left(\frac{u}{n} \right), \\ \text{Astigmatism: } S_{3,i} &= -\bar{A}_i^2 h_i \Delta_i \left(\frac{u}{n} \right), \\ \text{Field curvature: } S_{4,i} &= -H^2 c_i \Delta_i \left(\frac{1}{n} \right), \quad c_i = \frac{1}{r_i}, \\ \text{Distortion: } S_{5,i} &= \frac{\bar{A}_i}{A_i} (S_{3,i} + S_{4,i}). \end{aligned} \tag{3.15}$$

These coefficients are named Seidel coefficients after L. von Seidel (1821–1896).

H is Lagrange's invariant (see Sect. 2.5).

We have $H = n_1 \bar{h}_0 u_1$, where \bar{h}_0 is the object field height, or $H = -n_1 h_p \tan \bar{u}_1$, where h_p is the entrance pupil height.

The data required for initializing are:

\bar{h}_0 the object field height,

t_E the axial distance from object to entrance pupil, $\tan \bar{u}_1 = -\bar{h}_0/t_E$

h_p the entrance pupil height,

n_1 the refractive index in object space,

d_0 the distance from object to first surface

For the Chromatic aberration we have the surface coefficients:

$$\begin{aligned} \text{LCA: } C_{2,i} &= A_i h_i \Delta_i \left(\frac{\partial n}{n} \right) \\ \text{TCA: } C_{2,i} &= \bar{A}_i h_i \Delta_i \left(\frac{\partial n}{n} \right) \end{aligned} \quad (3.16)$$

with $\Delta_i \left(\frac{\partial n}{n} \right) = \left(\frac{\partial n'}{n'} - \frac{\partial n}{n} \right)_i$, $\partial n_i = n_i(\lambda_2) - n_i(\lambda_1)$, where λ_1, λ_2 are two different wavelengths, $\lambda_2 < \lambda_1$.

Again $\left(\frac{\partial n'}{n'} \right)_i = \frac{\partial n_{i+1}}{n_{i+1}}$, so that

$$\Delta_i \left(\frac{\partial n}{n} \right) = \frac{\partial n_{i+1}}{n_{i+1}} - \frac{\partial n_i}{n_i}.$$

Usually one takes $\lambda_2 = \lambda_F = 486.1$ nm and $\lambda_1 = \lambda_C = 656.3$ nm, and n_i is taken at $\lambda_d = 587.6$ nm.

The expressions for the coefficients $S_1 - S_4$ can be used always. When $A_i = 0$ (perpendicular incidence) the expression for S_5 given in (3.15) cannot be used. In that case the alternative formula [1, p. 142]

$$S_5 = h \bar{A}^3 \Delta \left(\frac{1}{n^2} \right) + \left(A \bar{A} h^2 - 2 \bar{A}^2 h \bar{h} \right) c \Delta \left(\frac{1}{n} \right) \quad (3.17)$$

can be used.

The relations between the third order aberration coefficients and the wavefront error coefficients of the fourth order (Sect. 3.1) are given by

$$b_1 = \frac{1}{8} S_1, \quad b_2 = \frac{1}{2} S_2, \quad b_3 = \frac{1}{4} (S_3 + S_4), \quad b_4 = \frac{1}{2} S_3, \quad b_5 = \frac{1}{2} S_5. \quad (3.18)$$

The system coefficients are obtained by adding the surface coefficients:

$$S_1 = \sum_{i=1}^k S_{1,i}, \text{ etc.} \quad (3.19)$$

This means that we see directly the effect of the surface aberrations on the aberrations of the system as a whole. This property is very important in lens design.

The additivity of aberrations is valid only for third order aberrations; for higher orders this property is lost.

For a ray with relative pupil coordinates x_r, y_r and relative object height η_r , the aberrations are given in terms of the Seidel coefficients by

$$\begin{aligned}\delta\eta' &= \frac{1}{2n'u'} \{ S_1 y_r (x_r^2 + y_r^2) + S_2 \eta_r (x_r^2 + 3y_r^2) + (3S_3 + S_4) \eta_r^2 y_r + S_5 \eta_r^3 \}, \\ \delta\xi' &= \frac{1}{2n'u'} \{ S_1 x_r (x_r^2 + y_r^2) + 2S_2 \eta_r y_r x_r + (S_3 + S_4) \eta_r^2 x_r \}.\end{aligned}\quad (3.20)$$

In the polar coordinates that we used before (3.5) this becomes

$$\begin{aligned}\delta\eta' &= \frac{1}{2n'u'} \{ S_1 \rho^3 \cos \varphi + S_2 \eta_r \rho^2 (2 + \cos 2\varphi) + (3S_3 + S_4) \eta_r^2 \rho \cos \varphi + S_5 \eta_r^3 \}, \\ \delta\xi' &= \frac{1}{2n'u'} \{ S_1 \rho^3 \sin \varphi + S_2 \eta_r \rho^2 \sin 2\varphi + (S_3 + S_4) \eta_r^2 \rho \sin \varphi \}.\end{aligned}\quad (3.21)$$

In (3.20) the aberrations in the image plane are given. Sometimes it is necessary to project the aberrations back to the object plane. For instance in a microscope we want to compare the aberrations with the details in the object, and with the Airy radius in the object plane (see Sect. 4.7 on diffraction).

When in (3.20) we replace the factor $1/2n'u'$ by $1/2nu$ we obtain the projected aberrations $\delta\xi$ and $\delta\eta$.

The expressions in brackets remain the same, because the relative object height η_r is identical to the relative image height; also relative pupil coordinates x_r, y_r are identical in entrance and exit pupil (in the paraxial approximation).

The maximum values of these aberrations are

$$\begin{aligned}\text{spherical: } \delta\eta' &= \delta\xi' \leq \frac{S_1}{2n'u'}, \\ \text{coma: } \delta\eta' &\leq 3 \frac{S_2}{2n'u'}, \quad \delta\xi' \leq \frac{S_2}{2n'u'} \\ \text{ast. and f.c.: } \delta\eta' &\leq \frac{(3S_3+S_4)}{2n'u'} \text{ (meridional),} \\ &\quad \delta\xi' \leq \frac{(S_3+S_4)}{2n'u'} \text{ (sagittal rays)} \\ \text{distortion: } \delta\eta' &\leq \frac{S_5}{2n'u'}, \quad \delta\xi' = 0.\end{aligned}\quad (3.22)$$

Note that $\delta\xi'_{\max} \leq \delta\eta'_{\max}$ always.

The curvature of the meridional image surface is given by $(3S_3 + S_4)/H^2$; the curvature of the sagittal image surface is given by $(S_3 + S_4)/H^2$; the quantity S_4/H^2 is called the Petzval curvature.

The chromatic aberrations are given by

$$\begin{aligned}\delta_\lambda \eta' &= \frac{1}{n'u'} \{C_1 y_r + C_2 \eta_r\}, \\ \delta_\lambda \xi' &= \frac{1}{n'u'} C_1 x_r.\end{aligned}\quad (3.23)$$

See Welford [1, pp. 206–207].

3.3.1 Calculation Scheme

The ray tracing scheme that we presented in Sect. 1.4 can be used also to calculate the third order aberration coefficients. The following steps must be taken:

1. Trace a marginal ray: the starting values are u_1 , the aperture angle (on the object side) and $h_1 = u_1 d_0$, where d_0 is the distance from the object plane to the first surface. With an object at infinity we have to take $u_1 = 0$ and $h_1 = -u_k' f'$, where u_k' is the aperture angle in image space.

- (1a) Calculate $(u/n)_i$ for all surfaces, and

$$(h\Delta)_i = h_i ((u/n)_{i+1} - (u/n)_i),$$
 see (3.15).
- (1b) Calculate $(nh/r)_i$ for all surfaces and

$$A_i = (nh/r)_i + (nu)_i$$

2. Trace a chief ray, with $\bar{u}_p = 1$, $\bar{h}_p = 0$ at the stop, or suitable starting values at the entrance or exit pupil. Scale the parameters of this ray with a factor $\tan w/\bar{u}_1$.

- (2a) Calculate $(n\bar{h}/r)_i$ for all surfaces and

$$\bar{A}_i = (n\bar{h}/r)_i + (n\bar{u})_i$$

3. Calculate $(K/n\bar{n}')_i$ for all surfaces. For the calculation of S_4 we still need the value of the Lagrange invariant

$$H = \bar{h}_0 (nu)_i = -h_p (n\bar{u})_p$$

When using the second version of H , do not forget the minus sign!

4. The coefficients C_1 and C_2 of the chromatic aberrations require the calculation of

$$\Delta(\delta n/n)_i = (\delta n/n)_{i+1} - (\delta n/n)_i$$

where $\delta n_i = (n_F - n_C)_i$ usually, and n_i is taken at $\lambda = 587.6$ nm.

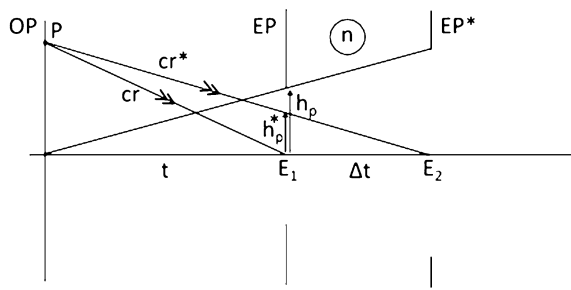
Note that this quantity has opposite signs on opposite sides of a glass (lens, plate, prism).

We give the complete calculation scheme in the following table.
The calculations can be checked in the following ways:

- u_1/u_{k+1} must be equal to M ,
- $h_1/-(nu)_{k+1}$ must be equal to f' , the effective focal length (EFFL) when the object is at infinity,
- $-\bar{h}_k + \bar{u}_{k+1}\bar{d}_k$, the image field height, must be equal to $f'\tan w$ when the object is at infinity or else to $M\bar{h}_0$, where \bar{h}_0 is the object height,
- $\bar{h}_i A_i - h_i \bar{A}_i$ must be equal to the invariant H for all surfaces.

Calculation scheme

	1	2	k		Formulas
r					
n					
n'					
d					
K					$K = (n' - n)/r$
d/n'					
nu					$n'u' = nu - Kh$
h					$h' = h + n'u'd/n'$
u/n					
$h\Delta$					$\Delta = \frac{u'}{n'} - \frac{u}{n}$
nh/r					$A = nu + nh/r$
A					
$n\bar{u}$					
\bar{h}					
$n\bar{h}/r$				\sum	$\bar{A} = n\bar{u} + n\bar{h}/r$
\bar{A}					
S_1					$S_1 = -h\Delta A^2$
S_2					$S_2 = -h\Delta A \bar{A}$
S_3					$S_3 = -h\Delta \bar{A}^2$
P					$P = K/n n'$
S_4					$S_4 = H^2 P$
S_5					$S_5 = \frac{\bar{A}}{A} (S_3 + S_4)$ or (3.17)
C_1					$C_1 = h A \Delta \left(\frac{\delta n}{n} \right)$
C_2					$C_2 = h \bar{A} \Delta \left(\frac{\delta n}{n} \right)$

Fig. 3.17 Stop shift

Exercise 5, Calculation of Seidel Coefficients

Using the ray data calculated in exercise 3 of Sect. 1.4, calculate the Seidel aberrations of Kingslakes dialyte lens.

Use the lens data $u_1 = 0$, $h_1 = f/12$, $w = 0.3839$.

Calculate also the chromatic aberration coefficients, with the following refractive index data:

Barium flint: $n_d = 1.6053$, $n_F = 1.61518$, $n_C = 1.60130$

Dense barium crown: $n_d = 1.6109$, $n_F = 1.61834$, $n_C = 1.60755$.

3.4 Stop Shift Equations

Some of the aberrations depend on the position of the stop. We see from Fig. 3.17 that when the entrance pupil shift from E_1 to E_2 , we obtain a new chief ray from the object point P.

All the aberrations that contain \bar{A} will change, viz. S_2 , S_3 , S_5 and C_2 .

From Fig. 3.17 we have that the new chief ray (cr^*) has ray parameters $\bar{h}^* = \bar{h} + \Delta q h$, $\bar{n}^* = \bar{n} + \Delta q(nu)$ in terms of the old chief ray and the marginal ray that is not changed, so that $\bar{A}^* = \bar{A} + \Delta q A$, with $\Delta q = \bar{h}_p^*/h_p$ in the “old” pupil.

Inserting this in (3.15) and (3.16) we find the *stop shift equations*.

$$\begin{aligned}
 S_1^* &= S_1, \\
 S_2^* &= S_2 + \Delta q S_1, \\
 S_3^* &= S_3 + 2\Delta q S_2 + \Delta q^2 S_1, \\
 S_4^* &= S_4, \\
 S_5^* &= S_5 + \Delta q(3S_3 + S_4) + 3(\Delta q)^2 S_2 + (\Delta q)^3 S_1, \\
 C_1^* &= C_1, \\
 C_2^* &= C_2 + \Delta q C_1,
 \end{aligned} \tag{3.24}$$

where a star denotes the coefficients for the new stop position, and Δq is the increment of the *q-factor* $q = \frac{\bar{h}}{h}$.

For a surface or a thin lens at the stop we have $\bar{h} = 0$ and so $q = 0$.

In terms of the shift of entrance pupil Δt we have from Fig. 3.17

$$\Delta q = \frac{\bar{h}_0}{h_p} \cdot \frac{\Delta t}{t + \Delta t}. \quad (3.25)$$

This value is equal for all surfaces in the system.

Applications of the stop shift equations are:

- calculation of the aberrations of a surface or a thin lens when those at the stop are known; this is specially important with thin lens calculations, see Sect. 4.3,
- correcting coma and astigmatism for two-component systems such as Petzval or telephoto lenses,
- correction of systems with a given stop, such as oculars.

3.5 Zero Seidel Conditions

There are a number of cases where some of the Seidel coefficients have a zero value. These cases follow from (3.15) and (3.16) of this chapter.

1. $A = 0$

This means that the incidence angle of the marginal ray is equal to zero. The object is conjugate to the center of curvature. We now have that

$$S_1 = S_2 = 0 \text{ and } C_1 = 0.$$

No spherical, coma and LCA. See Fig. 3.18a.

2. $\bar{A} = 0$

This means that the incidence angle of the chief ray is zero. The stop is conjugate to the center of curvature of this surface. We now have that

$$S_2 = S_3 = S_5 = 0 \text{ and } C_2 = 0.$$

No coma, astigmatism, distortion and TCA. See Fig. 3.18b.

3. $h = 0$

The object is conjugate to the vertex of this surface.

$$S_1 = S_2 = S_3 = 0 \text{ and } C_1 = C_2 = 0.$$

No spherical, coma or astigmatism. Also LCA and TCA are zero. See Fig. 3.18c.

4. $c = 0$

The surface is plane.

$$S_4 = 0$$

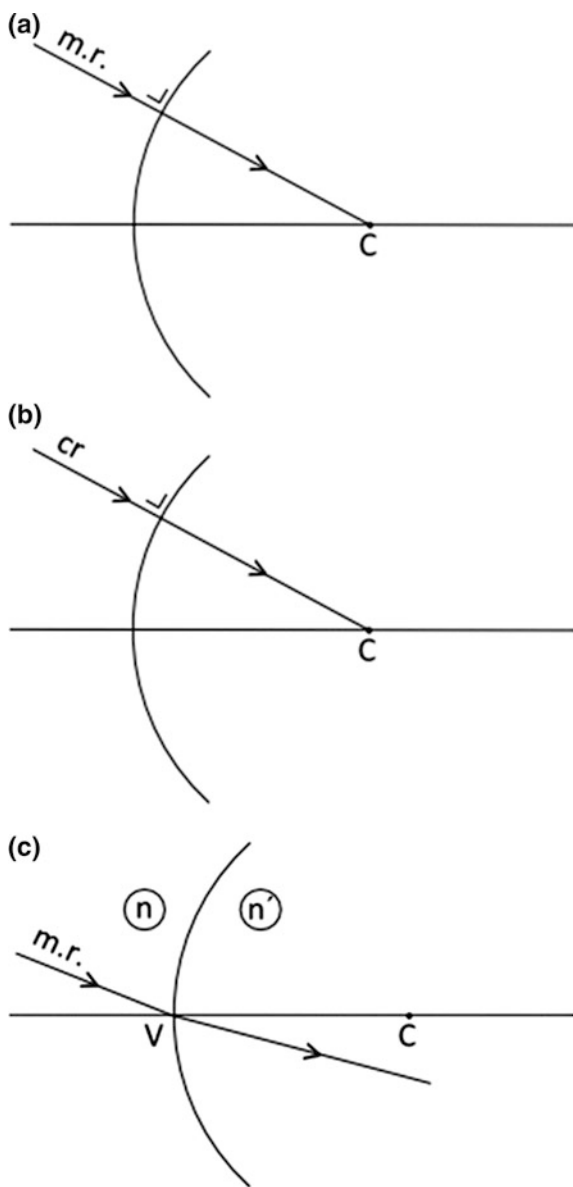
There is no field curvature. This is the only case for which the surface contribution to field curvature becomes zero.

Fig. 3.18 a A = 0, marginal ray at perpendicular incidence, C is conjugate to the center of the object.

b $\bar{A} = 0$, chief ray at perpendicular incidence, C is conjugate to the stop center.

c $h = 0$ for the marginal ray,

V is conjugate to the object center



$$5. \Delta\left(\frac{u}{n}\right) = 0$$

According to (3.15) we have

$$S_1 = S_2 = S_3 = 0$$

A surface in this condition is called *aplanatic*. This occurs when the surface is spherical and the object distance is $s = r(1 + n'/n)$. See Fig. 3.19.

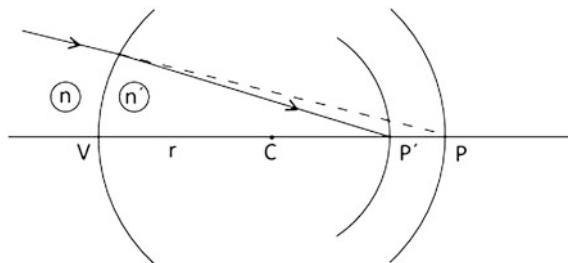


Fig. 3.19 $CP = \frac{n'}{n}r$, $CP' = \frac{n}{n'}r$, aplanatic surface, construction of Huygens

From the symmetry of the situation follows that a sphere around C with radius $n'r/n$ is imaged stigmatically on a sphere with radius nr/n' . The magnification is $M = s'n/sn' = n^2/n'^2$. From Lagrange's invariant follows that $u'/u = n'/n$.

The zero Seidel conditions should always be in the mind of a designer. Conditions 1 and 5 are applied in the design of microscope objectives. Condition 2 is active in concentric optical systems. Condition 3 and 4 are used in the correction of field curvature.

The importance of this subject is stressed by Kidger [2].

References

1. W.T. Welford, *Aberrations of Optical Systems*. (Taylor and Francis, London, 1986)
2. M. Kidger, *Fundamental Optical Design*. (SPIE Press, Bellingham, 2001)

Chapter 4

Lens Design Process

In this chapter we describe a systematic way of doing lens design. We show what to do first, how to proceed and reach the goal: a design that can lead to the production of a useful lens.

In Fig. 4.1 the phases of the lens design process are summed up in a flow diagram.

In the specification phase the type of lens to be designed is determined. In Sect. 4.1 we give an overview of the lens types that are treated in this book. This collection is far from complete; the choice was made in order to cover a representative selection of the problems that are met in the practice of lens design.

In this course we pay much attention to lay-out and thin lens predesign. When these phases are skipped, so that a starting system must be taken from the (patent) literature, or from the experience of the designer, the result of optimization may be disappointing. For an expert this may be feasible, but the non-expert can profit from the insights in the properties of the lens to be designed that can be obtained in these phases.

In the next phase a surface model is prepared, of which the aberration coefficients are calculated. The thin lenses are given thickness, while care is taken to preserve the paraxial properties of the predesign (and the colour correction). The surface contributions to the Seidel aberrations can be used to decide which parameters will be used as variables in the optimization phase.

The optimization phase is used to bring the design to the performance level that was indicated in the specification. The topic of optimization is discussed in Sect. 4.5; in this course the influence of optimization software is not so great as in most of the literature on lens design.

The optimized design must be prepared for production in the tolerancing phase. The sensitivity of the design for fabrication errors is calculated and the resulting degradation in the performance of the lens is estimated. In Sect. 4.6 a method is sketched to do this efficiently.

Because this course is concerned with lens design in the restricted sense of providing a prescription of the optical components, opto-mechanical aspects of lens design and optical fabrication technologies (including metrology) are not included.

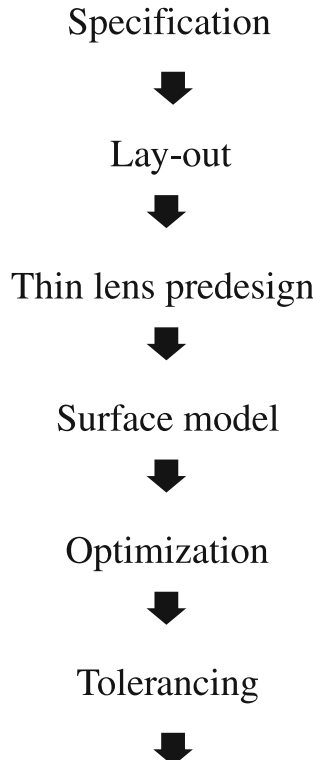


Fig. 4.1 Flow diagram of the lens design process

The arrow at the bottom of Fig. 4.1 is meant to remind the reader of this omission. In the books of Fischer [1] and Smith [2] these aspects are well considered.

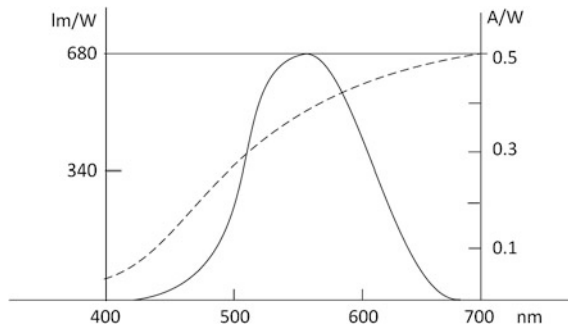
4.1 Specification

In the first phase of lens design we try to answer the question: what is the application for which we have to design a lens and what type of lens will fit to the application?

As we are concerned in this course with imaging applications we have to specify in the first place:

- the type and size of the object
- the spectrum and illuminance (irradiance) of the light used
- the size and sensitivity of the detector.

Fig. 4.2 Spectral sensitivity of a human eye (drawn curve) and a Si-detector (broken curve)



The object may be transparent or reflective; it may scatter light or act as a mirror. It may have details with high or low contrast. The details may be fine or coarse.

The object is far away (landscape, architecture) or just very near (under the microscope).

There is always a relation between the size of the object and the fineness of its details. This can be formulated as a limit on the number of image elements (“pixels”). So that a microscope has a small object field at the limit of resolution and a camera a great number of pixels (of the order of 10^7), corresponding to a larger field of view, at a moderate level of resolution.

There is a great difference in requirements between instruments for visual use and instruments with an electronic detector. We show the spectral sensitivity of the human eye and of a Si-detector in Fig. 4.2. Note the difference in scale between the two graphs, the units for the human eye are lumen/watt and for the detector ampere/watt.

The angular resolution of the human eye does not exceed a few tenths of a milliradian.

A CCD-camera with 10^7 pixels of $5 \mu\text{m}$, and a field angle of 20° will have an angular resolution limit of 0.11 mrad. It will depend on the camera lens how nearly this limit is approached.

The specification of the application of the lens to be designed will result in a number of paraxial parameters of the lens. For lenses with finite conjugates, such as a microscope objective, the most important parameters are

- field diameter
- aperture angle, or numerical aperture
- magnification
- distance from lens to object (working distance)
- distance from lens to image (tube length)
- length and diameter of the objective.

For instruments with the object at infinity, such as camera lenses, the paraxial parameters to specify are

- focal length
- back focal length (working distance)
- F-number
- field angle.

Oculars for telescopes and microscopes are treated as lenses with the object at infinity. We specify the focal length, the field angle, the diameter of the exit pupil and the eye relief.

In the specification phase we also have to describe the image quality that we expect from our design.

Important descriptors are

- resolution (periods per mm) as a function of field radius and defocus,
- contrast, in relation to detector noise,
- depth of focus,
- tolerances on field curvature and distortion,
- tolerances on shading.

With shading, inhomogeneity of illumination is meant; this is an important parameter in projection and inspection applications.

In the same group of applications telecentricity is often required (see Sect. 1.4). Also in lenses used in metrology applications telecentricity is recommendable.

In instruments for visual use aberrations of asymmetric character must be well corrected (coma, distortion and TCA), because the eye is very sensitive to asymmetries.

In infrared optics the contrast in the object is usually quite low; this merits extra attention in the design of optical systems. Also the wavelengths can be much larger than in the visible range ($10 \mu\text{m}$ at 300 K) so that diffraction phenomena are more prominent.

Finally the environment must be specified in which the lens will be used. The following factors can be mentioned

- physical, such as air temperature, -pressure and -humidity, shocks, vibrations, dust, (solar) radiation etc.; with space instrumentation size and weight are bound to limits,
- chemical (reactants, such as in sea water),
- biological (fungi),
- economical: cost, market price, batch size, delivery date, packaging and transport.

Our discussion of specification does not aim at completeness. The books of Fischer et al. [1, p. 9], Smith [2, pp. 3, 4] and Shannon [3, p. 5] contain more material. It is recommended to copy this and use it as a checklist.

4.1.1 Transmission of Lenses

Lenses do two things that are not intended: they reflect and absorb part of the light.

The losses by reflection are 4–5 % per uncoated surface. Before anti-reflection coatings were invented this was a problem; designers had to minimize the number of glass to air surfaces, which made the correction of aberrations more difficult. With anti-reflection coatings the loss per surface can be reduced to 1 % or less over most of the visible spectrum.

Loss of light is not the only problem; after an even number of reflections the light propagates again in the direction of the image plane. False reflections that reach the image plane can cause false images or a general loss of contrast (“glare”).

Optical glass has a good transmission for visible light. Some flint glasses look yellowish in thick layers; this is due to absorption on the blue side of the spectrum. In the near UV and the middle IR strong absorption occurs; this limits the number of materials that can be used in optical systems for those wavelengths.

4.1.2 Lens Types

To denote the type of a lens, we will use the typology of Kross et al. [4]. This classification departs from the number of components of the system, as fixed in the lay-out. A component can be a single lens, a thin doublet or triplet, or a more complicated group. The sign of the power of the component is denoted P or N.

For instance a Tessar has the classification PNP, a telephoto objective has PN, whereas a Petzval lens has PP.

A further refinement is made by denoting the lenses in a component by a lower case p or n. The Tessar becomes PN_pn, a split triplet ppPNP.

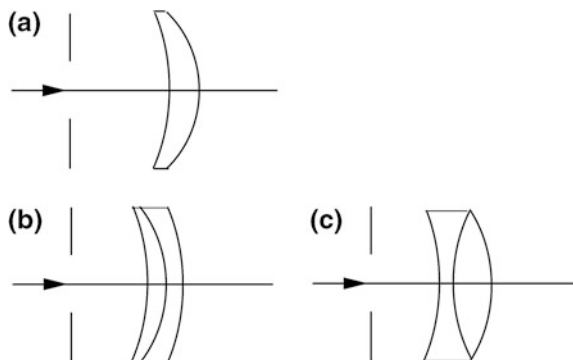
After specification of the properties of the system to be designed follows the choice of the type of lens that looks promising to fulfil the specifications.

We discuss four groups of lenses:

- camera lenses, this is the group with the largest number of different design forms, because the application are the most diverse; in the same group we also discuss a few projection lenses;
- telescope objectives, this group is divided into refractors (lenses) and reflectors (mirror systems);
- micro-objectives, a group that comprises three subgroups: microscope objectives, objectives for optical recording and projection lenses for opto-lithography (“stepper lenses”);
- oculars for telescopes and microscopes.

We will use different descriptors for each group, corresponding to the different applications.

Fig. 4.3 a Wollaston,
b Grubb, c Chevalier



4.1.3 Camera Lenses

The most important items in the specification of camera lenses are: the F-number, the field angle and the image quality. The F-number expresses the “speed” of the system; we gave its definition in Sect. 2.1. The field angle is usually given as the object field angle w or the *full field angle* $2w$. The image quality can be described in many ways. In Sect. 4.7 we will define the *modulation transfer function* and discuss its uses. In this section we will only give an estimate of the resolution (in periods per mm) on axis and its homogeneity in the field.

We discuss a selection of lens types that spans a history of about two hundred years of lens design.

Lenses that are used as design examples in this book are denoted by an asterisk*.

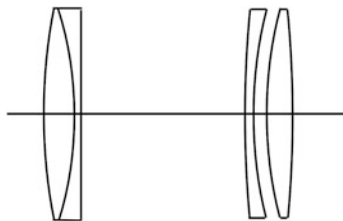
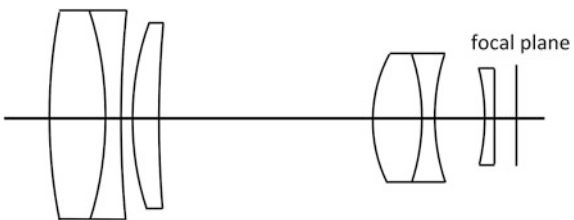
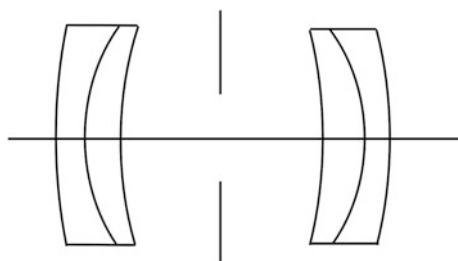
We begin with the Landscape Lens* (Wollaston 1812), in its original form a single lens with a remote stop. There are two models, with the stop in front or behind the lens. In Fig. 4.3a we show this first form.

Because this lens has uncorrected spherical aberration, its F-number is large, F/15 typically. The resolution is moderate, about 15 p/mm on axis and 10 p/mm in the field over a field of $2w = 30\text{--}40^\circ$ with a focal length of $f' = 100$ mm.

The single lens cannot be corrected for colour; Chevalier (1840) and Grubb (1857) improved this type by replacing the lens with a doublet, see Fig. 4.3c, b.

In the same period, and as a competitor to Chevalier, Petzval designed his portrait lens (1840). The type is still known as *Petzval lens**, we show the original version in Fig. 4.4. It consists of two doublets, of which the second has an airspace.

It is clear from Fig. 4.4 that the aperture is much larger, F/3.4 in the original design, over a field of $2w = 32^\circ$. The correction is excellent on axis, with a resolution of 25 p/mm, but much worse in the field. A modern application of the Petzval type is as a projection lens, we show the *Projection Ektar* of Schade (1948), that has a focal length of 56 mm, a field of 16 mm and an aperture of F/1.5. The resolution is 90 p/mm over the entire field. See Fig. 4.5.

Fig. 4.4 Petzval lens**Fig. 4.5** Ektar lens**Fig. 4.6** Dallmeyer's Rapid Rectilinear lens

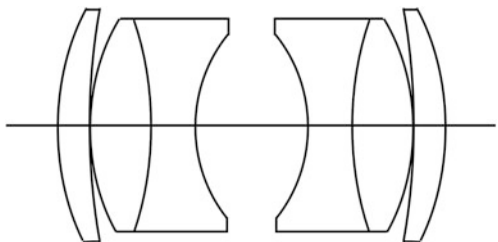
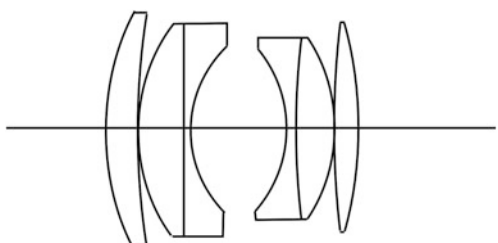
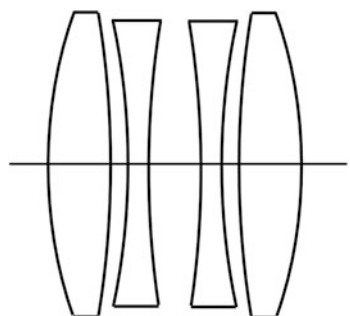
The correction of field aberrations (astigmatism, distortion) can be improved by two methods: making the distances between the components larger, and making the lens (more) symmetric. An early example is Dallmeyer's *Rapid Rectilinear* lens (1866), shown in Fig. 4.6.

This lens was preceded by Steinheil's Periskop (1862), but it had a better overall image quality. With a field of $2w = 50^\circ$ and an aperture of F/8 the Rapid Rectilinear has excellent correction of coma, distortion and lateral colour (TCA), made possible by the symmetry of the design. The meridional field curvature is well corrected, there is a rest of sagittal field curvature. The resolution is uniform over the field at about 20 p/mm.

This type of lens was developed further by Rudolph (Protar 1890) and von Hoegh (Dagor 1893).

Zeiss took a patent on Rudolph's *Planar** in 1896; it is shown in Fig. 4.7.

In comparison to the Rapid Rectilinear it has two components more. The thick doublets of the Planar have “buried surfaces”, where the refractive index step is small and the difference in V-number moderate. This results in a typical strong

Fig. 4.7 Planar lens**Fig. 4.8** Double Gauss**Fig. 4.9** Celor

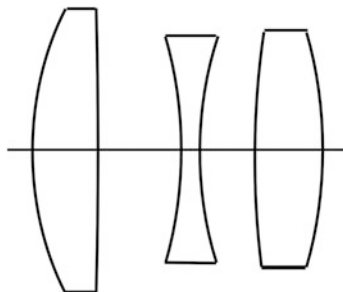
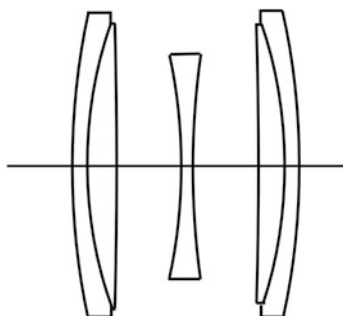
curvature of the inner surfaces that form a negative “air lens”. The aperture of the original Planar was F/4.5, the full field 40°, the resolution about 30 p/mm in the center of the field.

The Planar can be considered, according to Kidger [5, Chap. 4] as the prototype of the *Double Gauss** objective. The first step in this development was made by H. W. Lee (Opic 1920), who improved the aperture to F/2 with comparable image quality. A well-known modern Double-Gauss design is that of Mandler (1955), see Fig. 4.8.

With $f = 50$ mm, speed F/2, full field 44°, it has a uniform resolution of 30 p/mm.

The symmetric lens type was further developed by von Hoegh with the *Celor** (1897), shown in Fig. 4.9. With a focal length of 100 mm and an aperture F/5 it has a field of $2w = 60^\circ$.

Hoegh's Celor is completely symmetric; because the distances between its four elements are rather high it has a good correction for astigmatism. The “uneven”

Fig. 4.10 Triplet**Fig. 4.11** Heliar

aberrations (coma, distortion and TCA) can be corrected easily by a modest asymmetry. In a later model F/3.5 was obtained.

When the inner lenses of the Celor are combined into one negative lens (at or near the stop) we have a triplet. The *Cooke Triplet** (1895) was designed by H. D. Taylor, who followed a method of analytical design of which we also make use in this book (see [Sect. 4.3](#)). The Cooke Triplet is shown in Fig. 4.10.

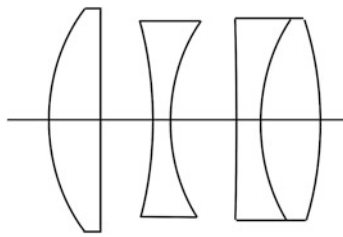
When the glasses of the Triplet have been chosen, we have five degrees of freedom left in the lay-out: three powers and two distances. That means that we can fix the system power and the Petzval sum (field curvature), correct longitudinal and transverse colour and most of distortion.

Triplets are near-symmetric systems, with the stop usually near to the middle lens. The forms of the three lenses provide three degrees of freedom more, that serve in the correction of spherical aberration, coma and astigmatism.

Triplets can take many different forms, leading to systems with high resolution and a narrow field (projection lenses or reproduction objectives) or systems with a wider field and a lower, but more uniform, resolution. Field angles from 10° to 35° , F# between 12 and 3.

There are many variants of the triplet, with extra lenses and with doublets. In [Sect. 6.4](#) we design a splitted triplet*. We also discuss the *Elmar** and the *Elmax**, lenses that were designed by Berek (1924) for the small “Leica” camera.

We show the *Heliar** (1902) by Harting in Fig. 4.11.

Fig. 4.12 Tessar

The *Tessar** (Rudolph 1901) was not developed as a *triplet* derivative, but rather as a simplified Protar. It is shown in Fig. 4.12. Because of its form the Tessar is usually assigned to the *triplet* family.

The *telephoto lens** consists of a positive first component and a negative second one. Its focal length is larger than the distance from its first surface to its focal plane. This lens can be corrected for field curvature easily, whereas distortion is more difficult to correct. We show a telephoto lens in Fig. 4.13. In Sect. 6.3 we discuss the design of several forms of this type.

A reversed tele-objective can be used as a *wide-angle** lens. This type has an enhanced back focal length, so that it can be used in a single lens reflex (SLR) camera. An example is shown in Fig. 4.14. This lens has a full field of 70° , aperture F/2.8, a resolution of 150 p/mm on axis and 40 p/mm in the field. It is sometimes called a retrofocus lens.

The wide angle lens can again be improved by making it symmetric. As examples of (nearly) symmetric wide-angle lenses we mention here the Angulon of Bertele (1951) and the Hologon of Glatzel (1966). The Angulon is shown in Fig. 4.15.

It has a full field of 75° , aperture F/5.6 and a resolution of 30 p/mm over most of the field. In Sect. 6.5 we discuss the Hologon and the design of a symmetric wide-angle lens.

4.1.4 Telescope Objectives

The lens system used as telescope objectives will be discussed first. The usual telescope objective is a doublet, that may have an airspace for aplanatic correction. A selection of doublets is shown in Fig. 4.16. With telescopes for terrestrial use cemented doublets are usually applied.

Telescope lenses will have a small field ($w \approx 3^\circ$) and a modest aperture (F/5). Resolution is expressed in angle units; with a visual telescope the resolution in the center of the field should be about $1/M$ min of arc, where M is the magnification of the telescope (see Sect. 2.4). The design of a telescope doublet is treated in Sect. 6.2.

In astronomical applications sometimes refractive objectives are used. When the object is characterized by low contrast and subtle shades of colour, such as in

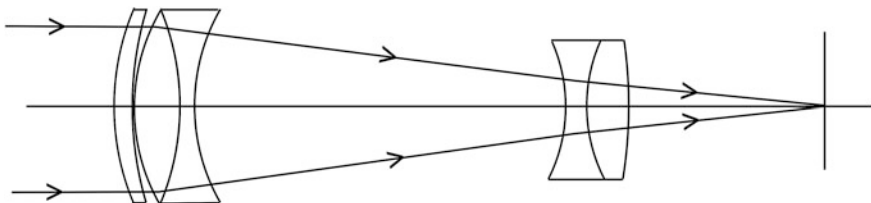
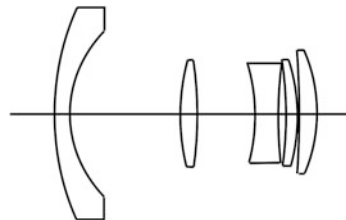
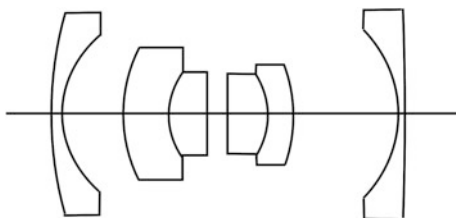
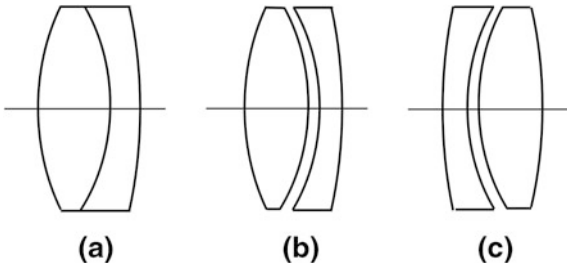
**Fig. 4.13** Tele-photo lens**Fig. 4.14** Retrofocus lens**Fig. 4.15** Angulon

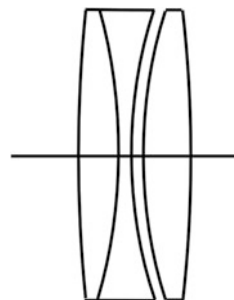
Fig. 4.16 Doublets:
a cemented,
b Fraunhofer,
c Steinheil



In the photography of planets and nebulae, the objective will be an apochromatic thin triplet. This type uses special glasses for an optimum colour correction. We show an apochromatic triplet in Fig. 4.17.

Astronomical telescopes usually have a reflective objective, often supported by refractive correction elements. When only mirrors are used, colour correction is not necessary.

Fig. 4.17 Apochromatic thin triplet



Newton's telescope (1668), shown in Fig. 4.18, uses a paraboloid objective and a flat mirror to reflect the light towards the ocular.

The image of a paraboloid is perfect on axis, but suffers from coma in the field. Therefore the field is limited to about 10 min of arc at an aperture angle of about $u' = 5^\circ$.

By the use of a secondary mirror, also aspheric, the correction can be improved. We will discuss this topic further in Sect. 6.7 and show only, in Fig. 4.19, the Cassegrain reflector.

With a paraboloid primary and a hyperboloid secondary mirror, this objective has a field of about 1° at an aperture of F/5.

Concentric systems have all surfaces centered in one point, where also the aperture stop is located. Such systems have, from symmetry, only spherical aberration and a curved image surface. The camera objective of Schmidt (1930), shown in Fig. 4.20, can have a field angle of 6° at an aperture of F/3. It has an aspheric corrector plate at the stop; we discuss this design in Sect. 6.7.

The angular resolution of astronomical objectives is usually perfect on axis. It is then given by

$$\delta\bar{u} = 0.6\lambda/f \sin u' \quad (4.1)$$

where λ is the wavelength, f the focal length and u' the aperture angle.

With $\lambda = 0.5 \mu\text{m}$, $f = 1 \text{ m}$ and $u = 0.1$ we have $\delta\bar{u} = 3 \cdot 10^{-6} \text{ rad}$, equivalent to 0.6 arcsecond.

Equation (4.1) will be derived in Sect. 4.7.

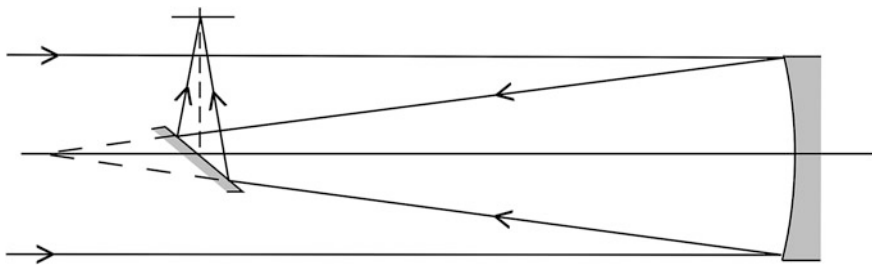


Fig. 4.18 Newton's telescope

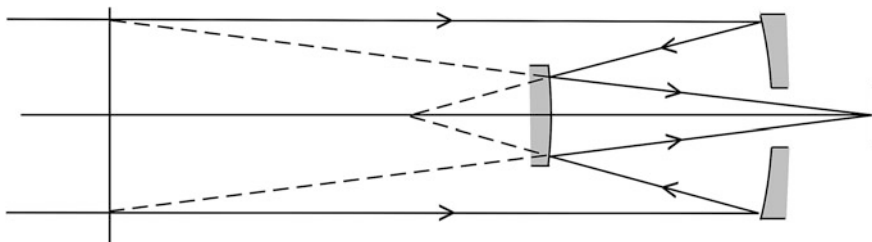


Fig. 4.19 Cassegrain reflector

Fig. 4.20 Schmidt objective

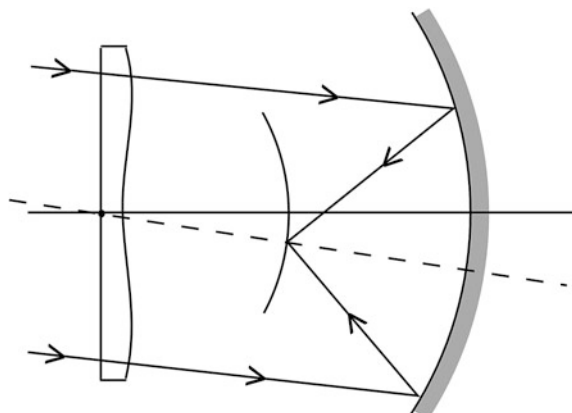
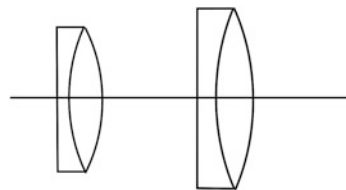
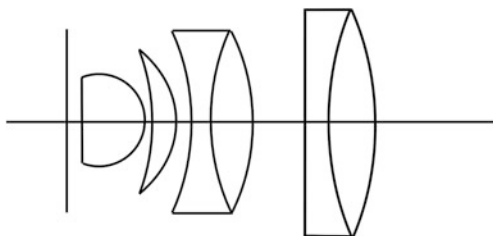


Fig. 4.21 Lister objective**Fig. 4.22** Amici objective

4.1.5 Micro-Objectives

The resolution of a microscope objective has a lower limit, given by (see Sect. 4.7)

$$\delta\eta = 0.6\lambda/\text{nsin } u \quad (4.2)$$

The quantity $\text{nsin } u$ is called the numerical aperture (NA). For instance with an immersion microscope with an NA of 1.2 we have $\delta\eta = 0.5\lambda$, about 0.2 μm in blue light.

Field angles of microscope objectives are small, about 2–3°. The diameter of the object field is $2\eta = 2wf$, where f is the focal length. The relation between focal length and magnification is given by

$$M = -\left(1 + \frac{t}{f'}\right) \quad (4.3)$$

where t is the tubus length (between 160 and 200 mm). An 10× objective with a tubus length $t = 180$ mm will have a focal length $f' = 20$ mm. The diameter of the object field will be about 2 mm (with $w = 3^\circ$).

The simplest microscope objectives, that are most frequently used, consist of two doublets in tandem, see Fig. 4.21. This type was greatly improved by Lister (1786–1869), as discussed in Sect. 6.6.

The Lister-type objectives can have a magnification of 10×, at an NA of 0.2.

A 20× objective can be obtained by adding to the Lister objective an aplanatic front lens, according to Amici (1786–1863). With a focal length of about 9.5 mm ($t = 180$ mm) and a field angle of 3° the field diameter will be about 1 mm. Numerical apertures range between 0.4 and 0.5.

Adding another aplanatic lens results in a 40× objective with a focal length of 4.4 mm and an NA of 0.6–0.7 (without immersion). Such an objective is shown in Fig. 4.22.

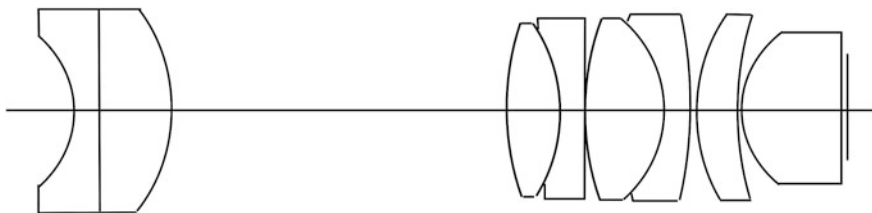
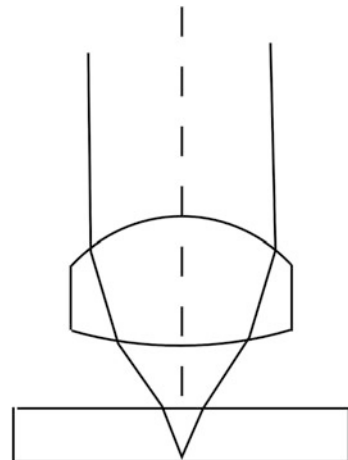


Fig. 4.23 Plan-apochromat

Fig. 4.24 Optical disk objective, after Broome [6]



The Lister-Amici line of objectives has *achromatic* correction, which means that the image distance is the same for red and blue light. The “green” rays will have a relative focusing error of about 0.2 %. The aberration correction will be good in the centre of the field, but there is always a quite serious field curvature, and astigmatism, distortion and lateral colour cannot be corrected.

This is not a great problem with visual use of the microscope, but with a solid-state detector we would prefer a flat, well corrected image field.

When we correct both field aberrations and secondary spectrum we obtain a *plan-apochromatic* objective. We show an example in Fig. 4.23. It has a focal length of 3 mm and a paraxial NA of 0.7.

The design of the microscope objectives mentioned in this paragraph is treated in Sect. 6.6.

A review of microscope objective designs has been given by Broome [6]. He points out that the objectives that are used in optical disk players are related to the microscope objectives that he describes. The design form chosen most frequently for optical disk objectives is a single lens with one or two aspheric surfaces. The numerical aperture is between 0.45 and 0.55 and the field smaller than 0.2 mm. The objective is mostly used in tandem with a collimator, to focus the beam of a diode laser on the back side of the optical disk. The diameter of the spot is about 1 μm . The lens and the disk should form an aplanatic system. In Fig. 4.24 we show such a design, from Broome’s chapter.

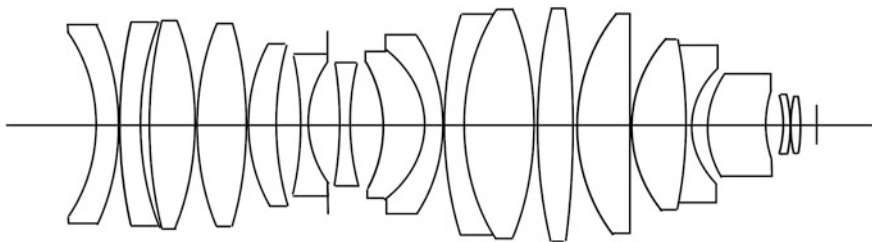
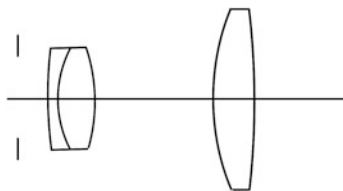


Fig. 4.25 Stepper lens, Williamson

Fig. 4.26 Kellner ocular



The “stepper lenses” that are used as projection systems in photolithography can be considered as offspring from flat-field microscope objectives. Especially the Zeiss S-Planar objective, designed by Glatzel [7] was crucial for this development.

We show a $5\times$ reduction lens, designed by Williamson [8], in Fig. 4.25.

It has an NA of 0.42, uses the mercury I-line (366.5 nm) for exposure and has a field diameter of 24 mm. Its resolution is about 0.5 μm , the wavefront errors are smaller than $\lambda/4$ over the whole field, distortion is smaller than 50 nm. These performance parameters are orders of magnitude better than those of the microscope objectives discussed above. The design of such complicated systems as stepper lenses exceeds the scope of this book.

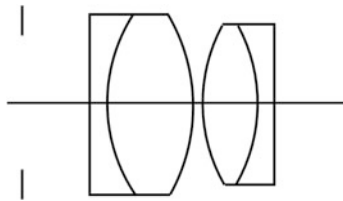
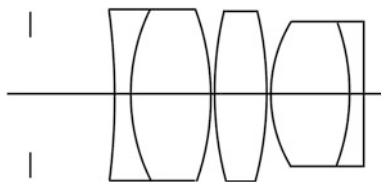
4.1.6 Oculars

The historic Huygens (1661) and Ramsden (1782) oculars follow the principle that a two-component system can be corrected for colour if the distance between the components is given by:

$$d = \frac{1}{2}(f_1 + f_2) \quad (4.4)$$

and the two components are made from the same material. We derive (4.4) and show the layout of these oculars in Sect. 5.1.

The *Kellner ocular* (1849), shown in Fig. 4.26, is the first modern eyepiece, with a better correction of colour and coma than the Ramsden, which it resembles.

Fig. 4.27 Plössl ocular**Fig. 4.28** Erfle ocular

It has a field angle of 25° and an eye relief of about $0.5f$, where f is its focal length (25 mm for a $10\times$ ocular). The design of a Kellner is treated in [Sect. 6.2](#).

The *Plössl ocular* (1860), also called symmetrical ocular, is composed from two cemented doublets. Many variants of this ocular are found in the literature, all more or less symmetrical. It has a larger eye-relief than the Kellner, up to $0.8f$, and a larger field angle, about 30° . We show a Plössl ocular in Fig. 4.27; it is the subject of a design exercise in [Sect. 6.2](#).

The Erfle ocular (1917) was designed as a wide field ocular for military purposes. It can be considered as a further development of the Plössl, by adding an extra lens. We show the original version in Fig. 4.28.

The field angle of an Erfle ocular can be larger than 40° .

We give an overview of the lenses discussed in this paragraph, with field angle (w) and aperture ($n \sin u$, F) as parameters in Fig. 4.29. Modern camera lenses are situated roughly along the curve denoted “camera lenses”. Microscope objectives, where only the numerical aperture varies greatly, along the line on the left. Telescope objectives occupy the region T, with the classical telescopes in the bottom, Schmidt systems in the top and objectives with corrector components in between. Oculars are found in the region O, with classical microscope oculars on the left and military telescope oculars on the right.

4.2 Lay-out

Lay-out is the paraxial phase of lens design. We start this phase by choosing the lens type that is best suited to the specifications. The most important parameters in this choice are aperture and field angle. A survey of lens types characterized by their field angle and numerical aperture was given in [Sect. 4.1](#).

After the choice of lens type we determine the powers and distances of the components, that we represent by thin lenses. With the more complicated designs,

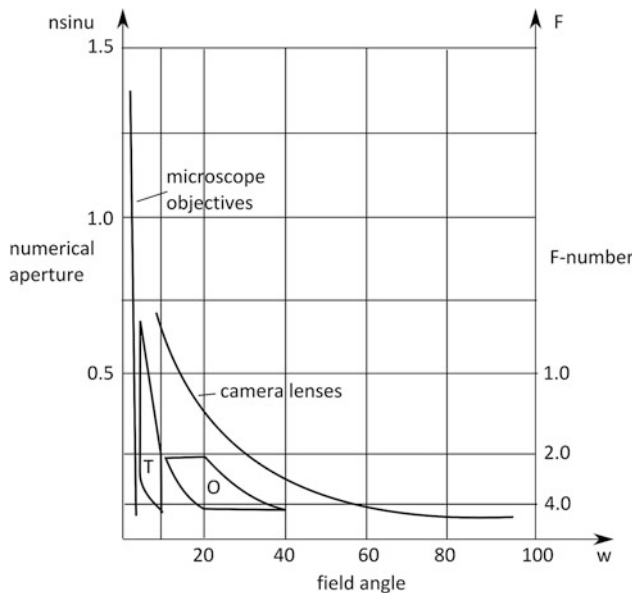


Fig. 4.29 Overview of lens types, T stands for telescope objectives, O denotes oculars

such as the design of zoom lenses, this can lead to a lot of algebra. The examples treated in this section are straight forward.

Also the primary chromatic aberrations are corrected in the lay-out, paraxial phase; these can be treated in the paraxial approximation.

We leave the third and higher order aberrations aside in the lay-out, with one exception: the field curvature. This has two reasons; the most important reason is that field curvature is difficult to correct in later phases of the design. Fortunately its coefficient (S_4) can be calculated simply, so that we can keep a check on it. Field curvature is independent of the form and position of components, and also of the position of the stop. The second reason to consider field curvature in the lay-out, paraxial phase of design is that it can be influenced by the component powers and by the choice of materials (glass, plastic, crystal). This choice also determines the correction of the chromatic aberrations. The correction of field curvature is therefore connected to the correction of chromatic aberrations (TCA and LCA).

4.2.1 Scale Factor

The focal length acts as the scale factor for the system to be designed. This scale factor depends on the application for which the system is intended.

In this course we take in many cases a focal length of 100 mm. In the literature this is a common value for the focal length of photographic objectives. In practice the focal length of photographic objectives will be adapted to the format of the detector (in the past photographic plates or film, nowadays mostly an electronic detector).

With telescope objectives the focal length depends on the magnification. The focal length of oculars have standard values of 50 (5 \times), 25 (10 \times), 12.5 (20 \times) mm. With a 10 \times ocular and a magnification $M = 10$ we have a focal length of the objective $f_{ob} = 250$ mm.

With microscope objectives the image distance is more or less standard, so that the focal length depends on the object magnification. Modern microscope objectives often have the object plane in their front focal plane, so that a tubus lens is necessary to form the image at a finite distance. The magnification is given by:

$$M = f_t/f_0$$

where f_t is the focal length of the tubus lens and f_0 the focal length of the objective.

With $f_t = 200$ mm and $M = 20$ we must have $f_0 = 10$ mm.

Some authors [9–11] normalize all dimensions in a system with respect to its focal length. This has the advantage that different designs can be compared more easily. On the other hand, theoretical derivations become more difficult to follow because the dimensions of the quantities involved are not clear. In this course we use the millimeter as unit throughout (sometimes we revert to μm 's).

A lay-out equation that we will use often is the *scale equation*, (1.29)

$$K = \sum_{i=1}^k \frac{h_i}{h_i} K_i, \quad u_i = 0 \quad (4.5)$$

where K is the system power, K_i are the component powers, h_i are the ray heights of a ray parallel to the axis.

When a system is scaled by a factor p , all radii, distances and also the focal length will be multiplied by p . All angles (aperture and field angles and incidence angles) will remain the same. Also the wavelengths of light remain the same, so that the diffraction limit of resolution (see Sect. 4.7) is invariant in a scale transformation. But the aberrations will grow in proportion as well, so that bigger systems can be brought to the limit of resolution more difficultly than smaller ones.

Stepper lenses of 1,000 mm long are therefore much more complicated than microscope objectives of 10 mm with the same numerical aperture.

4.2.2 Field Curvature

When the astigmatism of a system is corrected, the curvature (the reciprocal radius) of the image surface that touches the paraxial image plane in the axial point, is given by the Petzval sum P

For a thin lens system

$$P = \sum_{i=1}^k K_i/n_i \quad (4.6)$$

We will use this formula in the lay-out, it points out from the beginning which possibilities or problems one will have in obtaining a satisfactory flatness of the image surface.

With telescopes and classical microscopes, with which one uses only a small part of the image plane around the axis for accurate viewing, one aims at a value of P smaller than K .

When an electronic detector, such as a CCD, is used to record the image, the tolerance for field curvature is much narrower. This is also the case with objectives in photo-lithography (“stepper lenses”) that are used at high numerical aperture over a field of 30 mm diameter. There, with a projection wavelength of 248 nm, the focus tolerance is less than 1 μm and field curvature is not tolerated at all [12].

With simple photographic objectives, such as triplets and their variants, one tries to remain below 0.4 K. More sophisticated photographic lenses mostly have Petzval sums below 0.2 K. Still smaller values are found with wide-field objectives. There one takes occasionally a zero Petzval sum as the starting point of the calculations [13].

4.2.3 Distortion

Distortion is, as we have seen in Sect. 3.3, an aberration of the chief ray. A condition for the correction of distortion can be found by requiring that the total deviation of the chief ray is zero.

When an optical system is symmetric with regard to the stop plane, this condition is automatically fulfilled. Systems with small deviations from this symmetry can be easily corrected for distortion.

In a triplet with the stop at the central lens (see Fig. 4.30) this condition can be written

$$d_1 K_1 = d_2 K_3 \quad (4.7)$$

We will use this equation in the lay-out of triplets and triplet variants.

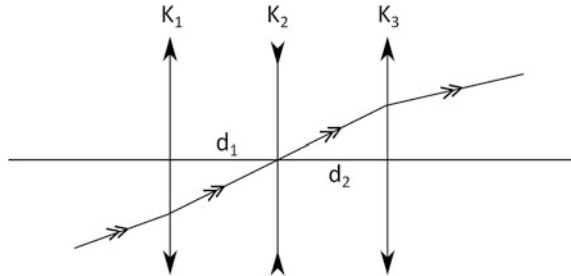
4.2.4 Axial Colour Correction

The basic condition for a stable image position along the optical axis for two different wavelengths can be written for a thin lens system,

$$C_1 = \sum_1^k h_i^2 K_i / V_i = h_1^2 K / V_s \quad (4.8)$$

where h_i is the ray height of the marginal ray and

Fig. 4.30 Notation for (4.7), triplet with stop at the second lens



$$1/V_i = \delta n_i / (n_i - 1)$$

where δn_i is the difference of n_i for two wavelengths,

$$\delta n_i = n_i(\lambda_1) - n_i(\lambda_2), \quad \lambda_1 < \lambda_2$$

and n_i is taken for a wavelength between λ_1 and λ_2 . Customarily the choice for a wavelength is $\lambda_1 = 486$ nm, the F-line of hydrogen, $\lambda_2 = 656$ nm, the C-line of hydrogen, and the third wavelength $\lambda_d = 588$ nm, the d-line of helium. The quantity

$$V = \frac{(n_d - 1)}{(n_F - n_C)} \quad (4.9)$$

is called Abbe's number.

The number V_s in (4.4) is a measure of the correction of axial colour. A value given by experience can be found for each type of optical system. With telescope objectives V_s should be of the order of 1,000, with photo-objectives from 200 to 500.

A system designed so that V_s is large enough is called an achromat. Such a system has an equal power for two wavelengths, usually the C- and F-lines.

For the d-line the power has a different value, the difference is called *secondary spectrum*.

When we define a *partial dispersion*

$$P_d = \frac{(n_F - n_d)}{(n_F - n_C)} \quad (4.10)$$

the secondary spectrum is given by

$$\delta K^{(2)} = \frac{K P_d}{V} = K(n_F - n_d)$$

A system that is corrected for secondary spectrum is called an apochromat.

In this course we do not treat the design of apochromats in detail. A clear and simple treatment of thin apochromats is given by Shannon [3, pp. 189–191]. See also Mercado [14].

4.2.5 Lateral Colour Correction

With a thin lens system, we have

$$C_2 = \sum_1^k h_i \bar{h}_i K_i / V_i \quad (4.11)$$

where \bar{h}_i is the ray height of the chief ray.

When the system is symmetric, with the stop in the middle, the values of \bar{h}_i for corresponding components on different sides of the stop will be opposite. This will make the correction of TCA easier for such a system.

In the case of a triplet, with the stop near the middle lens, we can find from the lay-out equations the simple condition

$$h_3/h_1 = V_3/V_1 \quad (4.12)$$

when (4.7) is also valid. This corrects lateral colour in the triplet.

Thin systems are not sensitive for lateral colour.

With systems with sizeable axial dimensions one will ensure enough degrees of freedom to solve this problem numerically.

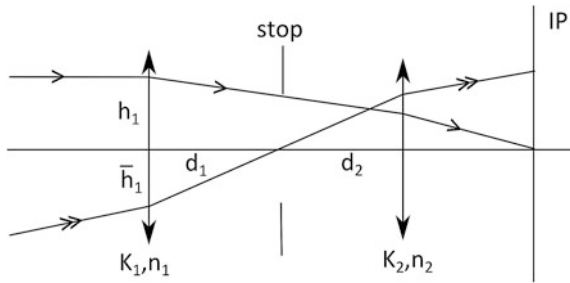
When one chooses for the first or last lens of a system an element built with two glasses of equal refractive index but different V-value, the correction of chromatic aberrations will be easier. In the design examples of this course we use this trick a couple of times.

4.2.6 Degrees of Freedom

Thus far we have considered focal length as a scale factor, field curvature, distortion and the primary chromatic aberrations. Field curvature and axial as well as lateral colour do not depend on the form of the lens elements. Our condition (4.7) on distortion relates only to the part of distortion that is form-independent. We will use the form factor in the next step of the design process: the thin lens predesign.

When we want to control the four parameters mentioned above (K , P , C_1 , C_2) and have some grip on distortion we must have at least five degrees of freedom in our lay-out.

The degrees of freedom that we use in the lay-out are: power (K_i), refractive index (n_i), dispersion (V_i) for each lens. When we have k lenses we have $k - 1$ distances between them. With the position of the stop included this gives $4k$ degrees of freedom with a system of k lenses.

Fig. 4.31 Lay-out example**Example**

As an example we consider a system of two thin lenses with the object at infinity. See Fig. 4.31.

This could be the lay-out for a simple projection lens.

The lay-out equations for this case are [see (4.5)–(4.8), (4.11)]

$$h_1 K = h_1 K_1 + h_2 K_2$$

$$P = K_1/n_1 + K_2/n_2$$

$$d_1 K_1 = d_2 K_2$$

$$C_1 = h_1^2 K_1 / V_1 + h_2^2 K_2 / V_2$$

$$C_2 = h_1 \bar{h}_1 K_1 / V_1 + h_2 \bar{h}_2 K_2 / V_2$$

our degrees of freedom are K_1 , K_2 , n_1 , n_2 , V_1 , V_2 , and d_1 , d_2 . Of these the last six are positive numbers. We will see that this restricts to a large degree our possibilities for correction.

In the first equations we have two choices: either K_1 and K_2 have the same sign or they have opposite signs.

When K_1 and K_2 have the same sign we cannot correct field curvature (P).

We can correct P better when K_1 and K_2 have opposite signs. Because

$$K = K_1 + K_2 - (d_1 + d_2)K_1 K_2$$

we can still have a positive value of K when K_1 or K_2 is negative. With $K_2 = -K_1$ we have

$$K = (d_1 + d_2)K_1^2$$

With this choice for the component powers, and $n_1 = n_2$ we could have $P = 0$. This looks nice, but when we consider also the remaining conditions we will be less pleased. With d_1 and d_2 both positive we cannot fulfill (4.7) when $K_2 = -K_1$. Distortion will then be more difficult to correct.

We would be able to make C_1 zero by the choice of V_1/V_2 such that

$$h_1^2/V_1 = h_2^2/V_2$$

but then we would get

$$C_2 = h_1 K_1 \left(\bar{h}_1 - \frac{h_1}{h_2} \bar{h}_2 \right) / V_1$$

and we cannot correct TCA because \bar{h}_1 and \bar{h}_2 have opposite signs.

The conclusion is that with $K_2 = -K_1$ we can correct field curvature and axial colour, but the correction of distortion and lateral colour is not possible.

It is now easy to see that with K_1 and K_2 both positive we cannot correct field curvature and axial colour, but we will do better with distortion and lateral colour. For a projection lens this is the better choice.

In the detailed treatment of design examples in [Chap. 6](#) of this course we will see that a solution of the dilemma to which we arrived in this example can be found in two ways. The colour correction can be solved by replacing both lenses by thin doublets. The correction of field curvature can be much improved by inserting a negative lens at the stop position between two positive lenses. See the lay-out of Petzval lens, telephoto and reversed telephoto objective, triplet and triplet variants in [Chap. 6](#).

4.2.7 Lay-out of a Zoom Lens

A zoom lens is a system that produces, on a fixed image plane, images with a variable magnification. This is realized by shifting components of the system. A great number of different zoom systems is described in the literature: Yamaji [[15](#)]. Zoom systems can be divided in two main groups: systems with mechanical compensation and optically compensated systems. In mechanically compensated systems usually one shift is used to change the magnification and another to correct focus. In optically compensated systems the moving elements are connected so that they perform the same movement. Therefore focus cannot be corrected exactly.

In this section we treat the lay-out, paraxial of a mechanically compensated zoom system, consisting of three thin lenses and a fixed camera lens. See Fig. [4.32](#).

The stop is in the camera lens, so that the illumination of the image plane stays the same in all zoom positions. Of the three thin lenses the first is fixed, the motion of the second lens governs the magnification and the third lens is used to correct focusing. With the camera lens focused at infinity, the three lenses act as a telescope. In practice a zoom system can also contain a focusing group, but for simplicity we leave that out.

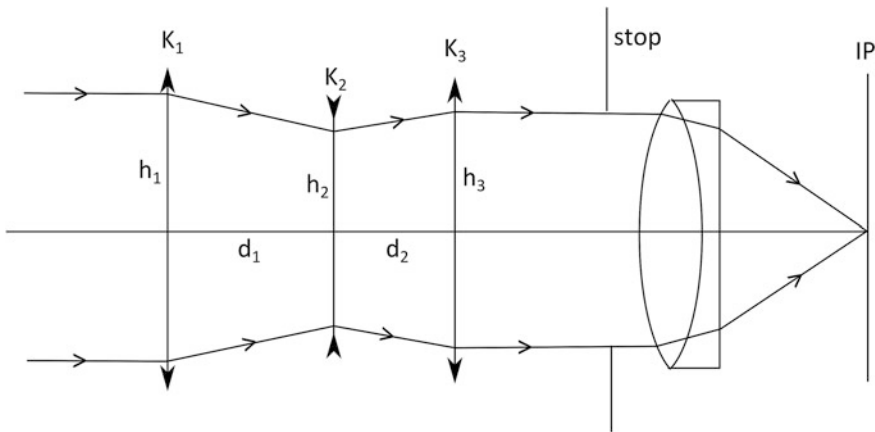


Fig. 4.32 Zoom system in front of a camera lens

With a telescope we must have (1.29)

$$h_1 K_1 + h_2 K_2 + h_3 K_3 = 0$$

Also, with $u_1 = 0$,

$$u_2 = -h_1 K_1, \quad u_3 = h_3 K_3,$$

so that

$$h_2 = h_1(1 - K_1 d_1) = h_3(1 - K_3 d_2)$$

The angular magnification of the telescope becomes

$$M = \frac{h_1}{h_3} = \frac{1 - K_3 d_2}{1 - K_1 d_1}$$

Using these results we find

$$M = \frac{-K_3}{K_1 + K_2 - d_1 K_1 K_2}$$

With the last two equations we can determine M and d_2 when d_1 and the powers are known.

Example

We take a reference system for which $K_1 = K_3$ and $M = 1$. Then we must also have $d_1 = d_2$.

For this system it follows that

$$1 - d_1 K_1 = -\frac{2K_1}{K_2}$$

With $d_1 K_1 = \frac{1}{2}$ follows $K_2 = -4K_1$

In the following table we list values of d_2 and M as functions of d_1

$d_1 K_1$	$d_2 K_1$	M	$(d_1 + d_2) K_1$
0	0.67	0.33	0.67
0.25	0.625	0.5	0.875
0.5	0.5	1	1
0.625	0.25	2	0.875
0.67	0	3	0.67

In the table, $d_1 + d_2$ is the distance from the first lens to the third lens. The range of movement of the third lens is $0.33f_1$, the second lens moves over a range of $0.67f_1$.

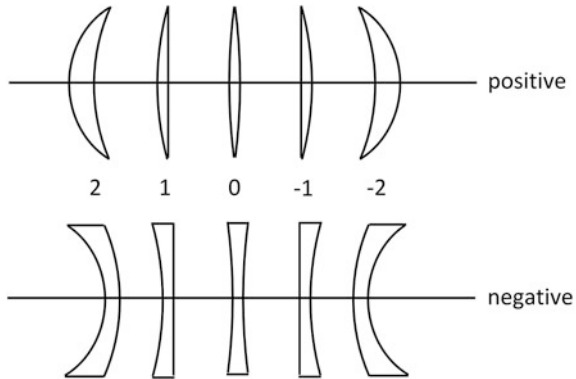
A paper of Jamieson [16] treats the lay-out and correction of optically compensated zoom systems. An ingenious method is described for solving the lay-out; this method is unfortunately not applicable to mechanically compensated systems. For the correction Jamieson uses the analytic method that we also use in this book for the thin lens design. He argues that this is sufficient for the design of zoom lenses, because with the analytical approach the variation of the aberrations can be controlled, which is the main goal with zoom systems. Moreover he argues that, for reasons of weight and space, zoom systems will use mainly thin lens elements so that giving thickness will not bring substantial changes in the aberration coefficients.

4.3 Thin Lens Predesign

This phase of the design process forms the transition between the lay-out phase and the optimization phase. It can be used to obtain an insight in the overall behavior of the aberrations of the system to be designed.

With the lay-out completed, we know the component powers of the lens, the distances between the components (and to object and image) and the optical glasses to be used. Longitudinal and transverse chromatic aberrations have been corrected. The Petzval sum is given and the distortion is corrected, both to a first approximation. With the remaining degrees of freedom (bendings of the lenses, stop position) we can correct the remaining aberrations and fine-tune distortion. After the transition to real lenses, resulting in a *surface model*, the system can be optimized.

Fig. 4.33 Thin lens forms for several values of the form factor



The most important property of the thin lens model is that the Seidel coefficients can be expressed analytically in the construction parameters of the system.

In this course we use the thin lens aberration formulas in the version of H. Coddington [19, p. 227]. Havlicek uses the version of Argentieri [9].

Kingslake [17] and Smith [2] use the g-sum method devised by Conrady [18].

The third order aberration coefficients of a thin lens can be expressed as follows in the construction data and the lay-out parameters.

We use the new variables

$$B = \frac{c_1 + c_2}{c_1 - c_2}, \text{ the } \textit{shapefactor}, \quad (4.13)$$

and

$$G = \frac{s' + s}{s' - s} = \frac{M + 1}{M - 1}, \text{ the } \textit{positionfactor} \quad (4.14)$$

The curvatures c_1 and c_2 can be calculated from (4.13) and $K = (n - 1)(c_1 - c_2)$, resulting in

$$\begin{aligned} c_1 &= \frac{1}{2}(B + 1) \frac{K}{(n - 1)} \\ c_2 &= \frac{1}{2}(B - 1) \frac{K}{(n - 1)}. \end{aligned} \quad (4.15)$$

We show lenses with different values of B in Fig. 4.33.

We suppose that the ambient medium is air. Then the aberration coefficients for a thin lens at the stop are given by

$$\begin{aligned}
S_1 &= \frac{h^4 K^3}{4} \left\{ \frac{n+2}{n(n-1)^2} B^2 + \frac{4(n+1)}{n(n-1)} BG + \frac{3n+2}{n} G^2 + \frac{n^2}{(n-1)^2} \right\}, \\
S_2 &= -\frac{h^2 K^2 H}{2} \left(\frac{n+1}{n(n-1)} B + \frac{2n+1}{n} G \right), \\
S_3 &= H^2 K, \\
S_4 &= \frac{H^2 K}{n}, \\
S_5 &= 0, \\
C_1 &= \frac{h^2 K}{V}, \\
C_2 &= 0.
\end{aligned} \tag{4.16}$$

The values of K , H , n and G will be known from the lay-out.

Usually also h is known, the marginal ray height. It can be found easily from a paraxial calculation.

H is the Lagrange invariant (see [Sect. 1.4](#))

V is the Abbe number

$$V = \frac{n_D - 1}{n_F - n_C}$$

where $\lambda_D = 589$ nm, $\lambda_F = 486$ nm, $\lambda_C = 656$ nm.

To obtain the aberration coefficients for a remote stop, denoted by a star, we use the stop shift equations ([Sect. 3.4](#)) in the form

$$\begin{aligned}
S_1^* &= S_1, \\
S_2^* &= S_2 + \frac{\bar{h}}{h} S_1, \\
S_3^* &= S_3 + 2 \frac{\bar{h}}{h} S_2 + \left(\frac{\bar{h}}{h} \right)^2 S_1, \\
S_4^* &= S_4, \\
S_5^* &= S_5 + \frac{\bar{h}}{h} (3S_3 + S_4) + 3 \left(\frac{\bar{h}}{h} \right)^2 S_2 + \left(\frac{\bar{h}}{h} \right)^3 S_1, \\
C_1^* &= C_1, \\
C_2^* &= C_2 + \frac{\bar{h}}{h} C_1.
\end{aligned} \tag{4.17}$$

The chief ray height \bar{h} can be found from a paraxial calculation.
Note that the case $h = 0$ does not lead to difficulties.

Welford [19, p. 234], remarks that the only aberration of a lens in a plane conjugate to the object is field curvature, given by $S_4 = \frac{H^2 K}{n}$. This can be shown by considering the surface formulas. See Sect. 3.3.

For a thin lens we have

$$C_1 = \frac{h^2 K}{V}, \quad C_2 = \frac{h \bar{h} K}{V}. \quad (4.18)$$

4.3.1 Spherical and Coma as Functions of B and G

From the formulas (4.16) we have that the minimum of S_1 as a function of B is obtained for

$$B = \frac{2(1 - n^2)}{n + 2} G.$$

With $n = 1.5$, $B \approx -0.7G$.

The minimum value of S_1 is then

$$S_{1,\min} = \frac{h^4 K^3}{4} \left(\frac{n^2}{(n-1)^2} - \frac{n}{n+2} G^2 \right).$$

This becomes zero for $n = 1.5$ when $G^2 = 21$.

When G and n are known we can find the value of B for which S_1 has a target value above the minimum.

See the example below.

Example

We take $n = 1.5$, $G^2 = 25$, $h' = 4$ and $K = 0.25$.

This gives, from (4.16), $S_1 = 9.3(B \pm 3.5)^2 - 1.5$. Spherical becomes zero for $B \pm 3.5 = \pm 0.4$, with the first minus sign for $G > 0$.

We have four solutions

$$\begin{aligned} G = 5, \quad B &= 3.1 \text{ or } 3.9, \quad M = 1.5 \\ G = -5, \quad B &= -3.1 \text{ or } -3.9, \quad M = \frac{1}{1.5}. \end{aligned}$$

The M values are both positive: virtual image

$|B| > 3$ means a meniscus lens.

4.3.2 Coma-Free Lens

We have zero coma for

$$B = \frac{(n - 1)(2n + 1)}{n + 1} G.$$

For $n = 1.5$ this becomes $B = -0.8G$.

This is not far from $S_{1,\min}$: $B = -0.7G$.

A single lens with zero coma (stop at lens) has also nearly minimum spherical.

Example

With

$$K = 0.01, \quad n = 1.5, \quad G = -1, \quad B = 0.8$$

we have

$$S_1 = 8.67 \frac{10^{-6}}{4} h^4, \quad S_2 = 0, \quad c_1 = 0.0225, \quad c_2 = -0.0025.$$

With $h = 10$, the transverse aberration becomes

$$\frac{S_1}{2u'} = 0.108 \text{ (mm)}.$$

The astigmatism coefficient is

$$S_3 = u'^2 \bar{h}_0^2 K,$$

where \bar{h}_0 is the field radius.

With $u' = 0.1$, $\bar{h}_0 = 10$ we have

$$S_3 = 0.01, \quad S_4 = 0.0067, \quad \delta\eta' = 0.183 \text{ (mm)}.$$

4.3.3 Correction of Thin Lens Systems

The thin lens aberration formulas (4.16) and (4.17) can be used for the correction of thin lens systems in the following way.

Supposing we know h , K , n and G from the lay-out we can for each lens calculate S_1 , S_2 , S_3 , S_4 as a function of B , when the lens is at the stop.

S_1 becomes a quadratic function of B ,

S_2 becomes a linear function of B ,

S_3 and S_4 are given by (4.16) as constants and S_5 is zero.

In S_2 , S_3 and S_4 we need the Lagrange invariant H , that is also known from the lay-out.

Using the equations (4.17), with the value of \bar{h} obtained from paraxial ray-tracing, we can find for each lens S_1^* , S_2^* , S_3^* and S_5^* as functions of B ; S_1 and S_4 do not depend on the position of the stop.

The functions S_1^* , S_2^* , S_3^* and S_5^* are quadratic functions of B ; S_4 does not depend on the form factor.

The Seidel sums $S_j = \sum_{i=1}^k S_{ji}$, where $j = 1, 2, 3, 5$ denote the aberration, and i is the number of the lens, $1 \leq i \leq k$, become quadratic functions of all the shape factors (or bendings) B_i of the component lenses.

Setting targets for the aberration coefficients, we can solve the equations for the B_i .

When we have k thin lenses and m aberrations the following situations can occur.

We have $k + 1$ degrees of freedom (k shape factors and the stop position). When $k + 1 > m$ it should be possible to find a suitable value for each aberration.

It is possible to select the most effective degrees of freedom.

When $k + 1 = m$ one can hope to find a solution; this depends on the target values of the aberrations. We will meet this situation in the correction of triplets, where the stop position is fixed and the three shape factors can be used to correct spherical, coma and astigmatism.

When $k + 1 < m$ it is not possible to correct all aberrations. The usual method is to minimize a weighted sum of squares of the aberration coefficients. This is discussed in [Sect. 4.5](#).

4.3.4 Exercise 6, Predesign of a Triplet

From Havliček [9] we have the following triplet lay-out (in our notation).

$$\begin{aligned} K_1 &= 1.733898K & n_1 &= 1.61924 & d_1 &= 0.115347f \\ K_2 &= -2.756850K & n_2 &= 1.61538 & d_2 &= 0.116172f \\ K_3 &= 1.721585K & n_3 &= 1.65510 \end{aligned}$$

$G_1 = -1$ (object at infinity), $h_2/h_1 = 0.8$, $h_3/h_1 = 0.854785$.

Calculate G_2 and G_3 from (4.14).

Take $h_1 = 7$ mm, $K = 0.01$, $f = 100$ mm, field radius $\bar{h}_F = 21.6$ mm.

Calculate q_1 and q_3 with $q_2 = 0$ (stop at the second lens).

Set up, according to the prescription of this section, the equations for S_1^* , S_2^* , S_3^* with B_1 , B_2 , B_3 as variables.

The equations can be solved numerically, graphically or by iteration.

We will discuss the methods of solution in [Sect. 6.4](#) where we treat the triplet.

4.4 Surface Model

When we have corrected the thin lens model we will give thickness to the lenses and consider the surface contributions to the third order aberrations.

Giving thickness is done in the following way. We insert a thickness between the first and second surface of each lens, equal to 10–15 % of its diameter, with a positive lens.

With a positive lens the edge thickness should be larger than 1 mm (sharp edges are difficult to make and to mount).

With negative lenses the central thickness should not be less than 6 % of the diameter, the edge thickness will then be sufficient.

The criterium of Fischer: “When it looks good, it is probably good”, can be used here [1].

We calculate the new power

$$K = K_1 + K_2 - \frac{dK_1 K_2}{n} \quad (4.19)$$

using the thin lens radii, and then scale r_1 , r_2 and d by a factor $\frac{K}{(K_1+K_2)}$.

Now the thick lens has the same power as the thin lens had before: $(K_1 + K_2)$.

The positions of the principal planes are found from the formulas (1.5) and (1.7).

$$\begin{aligned} V_2 H' &= -\frac{(n-1) c_1^* d^*}{n(K_1 + K_2)}, \\ V_1 H &= -\frac{(n-1) c_2^* d^*}{n(K_1 + K_2)}, \end{aligned} \quad (4.20)$$

where c_1^* , c_2^* are the scaled curvatures, and $K_1 + K_2$ is the power after scaling.

The distances between lenses in the thin lens model now become distances between principal planes:

$$d_i \Rightarrow H'_i H_{i+1}. \quad (4.21)$$

The aberrations of the surface model can now be calculated using the formulas (4.15) and (4.16) of Sect. 4.3.

The inverse procedure, making a thin lens from a real lens, is done as follows.

First we calculate the power of the real lens

$$K = (n-1) \left(c_1 - c_2 + d c_1 c_2 \frac{(n-1)}{n} \right). \quad (4.22)$$

Then we calculate the thin lens curvatures so that $\frac{c_1^*}{c_2^*} = \frac{c_1}{c_2}$.

When the thin lens must have power K ,

$$K = (n-1)(c_1^* - c_2^*) \quad (4.23)$$

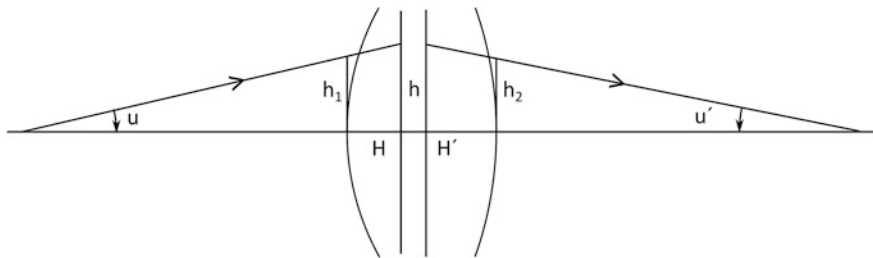


Fig. 4.34 Surface heights with a thick lens

we must take

$$\begin{aligned} c_1^* &= \frac{Kc_1}{(n-1)(c_1 - c_2)}, \\ c_2^* &= \frac{Kc_2}{(n-1)(c_1 - c_2)}. \end{aligned} \quad (4.24)$$

This makes that for the shape factor

$$B = \frac{c_1^* + c_2^*}{c_1^* - c_2^*} = \frac{c_1 + c_2}{c_1 - c_2}. \quad (4.25)$$

The distances between principal planes now become the distances between lenses:

$$H'_i H_{i+1} \Rightarrow d_i. \quad (4.26)$$

Note: in this section we have assumed that the surrounding medium is air.

4.4.1 Effect of Thickness on Aberrations

The effect of giving thickness on the aberration coefficients can be seen from Fig. 4.34.

In Fig. 4.34 the real lens is shown, with its principal planes H , H' . There is a difference between the ray heights h_1 , h_2 at the surfaces of the real lens and the ray height h at the equivalent thin lens. The aberration coefficients depend on powers of h ; specially spherical aberration, that is proportional to h^4 , is very sensitive to the change from thin to real lenses.

It is also clear from (4.20) that the effects of thickening depend on the form of the lens (or the positions of the principal planes) and its position (or the ray angles u , u').

4.5 Optimization

The goal of optimization is to produce a design that approaches as well as possible the functional properties and the quality required by the system specification. When this goal is reached, it makes no sense to improve the design further. The essential question is: is it good enough?

The input for optimization is a pre-design. As a pre-design we take a design that already gives us confidence that it can evolve to a design that is, as we called it above, good enough.

To estimate the potential of a pre-design we look at its Seidel coefficients and the resulting aberrations. And we consider the possibilities and degrees of freedom for further improvements (see [Chap. 5](#) on Design Strategies). We should not forget Fischer's criterion: "when it looks good, it is probably good", that can be used also in the negative sense. The input pre-design may be a surface model or, in some cases, even a thin lens pre-design. In this book we do not take designs from literature as pre-designs. To learn to be a designer one has to be able to set up a pre-design oneself.

In an optimization procedure an actual design is compared with an *ideal system* and changed in such a way that the differences between the actual design and the ideal system become as small as possible. The ideal system usually is described as a system where the paraxial laws of imaging (see [Chap. 1](#)) are valid. In the paraxial approximation each point of the object plane is imaged *stigmatically*, that is without aberrations, in a point of the image plane. This is valid for all possible object plane positions.

It can be shown, however, that with homogeneous refractive indices in object and image space, "not more than two surfaces may in general be sharply imaged by a rotationally symmetrical system". See Born and Wolf [20, Sect. 4.2] for a discussion on perfect imaging. We met already a case of perfect imaging in [Sect. 3.5](#) with the aplanatic surface.

In other words, the paraxial approximation cannot describe an ideal system, strictly speaking. Because of the simplicity of paraxial optics that we exploit in the lay-out phase and in the calculation of aberration coefficients we will nevertheless use the paraxial system image coordinates as a reference in optimization, conform to the usual practice in lens design software programs.

An alternative way of defining an ideal system is discussed in [21].

In optimization algorithms the design is represented by a *merit function* that expresses the difference in quality between the actual design and the ideal system.

The merit function usually has the form of a sum of squares:

$$F = \sum_m w_m (q_m - q_{mt})^2 \quad (4.27)$$

where the w_m are *weight factors*, positive numbers with $\sum_m w_m = 1$. The *quality parameters* q_m describe aspects of the quality of the system; q_{mt} are the *targets* for

these parameters. The targets are parameters of the ideal system, the weight factors are related to the function of the system.

Most of the quality parameters used in design software fall in one of the following categories:

- ray coordinates in the image plane, the targets of which are the paraxial coordinates,
- wavefront errors along a set of rays; the sum of squares of the wavefront errors E_i of rays from the same object point through an array of points in the entrance pupil describes the quality of the wavefront in the exit pupil in the same way as Strehl's number (see [Sect. 4.7](#)).
- aberration coefficients, the targets for which are found by tracing a number of finite rays (see [Sect. 4.5.4](#)).

Apart from these a number of other parameters can be used as components of the merit function. These are for instance the parameters that were fixed in the lay-out, such as the system focal length, of which we have shown in [Sect. 4.2](#) that it determines the scale of the system. Others are magnification, working distance, central and edge thickness of lenses, primary colour aberration coefficients, field angle, numerical aperture etc.

An alternative is the use of *solves*, specially *height* and *angle solves*, that change a construction parameter automatically in such a way that a lay-out parameter keeps a fixed value.

The solves can be used in the following way:

- the angle solve varies a radius in order to produce a fixed slope angle following the surface; this can be applied to each paraxial ray. An angle solve applied to a marginal ray can be used to control the focal length (EFL),
- the height solve varies the distance to a surface and controls the surface height. This solve can be used on a chief ray to find the position of the pupils, or on a marginal ray to find the object or image position, or to control magnification.

With a *pick-up* two construction parameters can be coupled; this is useful in the design of symmetric systems, for instance.

4.5.1 Weight Factors

The weight factors in the merit function are derived from the application of the lens to be designed. We consider first merit functions based on ray deviations.

Among the rays from a single object field point, rays through the central part of the pupil contribute most to the core of the point image; the rays through the outer parts of the pupil form a flare around this core. When a point image with a prominent core is wanted, one should give rays in the pupil centre more weight. For some applications the centre of the field should be well corrected and the

correction at the edge and in the corners of the field is not so important. We think of the classical portrait lenses, projection lenses and visual optical systems such as terrestrial telescopes and microscopes. In that case object points in the outer parts of the field can have a smaller weight.

When we combine ray deviations and wavefront errors (or aberration coefficients) as quality parameters, one should weight both groups differently. This can be achieved by different normalizations. For instance, ray deviations could be normalized by the Airy radius (see [Sect. 4.7](#)):

$$\Delta\eta' = 0.6\lambda/n \sin u' \quad (4.28)$$

and the wavefront errors by the wavelength λ .

Sometimes longitudinal aberrations (field curvatures, distortions, TCA) are used in the merit function. These could be normalized by the Rayleigh depth of focus:

$$\Delta z = \lambda/n \sin^2 u' \quad (4.29)$$

It is of prime importance not to include in the merit function aberrations that cannot be corrected, as this can lead to stagnation of the algorithm.

4.5.2 Variables and Constraints

The merit function is minimized by changing its *variables* under certain *constraints*. We will discuss the mathematics of optimization in a separate section below. As variables we can use construction parameters such as curvatures, distances, stop position, glass parameters (n , V , P). The constraints can take the form of inequalities or of functional relations between different variables.

With constraints in the form of inequalities the optimization program deals in the following way: when a variable has reached the limit, it is fixed there. Linear forms of constraints can be incorporated in the algorithm by an extra linear equation; nonlinear constraints have to be linearized. See Jamieson [[22](#), Chap. 5].

The variables that are used most frequently in optimization are curvatures and distances. In principle, curvatures are continuous variables; but the producer of the lens has usually a discrete set of tools available with the corresponding test glasses. To prevent high fabrication costs the design must be adapted to the tooling list of the producer. With a view to image quality radii smaller than, say, one-fifth of the focal length will cause difficulties in the correction of aberrations. This will lead to a constraint like $r_i \geq f/5$.

Distances are continuous and positive in refractive systems. When mirrors are used d can become negative, but then n will be negative as well, so that d/n is positive. This can be used as a constraint.

With lens thicknesses we formulated already a set of constraints in [Sect. 4.4](#); we repeat it here.

With a positive lens the central thickness should not be smaller than 10–15 % of the diameter of the lens; the edge thickness should be more than 1 mm.

With negative lenses the central thickness should be larger than 6 % of the diameter; the edge thickness is usually sufficient. Thicknesses are usually determined prior to optimization, but can be made variable for fine-tuning purposes.

Stop position and glass data are usually fixed in the lay-out phase, but they may be used as variables (in optimization) again in optimization. In the latter case care must be taken not to spoil the lay-out.

Glass data as variables have a special status. From the glass chart (n-V diagram) it can be seen that n and V are only available at discrete values in a limited existence region. Optimization programs have the possibility to use glass as a (two dimensional) variable. With continuous values of n and V this will lead to the introduction of non-existent “glasses” in the design. With discrete values only substitution of glasses is possible.

By splitting a lens element in two pieces that have (n , V) values on a line with the value needed the difficulty can sometimes be overcome.

4.5.3 Merit Functions

Because the result of optimization depends critically on the type and construction of the merit function used, we discuss several merit function types.

A frequently used merit function has a (two-dimensional) quality parameter: the ray deviation from the ideal position in the image plane. This ideal position can be the paraxial image point. The contribution of a single ray to the merit function is then given by

$$F_m = w_m \left\{ (X'_m - \xi_m)^2 + (Y'_m - \eta_m)^2 \right\} / \bar{a} \quad (4.30)$$

where X'_m , Y'_m are the image plane coordinates of the real ray and \bar{a} is the image field radius. The coordinates of the paraxial image point are ξ_m , η_m , usually $\xi_m = 0$.

Note that we normalize the ray coordinates by dividing through the field radius. Other components of the merit function also should be normalized in the same way.

For each object point a number of rays through different points of the entrance pupil should be traced. Representative object points (on the y -axis) should be selected. A recipe for the selection of rays is given by Jamieson [22, Chap. 4].

With refractive systems colour correction is usually necessary. The primary chromatic errors (LCA and TCA) are often already treated in the lay-out or the pre-design. For fine-correction the merit function will be minimized simultaneously at a number of wavelengths. One takes usually three wavelengths, two at the ends of the spectrum and one in the middle.

A different type of merit function uses the wavefront error (E in Sect. 3.1) along a ray as a quality parameter. In this case the wavelength is used for normalization. The merit function is related to Strehl's ratio (see Sect. 4.7).

From the wavefront-error-based merit function it is a natural step to a merit function based on aberration coefficients as quality parameters. Remember that the Seidel coefficients are proportional to the fourth order coefficients of the wavefront error. This leads to relatively simple and robust merit functions.

A merit function with only Seidel coefficients requires a minimum of calculations, but the correction state obtained will not be perfect as the higher order aberrations are ignored. It was part of the ability of designers in the pre-computer era to balance the Seidel aberrations against the higher orders. Lens design software can simulate this by extending the merit function by fifth order aberrations. Whereas calculating effort goes up sharply, the robustness of the algorithm remains. And a merit function with third and fifth order coefficients is still an approximation.

4.5.4 Aberration Balancing

Depending on the merit function used, the optimization algorithm will minimize the sum of squares of certain deviations from the ideal system.

For instance, the distances of ray intercepts in the image plane from the paraxial image point will be minimized for a number of field points. See the discussion of merit functions earlier in this section.

What happens to the third order aberration coefficients in that process? One could expect that all third order coefficients will be reduced to insignificant values. But that is not the case. Rather the aberrations are arranged in such combinations that the total effect on the point image is as small as possible. This process is called *aberration balancing*.

We give a simple example, the balancing of spherical aberration and defocus. The meridional aberration can be written

$$\delta\eta' = ay_r + by_r^3$$

where y_r is the meridional pupil coordinate (see Sect. 3.1).

When spherical aberration is fixed, defocus can be chosen so that the root-mean-square value of $\delta\eta'$ is smallest. It can be shown that this requires that $a/b = -1/2$.

With $a = 0$ the r.m.s. value of $\delta\eta'$ is $0.408b$.

With $a = -b/2$ the r.m.s. value becomes $0.288b$.

In practical situations the balancing process is much more complicated, taking along also the deviations of finite (non-paraxial) rays. The calculations will be executed by the computer. But the designer must compose a merit function that will produce a design of sufficient quality and present a suitable starting system.

In this book we pay attention to prepare starting systems that have properties that match as closely as possible to the systems that we want to design. In preparing a starting system we also discover which variables will be effective in optimization. This makes the composition of a merit function easier.

4.5.5 Fifth Order Aberrations

In this book higher order aberration are ignored for most of the time. To remember the reader of their existence we describe the aberrations of the fifth order and indicate their use in aberration balancing. From (3.1) of Sect. 3.1 follows that the fifth order aberrations in the image plane can be obtained by differentiation of the sixth order part of the wavefront error in the exit pupil. With a centered system and the object position on the y-axis we can write

$$\begin{aligned} E^{(6)} = & c_1 \rho^6 + c_2 \rho^4 y_r \eta_r + c_3 \rho^4 \eta_r^2 + c_4 \rho^2 y_r^2 \eta_r^2 + c_5 \rho^2 y_r \eta_r^3 \\ & + c_6 \rho^2 \eta_r^4 + c_7 y_r^3 \eta_r^3 + c_8 y_r^2 \eta_r^4 + c_9 y_r \eta_r^5 + c_{10} \eta_r^6 \end{aligned}$$

with $\rho^2 = x_r^2 + y_r^2$ as before.

The aberrations in polar coordinates, with $x_r = \rho \sin \varphi$ and $y_r = \rho \cos \varphi$, are given by

$$\begin{aligned} \delta\xi' = & -\frac{1}{n'u'} \{ 6c_1 \rho^5 \sin \varphi + 2c_2 \rho^4 \eta_r \sin 2\varphi + 4c_3 \rho^3 \eta_r^2 \sin \varphi + 2c_4 \rho^3 \eta_r^2 \cos^2 \varphi \sin \varphi \\ & + 2c_5 \rho^2 \eta_r^3 \sin 2\varphi + 2c_6 \rho \eta_r^4 \sin \varphi \} \\ \delta\eta' = & -\frac{1}{n'u'} \{ 6c_1 \rho^5 \cos \varphi + c_2 \rho^4 \eta_r (2\cos 2\varphi + 3) + 4c_3 \rho^3 \eta_r^2 \cos \varphi + 2c_4 \rho^3 \eta_r^2 (\cos^3 \varphi + \cos \varphi) \\ & + c_5 \rho^2 \eta_r^3 (\cos 2\varphi + 2) + 2c_6 \rho \eta_r^4 \cos \varphi + 3c_7 \rho^2 \eta_r^3 \cos^2 \varphi + 2c_8 \rho \eta_r^4 \cos \varphi + c_9 \eta_r^5 \} \end{aligned}$$

As we did in Sect. 3.1, we describe the terms of (4.2) one by one, give the aberration a name and show a zonal image, where this is necessary.

c₁. Fifth order spherical aberration

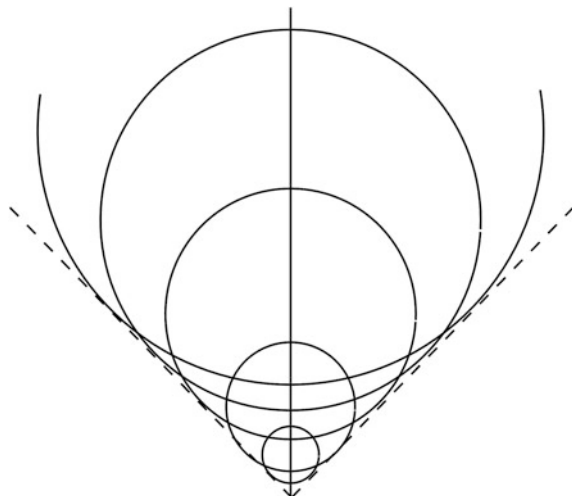
$$E = c_1 \rho^6, \quad \delta\xi' = -\frac{1}{n'u'} \cdot 6c_1 \rho^5 \sin \varphi, \quad \delta\eta' = -\frac{1}{n'u'} \cdot 6c_1 \rho^5 \cos \varphi$$

The zonal image has the same form as with third order spherical.
c₂. Fifth order (linear) coma

$$\begin{aligned} E = & c_2 \rho^4 y_r \eta_r, \quad \delta\xi' = -\frac{1}{n'u'} \cdot 2c_2 \rho^4 \eta_r \sin 2\varphi, \\ \delta\eta' = & -\frac{1}{n'u'} \cdot \rho^4 \eta_r (2\cos 2\varphi + 3) \end{aligned}$$

The zonal image has a form different from that of third order coma. See Fig. 4.35.

Fig. 4.35 Zonal figures of fifth order linear coma



c₃. Oblique spherical (sagittal) or “SOBSA”

$$E = c_3 \rho^4 \eta_r^2, \quad \delta\xi' = -\frac{1}{n'u'} \cdot 4c_3 \rho^3 \eta_r^2 \sin\varphi, \quad \delta\eta' = -\frac{1}{n'u'} \rho^3 \eta_r^2 \cos\varphi$$

This looks like third order spherical, but it depends quadratically on the object height.

c₄. Oblique spherical (meridional) or “TOBSA”

$$E = c_4 \rho^2 y_r^2 \eta_r^2, \quad \delta\xi' = -\frac{1}{n'u'} \cdot \rho^3 \eta_r^2 \cos^2\varphi \cdot \sin\varphi, \\ \delta\eta' = -\frac{1}{n'u'} \rho^3 \eta_r^2 (1 + \cos^2\varphi) \cdot \cos\varphi$$

This is SOBSA with an extra $\cos^2\varphi$ factor. The zonal image is given in Fig. 4.36.

c₅, c₇. Elliptic coma

$$E = c_5 \rho^2 y_r \eta_r^3 + c_7 y_r^3 \eta_r^3, \quad \delta\xi' = -\frac{1}{n'u'} \cdot c_5 \rho^2 \eta_r^3 \sin 2\varphi, \\ \delta\eta' = -\frac{1}{n'u'} \{ c_5 \rho^2 \eta_r^3 (\cos 2\varphi + 2) + 3c_7 \rho^2 \eta_r^3 \cos^2\varphi \}$$

These aberrations are comatic, depending on the third power of the field. The zonal image of c₅ is identical to that of third order coma. The zonal image of c₇ is a line along the η-axis, extending from 0 to $3c_7 \eta_r^3$.

Fig. 4.36 Zonal figures of TOBSA



$c_6, c_8.$ Fifth order field curvature and astigmatism

$$\begin{aligned} E &= c_6 \rho^2 \eta_r^4 + c_8 y_r^2 \eta_r^4, \quad \delta\xi' = -\frac{1}{n'u'} \cdot 2c_6 \rho \eta_r^4 \sin \varphi, \quad \delta\eta' \\ &= -\frac{1}{n'u'} (2c_6 \rho \eta_r^4 \cos \varphi + 2c_8 \rho \eta_r^4 \cos \varphi) \end{aligned}$$

Higher order forms of defocusing (c_6) and astigmatism (c_8).
 $c_9.$ Fifth order distortion

$$E = c_9 y_r \eta_r^5, \quad \delta\xi' = 0, \quad \delta\eta' = c_9 \eta_r^5$$

In Sect. 4.5 we considered aberration balancing. It will be clear from the description above that one form of aberration balancing can be found by the coupling of third order aberrations with their fifth order counterparts. We saw that each of the third order aberrations has such a counterpart; this leads to five possibilities of balancing. It is then necessary to calculate the relevant coefficients, which is more complicated with fifth order than with third order coefficients.

The use of oblique spherical and elliptic coma in aberration balancing is mentioned occasionally in the literature [1, p. 259]. There the balancing of field curvature and SOBSA is compared with the balancing of defocus and spherical. Elliptic coma could be used to counter the effects of third order coma in the field.

4.5.6 *Mathematics of Optimization

As a simple method of optimization we describe *linear variation*.

With a merit function as in (4.1), when we can give a linear description of the changes of the quality vector \vec{Q} due to the change vector of variables $\Delta \vec{x}$ as

$$\Delta \vec{Q} = \bar{A} \Delta \vec{x} \quad (4.31)$$

where \bar{A} is a matrix with components $\bar{A}_{ij} = \frac{\partial Q_i}{\partial x_j}$, we can take F equal to zero by taking

$$\Delta \vec{x} = \bar{A}^{-1}(\vec{Q}_t - \vec{Q}) \quad (4.32)$$

provided that the inverse matrix \bar{A}^{-1} exists. A necessary condition for the existence of the inverse is that \bar{A} is a square matrix. That means that the number of variables must be equal to the number of quality parameters.

When the Q_i are nonlinear function of the variables it is not possible to make \vec{Q} equal to \vec{Q}_t in one step. In that case smaller steps should be taken,

$$\Delta \vec{x} = \gamma \bar{A}^{-1}(\vec{Q}_t - \vec{Q}) \quad (4.33)$$

where $\gamma < 1$ must be chosen judiciously. The number of steps to reach the target vector is roughly equal to $1/\gamma$. At each step we should calculate the components \bar{A}_{ij} anew.

An application of damped linear variation can be found in thin lens predesign. When we take third order aberration coefficients as quality parameters, so that we have the merit function

$$F = \sum_i w_i (S_i - S_{it})^2$$

and use the form factors B_i as variables, as in Sect. 4.3, we have

$$\bar{A}_{ij} = \frac{\partial S_i}{\partial B_j}$$

Because in the thin lens model the S_i are in general quadratic functions of the B_i and because $S_i = \sum_j S_{ij}$, we can write

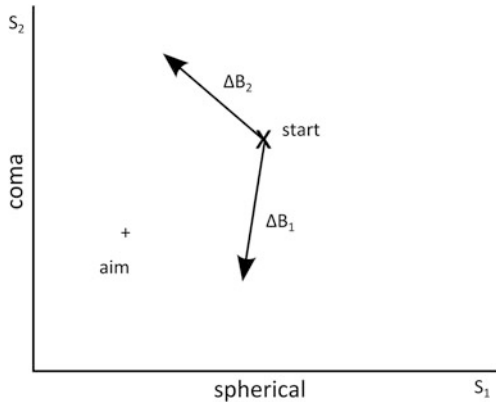
$$\bar{A}_{ij} = a_{ij} B_j + b_{ij}$$

where the constants a_{ij} and b_{ij} follow from the lay-out data.

For instance with a triplet, where we have three form factors, it is in principle possible to correct three aberrations. Because colour, field curvature and distortion follow from the lay-out in this case we could try to correct spherical, coma and astigmatism. The success of this trial will depend on the targets chosen; also the solution may result in impractical values of the form factors B_j .

Linear variation can be used fruitfully in optimization of thin lens designs “by hand”. The calculation of the \bar{A}_{ij} is very simple in this case.

Fig. 4.37 Optimizing two aberrations



In Fig. 4.37, after Kingslake and Johnson [17], we illustrate the correction of spherical and coma by linear variation, using changes of two form factors. In this way we want to bring the system from a start point (S_1 , S_2) to an aim (S_{1t} , S_{2t}).

By small variations of two form factors (or other degrees of freedom) we find two change vectors in the $S_1 - S_2$ plane. A suitable combination of these brings the system to the state of corrections designed by “aim”.

4.5.7 Damped Least Squares Algorithm

The optimization algorithm used most frequently in lens design software is the *damped least squares* (DLS) algorithm. When we have less variables than quality parameters to be corrected, as is usually the case in lens design, we cannot use linear variation. A minimum value of F can then be found in the following way. We write F in the following way:

$$F = \vec{Q}^t \cdot \vec{Q} \quad (4.34)$$

where \vec{Q} is a vector with components $\sqrt{w_i}(q_i - q_{it})$ and \vec{Q}^t is its transpose.

A change of F due to variable changes given by the vector $\Delta \vec{x}$ can be described by

$$F = F_0 + \vec{F}_0^t \cdot \Delta \vec{x} + \Delta \vec{x}^t \cdot \vec{F}'_0 \Delta \vec{x} \quad (4.35)$$

With

$$\vec{Q} = \vec{Q}_0 + \vec{A}_0 \Delta \vec{x} \quad (4.36)$$

for the changes of the quality parameters we have

$$\begin{aligned} F_0 &= \overrightarrow{Q_0^t} \cdot \overrightarrow{Q}_0 \\ \overrightarrow{F}'_0 &= 2\overrightarrow{A^t Q}_0 \\ \overrightarrow{F}''_0 &= \overrightarrow{A_0^t A_0} \end{aligned} \quad (4.37)$$

The suffix 0 in (4.35), (4.36) and (4.37) refers to the starting point.

In a minimum the gradient of F will be zero.

This leads to the equations

$$2\overrightarrow{A_0^t Q}_0 + \overrightarrow{A_0^t A_0} \Delta \overrightarrow{x} = 0 \quad (4.38)$$

Note that, although $\overrightarrow{A_0}$ is a rectangular matrix, $\overrightarrow{A_0^t A_0}$ is a square matrix, that has in general an inverse, so that the solution of (4.38) can be found as

$$\Delta \overrightarrow{x} = -2(\overrightarrow{A_0^t A_0})^{-1} \cdot \overrightarrow{A_0^t Q}_0 \quad (4.39)$$

As in linear optimization the changes of the variables should not be too large, as is implied by (4.36) above. This can be taken care of by adding a damping term $\lambda \Delta \overrightarrow{x}^t \Delta \overrightarrow{x}$ to the merit function. Instead of (4.39) we obtain

$$\Delta \overrightarrow{x} = -2(\overrightarrow{A_0^t A_0} + \lambda I)^{-1} \cdot \overrightarrow{A_0^t Q}_0 \quad (4.40)$$

The damping method described here is not the only one possible; by extending (4.36) by a second order term also damping will be introduced. The algorithm can be further extended to include constraint conditions on the variables.

The calculation of the inverse of matrices of a dimension higher than 3 is not something to be done by hand. With DLS this calculation has to be done at each step in the procedure. Also the extensions to second order terms of (4.36) and the inclusion of constraints make that the calculations can best be left to the computer. Only in thin lens predesign there are some modest opportunities for optimization by hand.

More details and literature on optimization can be found in the books by Gross et al. [23], Part 3], Haferkorn and Richter [24] and Jamieson [22].

A problem with DLS optimization is that it leads, from a given starting configuration, to the best accessible minimum of the merit function. The minimum that is found is a local minimum; there could be other minima with a better quality. Finding more or all minima of a given merit function is the subject of global optimization, for which we refer to the literature [23].

4.5.8 After Optimization

The results of optimization can be analyzed in many ways. From these we discuss five analysis techniques:

- spot diagrams
- aberration plots
- wave front error plots
- modulation transfer function (MTF)
- point spread function (PSF).

4.5.9 Spot Diagrams

A spot diagram is composed of the ray intercepts in the image plane of a substantial number of rays from a point object through different points in the entrance pupil. The distribution of rays in the pupil can have many forms, random or deterministic. A frequently chosen distribution takes ray positions on a number m of pupil radii with angles $2\pi/m$ in between.

On the radii the positions of n ray intercepts are given by

$$\rho_i = \sqrt{i/n}, \quad i = 1 \dots n$$

where ρ_i is the distance from the axis, in relative coordinates. In this way a quasi-uniform distribution is obtained, denoted as “ m arms, n rings”.

Spot diagrams will be produced for a number of field positions.

The use of spot diagrams has some advantages. The spot diagram uses not only rays of the meridional and sagittal fans, but also skew rays over the whole pupil. The design software will calculate the first and second order moments of the spot, from which distortion and r.m.s. spot radius follow. With a pixellated detector this is an important clue to decide whether lens and detector are well matched.

From the spot diagram it is difficult to distinguish between the different aberrations; this can be done better with the aid of aberration plots that are discussed below.

4.5.10 Aberration Plots

In these plots the following data are shown:

- meridional aberrations $\delta\eta'$ as a function of the relative meridional pupil height y_r ,
- sagittal aberrations $\delta\xi'$ as a function of the relative pupil coordinate x_r .

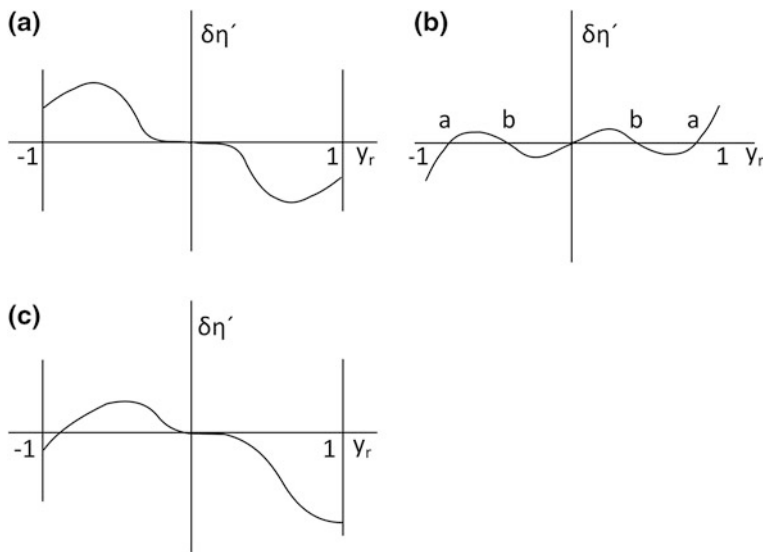


Fig. 4.38 a Aberration on axis. b Spherical and defocus. c Spherical and coma

The sagittal aberration plot is always symmetrical with respect to the meridional plane.

With the plots the vertical scale is given.

Usually plots are shown for each field point selected in the merit function. From these plots the following information can be obtained.

The plot connected to the axial object point shows spherical aberration. Because the aberration plots are calculated by finite ray tracing, without regard to the paraxial approximation, also higher order aberrations are included.

Without defocus the aberration plot will touch the y_r -axis in the axial point ($y_r = 0$). See Fig. 4.38a for an example.

By defocusing the plot can be tilted, so that the aberration becomes smaller on average. An example is given in Fig. 4.38b, that is derived from Fig. 4.38a by a rotation of the plot.

The aberration plot now has 5 zero points, meaning that it is composed from defocus and 3rd and 5th order spherical.

The slope of the plot of Fig. 4.38b in the axial point is proportional to defocus, the slope in the points b is proportional to 3rd order spherical and in the points a to 5th order.

The aberration plots for off-axis object points give information about the field aberrations.

Pure coma gives a parabolic $\delta\eta'$ plot and zero for the sagittal plot (see also Figs. 3.9 and 3.10 in Sect. 3.1); when spherical aberration is added to the $\delta\eta'$ plot it becomes asymmetrical; an example is given in Fig. 4.38c.

With field curvature the defocus, shown as the slope of the aberration curves for $y_r = 0$ and $x_r = 0$, depends on the field height. This is also the case for astigmatism that shows up as different defocus in the meridional and sagittal plots.

With distortion, the aberration $\delta\eta'$ is not zero for $y_r = 0$ and dependent on field height.

Aberration plots can be obtained for the wavelengths selected in optimization. Usually the plots for different wavelengths show small differences in the aberrations, even when the primary chromatic aberrations have been corrected.

When there is a rest of longitudinal chromatic (LCA) the plots for different wavelengths will have different slopes. When there is a rest of transverse chromatic (TCA) the plots for different wavelengths will intersect the vertical axis at different points.

In [Chap. 6](#), on design examples, the reader will find examples of aberration plots, used for the characterization of the designs discussed in that chapter.

4.5.11 Wavefront Error Plots

The data shown in these plots are the wavefront error along the meridional and sagittal axes in the exit pupil, $E(0, y_r)$ and $E(x_r, 0)$, usually for several field points and three wavelengths.

For the axial point the wavefront error has a second order component (defocus) and spherical aberration of fourth and higher (even) orders. Coma is of third (and higher uneven) order meridionally, and zero sagittally. Astigmatism is field dependent meridional defocusing; field curvature is field depending defocusing for both axes. Distortion gives linear wavefront error, dependent on third and higher orders of the field coordinate.

This analysis mode is most useful with near diffraction limited systems, such as microscope objectives.

4.5.12 Modulation Transfer Function

The modulation transfer function (MTF) is defined as the quotient of the contrast (or modulation depth) in the image plane and the contrast in the object plane, for an object with a sinusoidal intensity distribution, as a function of spatial frequency (number of periods per mm).

Background information about the calculation and properties of the MTF is given in [Sect. 4.7](#).

In optical design usually the following display modes of the MTF are used:

- MTF for different wavelengths, or an average over the spectrum,
- MTF for frequencies in radial and tangential direction (denoted by S and T, respectively),

- MTF (S and T) values for discrete frequencies as functions of defocus; this shows astigmatism and defocus,
- MTF (S and T) values for discrete frequencies as functions of the field height.

The MTF of a system without aberrations is used as a benchmark.

In [Chap. 6](#) a few examples of MTF curves can be found. In [1–3] much information on MTF is given.

4.5.13 Point Spread Function

The normalized intensity of the diffraction image pattern of a point object is called the *point spread function* (PSF). Some cross-section pictures of PSF's of systems without aberrations can be found in [Sect. 4.7](#) ([Figs. 4.48, 4.49](#)).

For optical systems that have small aberrations (wavefront error smaller than $\lambda/2$ peak to peak) the PSF is a useful diagnostic. In this book we are concerned with more modest designs, so that we will not use the PSF in that way. It will be seen in [Sect. 4.7](#) [([4.61](#)), ([4.62](#))] that PSF and MTF are strongly related.

The Strehl number, defined as the quotient of the intensity in the center of the PSF divided by the central intensity of an ideal PSF, is also used as a quality measure for systems with small aberrations. We give a short discussion of the Strehl number in [Sect. 4.7](#).

4.6 Tolerancing

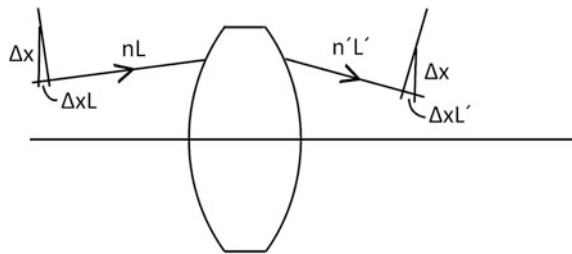
The last step in the design process consists in determining the sensitivity of the design to fabrication errors. This results in the specification of tolerance values for (classes of) fabrication errors. The most important of these are:

- centering errors, tilts and wedges,
- errors of curvature, distance and thickness,
- errors of refractive index and index gradients.

Most lens design programs find tolerances by calculating the effect of specific errors by ray tracing and applying statistical methods to find the effects of a combination of errors. This usually leads to a lot of extra ray tracing to be done (by the computer) and also to a great increase in computer output, to be analyzed by the designer.

In order to make tolerancing more easily understood, we offer here some general considerations that can be derived from eikonal theory [[25](#)]. We make use of the following theorem: the change in optical path length caused by a small perturbation is to a first approximation equal to the change in optical path, due to this perturbation, measured along the unperturbed ray. Changes of position and

Fig. 4.39 Optical path difference due to decentration



direction of the rays lead to changes of the optical length only in the second order of approximation.

In Fig. 4.39 we show the optical path difference caused by a shift Δx of a lens in the x-direction.

From Fig. 4.39 we have

$$\text{OPD} = (n'L' - nL)\Delta x \quad (4.41)$$

where $L \cdot L'$ are direction cosines and n, n' refractive indices on both sides of the lens.

In the general case of a vector shift ($\Delta x, \Delta y, \Delta z$) the change in optical path length becomes

$$\text{OPD} = (n'L' - nL)\Delta x + (n'M' - nM)\Delta y + (n'N' - nN)\Delta z \quad (4.42)$$

Using this formula we can establish tolerances for centering errors ($\Delta x, \Delta y$), distance and thickness errors (Δz). The formula describes the effects of displacements of surfaces, components or groups of components.

Note that with a plane surface we have $n'L' = nL$ according to Snell's law and also $n'M' = nM$. It is clear that a transverse shift ($\Delta x, \Delta y$) has no influence on the OPD when the surface is plane (and perpendicular to the z-axis). With a plane-parallel plate in air also $n' = n$ and $N' = N$ so that $\text{OPD} = 0$.

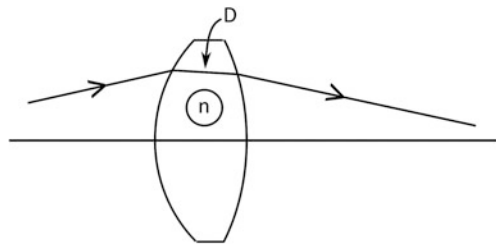
Rotation of a spherical surface about an axis perpendicular to the z-axis can be described by a rotation through the center of curvature C and a transverse displacement perpendicular to the axis of rotation. For instance a tilt about an angle α_x around an axis in the x-direction through the top of a spherical surface with radius r_k leads to a displacement

$$\Delta y = \alpha_x r_k \quad (4.43)$$

and a rotation around the center of curvature that has no effect on the OPD.

In this way the effects of surface tilt and wedge errors of components can be quantified.

The change of the optical path due to a change of surface curvature Δr is given by [25]

Fig. 4.40 Notation for (4.45)

$$\text{OPD} = \pm \Delta r \left(\left((n'L' - nL)^2 + (n'M' - nM)^2 + (n'N' - nN)^2 \right)^{\frac{1}{2}} - (n'N' - nN) \right) \quad (4.44)$$

where the plus sign is used when $n'N' - nN$ is positive and vice versa.

The OPD that follows from a change of refractive index Δn is given by

$$\text{OPD} = D\Delta n \quad (4.45)$$

where D is the path length through the lens along an unperturbed ray. See Fig. 4.40.

Equation (4.45) is similar to the equations used in Conrady's (D-d)-method [18] for the correction of chromatic errors.

The OPD values found from (4.44) and (4.45) are functions of even order of the ray coordinates y_r and η_r . Changes of curvature and refractive index leave the symmetry of the system intact. They lead to aberrations of uneven order, such as treated in Sect. 3.1. This is also valid for changes in distance and thickness.

In the following section we will see that breaking the symmetry leads to aberrations of even order. When there is a transverse gradient of refractive index, this is also the case.

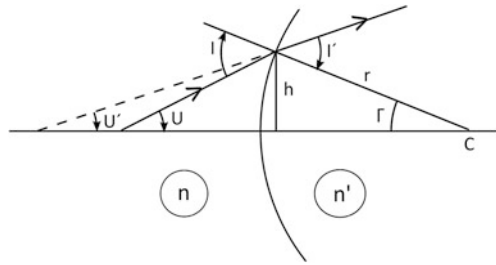
4.6.1 Third Order Analysis of Decentring Errors

To make use of the paraxial calculations that will be performed in the design examples of Chap. 6, for the calculation of tolerances, the formulas (4.41) to (4.44) of this section must be written in terms of the ray parameters h and u .

We will do this for meridional rays only; for the following reasons:

- the marginal and chief rays that we trace in the calculation of aberration coefficients are meridional rays;
- the aberrations of sagittal rays have lower maximal values than those of meridional rays (see Sect. 3.3); therefore we expect that the effect of perturbations will be smaller for sagittal rays as well.

Fig. 4.41 Meridional ray tracing, notation



Moreover it will be seen that the limitation to meridional rays will lead to simple formulas.

With lens design software the parameters of many traced rays are available, so that a more accurate picture of the effects of perturbations can be obtained.

In Fig. 4.41 the notation for the refraction of a finite meridional ray at a spherical surface is shown. A finite ray is a ray that makes finite angles with the optical axis and therefore is not always in the neighborhood of the axis. In the figure we use capital letters to denote angles, such as U and I , to make clear that a finite ray is traced.

From Fig. 4.41 it is seen that

$$I = U + \Gamma, \quad I' = U' + \Gamma, \quad \sin \Gamma = h/r$$

where h is the ray height and r the radius of curvature, so that

$$\begin{aligned} n \sin I &= n \sin U \cos \Gamma + n \cos U \sin \Gamma \\ n' \sin I' &= n \sin U' \cos \Gamma + n \cos U' \sin \Gamma \end{aligned}$$

Because $n' \sin I' = n \sin I$ we have

$$n' \sin U' - n \sin U = -(n' \cos U' - n \cos U) \tan \Gamma$$

Conventionally we take the $Y-Z$ plane as the meridional plane, so that $\sin U' = M'$, $\sin U = M$, and

$$n' M' - n M = -(n' \cos U' - n \cos U) \tan \Gamma \quad (4.46)$$

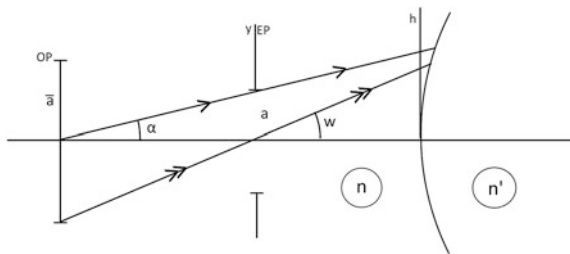
In a third order analysis we approach the quantities in the right hand side by:

$$\tan \Gamma = \frac{h}{r} + \frac{1}{3} \frac{h^3}{r^3}, \quad \cos U = 1 - \frac{1}{2} u^2, \quad \cos U' = 1 - \frac{1}{2} u'^2,$$

where h , u and u' are identified with paraxial parameters. To this approximation the OPD for a decentration Δy becomes [see (4.2)]

$$\text{OPD}_y = -\Delta y \left(\frac{h}{r} + \frac{1}{3} \frac{h^3}{r^3} \right) \left(n' - n - \frac{(n' u')^2}{2n'} + \frac{(nu)^2}{2n} \right) \quad (4.47)$$

Fig. 4.42 Notation for aperture angle (α) and field angle (w)



Between the paraxial parameters there is the relation

$$(n' - n)h/r = -n'u' + nu \quad (4.48)$$

To understand which aberrations follow from the OPD we must express h , u and u' in pupil and field coordinates. See Fig. 4.42 for the notation.

With a ray through the object center, $\eta = 0$, we have

$$nu = n \tan \alpha y_r, \quad n'u' = nu/\beta,$$

where α is the aperture angle and β the object magnification.

With a ray through the pupil center, $y = 0$, we have

$$nu = n \tan w \eta_r, \quad n'u' = nu/\beta_p,$$

where w is the field angle and β_p the pupil magnification. Note that all quantities relate to the surface under consideration. Only η_r and y_r are identical for all surfaces in a system and the system itself (this was the great invention of Seidel).

A general ray can be represented as an addition of both types of rays (see Sect. 1.6), with

$$\begin{aligned} nu &= n \tan \alpha y_r + n \tan w \eta_r \\ n'u' &= n \frac{\tan \alpha}{\beta} y_r + n \frac{\tan w}{\beta_p} \eta_r \end{aligned}$$

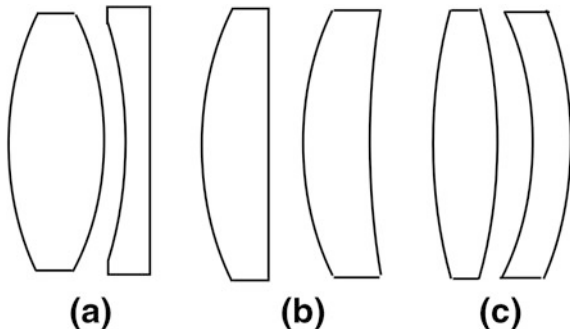
It follows that the OPD can be written

$$OPD_y = \Delta y (a_1 y_r + a_2 y_r^3 + b_1 y_r^3 + b_2 y_r^2 \eta_r + b_3 y_r \eta_r^2 + b_4 \eta_r^3)$$

where the different terms can be interpreted as follows:

- $a_1 y_r$ represents a transverse shift,
- $a_2 \eta_r^3$ and $b_4 \eta_r^3$ do not cause aberrations (but they are related to pupil errors)
- $b_1 y_r^3$ represents axial coma, independent of η_r ,
- $b_2 y_r^2 \eta_r$ represents a tilt of the image plane,
- $b_3 y_r \eta_r^2$ represents second order distortion.

Fig. 4.43 Three doublets from [26]



These aberrations are essentially different from the third order aberrations that we met thus far. This is connected to the fact that a decentration breaks the symmetry of an optical system.

We will use (4.47) to find the centering tolerances of a microscope objective. By following a marginal ray through the system we will obtain first the decentration sensitivity for all surfaces. From the condition that the OPD is not larger than $\lambda/4$ we find the tolerance values for Δy , per surface.

With a microscope objective the marginal ray gives the greatest contribution to the sensitivity ($\tan \alpha \gg \tan w$).

With systems where the field angle is not small also the chief ray should be used.

The ray data can be obtained, without additional ray tracing, from the results of the paraxial calculations tabulated for each system in Chap. 6.

In the following we describe the results of this procedure for a number of two-lens objectives that we studied in an earlier paper [26], where the construction data can be found.

The cross-sections are shown in Fig. 4.43.

The objective shown in Fig. 4.43a is a classical air-spaced doublet; at the third surface we expect a large sensitivity for transverse shifts. At a numerical aperture of 0.15 and a focal length of 100 mm it has an r.m.s. spot size of 2.2 μm within a field of $\pm 1^\circ$.

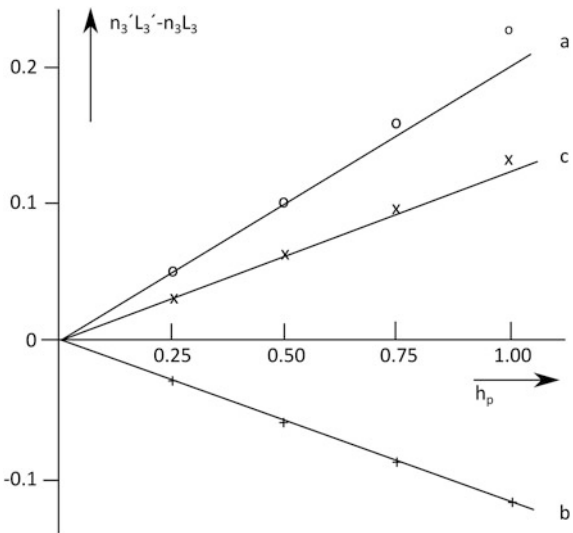
With the objective of Fig. 4.43b we have tried to make the sensitivity for decentering shifts as small as possible. It has an r.m.s. spot size of 12 μm for the same values of numerical aperture and field.

In the objective of Fig. 4.43c we have tried a trade-off between spot size and decentering sensitivity; we have inverted the second lens of the previous system. The r.m.s. spot size now becomes 3 μm .

In Fig. 4.44 we give the value of $n'L' - nL$ at the third surface for the three objectives, for rays parallel to the axis as a function of the relative pupil height.

The slope of the curves is now proportional to the image shift; the nonlinearity gives the amount of axial coma in microns per micron transverse shift.

Fig. 4.44 Sensitivity for decenter as a function of pupil height, a , b , c denote the systems in Fig. 4.43



When we tolerate one wavelength ($0.5 \mu\text{m}$) of axial coma the transverse shift tolerance is $12 \mu\text{m}$ for the air-spaced doublet, $400 \mu\text{m}$ for the second two-lens objective and $40 \mu\text{m}$ for the third objective.

4.6.2 Tolerances, Optimization and Strain

In the example that we described above we saw that fabrication errors lead to aberrations. Setting a tolerance limit on these aberrations leads to tolerances on the fabrication errors.

For most of the errors considered in this section: decentering, tilt and wedge, curvature errors, distance and thickness errors, we could express the sensitivity by a simple formula (4.41)–(4.44) in the direction cosines on two sides of a surface.

Following Glatzel [7] and Shafer [27] we consider an enhanced sensitivity for fabrication errors as an important system characteristic, leading to difficulties in the fabrication process [1] and higher costs of fabrication. These authors gave the name *strain* (German: Anspannung) to this characteristic. We propose to quantify the strain σ by the definition

$$\sigma = (n'L' - nL)^2 + (n'M' - nM)^2 + (n'N' - nN)^2$$

A design with a low value of σ is called by Shafer a relaxed design. The two-lens objective of Fig. 4.43b is typically such a design, with a very low sensitivity to centering errors.

In [25, 26, 28] the concept of strain was applied to optimization by including OPD's such as given in (4.41)–(4.44) in the merit function.

The conclusions of these experiments were twofold:

- it is possible to optimize a design, including strain, leading to well-corrected systems with a reduced sensitivity for e.g. centering errors and tilts, but
- when the reduction of strain is exaggerated, the image quality of the design will not be as good as that of a strained version.

In [28] it is pointed out that in relaxed systems the *induced* higher order aberrations are not corrected properly. Induced aberrations that occur in symmetric systems from the fifth order onward, constitute the part of surface aberrations that are induced by the aberrations of surfaces prior to the surface considered. Products of fourth order errors of the incoming wavefront are added to the *intrinsic* sixth order errors of the surface.

It follows that by adding a measure of strain the balancing of aberrations (see Sect. 4.5) can be improved.

4.6.3 Fabrication Errors

Earlier in this section expressions were given for the sensitivity of the optical path length to fabrication errors. The wavefront error resulting from the spread of the construction parameters can be calculated from these expressions [see (4.41)–(4.45)].

In the following table a set of representative error values are given for the error categories treated above.

Error	Values	Comment
Decenter	$\pm 0.05 \text{ mm}$	
Tilt	$\pm 0.05/r$	$r = \text{radius}$
Wedge	$\pm 0.025/r$	
Distance/thickness	$\pm 0.1 \text{ mm}$	
Radius	$\pm 0.01 \text{ mm}$	
Irregularity	0.5λ	$\lambda = \text{test wavelength}$
Refractive index	± 0.001	
Abbe number	$\pm 1 \%$	
Index gradient	$\pm 0.001/D$	$D = \text{surface diameter}$

These values are representative for camera lenses of modest performance. With high-performance lenses, such as stepper lenses and high-end microscope objectives the fabrication errors need to be much smaller. Not only because the wavefront errors must be smaller, but also because of the higher number of components in these systems. That means that for the fabrication of these systems special tools must be used. In general it will be necessary to talk with the workshop to make sure that what we have designed can also be produced.

When all contributions to the wavefront errors of the system have been calculated, an estimate must be made of their total effect on the performance of the produced lens. The usual assumption is that all errors are independent and have a zero average. The standard deviation of the total wavefront error is then equal to the root-mean-square of the component contributions.

In Sect. 6.6 we discuss the tolerance analysis of micro-objectives.

4.7 *Diffraction Theory for Lens Design

We summarize the results of diffraction theory that are used throughout this text in this section. We describe here a rudimentary theory that uses the scalar wave approximation.

We begin with the image of an axial point source (see Fig. 4.45) by a perfect lens. From the source departs a spherical wave; the lens transforms this wave into a converging spherical wave. From experiment it is known that the intensity distribution in the image plane has the form of a central maximum with weak rings around it. We describe the formation of this pattern by the interaction of spherical wavelets that depart from the wavefront in the exit pupil (see Fig. 4.46).

A wavelet from the surface element dS arrives in a point (x, y) on the image plane with a phase kl , where l is the optical path length (OPL) from (x_p, y_p) to (x, y) . When the pupil wavefront is spherical with radius r , the OPL from each point on the wavefront to the axial point $(0,0)$ of the image plane is equal to $n'r$. In the following we take $n' = 1$ for convenience.

The OPL to a point (x, y) in the neighborhood of $(0, 0)$ is, to a first order approximation, equal to

$$l = r - \frac{xx_p}{r} - \frac{yy_p}{r}$$

The amplitude of the wave in the image plane, $a(x, y)$, is now given by the *diffraction integral*

$$a(x, y) = \int_S a_p e^{ikl} dS / \lambda r$$

The factor $1/\lambda r$ keeps the energy budget in order.

Introducing l from above and taking a uniform pupil amplitude a_p we obtain

$$a(x, y) = \frac{a_p}{\lambda} \frac{e^{ikr}}{r} \int_S e^{-ik(xx_p + yy_p)/r} dx_p dy_p$$

We see immediately that in the axial point $(x = y = 0)$

$$a(0, 0) = a_p S e^{ikr} / \lambda r$$

where S is the pupil area.

Fig. 4.45 Imaging by a perfect lens

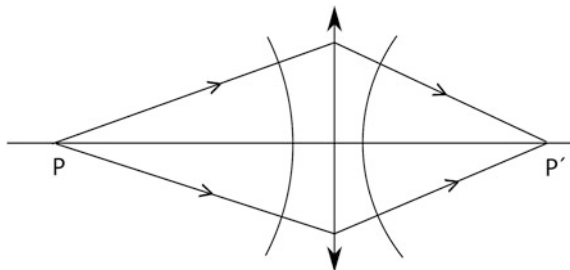
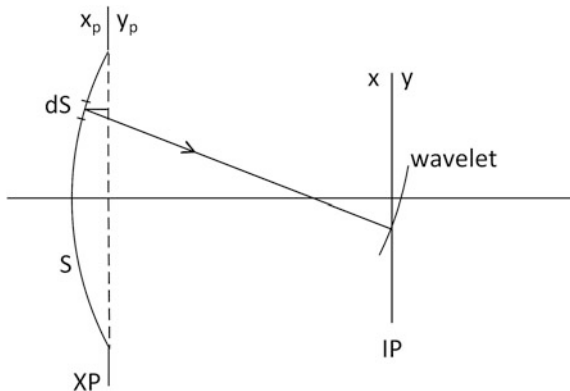


Fig. 4.46 Propagation from exit pupil (XP) to image plane (IP)



In the following we take, for convenience, a square pupil so that we can write

$$a(x, y) = \frac{a_p e^{ikr}}{\lambda r} \int_{-d/2}^{d/2} \int_{-d/2}^{d/2} e^{-ik(xx_p + yy_p)/r} dx_p dy_p$$

With these boundaries the integral is separable and we obtain easily

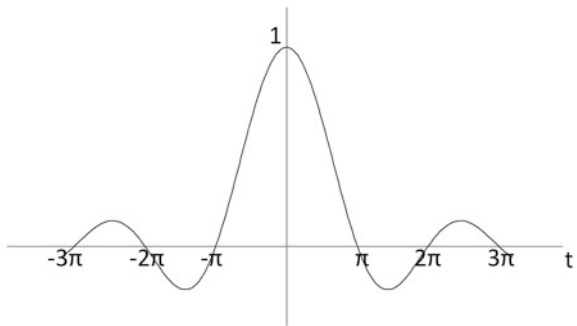
$$a(x, y) = \frac{a_p e^{ikr}}{\lambda r} d^2 \text{sinc}(kx \sin u') \text{sinc}(ky \sin u')$$

where $\sin u' = d/2r$ is the *numerical aperture* in image space. The last equation gives the amplitude distribution in the point diffraction image. Because of the symmetry in the exit pupil the amplitude is real.

The sinc function is defined by $\text{sinc}(t) = \frac{\sin(t)}{t}$, a picture of this function is given in Fig. 4.47.

The intensity distribution in the point image is given by

$$I(x, y) = \frac{a_p^2 d^4}{\lambda^2 r^2} \text{sinc}^2(kx \sin u') \text{sinc}^2(ky \sin u') \quad (4.49)$$

Fig. 4.47 The sinc function

The *point-spread function* (PSF) is defined by

$$h(x, y) = I(x, y)/I(0, 0) \quad (4.50)$$

From this definition and (4.7) follows that the PSF of an ideal (aberration free) lens with a square pupil is

$$h(x, y) = \text{sinc}^2(kx \sin u') \text{sinc}^2(ky \sin u') \quad (4.51)$$

Figure 4.48 gives a cross section and Fig. 4.49 gives the zero contours and the maximum values of $h(x, y)$ from (4.51). The distance between two zero contours is $\lambda/\sin u$. This is a measure of resolution in the image plane.

When the lens has a circular pupil, the amplitude distribution and the diffraction integral are best expressed in polar coordinates. We obtain, with $x = \rho \cos \varphi$, $y = \rho \sin \varphi$, $x_p = \rho_p \cos \varphi_p$, $y_p = \rho_p \sin \varphi_p$,

$$a(\rho, \varphi) = \frac{e^{ikr}}{\lambda r} \int_0^{\rho_p} \int_0^{2\pi} a_p e^{-ik\rho_p \cos(\varphi_p - \varphi)} \rho_p d\rho_p d\varphi_p$$

From the literature (see Born and Wolf [20, Sect. 8.5.2]) we have

$$a(\rho, \varphi) = \pi \rho_p^2 a_p \left[\frac{2J_1(k\rho \sin u')}{k\rho \sin u'} \right] \cdot \frac{e^{ikr}}{\lambda r}$$

where $J_1(t)$ is a Bessel function; for small values of t it is approximately equal to $\frac{1}{2}t$. It follows that $2J_1(t)/t = 1$ for $t \rightarrow 0$, and that the PSF for this case is

$$h(\rho, \varphi) = \left[\frac{2J_1(k\rho \sin u')}{k\rho \sin u'} \right]^2 \quad (4.52)$$

The PSF of a circular pupil is symmetric around the optical axis, a cross section is given in Fig. 4.50. The diameter of the first dark ring is equal to $1.22 \lambda/\sin u'$.

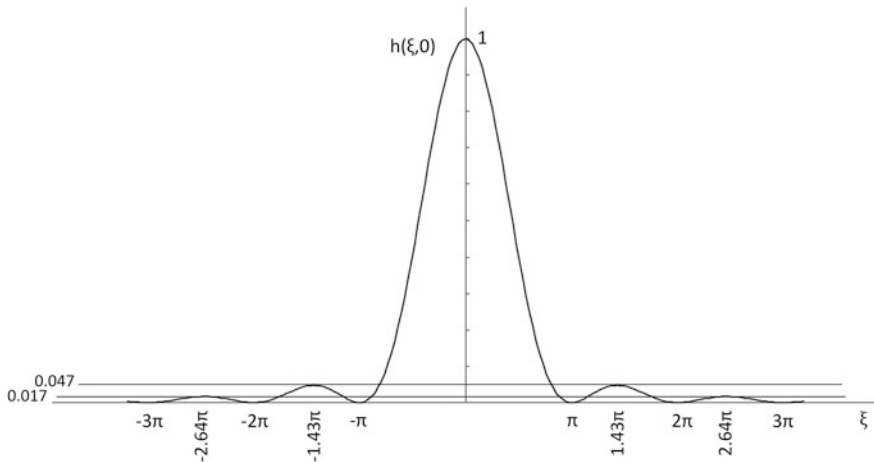
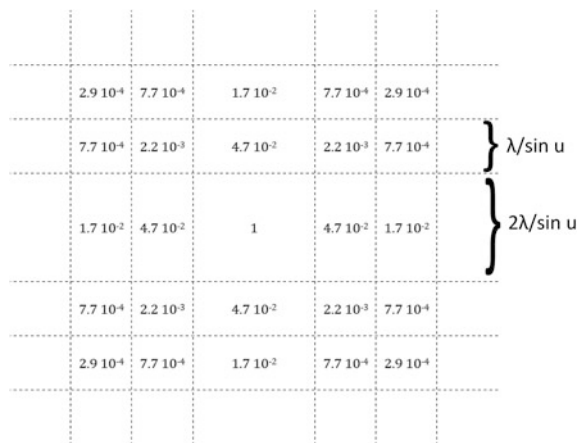


Fig. 4.48 Cross-section of the point-spread function (PSF) for a square pupil with $\xi = kx \sin u'$

Fig. 4.49 Zero contours and maximum values of the PSF of a square pupil



The resolution of a lens with a circular pupil is usually given as

$$\Delta x = 0.61 \lambda / \sin u' \quad (4.53)$$

when the wavefront aberration is zero. This is called the *Airy radius*.

We use the diffraction theory given above to derive two concepts that are important in characterizing the quality of lenses and lens designs. We mean the modulation transfer function (MTF) and the Strehl ratio.

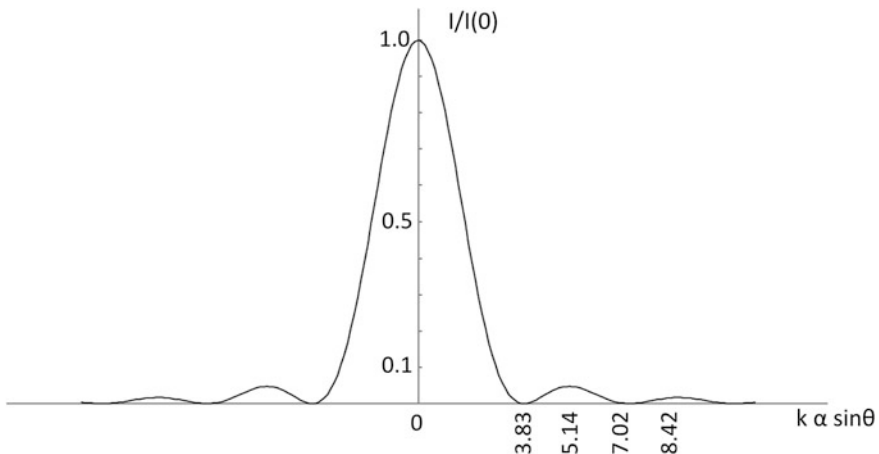


Fig. 4.50 Cross section of the Airy function (see 4.12)

4.7.1 Strehl Ratio

In this section we discuss the influence of aberration on the diffraction pattern and the PSF. When the pupil field has aberrations with a wavefront error $E(x_p, y_p)$ we obtain the diffraction integral,

$$a(x, y) = \int_S a_p e^{ikl} e^{ikE} dS / \lambda S$$

The *Strehl ratio* is defined as the maximum intensity in this diffraction pattern, divided by the maximum intensity of the ideal pattern.

With a uniform pupil amplitude a_p we obtain

$$R_{\text{Strehl}} = \left| \frac{\int_S e^{ikE} dS}{S} \right|^2 \quad (4.54)$$

By expanding e^{ikE} in a power series in kE and retaining first and second order terms we can show that

$$R_{\text{Strehl}} = 1 - \text{var}(kE) \quad (4.55)$$

where the variance of kE is defined as

$$\text{var}(kE) = \overline{k^2 E^2} - (\overline{kE})^2$$

where a bar denotes an average over the pupil area.

A more refined calculation (see Mahajan [29]) shows that

$$R_{\text{Strehl}} = e^{-(k\sigma)^2}, \quad k^2\sigma^2 = \text{var}(kE) \quad (4.56)$$

where σ is also called the root-mean-square wavefront error

$$\sigma = \text{rms}(E)$$

In practice we find that an excellent image quality is obtained when the value of $k\sigma$ is smaller than 0.4. This requires that

$$\text{rms}(E) < \frac{0.4\lambda}{2\pi} = 0.064\lambda \quad (4.57)$$

In the design of wafer stepper lenses values of r.m.s. (E) below 0.005λ are required. Geary [30, p. 358] calculates the minimum value of σ^2 for a balanced mixture of defocus and spherical.

The Strehl ratio shows the effect of aberrations on the central maximum of the PSF. The effect of aberrations on the side maxima can be described qualitatively as follows: the energy that is taken from the central maximum goes to the side maxima.

In the Airy pattern we observe that the rings will become stronger from moderate values of defocus or spherical; for higher values of these aberrations also the contrast in the pattern decreases.

With coma the energy is shifted to one side of the diffraction spot; the other side becomes steeper.

These effects are important in the design of cd player optics [31]. Spherical and defocus cause crosstalk between the tracks of a cd disk; coma gives rise to errors in the observed pit lengths.

4.7.2 Modulation Transfer

We consider the transfer of modulation depth from the object plane to the image plane, for an object with a sinusoidal intensity distribution. We assume that the object field is *incoherent*, so that we can consider the object as a continuous distribution of point sources of which the amplitudes are uncorrelated.

The object intensity is given by

$$I_{\text{ob}}(x_0, y_0) = I_0 \{ 1 + \mu \cos(2\pi x_0 f_x + 2\pi y_0 f_y) \} \quad (4.58)$$

where f_x, f_y are *spatial frequencies* and μ is the *modulation depth*, $0 < \mu < 1$.

We assume that the point spread function and the magnification M of the lens used for imaging of this object are constant over many periods of the cosine. That means that we can describe slow variations of the PSF and the magnification over the field of view of the lens.

Because each point source in the object gives rise to a diffraction spot, we can write for the intensity distribution in the image plane

$$I_{\text{im}}(x, y) = \iint I_{\text{ob}}\left(\frac{x'}{M}, \frac{y'}{M}\right) h(x' - x, y' - y) dx' dy' \quad (4.59)$$

where $h(x, y)$ is again the point spread function; in I_{ob} we have substituted x_0, y_0 by $x'/M, y'/M$.

Note that the PSF should, if necessary, take account of the wavefront aberrations in the exit pupil, so that we should use the definition

$$h(x, y) = \left| \frac{a(x, y)}{a(0, 0)} \right|^2$$

Inserting I_{ob} from (4.58) in (4.59) we obtain

$$I_{\text{im}}(x, y) = I_0 \left\{ H(0, 0) + \mu \left| H(f'_x, f'_y) \right| \cos(2\pi f'_x x + 2\pi f'_y y + \Phi) \right\} \quad (4.60)$$

where $f'_x = f_x/M, f'_y = f_y/M$ and

$$H(f'_x, f'_y) = \left| H(f'_x, f'_y) \right| e^{i\Phi(f'_x, f'_y)} = \iint h(x, y)^{2\pi i(xf'_x + yf'_y)} dx dy \quad (4.61)$$

The modulation depth of the image distribution becomes

$$\mu' = \mu \left| H(f'_x, f'_y) \right| / H(0, 0)$$

The function $\Phi(f'_x, f'_y)$, the *phase function*, can be interpreted as an image shift in the direction (f'_x, f'_y) , given by

$$\Delta = \Phi / 2\pi \sqrt{(f'^2_x + f'^2_y)}$$

With a symmetric, real PSF the phase function is zero and we can write

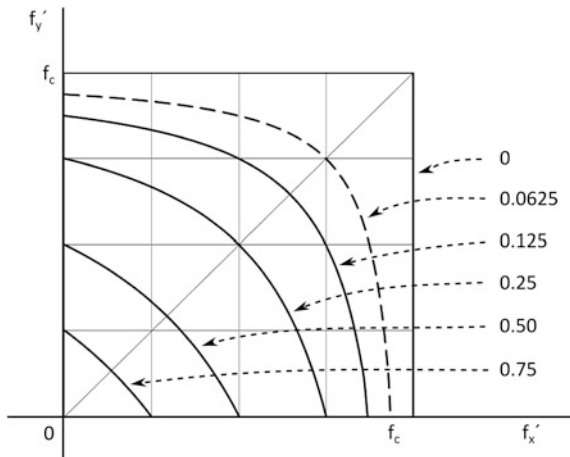
$$I_{\text{im}}(x', y') = I_0 \left\{ H(0, 0) + \mu H(f'_x, f'_y) \cos(2\pi f'_x x + 2\pi f'_y y) \right\}$$

From (4.60) we can define the *modulation transfer function* (MTF) as

$$T_\mu(f'_x, f'_y) \equiv \mu' / \mu = \left| H(f'_x, f'_y) \right| / H(0, 0) \quad (4.62)$$

Note that with a symmetric PSF the modulus bars can be omitted. This is strictly true with defocus and spherical aberration, where the wavefront aberration is uniform over the image field of view, and locally for field curvature and astigmatism. With coma and distortion we must take account of the phase function; with distortion the phase function is proportional to $\sqrt{(f'^2_x + f'^2_y)}$, so that we have an equal shift in the radial direction for all frequencies.

Fig. 4.51 Curves of equal MTF value in the spatial frequency (f'_x, f'_y) plane for a square pupil ($f_c = 2\sin u/\lambda$). Note the symmetry around the line $f'_x = f'_y$



With both coma and distortion, and also with astigmatism and field curvature, the MTF and the phase function are functions of the field coordinate.

The complex function

$$O(f'_x, f'_y) = H(f'_x, f'_y)/H(0, 0) \quad (4.63)$$

is called the *optical transfer function* (OTF).

Usually in optical design software the MTF can be calculated, and sometimes also the phase function. We will not use the OTF as such.

To conclude this section we give the MTF for an ideal, *diffraction limited*, lens. With the PSF of (4.51) that was derived for a square pupil, we obtain

$$\begin{aligned} T_\mu(f'_x, f'_y) &= \left(1 - \frac{f'_x}{f_c}\right) \left(1 - \frac{f'_y}{f_c}\right) \quad \text{for } 0 < f'_x < f_c, 0 < f'_y < f_c \\ T_\mu(f'_x, f'_y) &= 0 \quad \text{elsewhere,} \end{aligned}$$

with $f_c = 2\sin u/\lambda$, the cut-off frequency.

With a circular pupil we obtain

$$T_\mu(f_r) = \frac{2}{\pi} \left\{ \arccos\left(\frac{f_r}{f_c}\right) - \frac{f_r}{f_c} \sqrt{1 - \left(\frac{f_r}{f_c}\right)^2} \right\} \quad \text{for } 0 \leq f_r \leq f_c \quad (4.64)$$

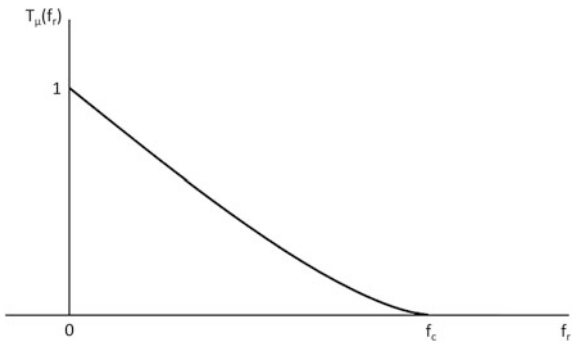
$$T_\mu(f_r) = 0 \quad \text{elsewhere,}$$

where $f_r^2 = f'_x^2 + f'_y^2$, and $f_c = 2\sin u/\lambda$ as before.

The functions are displayed in Figs. 4.51 and 4.52 respectively.

Note that in Fig. 4.51 the cut-off frequency for sinusoidal patterns in diagonal directions ($f'_x = \pm f'_y$) is equal to $\sqrt{2}f_c$.

Fig. 4.52 MTF of a circular, unaberrated pupil, with
 $f_c = 2\sin u/\lambda$



The MTF of (4.64) and Fig. 4.52, that is valid for a circular, unaberrated pupil, has $T_\mu(0) = 1$ and $T_\mu(f_c) = 0$. For $f_r > f_c$, $T_\mu(\rho) = 0$. This is also the case with aberrated systems.

References

1. R. Fischer, B. Tadic-Galeb, P.R. Yoder, *Optical System Design*, 2nd edn. (SPIE Press, 2008)
2. W. Smith, *Modern Optical Engineering*, 2nd edn. (SPIE Press, 2008)
3. R. Shannon, *The Art and Science of Optical Design* (Cambridge University Press, Cambridge, 1997)
4. J. Kross, *Typenkunde Optischer Systeme*. Thesis, Technische Universitaet, Berlin (1970)
5. M. Kidger, *Intermediate Optical Design* (SPIE Press, 2004)
6. B.G. Broome, Microscope objectives, in *Lens Design*, ed. by W.J. Smith, SPIE CR41 (1992), p. 325
7. E. Glatzel, New lenses for microlithography, in *SPIE Proceedings*, vol. 1780 (1992), p. 439
8. D.M. Williamson, The monochromatic quartet explained, in *Lens Design*, ed. by W.J. Smith, SPIE CR41 (1992)
9. F.I. Havlicek, Einführung in das korrigieren optischer Systeme, Wissenschaftlicher Verlagsgesellschaft (1960)
10. M. Berek, *Grundlagen der praktischen Optik* (W. de Gruyter, 1970)
11. Y. Matsui, K. Nariai, *Fundamentals of Practical Aberration Theory* (World Scientific, 1993)
12. J.R. Sheats, B.W. Smith, *Microlithography, Science and Technology* (Marcel Dekker, 1998)
13. F.I. Havlicek, J. Opt. Soc. Amer **41**, 1958 (1954)
14. R.I. Mercado, Design of apochromats and superachromats, in *Lens Design*, ed. by W.J. Smith, SPIE CR41 (1992), p. 270
15. K. Yamaji, Design of Zoom Lenses, in *Progress in Optics VI*, ed. by E. Wolf (North Holland, 1967), p. 107
16. T.H. Jamieson, Thin lens theory of zoom systems. Optica Acta **17**, 565 (1970)
17. R. Kingslake, R.B. Johnson, *Lens Design Fundamentals*, 2nd edn. (SPIE Press/Academic Press, 2010)
18. A.E. Conrady, *Applied Optics and Optical Design, Parts I and II* (Dover Books, 1985)
19. W.T. Welford, *Aberrations of Optical Systems* (Taylor and Francis, 1986)
20. M. Born, E. Wolf, *Principles of Optics*, 7th edn. (Cambridge University Press, Cambridge, 1999)

21. J.L.F. de Meijere, C.H.F. Velzel, Linear ray propagation models in geometrical optics. *J. Opt. Soc. Amer* **A4**, 1432 (1987)
22. T.H. Jamieson, Optimization Techniques in *Lens Design* (Adam Hilger, 1971)
23. H. Gross, F. Blechinger, B. Achtner, *Handbook of Optical Systems, Part III* (Wiley-VCH, New York, 2008)
24. H. Haferkorn, W. Richter, Synthese optischer Systeme, VEB Deutscher Verlag der Wissenschaften (1984)
25. C.H.F. Velzel, J.L.F. de Meijere, Sensitivity analysis of optical systems using the angle characteristic. *SPIE Proc.* **1168**, 164 (1989)
26. J.L.F. de Meijere, J.A. Schuurman, C.H.F. Velzel, The use of the pseudo-eikonal in the optimization of optical systems. *SPIE Proc.* **1013**, 2 (1988)
27. D. Shafer, Optical design and the relaxation response. *SPIE Proc.* **766**, 2 (1987)
28. C.H.F. Velzel, R Kruizinga, J.L.F. de Meijere, Lens design and tolerance calculations. *SPIE Proc.* **1780**, 439 (1992)
29. V. Mahajan, *Aberration Theory made Simple (TT6)* (SPIE Press, 1991)
30. J.M. Geary, *Introduction to Lens Design* (Willmann-Bell, 2002)
31. G. Bouwhuis et al., *Principles of optical disc systems* (Adam Hilger, 1985)

Chapter 5

Design Strategies

Every designer has a toolbox of methods and tricks, with which to solve the problems that arise in the lens design process. Kingslake and Johnson [1, Chap. 1] mentions thirteen procedures that he uses in his design examples. We cite here his remarks on this subject:

Lenses fall into several well-defined and well-recognized types,..... Each of these types, and indeed every form of lens, requires an individual and specific process for its design. Some lenses contain many refracting surfaces while some contain few. In some lenses there are so many available parameters that almost any glass can be used; in others the choice of glass is an important degree of freedom. Some lens systems favor a high relative aperture but cover only a small angular field, while other types are just the reverse.

We have tried to take his considerations further by connecting design strategies (methods, procedures, tricks) with design forms (types) by means of a matrix. See the table below.

We have divided the strategies into five groups, according to the objective of the strategy: colour correction, variables, symmetry, stops and field correction. These groups head the columns of the matrix.

The design forms are at the head of the rows; we go from the simple (singlet) to the complex (micro-objectives, stepper lenses) with one exception: we put mirror objectives last in the list.

With crosses we have indicated which strategies are important for the individual types. We discuss the matrix in detail in the rest of this chapter.

Types	Objective				
	Colour	Variables	Symmetry	Stops	Field
Singlet				x	x
Doublet	x			x	x
Apochromat	xx				
Ocular				x	x
Petzval lens	x			x	
Tele-objective	x	x			x
Wide-angle-lens	x	x			xx
Triplet	x	x	x	x	
Tessar, Heliar	x	x	x	x	
Angulon	x	x	x		x
Double Gauss	x	x	x		x
Lister objective	x				x
Flat-field objective	x		x		x
Stepper lens		x	x		xx
Cassegrain objective	x			x	
Schmidt camera	x		x	x	

5.1 Colour Correction

5.1.1 Optical Materials

The list of optical materials comprises glasses, plastics, crystals and also some fluids, all of them transparent in different parts of the spectrum.

In this book only optical glasses are considered; we limit our examples to the visible spectrum.

Special literature on optical materials is found in [2] and [3].

Optical glass is characterized by its refractive index (n) and its dispersion (V, P). The definition of refractive index was given in [Chap. 1](#) (1.1). Dispersion is the dependence of n on the wavelength of light.

An overall measure of dispersion in the visible spectrum is given by the quantity V , defined by

$$V = \frac{n_d - 1}{n_F - n_C} \quad (5.1)$$

where n_d , n_F , n_C denote the indices at the wavelengths $\lambda_d = 587.6 \text{ nm}$, $\lambda_F = 486.1 \text{ nm}$, $\lambda_C = 656.3 \text{ nm}$.

Sometimes we use also the partial dispersion coefficient P_d , defined as

$$P_d = \frac{n_F - n_d}{n_F - n_C} \quad (5.2)$$

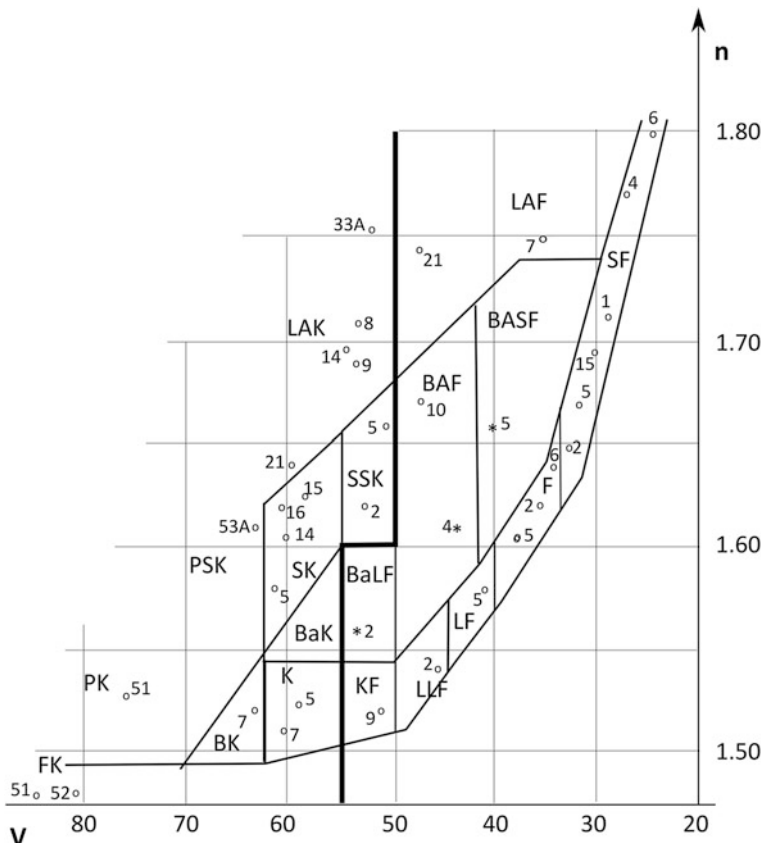


Fig. 5.1 Glass chart, with the glasses that are used in this book marked with a **o** (most) or a ***** (three KZFS glasses). The letters denote the glass types, glasses ending on K are crowns, those ending on F are flints

Producers of optical glass present an overview of their offer in a so-called *glass-chart*. This is a n-V diagram where the glasses are shown as points. In Fig. 5.1, which is adapted from O’Shea [4] we show a glass map with selected glasses from the company Schott. The glasses that we use in this book are denoted by little circles.

The region of the existence of optical glasses is divided in two parts, the crown glasses denoted by a K ("Kron") and the flint glasses denoted by F, roughly along the line $V = 50$, with the exception of the BaLF and KF glasses.

The data of the glasses that are used in the design examples in the Chap. 6 are shown in the following table. For each glass we give the values of n and V ; in Chap. 6 we will only give the names of the glasses. It is seen from the table and from Fig. 5.1 that n varies from 1.5 to 1.8, and V from 25 to 85. Note that a low value of V means a large dispersion.

	n	V	P _d
FK 51	1.48656	84.47	0.508
FK 52	1.48747	81.41	0.508
K 7	1.51112	60.41	0.509
N-BK 7	1.51680	64.06	0.507
N-K 5	1.52249	59.48	0.510
N-KF 9	1.52346	51.54	0.513
N-PK 51	1.52855	76.98	0.509
LLF 2	1.54344	45.47	0.516
N-KzFS 2	1.55836	54.01	0.509
LF 5	1.58144	40.85	0.519
N-SK 5	1.58193	61.27	0.508
N-SK 14	1.60311	60.60	0.509
F 5	1.60342	38.03	0.521
N-PSK 53A	1.61800	63.39	0.510
F 2	1.62004	36.37	0.522
N-SK 16	1.62041	60.32	0.509
N-SSK 2	1.62229	53.27	0.513
SK 15	1.62555	57.78	0.510
N-LAK 21	1.64049	60.10	0.507
F 6	1.64062	35.09	0.523
SF 2	1.64769	33.85	0.524
KzFS 5	1.65412	39.70	0.518
N-SSK 5	1.65844	50.88	0.514
N-BAF 10	1.67003	47.11	0.516
SF 5	1.67270	32.21	0.524
LAK 9	1.69100	54.70	0.510
N-LAK 14	1.69680	55.41	0.509
N-SF 15	1.69892	30.20	0.526
N-LAK 8	1.71300	53.83	0.510
N-SF 1	1.71736	29.51	0.526
N-LAF 7	1.74950	34.82	0.521
N-LAK 33A	1.75393	52.27	0.511
SF 4	1.75520	27.58	0.528
N-LAF 21	1.78800	47.51	0.514
SF 6	1.80518	25.43	0.529

5.1.2 Colour Correction of Thin Systems

A thin system is defined as a system where all distances are small compared with the system focal length. The classical way of correcting the power dispersion (dependence of power to wavelength) of a thin doublet is taking two glasses of different V-values and requiring that

$$\begin{aligned} K &= K_1 + K_2 \\ 0 &= \frac{K_1}{V_1} + \frac{K_2}{V_2} \end{aligned} \quad (5.3)$$

This follows from (4.4). Because the system is thin, we can take $h_1 = h_2$. From (5.3) we have

$$K_1 = \frac{V_1}{V_1 - V_2} K, \quad K_2 = \frac{-V_2}{V_1 - V_2} \quad (5.4)$$

When $V_1 > V_2$ (crown in front), K_1 is positive and K_2 negative; when $V_1 < V_2$ (flint in front), K_1 is negative and K_2 positive. Note that V is always positive, because $n_F > n_C$, and that flint glasses have lower V values than crown glasses (see Fig. 5.1).

With (5.4) the doublet has equal focal length for the wavelengths λ_C (red) and λ_F (blue). Such a doublet is called an *achromat*.

The focal length of an achromat for the wavelength λ_d is slightly different from that at λ_C and λ_F .

This is called *secondary spectrum*.

The secondary spectrum of a thin achromatic doublet, with powers given by (5.4), can be shown to be given by

$$\delta_2 K \equiv K_F - K_d = \frac{P_{d1} - P_{d2}}{V_1 - V_2} \cdot K_d \quad (5.5)$$

With traditional glasses, such as K5 and F2, we will find $\delta_2 K \approx 0.0005 K_d$. In the infrared and ultraviolet outside the visible spectrum the power deviations from K_d become rapidly larger.

The secondary spectrum can be reduced by taking FK 51 and N-KzFS 2 as glasses; now $\delta_2 K \approx 0.00002 K_d$. These glasses have about equal values of partial dispersion P_d , whereas their V -values differ strongly.

5.1.3 Apochromatic Thin Systems

With an achromat we have equal power (or focal length) for two wavelengths. A system for which the power is equal for three wavelengths is called an *apochromat*. The lay-out equations for a thin apochromat are:

$$\begin{aligned} K &= K_1 + K_2 + K_3 \\ \frac{K}{V_s} &= \frac{K_1}{V_1} + \frac{K_2}{V_2} + \frac{K_3}{V_3} \cong 0 \\ \frac{K_p P_{d1}}{V_1} + \frac{K_2 P_{d2}}{V_2} + \frac{K_3 P_{d3}}{V_3} &\cong 0 \end{aligned} \quad (5.6)$$

Three glasses must be found for which the three component powers are not too strong (for instance, smaller than 3 times the system power). The condition is that the value of the determinant

$$D = \begin{vmatrix} 1 & \frac{1}{V_1} & \frac{P_{d1}}{V_1} \\ 1 & \frac{1}{V_2} & \frac{P_{d2}}{V_2} \\ 1 & \frac{1}{V_3} & \frac{P_{d3}}{V_3} \end{vmatrix} \quad (5.7)$$

is not too small. $D = 0$ means that the glasses lie on a line in the P_d - V diagram. The glasses in Abbe's time (end of 19th century) had this property [5, Chap. 5]. Since then materials have become available that allow a workable solution for the apochromatic thin triplet and other apochromatic systems (such as microscope objectives).

5.1.4 Colour Correction in Two-Component Systems

The power of a two-component system is given by

$$K = K_1 + K_2 - dK_1 K_2 \quad (5.8)$$

See (1.26) of Sect. 1.3.

In (5.8), d is the distance between the components.

The power dispersion is given by

$$\delta K_{CF} = \frac{K_1}{V_1} + \frac{K_2}{V_2} - d \left(K_1 \frac{K_2}{V_2} + K_2 \frac{K_1}{V_1} \right) \quad (5.9)$$

We can make δK zero by an apt choice of d ; this is even possible when $V_1 = V_2$ and we obtain

$$d = \frac{1}{2} \left(\frac{1}{K_1} + \frac{1}{K_2} \right) = \frac{1}{2} (f_1' + f_2') \quad (5.10)$$

This principle of correction has been applied in classical oculars, those of Huygens and Ramsden. It turns out that it helps in the correction of TCA. The coefficient of TCA for a system of thin lenses of the same glass is given by

$$C_2 = \frac{h_1 \bar{h}_1 K_1}{V_1} + \frac{h_2 \bar{h}_2 K_2}{V_2} \quad (5.11)$$

From Fig. 5.2, that shows a lay-out of the Ramsden ocular, we see that $h_1 = 0$ and $\bar{h}_1 \cong 0$, so that C_2 is quite small. A practical version of the Ramsden ocular (see Sect. 6.2) has a smaller value of d so that C_2 is small, but not zero.

Fig. 5.2 Lay-out of the Ramsden ocular; f is the focal length of the ocular

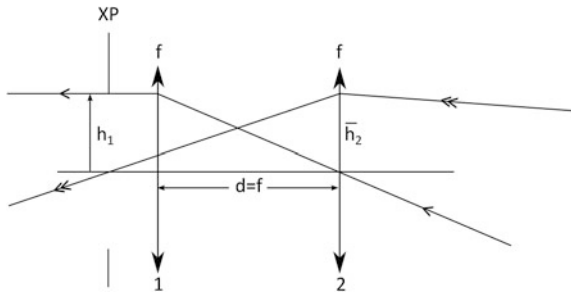
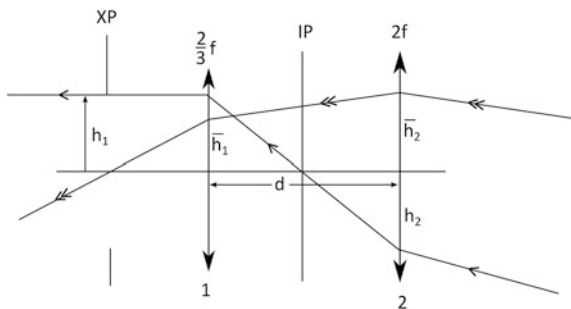


Fig. 5.3 Lay-out of the Huygens ocular; f is the focal length of the ocular, $d = 4f/3$



In the lay-out of the Huygens ocular shown in Fig. 5.3, we have $h_2 = -h_1$ and h_1, \bar{h}_2 both positive and nearly equal, so that C_2 is small.

The colour correction of general two-component systems, where d usually has a value different from $\frac{1}{2}(f'_1 + f'_2)$ and the stop position is not necessarily given, is governed by the following equations

$$\begin{aligned} \text{LCA: } & C_{1A} + C_{1B} = 0 \\ \text{TCA: } & C_{2A} + C_{2B} = q_A C_{1A} + q_B C_{1B} = 0 \end{aligned} \quad (5.12)$$

where A and B denote the components, and $q = \bar{h}/h$ as before. These equations can be solved by $q_A = q_B$, meaning two lenses in contact; this case was treated above. When we need the distance between the components (for instance to correct astigmatism) we must have $C_{1A} = C_{1B} = 0$. Two components at a distance must be corrected for colour separately. This applies to all lenses discussed in Sect. 6.3 on two-component systems.

5.1.5 Buried Surface

When we need a value of V or n that is not available in the glass catalogue, it is possible to divide the lens element in two pieces.

When we have the right value for n we can take two glasses with this index and different values of V and solve the equations

$$\begin{aligned} K &= K_1 + K_2 \\ \frac{K}{V} &= \frac{K_1}{V_1} + \frac{K_2}{V_2} \end{aligned} \quad (5.13)$$

for K_1 and K_2 so that we obtain the wanted value of V . This method can be applied in the design of Tessar. See Sect. 6.4.

It is also possible to obtain a value of n from two pieces with the same value of V by solving for K_1 and K_2 the equations

$$\begin{aligned} K &= K_1 + K_2 \\ \frac{K}{n} &= \frac{K_1}{n_1} + \frac{K_2}{n_2} \end{aligned} \quad (5.14)$$

This type of buried surface can be used to have a better control of higher order aberrations without disturbing colour correction [6, p. 19] and also for the reduction of field curvature.

5.1.6 Glass Selection

Earlier in this section we saw that for the colour correction of thin doublets (and also the doublet components of two-component systems) we need glasses with high and low values of the V -number. With a high value of the difference $V_1 - V_2$ we find relatively small power values of the doublet elements, see (5.4).

We found also materials for doublets that ensure a further correction of secondary spectrum. For the glass selection for thin apochromat triplets we refer to the literature [1, Sect. 5.6].

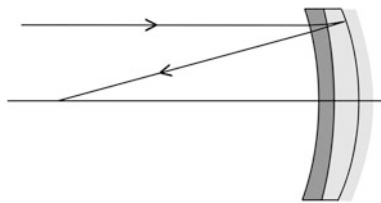
Glass selection in the design of triplets and triplet variants is a complicated subject. We will treat some aspects of it in Sect. 6.4.

With symmetrical four-component systems that are mainly applied in photography, the glass selection will occur in the same way as with two-component systems.

Glass selection is of prime importance in the design of high-power, flat field apochromatic micro-objectives, not only because of colour correction, but also with respect to field flattening. See Sect. 5.5 and Sect. 6.6 on micro-objectives.

With stepper lenses the source of radiation is either a high-pressure Hg-discharge or an excimer laser. As only one Hg-wavelength is used (g, h or i-line) the colour correction is relatively easy, also because the design has many degrees of freedom. With excimer laser illumination the situation is different. The spectral range of the source is small, but not zero because of wavelength drift. But at UV wavelengths of

Fig. 5.4 An achromatized Mangin mirror



248 nm and beyond the choice of materials is small: quartz glass (amorphous SiO₂) and CaF₂ or other fluorides. With care a sufficient correction of “colour” is possible.

In Sect. 6.7 we will treat some applications of aspheric surfaces. There we will discuss some mirror systems that have no need of colour correction at all.

In order to create degrees of freedom, refractive correction components can be introduced and mirrors can be transformed to katadioptric components (Mangin mirrors) so that colour correction becomes again necessary. With correctors colour aberrations are of minor importance, with Mangin mirrors we are with the doublets again. For applications of Mangin mirrors see Kidger [7, Chap. 13]. See also Fig. 5.4.

In many cases glass selection is done already in the lay-out phase of the design. Because it influences the quality of the end result this is a risk for the designer, who has to lean on his/her experience. It can be necessary to re-optimize with glasses in the neighborhood of the original selection.

5.2 Changing the Number of Variables

We discuss the following methods of changing the number of variables during one of the stages of the design process:

- splitting or adding lenses
- adding system properties
- adding an airspace
- aspherizing.

5.2.1 *Splitting or Adding Lenses*

When the designer judges that the “load” of a system component is too high, he/she has the option to divide the load over several elements. One way of estimating the load is comparing the aberration coefficients of the components (or surfaces).

A simple way to reduce the load of an element is splitting it into two or more elements near to each other. The sum of powers of these should be equal to the power of the original element.

Because the aberration coefficients S_1 and S_2 depend nonlinearly on power (see Sects. 3.3 and 4.3) the aberrations of the splitted component will be smaller than those of the original one.

The shape factors of the new elements must be adapted to reap the full profit of splitting. Note that also the position factors must be calculated anew. This can lead to a further decrease of the aberrations; see [8, Chap. 5].

Splitting is applied in the design of aplanatic focusing systems (for laser beams), microscope objectives and stepper lenses (see Sect. 6.6). In camera objective designs splitting often occurs; see Chap. 6, Sects. 6.4 and 6.5.

When we want to extend the performance of a system, it is an option to add one or more lenses. This happened with almost all types of camera lenses in the course of time [9]. With microscope objectives it leads to a modular design method, as we will see in Sect. 6.6.

A further degree of freedom can be obtained by shifting power between elements of a component, or even between components. This can change the paraxial parameters; one should be careful in using this stratagem.

5.2.2 Adding System Properties

Sometimes the lay-out of a system provides us with more degrees of freedom than we need according to the specification. By adding new, desirable properties to the system we can reduce the number of variables, taking care to preserve enough for the completion of the design.

We will give an example of this method by discussing the lay-out of a low power microscope objective. Such objectives usually consist of two achromatic doublets. Suppose that we want this system to be corrected for chromatic aberrations, spherical and coma.

It is clear that both components must be corrected separately for colour (see Sect. 5.1). We postpone the colour correction and begin the lay-out with two thin lenses with power K_1 and K_2 at a distance d . The power is given by

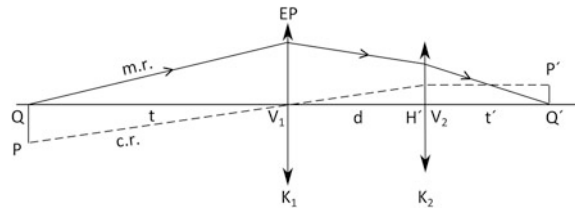
$$K = K_1 + K_2 - dK_1 K_2$$

and the positions of the principal planes by

$$\begin{aligned} V_2 H' &= -d \frac{K_1}{K}, \\ V_1 H &= -d \frac{K_2}{K}. \end{aligned}$$

With $V_2 Q' = t'$ and $V_1 Q = t$ the distance $q = QQ'$ from object to image is now given by

Fig. 5.5 Lay-out of a low-power microscope objective, notation



$$q = -t + d + t'.$$

The free working distance t' and the magnification μ are given. We have four degrees of freedom, K_1 , K_2 , d and t . Therefore we can make two choices for our variables.

We first take $K_2d = 1$. We obtain $K = K_2$ and $d = \frac{1}{K}$. When we put the stop at the first lens, the system is telecentric.

Secondly we make the deviations of the marginal ray equal at both components. We must have $h_1 K_1 = h_2 K_2$. Because $h_1/t\mu = h_2/t'$ this requires that

$$K_1 t\mu = K_2 t' = K t'.$$

This determines the lay-out (see Fig. 5.5).

The two components will be both achromats. We can correct spherical and coma by varying the bendings of both lenses.

We solve the lay-out with the stop at the first lens.

From the imaging equation $\frac{1}{s'} = \frac{1}{s} + K$ and $\mu = \frac{s'}{s}$ we have $s = \frac{(1-\mu)}{K\mu}$, $s' = \frac{(1-\mu)}{K}$.

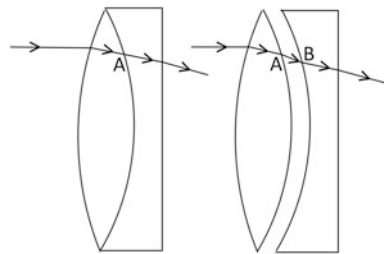
With $s = t - d$ and $s' = t' + \frac{K_1 d}{K}$, $d = \frac{1}{K}$ we obtain

$$t = \frac{d}{\mu}, \quad K = \frac{1-\mu}{2t'}, \quad d = \frac{2t'}{1-\mu}, \quad K_2 = K, \quad K_1 = \frac{(1-\mu)^2}{4t'}, \quad t = \frac{2t'}{(1-\mu)\mu}, \quad q = t' \left(1 - \frac{2}{\mu} \right).$$

In the following table we show a number of lay-outs that can be obtained, at different values of the magnification.

	$\mu = -1$	$\mu = -\frac{1}{2}$	$\mu = -\frac{1}{3}$	$\mu = -\frac{1}{5}$	$\mu = -\frac{1}{10}$
K_1	$\frac{1}{t'}$	$\frac{9}{16t'}$	$\frac{4}{9t'}$	$\frac{9}{25t'}$	$\frac{121}{400t'}$
K_2	$\frac{1}{t'}$	$\frac{3}{4t'}$	$\frac{2}{3t'}$	$\frac{3}{5t'}$	$\frac{11}{20t'}$
K	$\frac{1}{t'}$	$\frac{3}{4t'}$	$\frac{2}{3t'}$	$\frac{3}{5t'}$	$\frac{11}{20t'}$
d	t'	$\frac{4}{3t'}$	$\frac{3}{2t'}$	$\frac{5t'}{3}$	$\frac{200t'}{11}$
t	$-t'$	$-\frac{8}{3t'}$	$-\frac{9}{2t'}$	$-\frac{25t'}{3}$	$\frac{200t'}{11}$
q	$3t'$	$5t'$	$7t'$	$11t'$	$21t'$

We see that with $\mu = -\frac{1}{m}$, $q = t'(2m + 1)$.

Fig. 5.6 Adding an airspace

5.2.3 Adding an Airspace

Suppose that we take a cemented doublet apart and create a small airspace. Instead of the small ray deviation at A in the cemented doublet (see Fig. 5.6) we get much larger deviations from glass to air and back to glass at A and B in the airspace version. The ray height in B will be different from that in A, so that we obtain a “differential” aberration. Higher order aberrations are affected more strongly by differentiation than Seidel aberrations and primary parameters (such as LCD and TCA), so that adding an airspace is a means to influence the balance between third and higher orders.

We can also introduce different curvatures on both sides of the airspace; this helps in the correction of coma and higher order (“zonal”) spherical.

The balancing of different orders of spherical aberration is illustrated in Fig. 5.7.

When we have 3rd and 5th order spherical of opposite sign and equal value at the edge of the pupil, we have a rest of *zonal aberration* at $y_r = 0.7$. See Fig. 5.7a.

A more precise balancing can be obtained when 3rd and 7th order balanced against the fifth. See Fig. 5.7b.

The thickness of the airspace is a further degree of freedom; when the airspace becomes larger than a few mm we have a new design form called a dialyte. This form is used in the design of Celor, see Sect. 6.5.

5.2.4 Aspherizing

Aspheric surfaces are usually described by giving the axial coordinate z as a function of h^2 , where h is the distance from the axis. The description takes the form

$$z = \frac{h^2 c}{1 + \sqrt{1 - e(hc)^2}} + \sum_{n=2}^{\infty} A_{2n} \frac{(hc)^{2n}}{c} \quad (5.15)$$

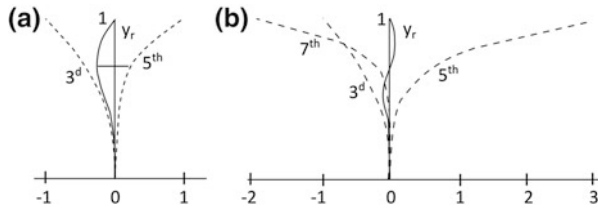


Fig. 5.7 Balancing spherical aberration, **a** between 3d and 5th order, **b** between 3d 5th and 7th order

The first term in (5.15) describes a conic section, with axial curvature c and eccentricity $1 - e$. Depending on the value of e , we have, with

- $e < 0$, a hyperbola,
- $e = 0$, a parabola,
- $e > 0$, an ellipse,
- $e = 1$, a circle.

To the conic section term separate terms can be added; e and the coefficients A_{2n} can be considered as extra degrees of freedom.

The additions to the third order aberrations caused by the aspherizing a surface are given by

$$\begin{aligned}\Delta S_1 &= \kappa h^4 (n' - n), \\ \Delta S_2 &= \kappa h^3 \bar{h} (n' - n), \\ \Delta S_3 &= \kappa h^2 \bar{h}^2 (n' - n), \\ \Delta S_5 &= \kappa h \bar{h}^3 (n' - n),\end{aligned}\tag{5.16}$$

where

$\kappa = c^3(e - 1)$ with a conoid surface, or $\kappa = 8c^3A_4$ with a fourth order asphericity.

When $\bar{h} = 0$ (surface conjugate to the pupil) only S_1 is different from zero.

With $h = 0$ (surface conjugate to the object) all third order terms are zero in (5.16).

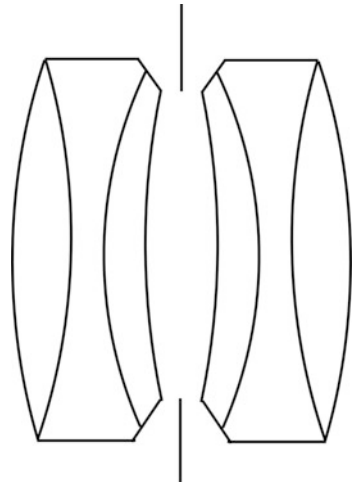
When $h = \bar{h}$ all third order terms are equal.

This gives a quick estimate of the influence of a fourth order asphericity.

Note that aspherizing does not change the paraxial parameters of the system. Also the field curvature is not influenced by aspherizing.

More material on aspherics can be found in Shannon's book [10, Chap. 7]. We will treat the application of aspheric surfaces in Sect. 6.7.

Fig. 5.8 A symmetric Dagor



5.3 Symmetries

The axial symmetry of the systems that we consider in this book makes that the wavefront error can be described as a function of the second order coordinates U , V , W that we defined in [Sect. 4.1](#). With wavefront errors of even order there will be transverse aberrations of uneven order only.

When the symmetry is broken, for instance by centring errors in the fabrication, aberrations of even order will arise as well. We met some of these in [Sect. 4.6](#) on tolerancing.

In this section we discuss some forms of additional symmetry: mirror symmetry and concentric symmetry. We add a description of the properties of aplanatic surfaces.

5.3.1 Mirror Symmetry

Systems that have a symmetry plane perpendicular to their axis (with the stop in the symmetry plane) are often used as a starting point for the design of camera objectives. Examples are Dagor and Biotar, from which the Double-Gauss type was developed [9]. Actual Double-Gauss objectives usually depart slightly from mirror symmetry: one speaks of “symmetric” and “hemi-symmetric” systems.

In Fig. 5.8 we show a symmetric Dagor, designed by P. Rudolph.

When a symmetric system is used at a magnification $M = -1$, it follows from symmetry that distortion, coma and lateral colour are absent. This can be seen from (3.15) of [Sect. 3.3](#), because the values of $\bar{A} = \bar{n}$ in both halves of the systems are opposite. It is illustrated in Fig. 5.9, where we have assumed that spherical and

Fig. 5.9 The Symmetric Principle (after Kingslake and Johnson [1])

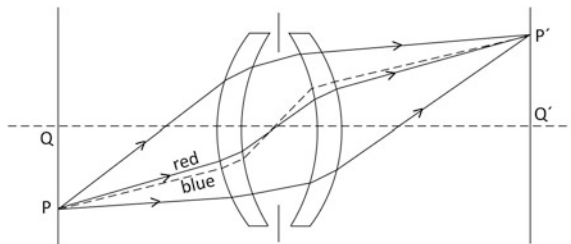
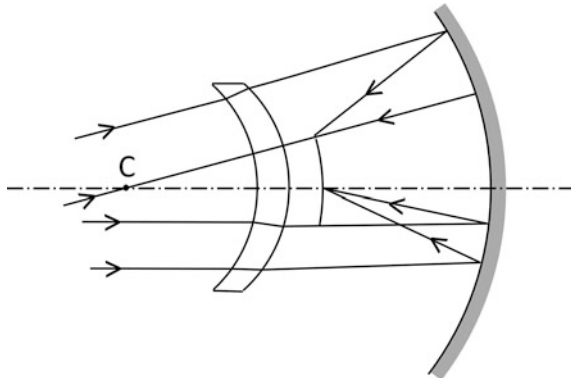


Fig. 5.10 Bouwers telescope objective



meridional field curvature, as well as longitudinal colour, have been corrected. This makes the figure more clear without changing its message.

Symmetric systems are often used with object at infinity, or far away. Then the freedom of distortion is only given when the position of the pupils is independent of the field, which is usually not the case with wide-angle lenses. Also lateral colour can only be corrected when the pupil positions do not depend on wavelength.

Usually coma can be corrected by a small asymmetry.

We discuss examples of mirror-symmetric systems in Sect. 6.5.

5.3.2 Concentric Systems

When all surfaces of a system have a common center of curvature, and the stop is at the center too, the system is called concentric. A concentric system can only have spherical aberration (of all orders); each line through the center is an axis of symmetry.

The image field and the object field will be concentric as well. See Fig. 5.10 where we show a telescope objective designed by Bouwers [11]. In Sect. 6.7 we discuss the Schmidt camera, a concentric system with an aspheric corrector at the stop.

Fig. 5.11 Aplanatic surface,
 $CP = \frac{n'}{n}r$, $CP' = \frac{n}{n'}r$

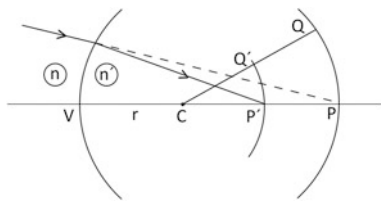


Fig. 5.12 Aplanatic lenses: a
 planar-aplanatic, b
 concentric-aplanatic

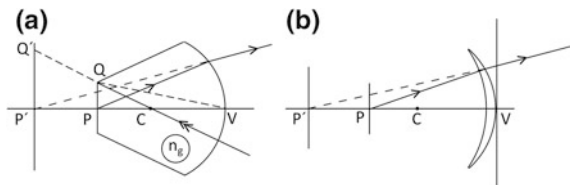
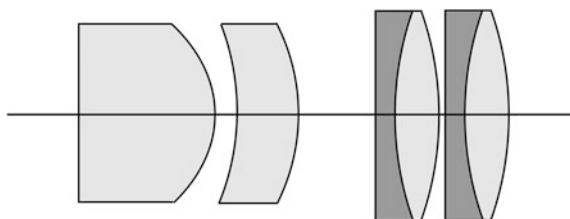


Fig. 5.13 Achromat NA
 0.65/40x. Scale 10:1



Although in practice there are few strictly concentric systems, the idea of concentricity is in the background of many designs: the triplet and its relatives and wide-angle lenses such as Glatzel's Hologon (see Sect. 6.5).

5.3.3 Aplanatic Surfaces

In Sect. 3.5 we introduced the aplanatic surface. See Fig. 5.11 for the notation.

A spherical surface can make a stigmatic image P' of an object P when the axial distance CP is equal to $n'r/n$. The image is found at $CP' = nr/n'$.

With aplanatic surfaces lenses can be constructed, as shown in Fig. 5.12. The lens of Fig. 5.12a is used often as a front lens in high power microscope objectives, at a magnification $M = n^2$. In the thin lens of Fig. 5.12b, the first surface is centered on P (so that $A = ni = 0$, see Sect. 3.5). The second surface is aplanatic, the magnification is now $M = n$. The two lenses of Fig. 5.12 can be used as a *duplex front* in a microscope objective; this part of the objective multiplies the (paraxial) numerical aperture by a factor of n^3 . An example is given in Fig. 5.13. For an application see Sect. 6.6.

5.4 Stops and Diaphragms

In Sect. 1.5 we considered stops and pupils; the stop shift equations were given in Sect. 3.4. In this section we discuss the position of the stop as a design variable. A related subject, vignetting, is also treated in this section.

5.4.1 Stop Position

A pure example of the use of the stop as a design variable is the landscape lens (see also Sect. 4.1). For a simple camera objective we use a single lens or a thin doublet, that will have a finite value of S_1 . We position the stop so that coma is corrected. We must have

$$q = -\frac{S_2}{S_1} \quad (5.17)$$

With (3.24) of Sect. 3.4 we can calculate the position of the stop. Now we use the form factor (bending) of the lens to correct astigmatism. With the stop shift equation

$$S_3^* = S_3 + 2qS_2 + q^2S_1 \quad (5.18)$$

and (5.17) we find that we will have $S_3^* = 0$ when

$$S_1S_3 = S_2^2 \quad (5.19)$$

This example is worked out further in Sect. 6.1.

There are cases where the stop position of a system is given. For instance, when two optical systems are coupled. When the light from system 1 must enter system 2 without losses, the entrance pupil of system 2 must coincide with the exit pupil of system 1.

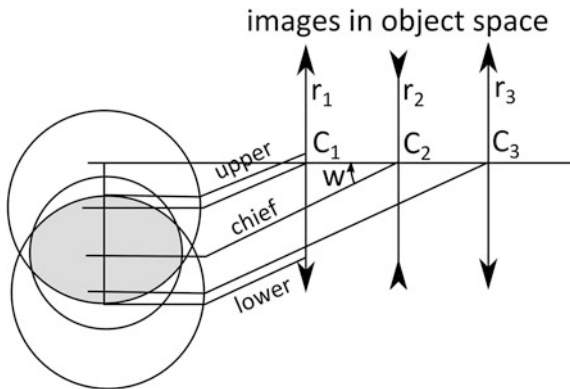
Oculars are good examples; the light from the lens must be coupled into the eye of the user. Therefore the exit pupil of an ocular must be at some distance (called the *eye relief*) from the last surface of the system. See Sect. 6.2.

With more complicated systems the stop shift equations can be used, in the thin lens predesign, to estimate the possibilities for correction. We give the example of a two-component system of which both components are corrected for spherical and coma. The stop shift equations now reduce to

$$S_5^* = q_1(3S_{31} + S_{41}) + q_2(3S_{32} + S_{42}) \quad (5.20)$$

and we can immediately see what the residual distortion will become. When the stop position is free we can use a stop shift for correction. In Sects. 6.3–6.6 there will be many examples of this use of the stop shift equations.

Fig. 5.14 Vignetting in a triplet (thin lens) design. The upper and lower rim rays (for $w = 25^\circ$) and the chief ray are shown



5.4.2 Vignetting

Kingslake and Johnson [1] has the following method to make a vignetting diagram (see Fig. 5.14). It is applied here to a triplet. The method uses the thin lens model of the system. The second and third lens are imaged in the object space. Their image radii and central points r_2 , r_3 , C_2 , C_3 are now known. Together with r_1 , C_1 this gives three circles in a given oblique direction ($w = 25^\circ$ in the figure). The overlapping part of the three circles (hatched in the figure) is the free aperture.

Vignetting reduces the radiation flux in oblique directions. In the design of photographic objectives, vignetting is used to cut off rays that have severe aberrations. Higher order aberrations, such as oblique spherical, can be reduced by just a little vignetting of the meridional fan. See Kingslake's dialyte and double-Gauss designs [1, pp. 242–249].

Note that the effect of vignetting is strongest in the meridional ray fan. But there the aberrations are usually larger than in the sagittal fan.

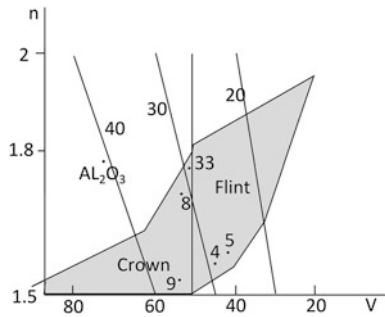
5.5 Field Correction

In this section we treat methods to correct field curvature, astigmatism and distortion.

5.5.1 Field Curvature

Among the third order aberrations, field curvature has a special position. Its coefficient depends only on the powers and refractive indices, as we have seen in Sects. 3.3, 3.4 and 4.3. Care must be taken to correct field curvature in the early

Fig. 5.15 Schematic version of the glass chart. Existing glasses are in the grey area. Contours of $V/n = 20, 30, 40$ are shown



stages of the design process. We discuss the following methods to correct or reduce field curvature:

- glass selection,
- components of negative power,
- use of mirrors.

Glass selection is important with thin systems, where we have no other possibility to correct field curvature. The Petzval sum of a thin doublet achromat is given by

$$P = \left(\frac{V_1}{n_1} - \frac{V_2}{n_2} \right) \frac{K}{V_1 - V_2} \quad (5.21)$$

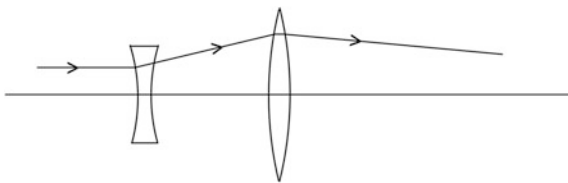
meaning that $V_1/n_1 - V_2/n_2$ should be small and $V_1 - V_2$ large to make P/K small. It is easy to see from the glass chart that this is not well possible for existing glasses. See Fig. 5.15, where we have drawn contours of $V/n = 20, 30, 40$ in the glass chart. We see that on these contours, within the region of existence, the variation of V is limited.

In the following table we give the results for different glass combinations. In the table we use the Schott code to indicate the indices and dispersion parameters of the glasses. In this code the first three numbers denote the first three decimals of n , the following three numbers denote $10 V$.

Table, Field curvature in doublet achromats

Glass 1	Code	K_1/K	Glass 2	Code	K_2/K	P/K
K5	524592	2.56	F2	624361	-1.56	0.72
LAK 8	716536	4.12	LF 5	585406	-3.12	0.43
LAK 33	757522	4.50	LF 5	585406	-3.50	0.35
Al_2O_3	771720	2.56	LLF 4	564450	-1.56	0.42
Al_2O_3	771720	3.60	N-KF 9	523515	-2.60	0.35

Fig. 5.16 Reduction of field curvature



As a benchmark we show a doublet with “old” glasses. With glasses with high indices for the crowns and low indices for the flints we can obtain reduction of field curvature, but the component powers of the doublet become quite high. Such a lens is called a new-achromat [1, p. 305]. We have introduced Al_2O_3 as a “crown glass”, with n , V values outside the glass region, to show that reduction of the Petzval sum is possible, with decent values of the powers, but at a price.

When we use components with powers of opposite sign at a distance, a reduction of field curvature can be obtained. This can be used in the design of two-component systems and triplets.

Kidger [7] gives a lay-out of the tele-objective with two components of powers K and $-K$ at a distance $d = 1/K$; it has system power K and zero Petzval sum.

A triplet design of Kingslake and Johnson [1, p. 116] has glasses SK 16 (622602) and SF 2 (627366) and a Petzval sum $P = 0.38 K$.

A meniscus lens with radii of equal magnitude also has a zero Petzval sum. The power of such a lens is

$$K = c^2(n - 1)^2 \cdot d/n \quad (5.22)$$

In flat-field microscopes, stepper lenses and wide-field camera objectives the combination occurs of a negative component in front of a positive one. See Fig. 5.16.

Because the negative component increases the ray height of the marginal ray, the positive lens can produce a higher deviation. The combination has a reduced Petzval sum as compared with a single positive component with the same ray deviation.

In Sect. 3.5 it was noted that a surface in a plane conjugate with the object plane has no aberrations except the field curvature. It also does not change image position and magnification. In systems with an inherent positive field curvature, such as the Petzval objective, a negative lens near the image plane can therefore be used as a *field flattener*.

A spherical mirror has a field curvature coefficient

$$S_4 = 2H^2c = -H^2K \quad (5.23)$$

With a positive power it has a negative field curvature.

The Dyson lens of Fig. 5.17, that has been used as a 1:1 projection lens in photolithography [12] does not have third order aberrations when $c_m = (n - 1) c_g/n$. It is a concentric system with compensated field curvature.

Fig. 5.17 The Dyson lens has no third order aberrations if $r_m = \frac{n}{n-1} r_g$

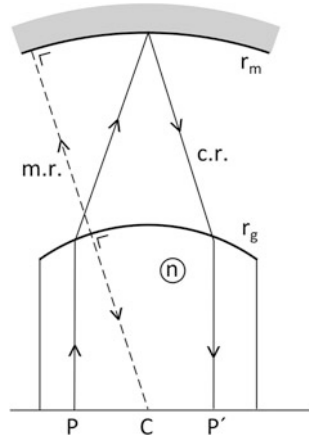
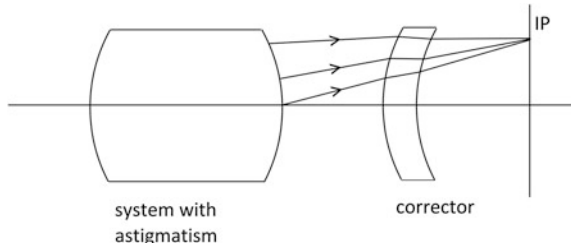


Fig. 5.18 Correction of astigmatism



5.5.2 Astigmatism

A thin system has astigmatism given by

$$S_3 = H^2 K \quad (5.24)$$

when it is in contact with the stop. In Sect. 5.4 we saw already that astigmatism can be corrected by a remote stop when we have some spherical available. In general we can correct astigmatism only when we have not too small distances between the components. Simultaneous correction of spherical, coma and astigmatism will then succeed only when the components have finite amounts of spherical and coma.

A thin meniscus, acting as a tilted plate of which the tilt is roughly proportional to the field angle, can be used to correct residual astigmatism. See [8, p. 77] and Fig. 5.18. For the aberrations of a tilted plate see [13, Sect. 7.8].

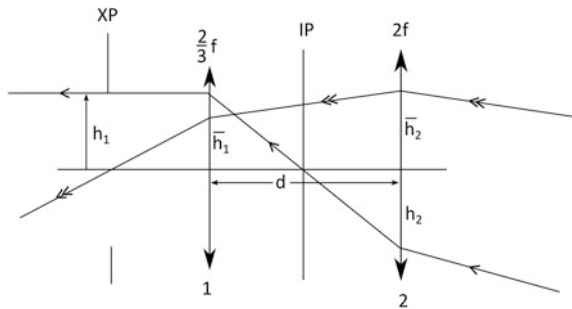


Fig. 5.19 Lay-out of the Huygens ocular

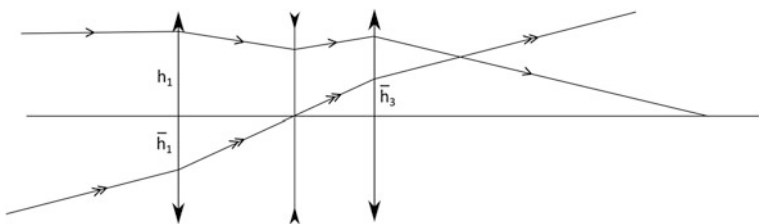


Fig. 5.20 Triplet lay-out

5.5.3 Distortion

We have found three situations where distortion is absent:

- with a thin system at the stop (see 4.17)
- with a system with mirror symmetry, at magnification $M = -1$ (see Sect. 5.3)
- with concentric systems, when we allow a concentric image field (also Sect. 5.3).

This can give a hint how the Correction of distortion can be tackled.

In many design situations the Correction of astigmatism and field curvature is contrary to the Correction of distortion.

We give two examples. In Fig. 5.19 we show the lay-out of the Huygens ocular again.

The chief ray heights \bar{h}_1, \bar{h}_2 are both positive, and the marginal ray heights h_1, h_2 have opposite signs. This means that the leading terms of distortion oppose each other and the leading terms of astigmatism add up, as well as the two terms of field curvature (see 4.17). The balancing of distortion will be easier than of astigmatism.

The second example concerns a triplet lay-out, Fig. 5.20. Here we have opposite values of \bar{h}_1 and \bar{h}_3 , with $\bar{h}_2 = 0$, and positive values of h_1, h_2 and h_3 . Again the leading distortion terms are balanced and all leading astigmatism terms

add up, but the second component has a negative contribution. Distortion in the Cooke triplet (Sect. 6.4) can be corrected quite well, but meridional field curvature is more difficult.

References

1. R. Kingslake, R.B. Johnson, *Lens Design Fundamentals*, 2nd edn. (SPIE Press/Academic Press, Washington, Massachusetts, 2010)
2. S. Musikant, *Optical Materials* (Marcel Dekker, New York, 1985)
3. G. Litfin (ed.), *Technische Optik in der Praxis*, 2nd edn. (Springer, Germany, 2001)
4. D. O'Shea, *Elements of Modern Optical Design* (Wiley, New York, 1985)
5. D. Shafer, Optical design and the relaxation response. SPIE Proc. **766**, 2 (1987)
6. F.I. Havlicek, Einführung in das korrigieren optischer Systeme, Wissenschaftlicher Verlagsgesellschaft (1960)
7. M. Kidger, *Fundamental Optical Design* (SPIE Press, Washington, 2001)
8. R. Fischer, B. Tadic-Galeb, P.R. Yoder, *Optical System Design*, 2nd edn. (SPIE Press, Washington, 2008)
9. R. Kingslake, *A History of the Photographic Objective* (Academic Press, Massachusetts, 1989)
10. R. Shannon, *The Art and Science of Optical Design* (Cambridge University Press, Cambridge, 1997)
11. A. Bouwers, *Achievements in Optics* (Elsevier, Amsterdam, 1946)
12. J.R. Sheats, B.W. Smith, *Microlithography, Science and Technology* (Marcel Dekker, New York, 1998)
13. W. Smith, *Modern Optical Engineering*, 2nd edn. (SPIE Press, Washington, 2008)

Chapter 6

Design Examples

In this chapter we discuss a number of designs in more detail. We take our examples from the following categories of systems

- thin systems,
- telescopes, especially the oculars,
- two-component, asymmetric objectives,
- triplets and related systems,
- symmetric four-component systems,
- micro-objectives,
- mirror objectives.

We will treat the different design examples of this chapter in different ways.

With the thin systems that we will consider, singlets and thin doublets, we will treat the thin lens predesign in detail. The results of that ([Sect. 6.1](#)) will be used many times in the following sections.

The design of a simple telescope in [Sect. 6.2](#) is completed by a third order analysis and computer optimization.

In the following [Sects. 6.3, 6.4, 6.5](#), we also perform the complete design process, without the tolerance calculations.

In [Sect. 6.6](#) we also show how centring tolerances can be calculated by the method outlined in [Sect. 4.6](#).

In [Sect. 6.7](#) we treat the application of aspherical surfaces in the third order only, because this shows the principles of this technique most clearly.

We will finally treat mirror objectives by considering the third order aberrations of two-mirror systems, as in the work of Schwarzschild [1].

6.1 Thin Systems

A thin system is defined as a system where the distances between the components are small compared to the system focal length.

6.1.1 Single Lens

We discuss first the application of a single lens as a landscape lens. It is clear that we cannot correct chromatic aberrations in this case; the only thing that is possible is to select a glass with low dispersion (high V value).

We will use the two degrees of freedom: stop position and bending; the focal length of our lens we take as $f = 100$ mm.

The first four Seidel coefficients of a thin lens at the stop we write as

$$\begin{aligned} S_1 &= \frac{1}{4} h^4 K^3 \{ \mu_1 B^2 + \mu_2 BC + \mu_3 C^2 + \mu_4 \}, \\ S_2 &= -\frac{1}{2} h^2 HK^2 \{ \mu_5 B + \mu_6 C \}, \\ S_3 &= H^2 K, \\ S_4 &= \frac{H^2 K}{n}, \end{aligned} \quad (6.1)$$

where we use the notation of H. Coddington as given in the book of van Heel [2, Chap. 9].

We show a table of the μ_i coefficients below, from Van Heel [3].

$n =$	1.5	1.55	1.6	1.65	1.7	1.75	1.8
$\mu_1 = \frac{n+2}{n(n-1)^2}$	9.33	7.57	6.25	5.24	4.44	3.81	3.30
$\mu_2 = \frac{4(n+1)}{n(n-1)}$	13.33	11.96	10.83	9.88	9.08	8.38	7.78
$\mu_3 = \frac{3n+2}{n}$	4.33	4.29	4.25	4.21	4.18	4.14	4.11
$\mu_4 = \frac{n^2}{(n-1)^2}$	9.00	7.94	7.11	6.44	5.90	5.44	5.06
$\mu_5 = \frac{(n+1)}{n(n-1)}$	3.33	2.99	2.71	2.47	2.27	2.10	1.94
$\mu_6 = 2 + \frac{1}{n}$	2.67	2.65	2.62	2.61	2.59	2.57	2.56

With a remote stop we have, as in (4.17) the stop shift equations

$$S_2^* = S_2 + \left(\frac{\bar{h}}{h} \right) S_1, \quad S_3^* = S_3 + 2 \left(\frac{\bar{h}}{h} \right) S_2 + \left(\frac{\bar{h}}{h} \right)^2 S_1,$$

where $\bar{h} = wt$, w is the field angle and t is the distance from the entrance pupil to the lens.

We will take $\frac{\bar{h}}{h} = -\frac{S_2}{S_1}$ so that $S_2^* = 0$ and $S_3^* = S_3 - \frac{S_2^2}{S_1}$.

Correction of coma and astigmatism requires $S_3 = \frac{S_2^2}{S_1}$.

Using the thin lens aberration formulas (6.1), we can write this as a quadratic equation in B

$$(\mu_1 B^2 + \mu_2 BG + \mu_3 G^2 + \mu_4) = (\mu_5 B + \mu_6 G)^2$$

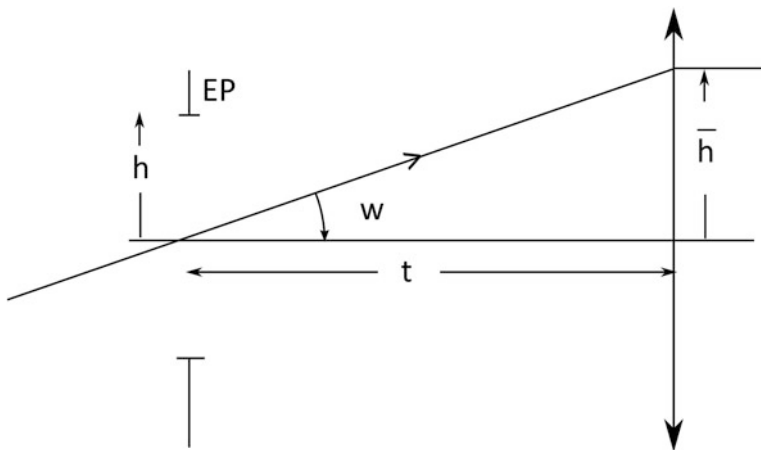


Fig. 6.1 Lay-out of landscape lens

or, with $G = -1$ (object at infinity),

$$(\mu_1 B^2 - \mu_2 B + \mu_3 + \mu_4) = (\mu_5 B - \mu_6)^2.$$

As an example we take $n = 1.5$; with the constants from the table we have the solutions

$$B_{(1)} = -1 \text{ and } B_{(2)} = 3.5.$$

For these values we want to calculate $\frac{\bar{h}}{h}$. The paraxial data that we need, are chosen as $\tan w = \frac{1}{3}$, $h = 4 \text{ mm}$, $H = hw = 1.33$, $K = 0.01$ (See Fig. 6.1).

For the first solution we now find

$$S_1 = 0.0023, S_2 = -0.0063, \frac{\bar{h}}{h} = 2.74, \bar{h} = 10.96, t = 32.86.$$

The curvatures of the lens are [see (4.15)]

$$c_1 = 0, c_2 = -0.02.$$

For the second solution we find

$$S_1 = 0.0052, S_2 = 0.0096, \frac{\bar{h}}{h} = -1.85, \bar{h} = -7.38, t = -22.15.$$

The curvatures of the lens are

$$c_1 = 0.045, c_2 = 0.025.$$

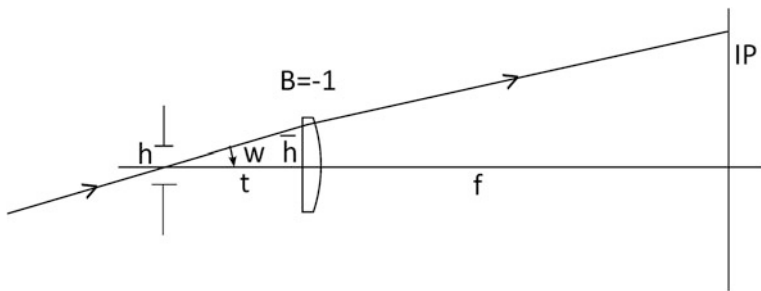


Fig. 6.2 Landscape lens, first solution

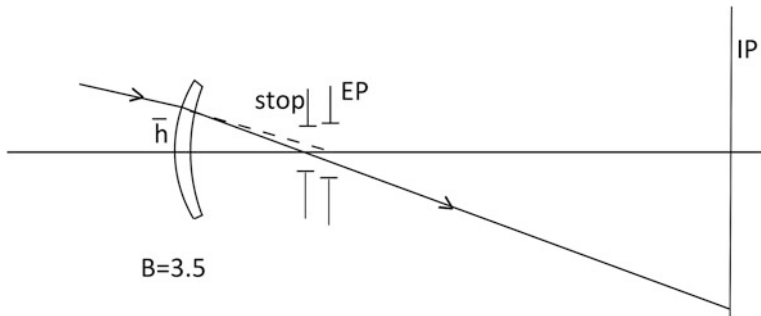


Fig. 6.3 Landscape lens, second solution

See Figs. 6.2 and 6.3.

The field curvature is $S_4 = 0.0118$, the aberration is $\delta\eta' = \delta\xi' = 0.147$ mm at the edge of the field, and 0.037 mm at half field.

The aberration due to spherical is $\delta\eta' = \delta\xi' = 0.029$ mm (first solution).

The lens is corrected as well as possible. Note that the plane-convex lens in the first solution does not have minimum spherical aberration. When we turn this lens around ($B = 1$) we have $S_1 = 0.0006$, very near to the minimum.

6.1.2 Doublets

The design of doublets is relatively straightforward and can be described by a clear procedure, as we shall see below. Doublets are used as telescope objectives, aplanatic, achromatic or apochromatic (see Sect. 6.2). Also doublets are indispensable as achromatic modules in two-component and four-component systems (Sects. 6.3 and 6.5), and in micro-objectives (Sect. 6.6). Although the original Cooke triplet was composed from single lenses, later members of the triplet family contain again doublets (see Sect. 6.4).

My teacher in Delft Technical University, professor Bram van Heel (1903–1966), was sometimes called by colleague designers “the doublet designer”. He considered that as a compliment. A later teacher, John McDonald [4], phrased the importance of doublet design as follows: “For example, the design of a “simple” achromatic doublet encompasses many of the pitfalls and many of the tricky parts of aberrational optical design and, indeed, anyone who has designed and finalized a design for a simple achromatic doublet can go on to drive safely on the highroad of optical design”.

The correction of axial chromatic aberration (LCA) was discussed in Sect. 4.2 in general terms.

With a thin doublet we have

$$C_1 = h^2 \left(\frac{K_1}{V_1} + \frac{K_2}{V_2} \right)$$

and $K = K_1 + K_2$, so that

$$K_1 = K \frac{V_1}{V_1 - V_2}, \quad K_2 = K \frac{-V_2}{V_1 - V_2}$$

for a crown-in-front doublet, and vice versa for a flint-in-front one.

Example: with $V_1 = 60$, $V_2 = 36$ we have $K_1 = 2.5$ K, $K_2 = -1.5$ K. These are normal values for an “old achromat”.

As the astigmatism of a thin system at the stop cannot be corrected, we treat this aberration first. We have

$$S_3 = H^2 K.$$

With $K = 0.01 \text{ mm}^{-1}$, $h = 5$ and $w = \frac{1}{20}$ we have $S_3 = 0.000625$.

The field curvature is given by

$$S_4 = H^2 \left(\frac{K_1}{n_1} + \frac{K_2}{n_2} \right).$$

In Sect. 5.5 we discussed the Petzval sum of thin doublets, for the example given above $n_1 = 1.524$ and $n_2 = 1.624$ are acceptable, this gives $S_4 = 0.72 \text{ H}^2 \text{K}$.

Now we can calculate the aberrations

$$\delta\eta' = \frac{(3S_3 + S_4)}{2n'u'} = 0.023 \text{ (mer.f.c.)},$$

$$\delta\xi' = \frac{(S_3 + S_4)}{2n'u'} = 0.011 \text{ (sag.f.c.)}.$$

We saw in Sect. 5.5 that by taking new glasses the Petzval sum can be reduced to about 0.45 K.

Before we consider spherical aberration and coma, we look first at the secondary spectrum. The difference in focal length between the F-line (486 nm) and the d-line (588 nm) is given by

$$\Delta f = f \frac{P_{d1} - P_{d2}}{V_1 - V_2}$$

where P is the partial dispersion (see Sect. 5.1) given by

$$P_d = \frac{n_F - n_d}{n_F - n_C}.$$

For “old” glasses $P_{d1} - P_{d2}$ would be of the order of 0.01, with $V_1 - V_2 \cong 25$, so that $\frac{\Delta f}{f} \cong 0.0004$. With “new” glasses, such as FK 51 and FK 52, $V_1 - V_2$ can be twice as high with the same value of $P_{d1} - P_{d2}$, so that $\frac{\Delta f}{f} \cong 0.0002$. With an aperture angle $u' = 0.05$ we obtain the aberration $\delta\eta' = 0.001$ for the d-line. This is much smaller than the aberrations due to field curvature and astigmatism.

Kingslake points out that an apochromatic doublet can be obtained when two glasses are chosen with equal partial dispersions and different values of n and V [5, Sect. 5.5].

He takes FK 52 and KzFS 2, $P_1 = P_2 = 0.4562$, $V_1 = 82$, $V_2 = 54$,

See also the paper of Mercado [6].

Correction of Doublets

The procedure for the correction of the monochromatic aberrations with a thin aplanatic doublet is as follows.

We write the equations for S_1 and S_2 , from (6.1)

$S_1 = S_{1a} + S_{1b}$, with

$$S_{1a} = \frac{1}{4} h^4 K_a^3 (\mu_{1a} B_a^2 + \mu_{2a} B_a G_a + \mu_{3a} G_a^2 + \mu_{4a})$$

$$S_{1b} = \frac{1}{4} h^4 K_b^3 (\mu_{1b} B_b^2 + \mu_{2b} B_b G_b + \mu_{3b} G_b^2 + \mu_{4b})$$

$S_2 = S_{2a} + S_{2b}$, with

$$S_{2a} = -\frac{1}{2} h^2 K_a^2 H (\mu_{5a} B_a + \mu_{6a} G_a)$$

$$S_{2b} = -\frac{1}{2} h^2 K_b^2 H (\mu_{5b} B_b + \mu_{6b} G_b)$$

where a denotes the front lens of the doublet and b the rear lens. The constants μ_i , with $i = 1 \dots 6$, were defined in the first part of this section, where also a table of μ_i as functions of the refractive index was given.

The position factors G_a and G_b follow from the condition for achromasy, as do the powers K_a and K_b , see above.

An aplanatic doublet must have $S_1 = 0$ and $S_2 = 0$.

$S_2 = 0$ leads to a linear relation between B_a and B_b . Using this relation we can eliminate one of the form factors from the equation $S_1 = 0$, so that a quadratic equation for B_a or B_b remains, from which the unknown can be solved. When B_a (or B_b) is known, B_b (or B_a) can be calculated from the coma condition.

The curvatures of the doublet can be calculated with (4.15):

$$c_1 = \frac{1}{2}(B + 1) \frac{K}{(n - 1)}$$

$$c_2 = \frac{1}{2}(B - 1) \frac{K}{(n - 1)}$$

Example

We choose glasses with

$$n_a = 1.70, V_a = 60, n_b = 1.60, V_b = 36$$

With $K = 0.01$ we now have

$$K_a = 0.025, K_b = -0.015$$

Taking $h = 10$ and $\tan w = 0.05$, so that $H = -0.5$

The position factors are given by

$$G_a = -1, G_b = (K + K_a)/K_a - K = 0.2333$$

We have the constants, from the table

μ_1	μ_2	μ_3	μ_4	μ_5	μ_6	
4.44	9.08	4.18	5.90	2.27	2.59	for $n = 1.7$
6.25	10.83	4.25	7.11	2.71	2.62	for $n = 1.6$

so that we obtain

$$S_1 = 0.03906(4.44B_a^2 - 9.08B_a + 10.08) - 0.008438(6.25B_b^2 + 25.27B_b + 30.25)$$

$$= (0.1734B_a^2 - 0.3547B_a + 0.3937) - (0.05273B_b^2 + 0.2132B_b + 0.2552)$$

$$S_2 = 0.01563(2.27B_a - 2.59) + 0.00563(2.71B_a + 6.11)$$

The coma condition $S_2 = 0$ leads to

$$B_b = -2.197B_a + 0.401$$

Elimination of B_b from $S_1 = 0$ gives

$$S_1 = 0.0811B_a^2 + 0.2065B_a + 0.0470 = 0$$

that has two solutions:

1. $B_a = -0.2102, B_b = 0.8624$
2. $B_a = 2.756, B_b = -5.654$

The first solution has the radii ($r_i \equiv 1/c_i$, in mm.)

$$\begin{aligned}r_1 &= 70.905 \\r_2 &= -46.273 \\r_3 &= -42.955 \\r_4 &= 581.395\end{aligned}$$

The radii of the second solution are

$$\begin{aligned}r_1 &= 14.910 \\r_2 &= 32.430 \\r_3 &= 17.190 \\r_4 &= 12.023\end{aligned}$$

Of the latter solution, three radii are smaller than $f/5$.

We show the lay-out of these doublets in Fig. 6.4. It is clear from the figure that the second solution is less useful than the first.

6.1.3 Aplanatic Doublets

We begin with a doublet with two “old” glasses, F 2 and K 5, so that $K_1 = 2.56$ K, and $K_2 = -1.56$ K. For glass data see the table in Sect. 5.1.

The Petzval sum is $P = 0.72$ K.

Inserting these data in the formulas for S_1 and S_2 , (6.1), we find the following solution for

$$\begin{aligned}S_1 &= 0, S_2 = 0 \\B_1 &= 1.62, B_2 = 4.79 \quad \text{or} \quad B_1 = -0.90, B_2 = 3.43.\end{aligned}$$

We discard the first solution because of the high value of B_2 .

The second solution has the radii, with $K = 0.01$,

$$\begin{aligned}r_1 &= 409.84 \\r_2 &= -21.55 \\r_3 &= -18.05 \\r_4 &= -32.78.\end{aligned}$$

The radii r_3 and r_2 are quite small (see Fig. 6.5). We cannot expect a good image quality from this doublet.

When we take the glasses N-SK5 and N-SF6, with $n_1 = 1.589$, $V_1 = 61.2$, $n_2 = 1.805$, $V_2 = 25.4$ we find $K_1 = 1.71$ K, $K_2 = -0.71$ K.

The Petzval sum is now $P = 0.68$ K.

Fig. 6.4 A healthy (a), and a sick (b) doublet

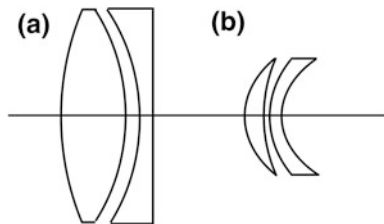
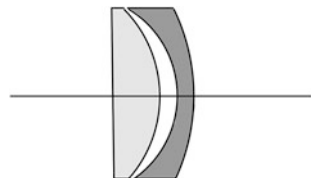


Fig. 6.5 A rough outline of the F 2-K 5 doublet



Inserting these data in the thin lens formulas for S_1 and S_2 , we find the following aplanatic solutions

1. $B_1 = 0$, $B_2 = 2.68$,
2. $B_1 = 19.14$, $B_2 = -152.35$.

The second solution is clearly not practical. Figure 6.6 shows a rough outline of the first solution of this doublet. It is of the split Fraunhofer type (“crown-in-front”).

The data for the previous example were taken from Kidger's book [7, p. 180]. The book follows a different strategy: correct first S_1 and afterwards optimize coma. From

$$S_1 = \frac{h^4 K^3}{4} \left\{ \left(31.07(B_1 - 0.86)^2 + 3.15 \right) - \left(1.18B_2^2 + 10.63B_1 + 21.81 \right) \right\}$$

we find $S_1 = 0$ for $B_1 = 0.86$, $B_2 = 0.97$ or -9.98 , $S_2 = 0.0045$ or -0.0049 .

With $B_1 = 0.7$, $B_2 = 0.97$ we obtain $S_1 = 0.0008$, $S_2 = 0.0038$.

A sketch of the doublet; with the curvatures and radii, is found below. See Fig. 6.7.

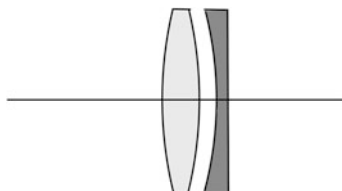
This is a typical Fraunhofer doublet.

With $B_1 = 1$, $B_2 = -9.98$ we obtain $S_1 = 0.0040$.

See the sketch and curvatures plus radii below, Fig. 6.8.

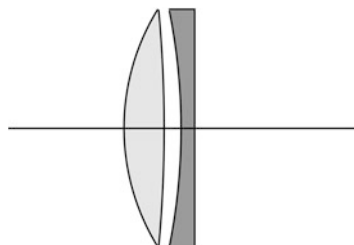
This looks like the Gauss doublet of Kidger. His Fig. 8.15 is missing, see also [7, p. 177].

Fig. 6.6 A rough outline of the N-SK5, N-SF6 doublet



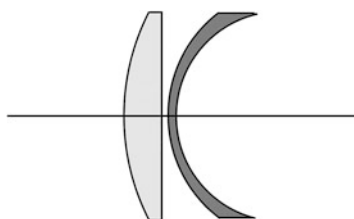
$$\begin{aligned}r_1 &= 68.9 \text{ mm} \\r_2 &= -68.9 \text{ mm} \\r_3 &= -61.3 \text{ mm} \\r_4 &= -134.1 \text{ mm}\end{aligned}$$

Fig. 6.7 The Fraunhofer solution of Kidger's doublet



$$\begin{aligned}r_1 &= 40.5 \text{ mm} \\r_2 &= -229.6 \text{ mm} \\r_3 &= -115.1 \text{ mm} \\r_4 &= 7559 \text{ mm}\end{aligned}$$

Fig. 6.8 The Gauss solution of Kidger's doublet



$$\begin{aligned}r_1 &= 40.5 \text{ mm} \\r_2 &= \text{plane} \\r_3 &= 23.1 \text{ mm} \\r_4 &= 19.2 \text{ mm}\end{aligned}$$

6.1.4 Cemented Doublets

For the correction of coma and spherical we have in principle two degrees of freedom available, the bendings B_1 and B_2 .

With a cemented doublet B_1 and B_2 are related as follows

$$\frac{(B_1 - 1)V_1}{(n_1 - 1)} = -\frac{(B_2 + 1)V_2}{(n_2 - 1)}.$$

This follows directly from $c_2 = c_3$ and (4.15) of Sect. 4.3.

With an airspaced doublet this relation will be approximately fulfilled, when the airspace is small.

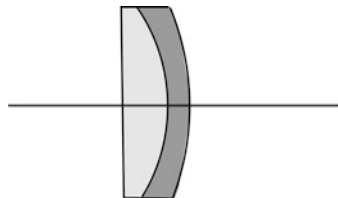
We therefore have two ways of correcting the doublet:

- obeying the cementing condition and choosing the glasses in such way that spherical and coma are both small, or
- neglecting the cementing condition and correcting spherical and coma.

With the first method we find the classical Fraunhofer and Steinheil doublets.

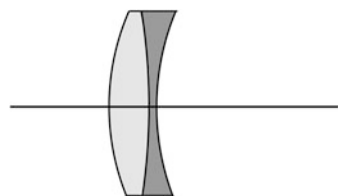
With the second method we also find the Gauss doublet.

Fig. 6.9 Cemented doublet with $B_1 = -1$, $B_2 = 5$, a right-handed doublet



$r_1 = \text{plane}$
 $r_2 = -28.5 \text{ mm}$
 $r_3 = -28.1 \text{ mm}$
 $r_4 = -42.2 \text{ mm}$

Fig. 6.10 Cemented doublet with $B_1 = 0.45$, $B_2 = 0.64$, a left-handed doublet



$r_1 = 39.28 \text{ mm}$
 $r_2 = -103.5 \text{ mm}$
 $r_3 = -102.8 \text{ mm}$
 $r_4 = 46.79 \text{ mm}$

Cemented Doublets, Examples

To design a cemented doublet the strategy is usually to combine the cementing condition with $S_1 = 0$.

With the glasses BK 7 and SF 1 we find the solutions

$$(B_1, B_2) = (-1.04, 5.03) \text{ with } S_2 = -0.00503 \text{ and } (B_1, B_2) = (0.45, 0.64).$$

The curvatures and radii of these solutions, and a 1:1 sketch of both, are shown in Figs. 6.9 and 6.10.

The following example comes from the book of van Heel [2]. Van Heel describes several cemented doublets. We take here his “one-radius” doublet.

The glasses are from the catalogue of Chance Bros., Birmingham U.K.

With HC1: 517607 and F: 620363 we find $K_1 = 2.49 \text{ K}$, $K_2 = -1.49 \text{ K}$, $G_2 = 2.34$.

With $B_1 = 0$, $B_2 = 1$, we calculate

$$S_1 = 0.0026, S_2 = 0.0025 \quad \text{with} \quad h = 10, K = 0.01, H = \frac{1}{6}, \tan w = \frac{1}{60}.$$

This is an excellent result in view of the large aberration values of the components.

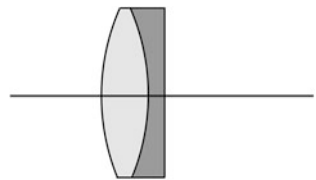
The curvatures are $c_1 = -c_2 = -c_3 = 0.024$, $c_4 = 0$.

Radii $r_1 = -r_2 = -r_3 = 41.52$, $r_4 = \text{plane}$.

A sketch is shown in Fig. 6.11.

This completes our treatment of the thin lens design of (thin) doublets. We have still to show how the aberrations behave after the transformation to real lenses, and how to optimize the design further by ray-tracing.

Fig. 6.11 van Heel's “one radius” doublet



6.1.5 Surface Model of a Doublet

As our example for further optimization we take the airspaced Fraunhofer doublet.

The glass data of this doublet were given above.

With a free diameter of 20 mm, the central thickness of the positive lens should be chosen as 2.5 mm (see Sect. 4.4). We take the central thickness of the negative lens as 2 mm. The airspace has a central thickness of 0.06 mm when we have edge contact between the lenses.

The lens data, corrected for thickness, are

#	r	d	n'	Glass	Φ	V
1	68.36	2.48	1.589	N-SK 5	20	61.24
2	-68.36	0.06	Air	-	20	-
3	-63.18	1.98	1.805	N-SF 6	20	25.42
4	-144.65	98.052	Air	-	20	-

We calculate the surface contributions to the third order aberrations using the paraxial ray-tracing scheme presented in Sects. 1.4 and 3.3.

With the pupil in the first surface, $h_1 = 10$ and $w = -1^\circ$, the Lagrange invariant is -0.1754 . The results of this calculation are shown below. We follow the format of Kidger's book [8], for the ease of comparison.

#	h	nu	A	\bar{h}	$n\bar{u}$	\bar{A}	Δ
1	10.0000	0	0.1463	0	-0.01754	-0.01754	-0.03412
2	9.8655	-0.08616	-0.3155	-0.02737	-0.01754	-0.01690	-0.1370
3	9.8552	-0.1711	-0.3271	-0.02841	-0.01730	-0.01685	0.1570
4	9.8052	-0.0455	-0.1679	-0.04799	-0.01766	-0.01706	-0.0861

#	S ₁	S ₂	S ₃	S ₄	S ₅
1	0.00730	-0.000876	0.000105	0.000167	-0.0000326
2	0.13454	0.007207	0.000386	0.000167	0.0000296
3	-0.16565	-0.008533	-0.000440	-0.000217	-0.0000339
4	-0.02380	0.002418	0.000245	0.000094	0.0000344
Σ	-0.00001	0.000216	0.000297	0.000211	-0.0000025

With the thin lens model we found $S_1 = 0$ and $S_2 = 0.00016$. The values of S_3 and S_4 are close to those found by Kidger (as they should be, because we cannot change them).

The distortion is small, as expected.

6.1.6 Exercise 7, Predesign of a Chevalier Lens

In this section we have made thin lens predesigns of a singlet landscape lens and of airspaced and cemented doublets. For an exercise we take the Chevalier lens, which is a landscape lens with a doublet. See Fig. 4.1 of [Sect. 4.1](#).

As this is the first design exercise, we describe the assignment in detail. As we can see from the figure, the system has a stop in front and a cemented doublet (flint in front) at some distance behind it.

First you should make a drawing of the lay-out. The stop radius a and the distance t between stop and doublet, together with the focal length $f' = 1/K$ of the doublet will be the lay-out parameters.

In this course we always begin with $f' = 100$ mm; if required, for instance when you want to use the lens in an existing camera, the scale of the lens can be adapted afterwards.

For the predesign we choose $F = 12.5$, so that $a = 4$ mm; the field angle will be 30° , so that $\tan w = 0.5774$. Therefore $h = 4$ and $\bar{h} = 0.5774 t$ at the lens, so that $q = \bar{h}/h = 0.1444 t$.

As a goal for the predesign we give that the meridional field curvature and the coma must be corrected, so that $3\bar{S}_3 + S_4 = 0$ and $\bar{S}_2 = 0$.

S_4 will be positive, so that \bar{S}_3 must take a negative value; this is easier done when S_4 has a low value. With classical glasses the Petzval sum will be about $P = 0.7/f' = 0.007$. With “modern” glasses, with a high index crown and a low index flint we can have a lower Petzval sum, as we saw in [Sect. 5.5](#). We choose in this case the glasses N-LAK 9 and LF 5. With these glasses (see the glass list in [Sect. 5.1](#)) we have $K_a = -0.029473$, $K_b = 0.039473$ and $P = 0.453/f'$.

Now the aberrations of the thin lens model can be considered. From [Sect. 4.3](#) ([4.10](#)) we have for S_1 with the lens at the stop

$$S_1 = \frac{1}{4}h^4 K_a^3 I_a + \frac{1}{4}h^4 K_b^3 I_b,$$

where I_a and I_b are quadratic polynomials in the form and position factors (B and G) of the doublet elements. With an achromatic doublet we have

$$\frac{K_a}{K_b} = -\frac{V_a}{V_b}$$

so that we can write

$$S_1 = \frac{1}{4} h^4 K_b^3 \left(I_b - \left(\frac{V_a}{V_b} \right)^3 I_a \right)$$

In the same way we have

$$S_2 = \frac{1}{2} h^2 K_b^2 \left(\Pi_b + \left(\frac{V_a}{V_b} \right)^2 \Pi_a \right)$$

where Π_a and Π_b are linear in B_a , G_a and B_b , G_b , respectively. We also have

$$S_3 = H^2 K_b \left(1 - \frac{V_a}{V_b} \right)$$

With the glasses chosen we have $V_a/V_b = 0.7467$.

We saw in the first part of this section that we must have, because of the stop shift equations,

$$q = -\frac{S_2}{S_1}, \quad S_3 = \frac{S_2^2}{S_1}$$

to find $\bar{S}_2 = 0$, $\bar{S}_3 = 0$, with a remote stop.

When we want to make $3S_3 + S_4$ equal to zero the second condition becomes

$$S_3 + \frac{1}{3} S_4 = S_2^2 / S_1$$

Inserting the expressions for S_1 , S_2 , S_3 and S_4 and using $V_a/V_b = 0.7467$ we obtain

$$0.2915(I_b - 0.4163I_a) = (\Pi_b + 0.5577\Pi_a)^2 \quad (6.2)$$

The form of the polynomials I_a , I_b , Π_a and Π_b are given in (4.16) and in (6.1).

We have to use the indices n_a and n_b to obtain the constants in these polynomials.

The position factors for this case are given by

$$G_a = -1, \quad G_b = \frac{K_a + K}{K_a - K} = 0.5980.$$

The form factors B_a and B_b are not independent, because in the Chevalier lens a cemented doublet is used. The cementing condition was given in the second part of this section as

$$-\frac{(B_a - 1)V_a}{(n_a - 1)} = \frac{(B_b + 1)V_b}{(n_b - 1)} \quad (6.3)$$

When we use (6.3) to eliminate B_a from (6.2) we obtain a quadratic equation in B_b .

From this point on we ask you to complete the predesign. You have to do the following steps:

1. Express B_a in terms of B_b by (6.3), using the values of n_a , V_a , n_b , V_b from the glass list in Sect. 5.1.
2. Give numerical values to the constants in I_a , I_b , Π_a and Π_b .
3. Eliminate B_a from I_a and Π_a , using the result of step 1.
4. Write (6.2) as a condition on B_b only and solve for B_b . Calculate the B_a values corresponding to the values found for B_b .
5. Calculate the radii of the doublet for the solutions found.
6. Calculate S_1 and S_2 (at the stop) and the values of q corresponding to both solutions, and t from those.

As before you will find a positive and a negative value for t , the Chevalier lens has the positive value. Make a sketch of the two systems that you have found. When you have read Sects. 6.2 and 6.3 you can come back to this exercise, give thickness to the design and optimize it.

6.2 Design of a Telescope

We design a simple, refracting telescope. For the objective we take the Fraunhofer aplanat that we considered in detail in Sect. 6.1. We scale its dimensions up to a focal length of 250 mm. The aberrations go up as well, with the same factor 2.5. Note that the wavelength and the numerical aperture do not scale up, so that the Airy radius remains the same ($\approx 3 \mu\text{m}$).

The ocular remains to be designed. We will do this in two phases: first we calculate the aberrations of a Ramsden ocular. This is the simplest type of ocular, we will use it as a benchmark. Then we will design a Kellner ocular, which is a variation on the Ramsden.

In the book of Kidger [7] the results of the design of several types of oculars are shown (Chap. 11). Here we show the design of only one type, the Kellner ocular, from scratch.

The data of the Ramsden ocular are EFL = 24.9650 mm, H = 0.6699 mm.

Surface	Radius	Distance	Index	V	cl.rad.	Glass
1#	Plane	12	1		2.5	
2	Plane	3	1.516798	64.14	6.5	N-BK7
3	-17.66	10.99	1		6.5	
4	21.375	3	1.516798	64.14	8.5	N-BK7
5	Plane	9.11604	1		8.5	

The paraxial calculations of the marginal and chief rays give the following results:

Surface	h	$n\mu$	\bar{h}	$n\bar{\mu}$	Δ	A	\bar{A}
1	2.5	0	0	0.26795			
2	2.5	0	3.21540	0.26795	0	0	0.26795
3	2.5	0	3.74586	0.26795	-0.07316	-0.21742	-0.05373
4	1.11069	-0.07316	6.75234	0.15835	-0.02963	-0.02120	0.47425
5	0.91288	-0.10014	6.74263	-0.00491	-0.05661	-0.10014	-0.00491

The third order aberration coefficients become

	S_1	S_2	S_3	S_4	S_5
2	0	0	0	0	-0.02719
3	0.008432	0.002110	0.000528	0.008658	0.002299
4	-0.000014	0.000331	-0.007403	0.007153	0.005593
5	0.000518	0.000025	0.000001	0	0
Σ	0.008936	0.002466	-0.006874	0.015811	-0.01930

Because for surface 2, $A = 0$, we must use the alternative formula for distortion, (Sect. 3.17).

These results agree with those of Kidger for the same system, with the exception of the distortion coefficient of the plane surface 2. We calculated the chromatic aberration coefficients from a thin lens model and found $C_1 = 0.003229$, $C_2 = 0.006537$. This agrees well enough with Kidger's values.

6.2.1 Design of a Kellner Ocular

From the data of the Ramsden ocular we derive the following lay-out

	φ	d	h	Clear radius
Pupil	-	10.57	2.5	2.5
Lens 1	0.030	19	2.5	5
Lens 2	0.025	250	1.075	8

From this lay-out we have $f = 25.54$ mm. With $w = 0.28667$ and $h_p = 2.5$ we have $H = -0.7166$.

We find $\bar{h}_1 = 3.03075$, $\bar{h}_2 = 6.75$, $d_2 = 250$ mm.

The back focal length is 10.55 mm.

The first lens will be executed as a doublet, for which we will use the glasses N-SK 5, N-SF 6.

With these we find

$$K_{1a} = -0.0213, \quad K_{1b} = 0.0513.$$

We will also use N-SK 5 for the second lens.

We can directly make an estimate of the chromatic aberration coefficients.

Because lens1 is an achromat we have $C_{11} = C_{21} = 0$, and $C_1 = \frac{h_1^2 K_1}{V_2} = 0.00047$,
 $C_2 = \frac{h_2 \bar{h}_2 K_2}{V_2} = 0.00297$.

For the monochromatic aberrations we use the stop shift equations, that we report below.

$$\begin{aligned} S_1 &= S_{11} + S_{12}, \\ S_2 &= S_{21} + q_1 S_{11} + S_{22} + q_2 S_{12}, \\ S_3 &= S_{31} + 2q_1 S_{21} + q_1^2 S_{11} + S_{32} + 2q_2 S_{22} + q_2^2 S_{12}, \\ S_4 &= S_{41} + S_{42}, \\ S_5 &= S_{51} + q_1(3S_{31} + S_{41}) + 3q_1^2 S_{21} + q_1^3 S_{11} + S_{52} + q_2(3S_{32} + S_{42}) \\ &\quad + 3q_2^2 S_{22} + q_2^3 S_{12}, \end{aligned} \tag{6.4}$$

with $q_1 = \frac{\bar{h}_1}{h_1}$, $q_2 = \frac{\bar{h}_2}{h_2}$.

As degrees of freedom we use the shape factors B_a , B_b of the components of the doublet. The second lens is given the shape factor of $B_2 = 1$.

Using the formulas for spherical and coma of (6.1) we find the intrinsic values of S_{1a} and S_{1b} , S_{2a} and S_{2b} .

We chose $B_b = 0.17$, because this gives nearly minimum spherical aberration S_{1b} , and a small value of S_{2b} .

With the cementing condition (6.3) we obtain $B_a = -2.85$.

Now we find, with $q_1 = 1.21$ and $q_2 = 6.28$.

$$\begin{aligned} S_{1a} &= -0.005465, \quad S_{1b} = 0.009440, \\ S_{2a} &= -0.008218, \quad S_{2b} = 0.000500, \\ S_{2a}^* &= -0.008218 - 1.21 \cdot 0.005465 = -0.014347, \\ S_{2b}^* &= 0.000500 + 1.21 \cdot 0.009440 = 0.011922, \\ S_{11} &= 0.003975, \quad S_{21} = -0.002425, \end{aligned}$$

where we used $G_a = -1$, $G_b = 2 \frac{V_a}{V_b} - 1 = -0.1699$.

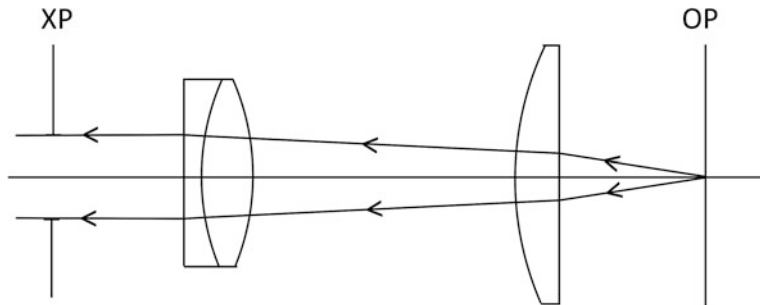


Fig. 6.12 Kellner ocular, version 1. Scale 2:1

With $G_2 = -8.58$, $B_2 = 1$ we have $S_{12} = 0.001217$, $S_{22} = 0.002626$ and for the system $S_1 = 0.005192$, $S_2 = 0.000201$.

Using the formulas of Sect. 4.3 we find $S_3 = 0.014303$, $S_4 = 0.03072$, $S_5 = 0.06086$.

The figures are not bad for the first try. Radii and curvatures, and a rough sketch of the system, are given below. See also Fig. 6.12.

In this book usually optical systems are drawn in such a way that the light comes from the left. In Fig. 6.12 this is not the case because oculars are usually designed from the side of the eye. This is somewhat easier because the marginal ray is then parallel to the optical axis.

Radii of the Kellner Ocular

	c	r
2	0.02354	42.46 mm
3	0.05001	20.00
4	-0.03745	-26.70
5	0.04244	23.76
6	0	Plane

When we change this system a bit, taking $B_a = -3$, $B_b = 0.2147$, we obtain the following coefficient values:

S_1	S_2	S_3	S_4	S_5
0.004702	-0.000886	0.00985	0.03072	0.05324 V_2

Spherical, astigmatism and distortion have become better, at the cost of some increase of coma. Field curvature has remained the same; it is about twice as large as with the Ramsden ocular, partly because of our choice of glass (N-SF 6, N-SK 5).

When we transform the thin lenses of this design into real lenses, we obtain the construction data shown below. We calculate the position of the pupil (the eye relief). With $M = 10$ we have $f_{ob} = 243.843$. We trace a chief ray from the center of the entrance pupil at a distance of $243.843 + 7.7364 = 251.579$ mm from V_6 and obtain $d_1 = 12.8728$ mm.

Construction data of the Kellner ocular, version 2

EFL = 24.3843

r	d	n'	V	c.r.	Glass
1		12.873	1		2.5
2	36.4697	1.4472	1.805	25.4	7
3	18.2349	4.7725	1.589	61.2	7
4	-27.9095	17.3924	1		7
5	23.5626	4.0000	1.589	25.4	10
6	Plane	7.7364	1		10

Comparison of the aberration coefficients of different designs

S ₁	S ₂	S ₃	S ₄	S ₅	
0.005197	0.000654	0.014303	0.03072	0.06086	V ₁
0.004082	-0.001885	0.009840	0.029802	0.07800	K
0.008936	0.002466	-0.006874	0.01581	0.02333	R
0.004702	-0.000886	0.00985	0.03072	0.05324	V ₂

The first line and the fourth, marked V₁ and V₂, show the coefficients of the two Kellner oculars that we discussed. The second line, marked K, shows the coefficients of the Kellner ocular from Kidger's book. The third line, marked R, shows the coefficients of the Ramsden ocular of pp. 105 and 106.

To conclude this section we compare the aberrations of the objective (see p. 102) and the ocular. We multiply the aberration coefficients of the objective by a scale factor of 2.5.

We obtain the coefficients:

	S ₁	S ₂	S ₃	S ₄	S ₅
Objective	-0.00003	0.00054	0.00075	0.00053	-0.00001
Ocular	0.00470	0.00087	0.00985	0.03072	0.00532

6.2.2 Inverting System

As the Kepler telescope produces an inverted image, an inverting system must be added to it in terrestrial applications. This can be done by adding a lens with a

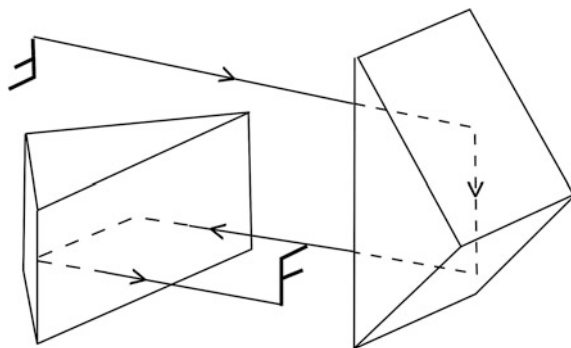


Fig. 6.13 Porro prism system; the inverted image from the objective is erected by the prisms

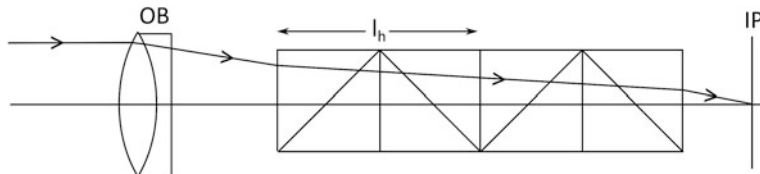


Fig. 6.14 Tunnel diagram of the Porro system with objective and image plane

negative magnification to the ocular, by which the *terrestrial ocular* is formed. A terrestrial ocular makes the telescope significantly longer and less handy in use.

The inverting prism system, invented by Porro ($\pm 1,850$) makes the telescope more compact; it is shown in Fig. 6.13.

When the prisms are unfolded, so that a *tunnel diagram* is generated, it is seen that the system is equivalent to a plane-parallel plate of thickness

$$d = 2l_h,$$

where l_h is the length of the hypotenuse plane, see Fig. 6.14.

When the prism has its first surface about halfway across the focal distance of the telescope objective, l_h will be somewhat larger than $2a + 2\bar{a}$, where $2a$ is the diameter of the objective and $2\bar{a}$ the diameter of the intermediate image field. In the telescope objective that we are designing we obtain $l_h > 70$ mm; we will take $l_h = 75$ mm. We have a plate of $d = 150$ mm thickness that replaces d/n distance in air. With $n = 1.518$ (BK 7) we have $d/n = 98.8$ mm.

The axial distance between the input and output planes of the Porro system can be made zero by cementing the component prisms, so that the telescope becomes nearly 100 mm shorter.

Unfortunately the glass volume is about $\frac{1}{4}l_h^3$, with a density of 2.5 g/cm^3 this gives a mass of 0.263 kg, so that a binocular with two Porro prisms becomes 0.526 kg heavier.

The aberration coefficients of a plane-parallel plate are given by Welford [9, p. 234]:

$$\begin{aligned}
 S_1 &= -\frac{n^2 - 1}{n^3} \cdot u^4 d \\
 S_2 &= \frac{\bar{u}}{u} S_1 \\
 S_3 &= \left(\frac{\bar{u}}{u}\right)^2 S_1 \\
 S_4 &= 0 \\
 S_5 &= \left(\frac{\bar{u}}{u}\right)^3 S_1 \\
 C_1 &= -\frac{\delta n}{n^2} u^2 d \\
 C_2 &= \frac{\bar{u}}{u} C_1
 \end{aligned} \tag{6.5}$$

independent of the position of the plate.

We apply these formulas to our telescope design.

With $u = 0.1$, $\bar{u} = 0.04$, $d = 150$, $n = 1.518$ we have

$$S_1 = -0.00559, \quad S_2 = -0.00223, \quad S_3 = -0.000859, \quad S_5 = -0.000358$$

and with $\delta = n_F - n_C = 0.008054$ for BK 7,

$$C_1 = -0.00521, \quad C_2 = -0.00208$$

The monochromatic aberrations balance nicely those of the combination of objective and ocular.

For the ocular we found

$$C_1 = 0.00047, \quad C_2 = 0.00297$$

so that TCA is well corrected, and LCA must be improved.

6.2.3 Optimization of the Telescope Design

The predesign has a doublet with an airspace. See Fig. 6.6.

In the optimization we changed the doublet into a cemented one. The first optimization run was done with the glasses of the predesign. We optimized the r.m.s. spot radius for three fields: 0, 1.5 and 2°, with an infinite EFL. This did not result in significant improvement, so that we do not show coefficients or ray fan plots.

In a second run we let the computer find a different choice of glasses. With N-SK 2 and N-BASF 2 for the doublet glasses the correction improved, the main

change being the vanishing of the meridional field curvature. We give the lay-out of the resulting system and ray-fan plots for the three fields in Fig. 6.15a, b. Note that the aberrations are given in milliradians, because the system is telescopic. In the center of the field the aberrations are below 1 mrad; the resolution of the human eye is about 0.4 mrad. The remaining aberrations are astigmatism (about 4 mrad at the edge of the field) and about 1 mrad of TCA.

The prescription of the optimized system is given below. Surface 6 is the intermediate image plane, surface 12 is the exit pupil. The diameter of the exit pupil is 5 mm in this prescription; with a diameter of 2 mm the aberrations at the edge of the field will be smaller than 2 mrad.

Surface data summary:

Surf	Radius	Thickness	Glass	Diameter
OBJ	Infinity	Infinity		0
STO	183.3102	10.00097	N-SK 2	50
2	-94.0289	9.99993	N-BASF 2	49.82282
3	-499.4414	100		49.32021
4	Infinity	150	N-BK 7	36.01735
5	Infinity	41.62677		22.94478
6	Infinity	7.736		17.47828
7	Infinity	4	N-SK 5	19.5703
8	-23.563	17.392		19.87526
9	27.91	4.773	N-SK 5	14.04767
10	-18.235	1.447	N-SF 6	13.06061
11	-36.47	10.873		12.5818
12	Infinity			5

6.2.4 Exercise 8, Predesign of a Plossl Ocular

The thin lens predesign of a Plössl ocular (see Fig. 4.27 of Sect. 4.1) can be approached in the following way. As a lay-out we take two thin doublets. With a focal length of the ocular of 25 mm, we give these doublets a focal length of 50 mm each. For the thin lens design we take zero distance between the doublets. The notation of the lay-out is given in Fig. 6.16.

As is usual in the design of oculars, we take the stop to the left. This is the exit pupil of the telescope; the objective is far away to the right, the chief ray points to the centre of the objective where the entrance pupil is located.

When we want to correct coma and astigmatism with a remote pupil and a positive power sum we must fulfill the conditions

$$q = -\frac{S_2}{S_1}, \quad S_3 = \frac{S_2^2}{S_1} \quad (6.6)$$

as with the landscape lens.

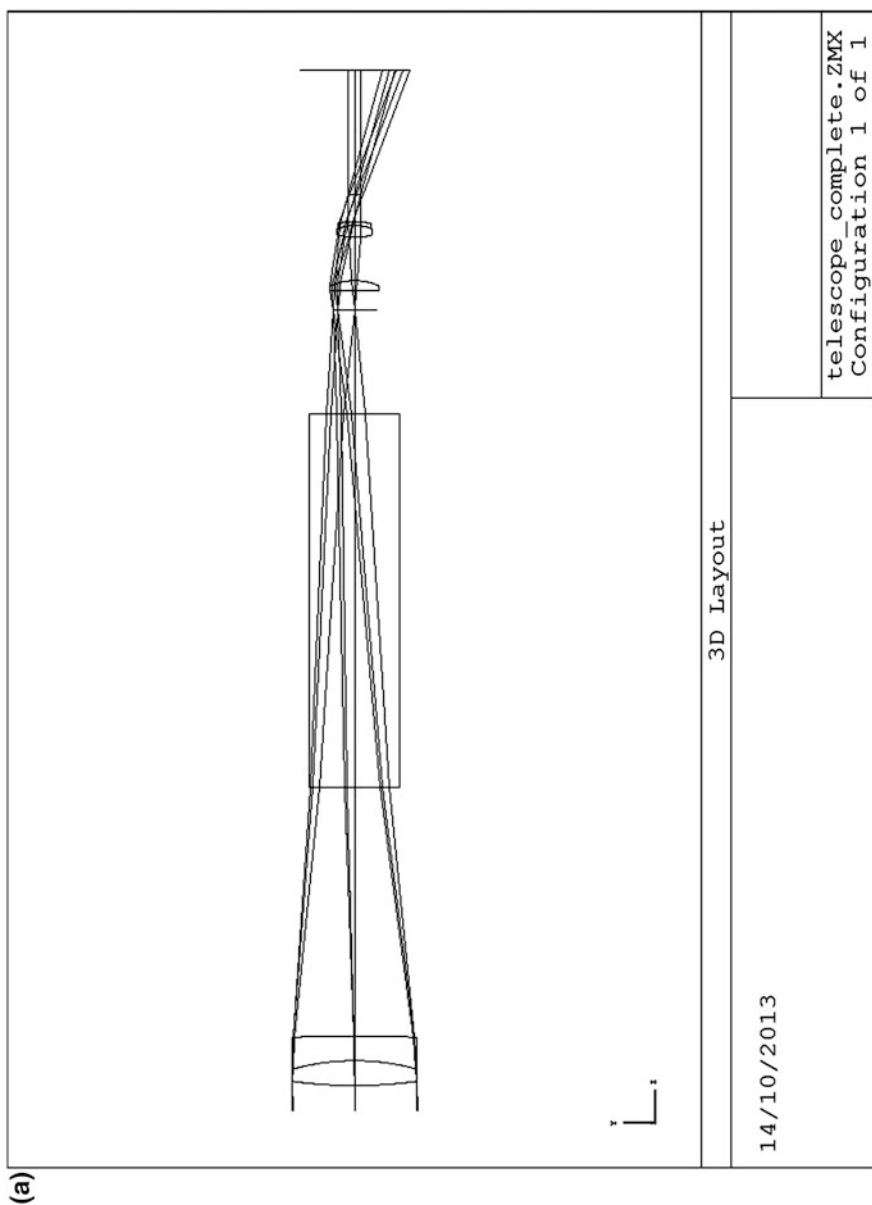


Fig. 6.15 a Telescope, lay-out. b Telescope, aberrations

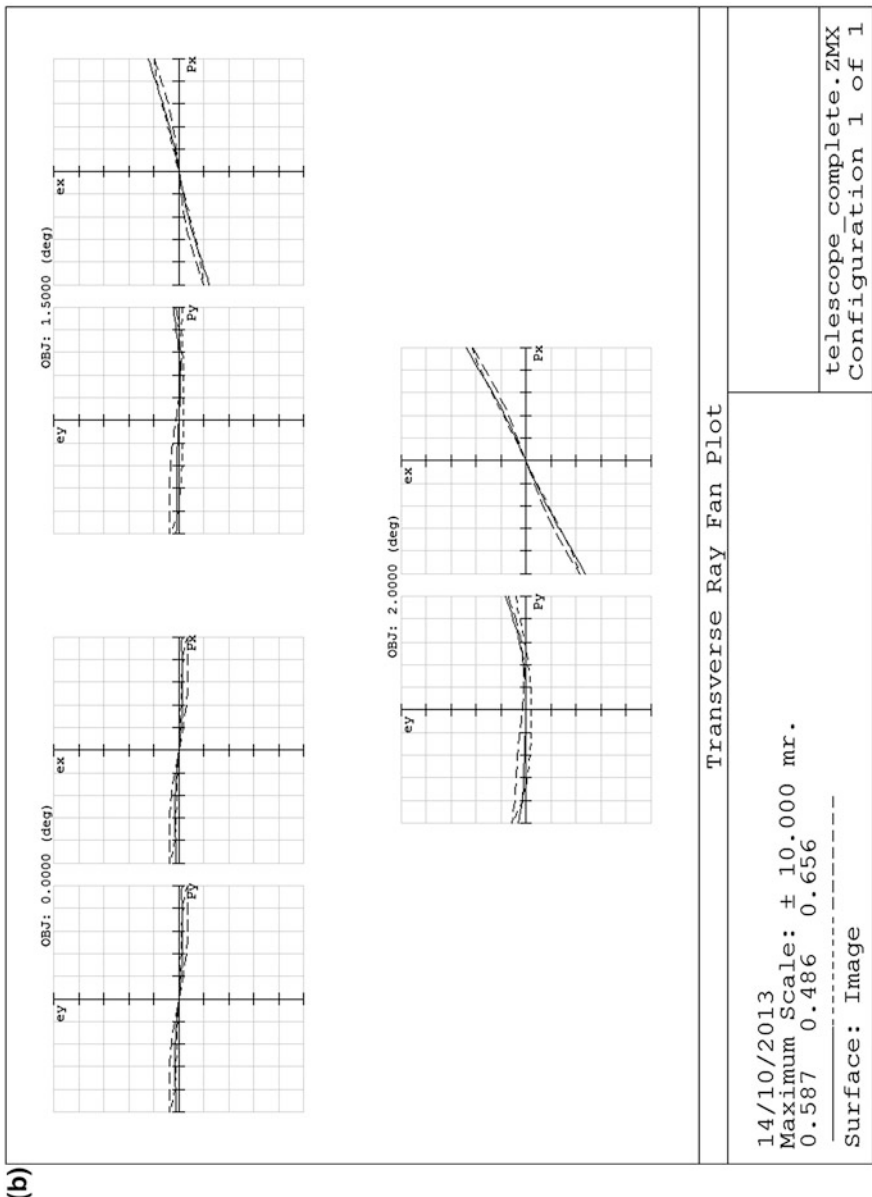


Fig. 6.15 (continued)

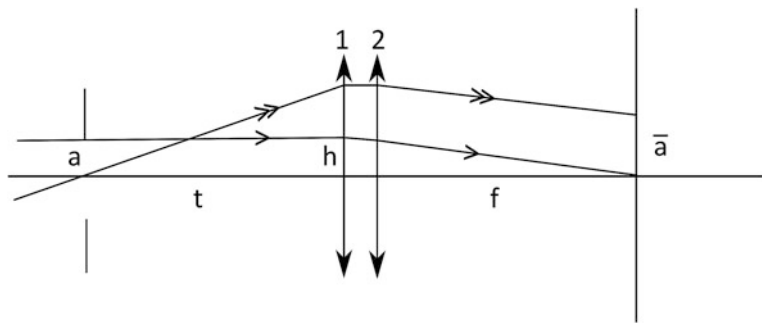


Fig. 6.16 Notation for the Plössl ocular

As glasses for the achromatic doublets we use the same glasses as in exercise 7, N-LAK 9 and LF 5, because these give a low value of the Petzval sum, $P = 0.453 \text{ K}$ for each doublet (and also for the combination).

We will take cemented doublets so that for each doublet the cementing condition

$$-\frac{(B_a - 1)V_a}{(n_a - 1)} = \frac{(B_b + 1)V_b}{(n_b - 1)} \quad (6.7)$$

must be valid. This will be used to eliminate one of the form factors for each doublet. For each of the doublet elements we find S_1 , S_2 and S_3 from the (4.16) that give the coefficients for the lens at the stop.

As in exercise 7 we use the notation

$$S_{1i} = \frac{1}{4} h^4 K_i I_i, \quad S_{2i} = \frac{1}{2} h_i^2 H K_i^2 \Pi_i, \quad S_{3i} = H^2 K_i$$

where the suffix i denotes the lens element and where I_i and Π_i are polynomials given by

$$\begin{aligned} I_i &= \frac{(n_i + 2)}{n_i(n_i - 1)^2} B_i^2 + \frac{4(n_i + 1)}{n_i(n_i - 1)} B_i G_i + \frac{3n_i + 2}{n_i} G_i^2 + \frac{n_i^2}{(n_i - 1)^2} \\ \Pi_i &= \frac{(n_i + 1)}{n_i(n_i - 1)} B_i + \frac{2n_i + 1}{n_i} G_i \end{aligned}$$

We have to add the contributions of all four doublet elements, i taking values 1a, 1b, 2a, 2b.

Because for each doublet the element powers have the ratio $K_a/K_b = -V_a/V_b$, where a denotes the negative element we have for the first doublet

$$\begin{aligned} S_{11} &= \frac{1}{4} h^4 K_{1b}^3 \left(I_{1b} - I_{1a} (V_a/V_b)^3 \right) \\ S_{21} &= \frac{1}{2} h^2 H K_{1b}^2 \left(II_{1b} - II_{1a} (V_a/V_b)^2 \right) \\ S_{31} &= H^2 K_{1b} (1 - V_a/V_b) \end{aligned}$$

When we eliminate B_{1a} by the cementing condition, S_{11} and S_{12} depend only on the variable B_{1b} , as G_{1a} and G_{1b} follow from the lay-out.

Plössl oculars occur in many different configurations, equal and unequal doublets, in tandem or in a symmetric or hemi-symmetric configuration. We will take the case of two equal, cemented doublets in symmetric configuration. This makes $B_{2a} = -B_{1b}$, $B_{2b} = -B_{1a}$, and we can write the aberrations as

$$\begin{aligned} S_1 &= \frac{1}{4} h^4 K_{1b}^3 \left(I_{1b} + I_{2a} - (V_a/V_b)^3 (I_{1a} + I_{2b}) \right) \\ S_2 &= \frac{1}{2} h^2 H K_{1b}^2 \left(II_{1b} + II_{2a} - (V_a/V_b)^2 (II_{1a} + II_{2b}) \right) \\ S_3 &= H^2 K_{1b} \cdot 2(1 - V_a/V_b) \end{aligned} \quad (6.8)$$

With our choice of glass we have $V_a/V_b = 0.7467$.

S_1 and S_2 still contain the position factors G_{1a} , G_{1b} , G_{2a} , G_{2b} that can be calculated from the lay-out data

$$\begin{aligned} K_{1a} &= -0.058946, \quad K_{1b} = 0.078946, \\ K_{2a} &= 0.078946, \quad K_{2b} = -0.058946 \end{aligned}$$

and $1/s_1 = 0$.

The condition to be solved for B_{1b} is, from (6.6) and (6.8)

$$\begin{aligned} 2(1 - V_a/V_b) \left(I_{1b} + I_{2a} - (V_a/V_b)^3 (I_{1a} + I_{2b}) \right) \\ = \left(II_{1b} + II_{2a} - (V_a/V_b)^2 (II_{1a} + II_{2b})^2 \right) \end{aligned}$$

This condition is independent of h , $H = -a \tan w$ and K_{1b} . When we take $a = 2$ also $h = 2$. The value of t will be found when we calculate S_1 and S_2 , the value of $H = -a \tan w$ can be determined when we discuss the distortion of the ocular.

The assignment for this exercise consists of the following steps:

1. Calculate the position factors G_{1a} , G_{1b} , G_{2a} , G_{2b} .
2. Take the constants in the expressions I_i and II_i in (7) from Exercise 7.
3. With n_a , V_a and n_b , V_b write B_{1a} as a function of B_{1b} . Write B_{2b} as a function of B_{1b} (remember that $B_{2a} = -B_{1b}$ and $B_{2b} = -B_{1a}$).
4. With the position factors and the constants write the expressions for S_{11} , S_{12} , S_{21} and S_{22} . Eliminate B_{1a} from S_{11} and S_{12} and B_{2b} from S_{21} and S_{22} using the expressions found in Step 3.

5. Write the condition $S_3 = S_2^2/S_1$ as a quadratic equation in B_{1b} and solve for B_{1b} . Calculate B_{1a} , B_{2a} , B_{2b} with the result of Step 3. Calculate the radii of both doublets.
6. With $q = t \cdot \tan w/h$ we can write

$$t \cdot \tan w/h = -S_2/S_1$$

Because S_2 is proportional to $H = -a \tan w$ and $h = a$ (see Fig. 6.16) we find from (6.8)

$$t = \frac{1}{K_{1b}} \cdot \frac{I_c}{I_c}$$

where I_c , I_{IIc} are the expressions in brackets in S_1 and S_2 respectively in (6.8). Determine t , make a sketch of the system.

7. From the stop shift (4.17)

$$S_5 = q(3S_3 + S_4) + 3q^2S_2 + q^3S_1$$

determine S_5 as a function of $\tan w$.

When you accept 1 % of distortion, which value of $\tan w$ would you allow?

6.3 Two-Component Systems

A two-component system consists of two thin systems, separated by a distance that is not small compared to the focal lengths of the components.

Two-component systems form a large and varied group of optical systems, that are moreover easily accessible for the thin lens design method that we recommend in this course.

In Figs. 6.17, 6.18, 6.19 and 6.20 we show some examples of two-component lenses, without further comment as to their application and properties. We will discuss the design of these lenses in the following sections.

But these examples do by no means exhaust the store of two-component lenses. We mention here the oculars that we designed in the previous section; the classical Huygens, Ramsden and Kellner oculars are two-component systems with a fixed, remote stop. We will in the following use the stop position as a variable.

Low-power microscope objectives often have a construction that resembles very much the Petzval lens. We will come back to microscope objectives in Sect. 6.6.

The Galilei telescope is a two-component system that resembles very much the telephoto lens; we will discuss it when we treat the design of telephoto lenses.

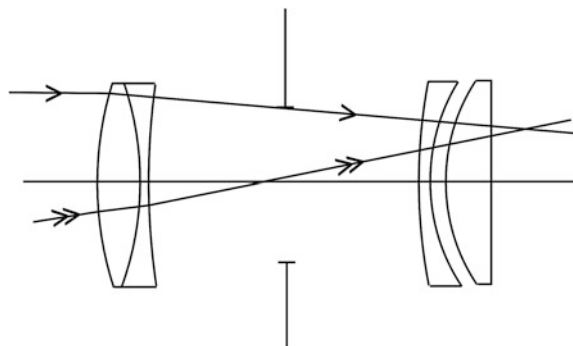


Fig. 6.17 Petzval lens

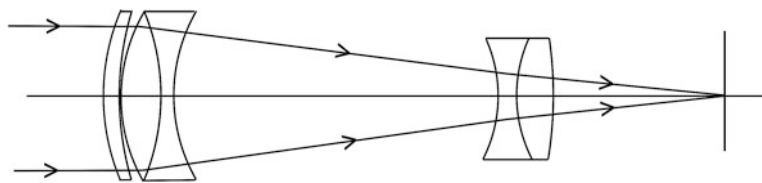


Fig. 6.18 Telephoto lens

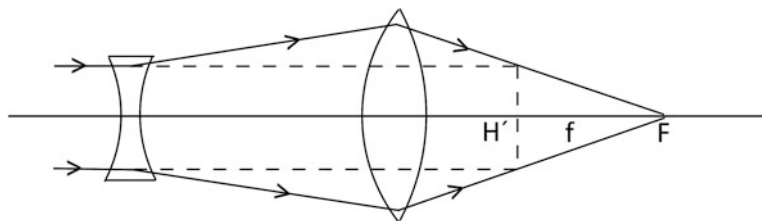
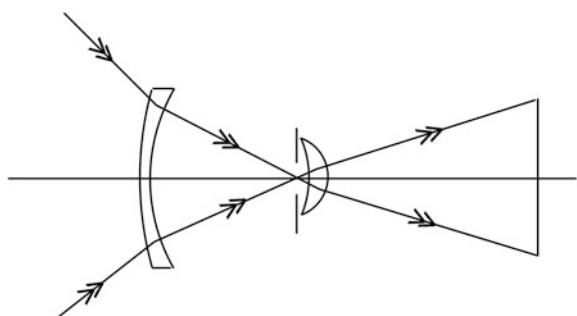


Fig. 6.19 Reversed telephoto lens

Fig. 6.20 Wide-angle lens



It is not necessary that a two-component lens consist of two or more lenses: a thick lens can be a two-component system when its central thickness is not small compared to the focal lengths of its end surfaces. We do not discuss these lenses further in this section.

In the typology of Kross [10], the Petzval lens and the Lister objective are of type PP.

The telephoto lens and the Galilei telescope are of type PN.

The type NN does not occur as an independent lens type (like the N p.n doublet), but it is sometimes found as a module in compound lens types.

To conclude this brief survey of two-component systems we point out the systems with mirror symmetry, that group is closely related to, and partially overlaps, the group of two-component systems.

The lay-out conditions for a two-component system are usually of the form

$$\begin{aligned} K &= K_1 + \frac{h_2}{h_1} K_2, \\ \sum P &= + \frac{K_2}{n_2}, \frac{K_1}{n_1}, \\ C_1 &= h_1^2 \frac{K_1}{V_1} + h_2^2 \frac{K_2}{V_2}, \\ C_2 &= h_1 \bar{h}_1 \frac{K_1}{V_1} + h_2 \bar{h}_2 \frac{K_2}{V_2}. \end{aligned} \tag{6.9}$$

We showed on pp. 73 and 74 that a general two-component system must be corrected for colour by making V_1 and V_2 both large enough. This requires that both components must be achromatized. V_1 and V_2 are then the equivalent V-numbers of the two achromats. Likewise, n_1 and n_2 are the equivalent indices of the components. See below for a definition of these equivalent values.

Equivalent Index and Dispersion (Abbe) Number

A thin system with power K_s , given by

$$K_s = \sum_i K_i$$

has equivalent refractive index n_s and dispersion number V_s given by

$$\frac{K_s}{n_s} = \sum_i \frac{K_i}{n_i}, \quad \frac{K_s}{V_s} = \sum_i \frac{K_i}{V_i},$$

so that

$$\begin{aligned} n_s &= \frac{\sum_i K_i}{\sum_i \frac{K_i}{n_i}}, \\ V_s &= \frac{\sum_i K_i}{\sum_i \frac{K_i}{V_i}}. \end{aligned} \quad (6.10)$$

Aberrations of a Two-Component System

The monochromatic component aberrations must be found from the equations

$$\begin{aligned} S_1 &= S_{11} + S_{12} & S_4 &= S_{41} + S_{42} \\ S_2 &= S_{21} + q_1 S_{11} + S_{22} + q_2 S_{12} \\ S_3 &= S_{31} + 2q_1 S_{21} + q_1^2 S_{11} + S_{32} + 2q_2 S_{22} + q_2^2 S_{12} \\ S_5 &= S_{51} + q_1(3S_{31} + S_{41}) + 3q_1^2 S_{21} + q_1^3 S_{11} + S_{52} + q_2(3S_{32} + S_{42}) + 3q_2^2 S_{22} + q_2^3 S_{12} \end{aligned} \quad (6.11)$$

with $q_1 = \frac{\bar{h}_1}{h_1}$, $q_2 = \frac{\bar{h}_2}{h_2}$.

These equations can be interpreted as follows. $S_i (i = 1, \dots, 5)$ are the aberration coefficients of the system as a whole.

$S_{i1}, S_{i2} (i = 1, \dots, 5)$ are the aberration coefficients of the components, with the stop at each component, respectively.

As always, h_j in $q_j = \frac{\bar{h}_j}{h_j}$ is the ray height of the marginal ray at component j ($j = 1, 2$), and \bar{h}_j is the ray height of the chief ray at component j .

Suppose that we want to design a two-component system with target values \bar{S}_i of the aberration coefficients, and a given value of K , the power of the system.

When the lay-out is given, that is when we know K_1, K_2 and d , and also n_1, n_2, V_1, V_2 , and \bar{h}_0, s_1, h_p , we find that q_1 and q_2 are fixed.

Also we can calculate $S_{31} = H^2 K_1$, $S_{32} = H^2 K_2$, $S_{41} = H^2 \frac{K_1}{n_1}$ and $S_{42} = H^2 \frac{K_2}{n_2}$.

Note that the Lagrange invariant is given by

$$H = -n_1 \frac{h_p \bar{h}_0}{s_1} \text{ (or } +n_1 h_p \tan w \text{ when } s_1 \rightarrow \infty\text{)}.$$

We can take $S_{51} = S_{52} = 0$ in the thin lens model. The four unknowns $S_{11}, S_{12}, S_{21}, S_{22}$ can be found from the four equations (3). The four form factors of the achromatized components must be chosen so that S_{11}, S_{12}, S_{21} and S_{22} have the values required by these equations.

Below we apply this procedure to a practical design problem. We will see that there are different strategies to obtain a useful predesign. For an alternative treatment see Hopkins and Rao [11].

6.3.1 The Retinascope (Fundus Camera)

A retinascope serves to project an image of the retina (or fundus) of the human eye on a CCD target.

A schematic diagram of a retinascope is given in Fig. 6.21. On the left we find a simplified eye model, consisting of a curved object surface, representing the retina, and a thin lens with a power of 60 dp ($f' = 16\frac{2}{3}$ mm). The lens is situated at the exit pupil of the eye, which acts as the aperture stop of the system. We assume that the curvature of the object surface is chosen so that the beams that leave the pupil from points of the retina are parallel; herewith we neglect the eye's aberrations.

An "eye lens" makes an image of the retina in its focal plane. We have chosen a focal length of 32 mm for the eye lens, its distance to the stop is 40 mm. the stop is imaged at 160 mm behind the eye lens. The diameter of the intermediate image is about 20 mm, this corresponds to 10.4 mm on the retina.

The intermediate image is imaged on the CCD by an objective situated behind the stop image. The objective has a focal length of 25.6 mm and is situated at the same distance behind the stop, so that we have image telecentricity (see Sect. 1.5). The magnification of the system is $M = 0.4$.

The illumination of the retina is problematic in a retinascope, because the reflection coefficient of the retina is small, of the order of 0.01. The cornea already reflects about 3 % of the incoming light, and also the surfaces of the eye lens will reflect some light in the direction of the objective that can disturb seriously the image on the CCD.

In the diagram of Fig. 6.21 we have placed a point light source next to the objective. We show the illuminating rays as interrupted lines. The point source is imaged on the eye pupil, outside the part of the pupil that is conjugated to the objective pupil. In this way we prevent the cornea reflection to enter the objective.

The eye lens of a retinascope has a remote stop. Therefore it can be considered as a landscape lens (see Sect. 6.1 and also [12, Chap. 9]). The correction possibilities with a single lens or achromat are limited in this case.

In practice one uses thick meniscus lenses, with one or two aspheric surfaces (so-called ophthalmic lenses).

An alternative is to use an ocular of the Plössl type (see Exercise 8, also [13]), that consists of two achromats in tandem. This gives a better correction of the intermediate image, but it is more difficult to avoid disturbing reflections.

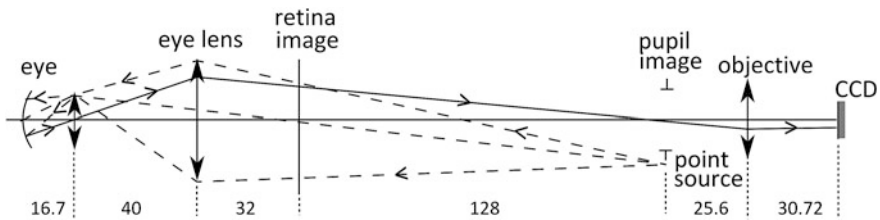


Fig. 6.21 Lay-out of a retinascope with point source illumination

6.3.2 Exercise 9, Design of an Eye Lens

With the formulas (4.13–4.16) of Sect. 4.3 calculate the form of the eye lens for which coma is zero and astigmatism has a minimum value. The lay-out is given in Fig. 6.21. Take 4 mm for the pupil radius of the eye and 0.3 for the field angle. The glass is BK 7. Compare the aberration coefficients of this lens to those of the landscape lens (first solution) that we discussed in the first part of Sect. 6.1. Could we make \bar{S}_3 smaller by choosing another glass? Consult the table of van Heel in Sect. 6.1.

Design of the Objective

We concentrate now on the design of the objective for the retinascope.

We chose a magnification of $M = -0.20$, so that the diameter of the CCD image is 4.9 mm, which just fits on a $\frac{1}{4}$ -inch CCD target. We follow the lay-out for PP two-component systems given in Sect. 5.2. That means that we have the stop at the first component and obtain image telecentricity, as in the diagram of Fig. 6.21.

The lay-out of the objective is shown in general terms in Fig. 6.22. With $M = -0.20$ we have, taking $t = -128$ mm, $d = 25.6$ mm, $K = K_2 = 0.039$, $K_1 = 0.0234$. We have now fixed q_2 ; from formula (6.11) we find $q_2 = -\frac{5}{6}$.

The Helmholtz invariant is $h_p \tan w = 0.3125$ (mm). As glasses we choose SK5 and F5.

The powers of the doublet components now become:

$$K_{a1} = 0.06153, K_{b1} = -0.03813.$$

$$K_{a2} = 0.10254, K_{b2} = -0.06354.$$

We can use different strategies to correct the Seidel aberrations of the objective. It would be erroneous to take aplanatic doublets for the components. In that case spherical and coma are corrected, as well as longitudinal and lateral colour. But it is not possible to correct astigmatism, field curvature and distortion. The resulting design will have a small useable field.

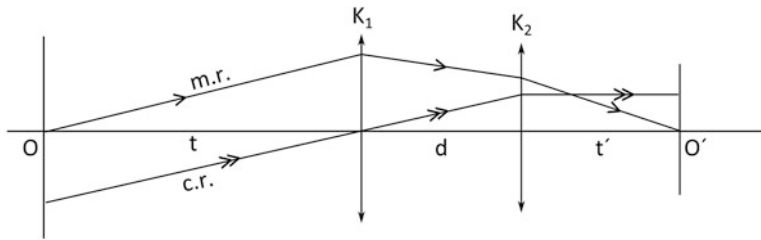


Fig. 6.22 Notation for the lay-out of the retinascope objective

Thin Lens Design

From (6.11) with $q_1 = 0$ we obtain the equations

$$\begin{aligned}\bar{S}_1 &= S_{11} + S_{12} \\ \bar{S}_2 &= S_{21} + S_{22} + q_2 S_{12} \\ \bar{S}_3 &= S_{31} + S_{32} + 2q_2 S_{22} + q_2^2 S_{12} \\ \bar{S}_5 &= q(3S_{32} + S_{42}) + 3q_2 S_{22} + q_2^3 S_{12}\end{aligned}\tag{6.12}$$

We will set the targets $\bar{S}_1 = 0$, $\bar{S}_2 = 0$ to correct the centre of the field, so that

$$S_{11} = -S_{12} \quad \text{and} \quad S_{21} = -S_{22} - q_2 S_{12}$$

From the last two equations of (6.12) we will find S_{12} and S_{22} . Note that S_{31} , S_{32} and S_{42} are given from the lay-out. From (6.12) we can derive three different strategies for the correction of the third order aberrations of the thin lens model.

I. We correct all aberrations.

In this case \bar{S}_3 and \bar{S}_5 are zero.

From (6.12) with all left sides zero, we find

$$\begin{aligned}S_{12} &= (3S_{31} - S_{32} - 2S_{42})/q_2^2 \\ S_{22} &= (-S_{31} + 2S_{32} + S_{42})/q_2\end{aligned}\tag{6.13}$$

II. We correct spherical, coma and distortion.

The last two equations of (6.12) now become

$$\begin{aligned}\bar{S}_3 &= S_{31} + S_{32} + 2q_2 S_{22} + q_2^2 S_{12} \\ 0 &= 3S_{32} + S_{42} + 3q_2 S_{22} + q_2^2 S_{12}\end{aligned}$$

We can now introduce an extra target, we choose $S_{12} = 0$ because we now have $S_{11} = 0$ and $S_{21} = -S_{22}$. We find

$$\begin{aligned} S_{22} &= -S_{21} = \left(S_{32} + \frac{1}{4} S_{42} \right) / -q_2 \\ \bar{S}_3 &= S_{31} - S_{32} - \frac{2}{3} S_{42} \end{aligned} \quad (6.14)$$

III. We correct spherical, coma and astigmatism.

The last two equations of (6.12) become

$$\begin{aligned} 0 &= S_{31} + S_{32} + 2q_2 S_{22} + q_2^2 S_{12} \\ \frac{\bar{S}_5}{q_2} &= 3S_{32} + S_{42} + 3q_2 S_{22} + q_2^2 S_{12} \end{aligned}$$

When we again take $S_{12} = 0$ we find

$$\begin{aligned} S_{22} &= (S_{31} + S_{32}) / -2q_2 \\ \frac{\bar{S}_5}{q_2} &= \frac{3}{2} (S_{32} - S_{31}) + S_{42} \end{aligned} \quad (6.15)$$

In the formulas (6.11) there is no possibility of correcting field curvature (S_4). We estimate the Petzval sum of the total system (eye lens plus objective) as

$$P = \frac{2}{3} (0.030 + 0.039) = 0.046.$$

With $H = 0.3125$ we now have $S_4 = 0.00449$. The aberration on the CCD, at the edge of the field, becomes $\frac{S_4}{2H} = 0.00719$ mm, corresponding to 35 p/mm. At half field this becomes 140 p/mm

I. From the formulas (6.13) we obtain the component aberrations, with $\bar{S}_3 = \bar{S}_5 = 0$,

$$\begin{aligned} S_{11} &= -S_{12} = -0.01344 \\ S_{21} &= 0.02045, \quad S_{22} = 0.00925 \end{aligned}$$

Using the thin lens formulas for spherical and coma (4.16) we find the following solutions for the form factors of the components (Note that the solutions for the first and second doublet are independent, so that there are in fact four solutions).

$$(1) \quad B_{a1} = -0.7697, \quad (2) \quad B_{a1} = 1.7711, \\ B_{b1} = 2.0392, \quad B_{b1} = -4.7788,$$

for the first doublet, and

$$(1) \quad B_{a2} = -0.8280, \quad (2) \quad B_{a2} = 1.9400, \\ B_{b2} = 2.2533, \quad B_{b2} = -5.1755,$$

for the second doublet.

We prefer the first solutions because of the moderate values of the form factors. From the glass data the radii become (in mm):

$$\begin{aligned} r_1 &= 83.472, & r_5 &= 67.066, \\ r_2 &= -10.862, & r_6 &= -6.310, \\ r_3 &= -10.479, & r_7 &= -5.876, \\ r_4 &= -30.647, & r_8 &= 15.261. \end{aligned}$$

A scale drawing of this solution is given in Fig. 6.23.

II. With the second strategy we expect an astigmatism (of the objective) of $\bar{S}_3 = 0.00311$.

The conditions on the component aberrations are $S_{11} = S_{12} = 0$; $S_{21} = -S_{22} = +0.00522$.

We find the following solutions for the form factors of the components:

$$(1) \quad B_{a1} = -0.1178, \quad (2) \quad B_{a1} = 2.3989, \\ B_{b1} = 0.3128, \quad B_{b1} = -5.8090,$$

for the first doublet, and

$$(1) \quad B_{a2} = -0.3461, \quad (2) \quad B_{a2} = 2.1169, \\ B_{b2} = 1.2969, \quad B_{b2} = -5.3128.$$

for the second doublet. Again we prefer the first solution.

With these the radii become

$$\begin{aligned} r_1 &= 21.791, & r_5 &= 17.641, \\ r_2 &= -17.198, & r_6 &= -8.569, \\ r_3 &= -24.260, & r_7 &= -8.321, \\ r_4 &= 46.344, & r_8 &= 64.371. \end{aligned}$$

III. With the third strategy we will have a residual distortion $\bar{S}_5 = 0.00389$.

The conditions on the component aberrations become $S_{11} = S_{12} = 0$; $S_{21} = -S_{22} = 0.00365$. The solutions for the component form factors are

$$(1) \quad B_{a1} = -0.2490, \quad (2) \quad B_{a1} = 2.1991, \\ B_{b1} = 1.1271, \quad B_{b1} = -5.4421,$$



Fig. 6.23 Scale drawing (5:1) of retinascope objective I

for the first doublet, and

$$(1) \quad B_{a2} = -0.4060, \quad B_{a2} = 2.0632, \\ B_{b2} = 1.3996, \quad B_{b2} = -5.2271.$$

The radii for the first, preferred, solutions become

$$\begin{aligned} r_1 &= 25.598, & r_5 &= 19.420, \\ r_2 &= -15.391, & r_6 &= -8.204, \\ r_3 &= -14.972, & r_7 &= -7.965, \\ r_4 &= -250.573, & r_8 &= -47.827. \end{aligned}$$

For a scale drawing see Fig. 6.24.

When we compare the three predesigns we see that the first has a smallest radius of -5.9 mm. The other two have -8.3 and 8.0 mm respectively.

Because in the application resolution is important and some distortion can be tolerated, we will discuss in the following the third version. We are ready now with the thin lens design of our retinascope objective.

6.3.3 Exercise 10a, Thin Lens Design of a Retinascope Objective

Using the given lay-out data and the formulas for achromatizing (5.4) and thin lens aberrations (4.10), try to reproduce the thin lens designs obtained above, but with a different choice of glasses.

The targets are, respectively

1. $\bar{S}_1 = \bar{S}_2 = \bar{S}_3 = \bar{S}_5 = 0$,
2. $\bar{S}_1 = \bar{S}_2 = \bar{S}_5 = 0$, $\bar{S}_3 \neq 0$,
3. $\bar{S}_1 = \bar{S}_2 = \bar{S}_3 = 0$, $\bar{S}_5 \neq 0$.

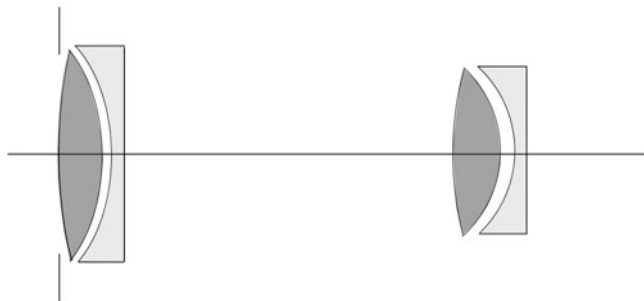


Fig. 6.24 Scale drawing (5:1) of retinascope objective III

Surface Model of the Retinascope Objective

To obtain a surface model we use the following procedure. We give thickness to the lenses of each component, and determine the power and the position of the principal planes for each component. Then we scale up the dimensions, as described in Sect. 4.4.

Finally we place the two components at the distance that corresponds to the distance between the two components in the thin lens model. This means that we must take $H'_1 H_2 = d$ (see the notation in Fig. 6.22). Together with the object distance $OH_1 = t$ and the image distance $H'_2 O' = t'$ we can obtain the complete surface model. From the lay-out we have $OH_1 = 128 \text{ mm}$, $H'_2 O' = 15.393 \text{ mm}$, and $H'_1 H_2 = 25.641 \text{ mm}$. We will use these data below to calculate the distances d_0 , d_4 and d_8 .

We now begin by giving realistic values to the remaining thicknesses according to the guidelines given in Sect. 4.4. We take $d_1 = 2 \text{ mm}$, $d_2 = 0.1 \text{ mm}$, $d_3 = 1 \text{ mm}$ for the first doublet, and $d_5 = 2.5 \text{ mm}$, $d_6 = 0.1 \text{ mm}$, $d_7 = 1 \text{ mm}$ for the second doublet. The distance d_5 is longest because of the small value of r_6 .

Using the radii given (version III) and the indices $n_2 = n_6 = 1.59142$, $n_4 = n_8 = 1.60718$ we trace paraxial rays, parallel to the axis, through both components from the front as well as the back side. In this way we find the powers and the positions of the principal planes for both components.

The result is, for this case

$$K_1 = 0.023590, K_2 = 0.039012$$

$$H_1 V_1 = 0.074, H'_1 V_4 = 2.049, H_2 V_5 = -0.406, H'_2 V_8 = 1.919$$

According to the lay-out the components should have the powers $K_1 = 0.0234$ and $K_2 = 0.0390$.

Therefore we have to scale up both components by the factors $p_1 = 0.9919$ and $p_2 = 0.9997$, respectively. That means that radii and distances must be divided by these scale factors.

For the positions of the principal planes we obtain

$$H_1 V_1 = 0.074, H'_1 V_4 = 2.065, H_2 V_5 = -0.406, H'_2 V_8 = 1.919.$$

With these we calculate the remaining distances

$$d_0 = OV_1 = OH_1 + H_1 V_1 = 128 + 0.074 = 128.074,$$

$$d_4 = V_4 V_5 = V_4 H'_1 + H'_1 H_2 + H_2 V_5 = -2.065 + 25.641 - 0.406 = 23.170,$$

$$d_8 = V_8 O' = V_8 H'_2 + H'_2 O = -1.919 + 15.393 = 13.474.$$

We now obtain the system specification.

#	Radius	Thickness	Glass	Diameter
0	Plane	128.074	Air	20
1	25.807	2.016	N-SK 5	8.5
2	-15.517	0.101	Air	8.5
3	-15.094	1.008	F 5	8.5
4	-252.619	23.170	Air	8.5
5	19.426	2.501	N-SK 5	9.5
6	-8.206	0.100	Air	9.5
7	-7.967	1.000	F 5	9.5
8	-47.886	13.474	Air	9.5
9	Plane	-	-	4

We have described the procedure to obtain a surface model from a thin lens predesign in detail. We do so for two reasons

- the procedure is tedious and it is easy to make errors in it (especially signs);
- these things are almost never described in books on lens design (Conrady and Kingslake are exceptions).

6.3.4 Exercise 10b, Surface Model of a Retinascope Objective

Using the results of exercise 10a, obtain a surface model for one of the predesigns.

Retinascope Objective, Paraxial Calculations

#	nu	h	n <u>u</u>	<u>h</u>	A	hΔ	hΔ
1	0.03318	4.25	0.07808	0	0.1979	0.0781	-0.2488
2	-0.06421	4.1686	0.07808	0.0989	-0.4917	0.0679	-0.8243
3	-0.22310	4.1461	0.07431	0.1064	-0.4978	0.0673	0.8346
4	-0.05663	4.1108	0.07859	0.1557	-0.0302	0.0796	-0.1825
5	-0.06620	2.5770	0.07822	1.9680	0.0666	0.1795	0.0234
6	-0.14465	2.3497	0.01830	1.9967	-0.6003	-0.3689	-0.6036
7	-0.31399	2.3183	-0.12560	1.9842	-0.6050	-0.3747	0.6047
8	-0.13732	2.2328	0.02562	2.0001	-0.2123	-0.0415	-0.2812

S ₁	S ₂	S ₃	S ₄	S ₅	C ₁	C ₂	
1	0.00974	0.00384	0.00152	0.00141	0	0.00509	0.00201
2	0.19933	-0.02753	0.00380	0.00234	-0.00085	0.01240	-0.00171
3	-0.20861	0.02794	-0.00378	-0.00244	0.00084	-0.02042	0.00276
4	0.00017	-0.00044	0.00115	0.00015	-0.00342	0.00123	-0.00323
5	-0.00010	-0.00028	0.00075	0.00187	0.00707	0.00103	0.00279
6	0.21753	0.13368	0.08215	0.00442	0.05320	0.00853	0.00524
7	-0.22131	-0.13705	-0.08487	-0.00463	-0.05543	-0.01388	-0.00860
8	0.01131	0.00216	0.00043	0.00077	0.00023	0.00469	0.00092
Σ	0.00806	0.00232	0.00115	0.00389	0.00164	-0.00133	0.00018

$$u_9 = -0.16505 \quad h_9 = 0.00083 \quad M = -0.20032 \\ \bar{u}_9 = 0.00023 \quad \bar{h}_9 = 2.0082$$

We summarize these results as follows:

$$\begin{aligned} S_{11} &= 0.00243 & S_{21} &= 0.00381 & S_{31} &= 0.00269 & S_{41} &= 0.00145 \\ S_{12} &= 0.00743 & S_{22} &= -0.00149 & S_{32} &= -0.00154 & S_{42} &= 0.00243 \\ S_1 &= 0.00986 & S_2 &= 0.00232 & S_3 &= 0.00115 & S_4 &= 0.00388. \end{aligned}$$

The residual distortion is $S_5 = 0.00164$.

Coma and astigmatism are corrected quite well, field curvature is what we expected.

Only spherical aberration is out of balance, especially in the second doublet.

We tried to improve the overall correction by bending the negative lens of the second doublet somewhat more. With $r_7 = -7.745$ and $r_8 = -40.863$ (mm) we obtain

$$\begin{aligned} S_{11} &= 0.00243 & S_{21} &= 0.00381 & S_{31} &= 0.00269 \\ S_{12} &= 0.00243 & S_{22} &= -0.00643 & S_{32} &= -0.00529 \\ S_1 &= 0.00486 & S_2 &= -0.00262 & S_3 &= -0.00260. \end{aligned}$$

Spherical aberration has been improved by a factor 2, coma and astigmatism have changed sign. Although the absolute value of astigmatism has doubled, this leads to a better balancing with field curvature. The meridional field curvature

$3S_3 + S_4$ is now -0.00392 instead of 0.00733 before; the sagittal field curvature $S_3 + S_4$ is 0.00128 instead of 0.00503 .

We used only one variable for optimization; a better result can be obtained by optimization with all four form factors as variables (this leaves colour correction intact).

It is interesting to compare these results with those of other authors (see the comment below). In the book of Kidger [7] a design of a “Petzval lens” is described that resembles our objective.

We note the third order coefficients:

	S_1	S_2	S_3	S_4	S_5
K.	0.02824	0.00623	-0.03273	0.13244	0.016927
	0.00986	0.00232	0.00115	0.00388	0.00164

where K. denotes Kidger’s system.

Also the paraxial parameters are different:

	f	u'	$\tan w$	H
K.	100	0.25	0.16	-3.8
	25.6	0.166	0.08	-0.31

The ratio of focal lengths is $100/25.6 = 3.9$.

We have to divide Kidger’s coefficients by this scale factor. We obtain

	S_1	S_2	S_3	S_4	S_5
K.	0.00724	0.00160	0.00039	0.03396	0.00434

Moreover, Kidger’s design has a larger aperture and field angle than ours. The aperture ratio is $\rho_u = 0.25/0.166 \cong 1.5$; the field angle ratio is $\rho_w = 0.16/0.08 = 2$.

We have to divide Kidger’s coefficients also by factors derived from these, to make a comparison more realistic. S_1 is divided by ρ_u^4 , S_2 by $\rho_u^3 \rho_w$, S_3 and S_4 by $\rho_u^2 \rho_w^2$ and by $\rho_u \rho_w^3$.

We now obtain the comparison.

	S_1	S_2	S_3	S_4	S_5
K.	0.00143	0.00023	-0.00093	0.00377	0.00036
	0.00986	0.00232	0.00115	0.00388	0.00164

Using Kidger’s design as a benchmark, we see that spherical and coma could be better corrected; the other coefficients are about right.

Note that Kidger’s design has been optimized, whereas ours is derived directly from the thin lens predesign.

The objective of the predesign was to correct fully spherical, coma and astigmatism; we see that the surface model needs some further correction to bring it to the level of Kidger's design.

We checked the predesign, using the Zemax software, and found substantially the same values for the coefficients. It turns out that the Schott catalogue, that is used by Zemax, has different values for the refractive indices from those of the book of Laikin, Lens Design.

The values used by Zemax are

$$\begin{aligned} \text{SK5: } n_d &= 1.589130, \quad V_d = 61.2668 \\ \text{F5: } n_d &= 1.603420, \quad V_d = 38.029 \end{aligned}$$

Therefore we can expect different values of the aberration coefficients.

We optimized this system by varying the radii of both doublets, and found the following results.

6.3.5 Exercise 11, Linear Optimization of a Retinascope Objective

Using the linear optimization procedure described in [Sect. 4.5](#), the reader should assess the effects of small changes of the form factors of the solution (1.1) of the predesign version III.

From this assessment a correction of the eight radii should be obtained that should result in a better correction of spherical, coma and astigmatism of the retinascope objective.

This should be checked by a paraxial calculation, followed by a calculation of the third order coefficients. The scheme of [Sect. 3.3](#) can be used for this purpose.

Optimization of the Retinascope Objective

The objective has an EFL of 26 mm, an image space F-number of F/3 and an object field radius of 10 mm. We optimized the spot size at fields of 0, 7.07 and 10 mm. The paraxial magnification was $M = -0.2$. The r.m.s. spot sizes in the image are found, after optimization, as 2, 1.7 and 3.5 μm . This is sufficient because the image sensor used has pixels of 5.3 μm diameter.

The lay-out of the system, the ray fan plots, the spot diagrams and the MTF are shown in Fig. [6.25](#)a–d. It is seen from the ray fan plots that there is a rest of astigmatism; this also shows up in the MTF values at 10 mm field.

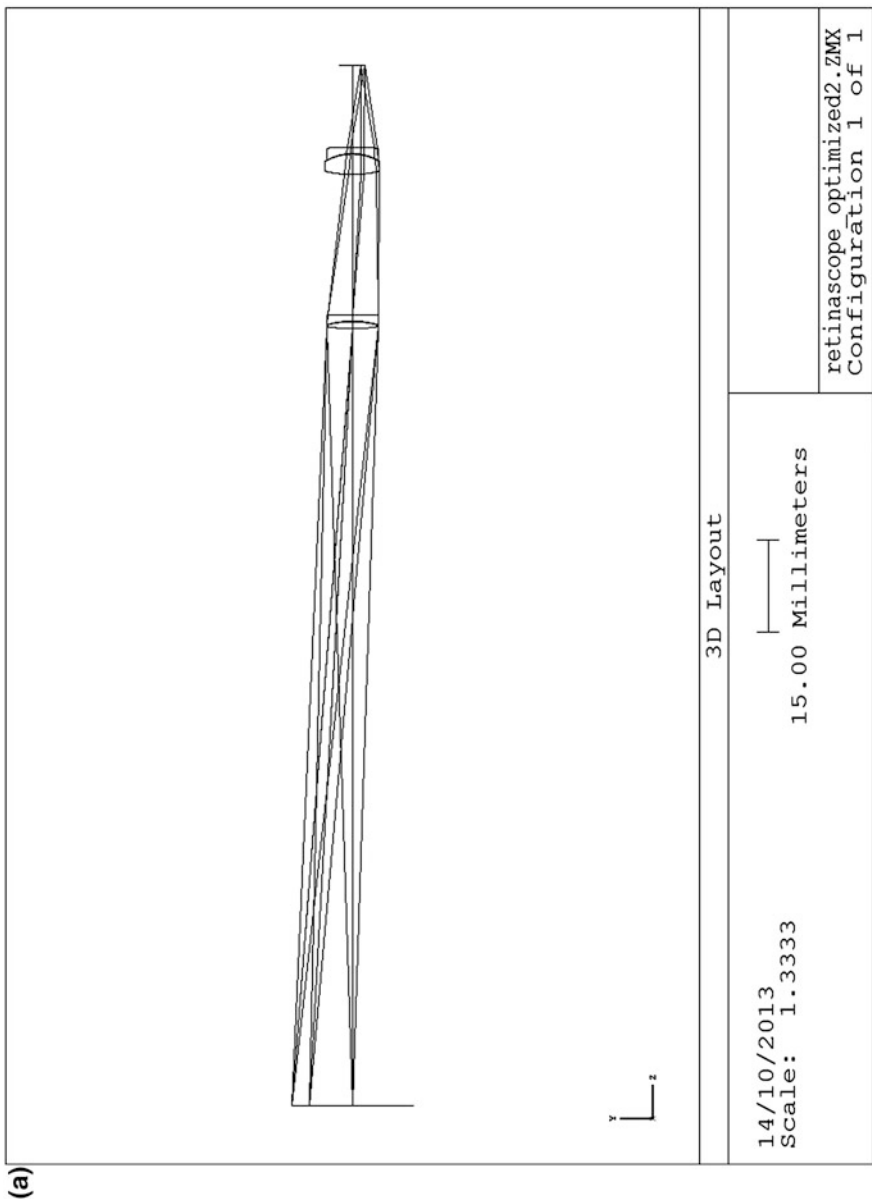


Fig. 6.25 **a** Retinascope objective, lay-out. **b** Retinascope objective, aberrations. **c** Retinascope objective, spot diagrams.
d Retinascope objective, MTF

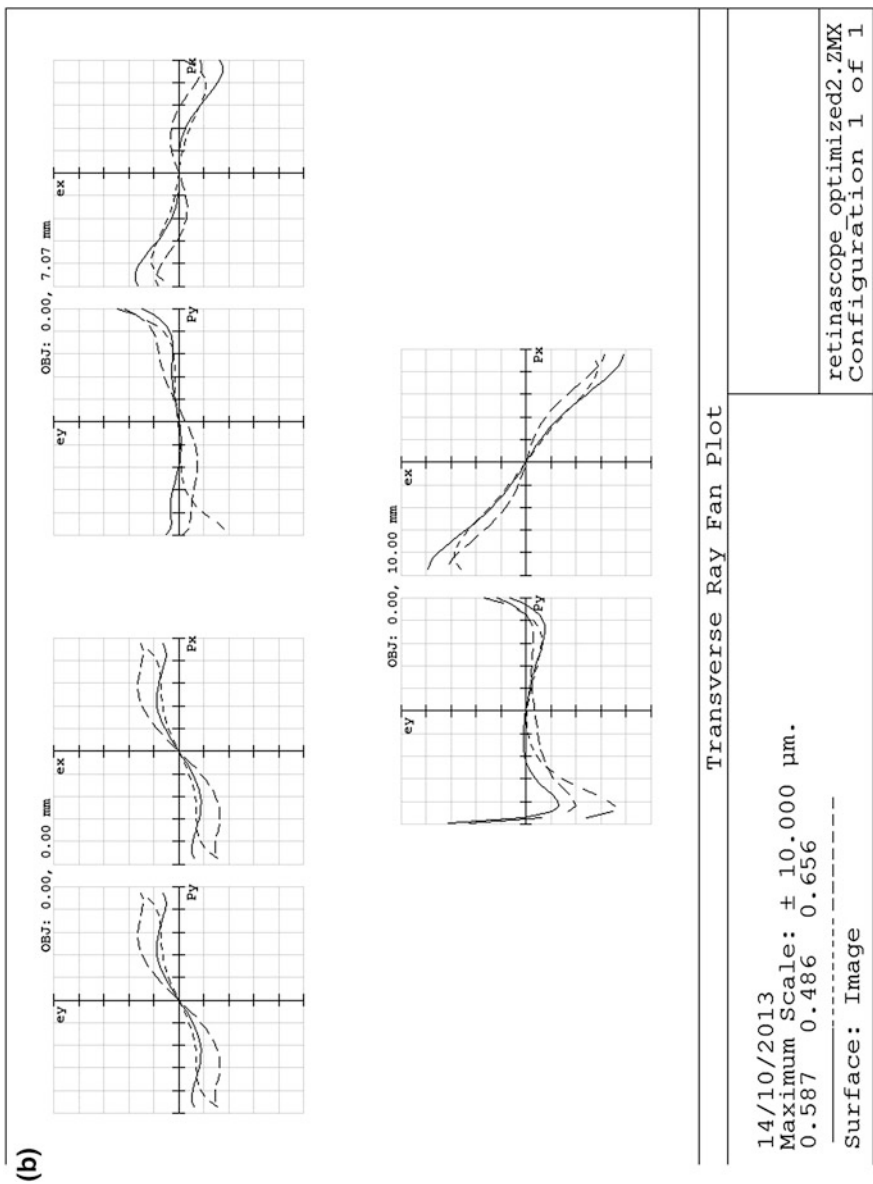


Fig. 6.25 (continued)

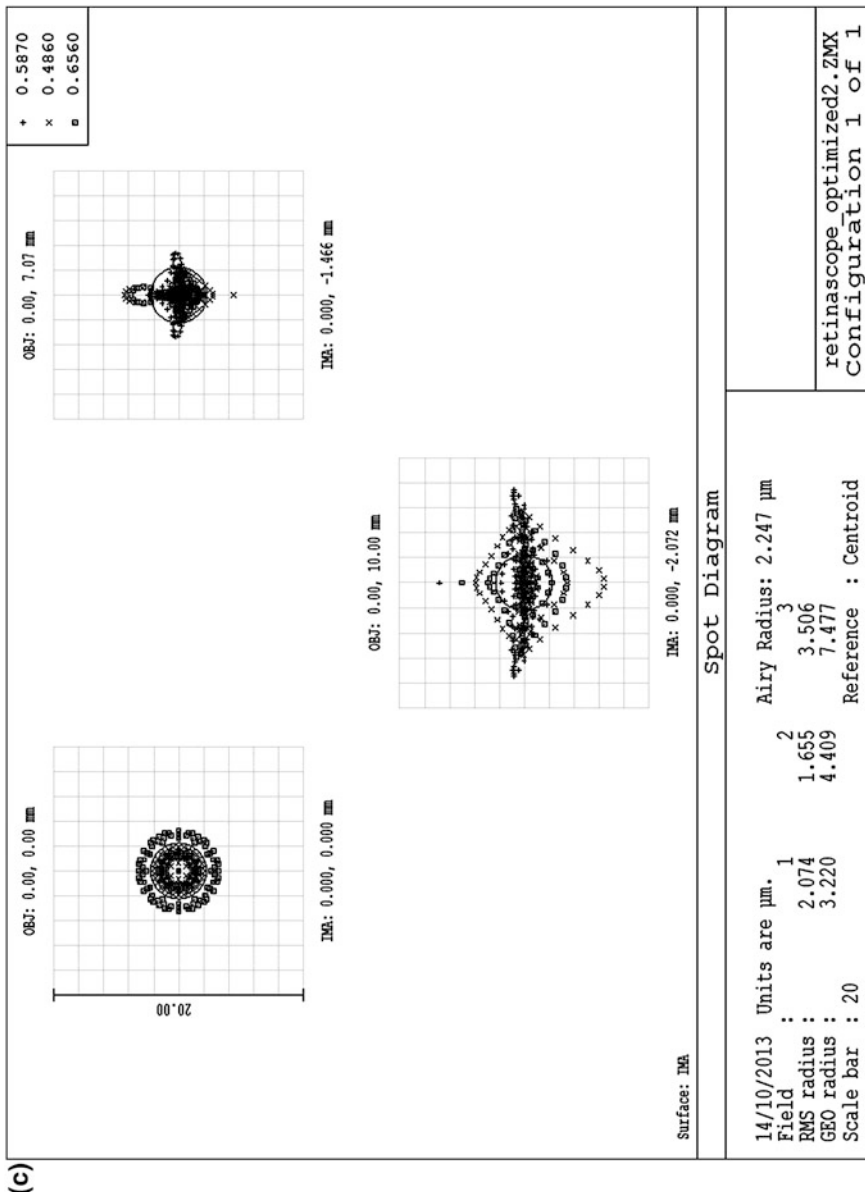


Fig. 6.25 (continued)

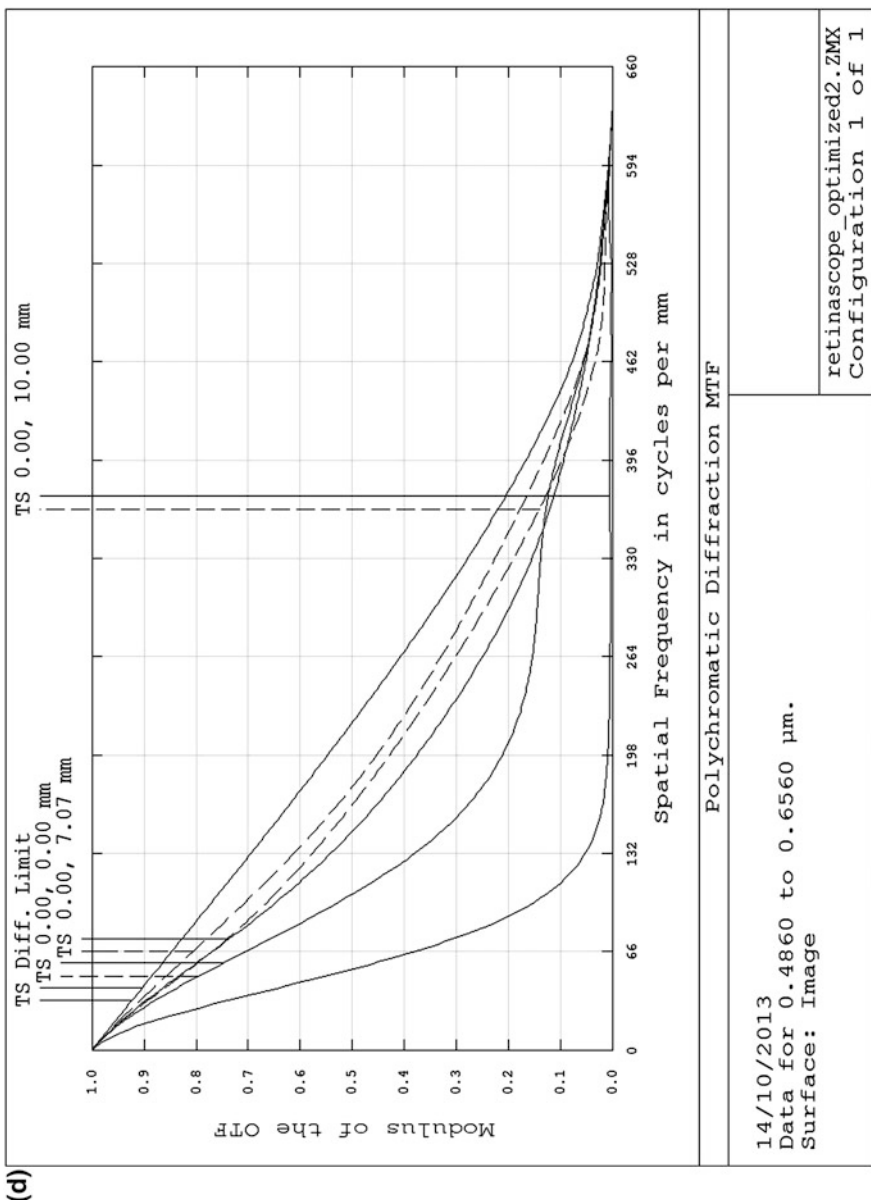


Fig. 6.25 (continued)

The prescription of this design is shown in the table below.

Surface data summary

Surf	Radius	Thickness	Glass	Diameter
OBJ	Infinity	128.074		20
STO	25.78226	1.1522	SK5	8.5
2	-15.65843	0.101		8.503008
3	-15.01059	0.999814	F5	8.478038
4	-193.4247	23.17		8.521683
5	18.23677	3.354283	SK5	8.955196
6	-8.878008	0.1		8.6643
7	-8.591382	0.9998633	F5	8.540485
8	-83.43639	13.474		8.235591
IMA	Infinity			4.153446

Comparison of Different Designs

To compare different designs, we follow a scaling procedure that reduces the third order aberrations of one of the systems to the values that they would have when the system would have the same paraxial parameters (focal length, aperture, field angle and Helmholtz invariant) as the system it is compared with.

Calling one system the benchmark and the other the test system we form the ratio's

$$\begin{aligned}\rho_f &= f(\text{benchmark})/f(\text{test}) \\ \rho_u &= u'(\text{benchmark})/u'(\text{test}) \\ \rho_w &= \tan w(\text{benchmark})/\tan w(\text{test})\end{aligned}$$

The product of these ratio's is the ratio of the Helmholtz invariants.

We reduce the third order coefficients of the benchmark system by the following factors:

$$\begin{aligned}S_1 &\text{ by the factor } \rho_f \rho_u^4 \\ S_2 &\text{ by the factor } \rho_f \rho_u^3 \rho_w \\ S_3 \text{ and } S_4 &\text{ by the factor } \rho_f \rho_u^2 \rho_w^2 \\ S_5 &\text{ by the factor } \rho_f \rho_u \rho_w^3.\end{aligned}$$

We could also multiply the test system coefficients by these factors.

In this way we have a fair comparison of the aberrations of both systems.

Many authors [12, 14, 15] use the focal length as a unit of length, $f = 1$. In this course we refrain from doing so, to avoid confusion (see the comment in Sect. 4.2). By the method outlined here a comparison between designs is always possible.

6.3.6 The Petzval Lens

We cite the introductory remarks of Berek [12]. “The Petzval portrait lens is the first high-aperture photographic objective; it is still applied often today, mainly for film projection. Also microscope objectives of low and moderate power are seen to be constructed in the same way if one counts the surfaces not from the side of the illuminator but from the long conjugate side, that is the side of the ocular”.

A modern application of the Petzval lens would be as a projection lens in a projector. Because of its reasonably high aperture and moderate field angle it fits this application well.

Lay-out

As data for the lay-out we take the focal length f , the back focal length s_2' and the distance d between the components.

From equation (1.28) we find

$$s_2' = (1 - dK_1)/K$$

so that

$$K_1 = (s_2' K - 1)/(-d)$$

and with (1.26)

$$K_2 = (K - K_1)/(1 - dK_1)$$

With $s_2' = 1/2f$, $d = f$, $K = 0.01 = 1/f$ we now have

$$K_1 = 0.005, \quad K_2 = 0.01 = K, \quad d = 100, \quad s_2' = 50$$

The second doublet in Petzval’s design has flint in front. Havliček [16, Chap. 1] recommends to take the ratio K_{2a}/K_{2b} so that the marginal ray becomes parallel to the optical axis between the components of this doublet. Variation of the distance between these components can then be used for the fine-tuning of coma and astigmatism [14]. Now the first doublet and the first lens of the second doublet form a Galilei telescope (see Fig. 6.26), so that we have

$$d = f_1 + f_{2a}$$

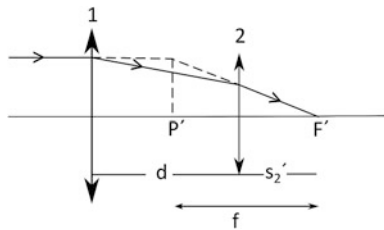
This can be written

$$K_{2a} = \frac{-K_1}{1 - dK_1}$$

With $K_2 = K_{2a} + K_{2b}$, which is still approximately true, we find

$$\frac{K_{2a}}{K_{2b}} = \frac{-K_1}{K}$$

Fig. 6.26 Petzval lens layout, notation



Achromatizing the second doublet, we must have

$$\frac{K_{2a}}{K_{2b}} = -\frac{V_{2a}}{V_{2b}}$$

as was shown in Sect. 5.1, so that in our glass choice we must have

$$\frac{V_{2a}}{V_{2b}} = \frac{K_1}{K}$$

With $s' = \frac{1}{2}f$, $d = f$ we have $K_1 = \frac{1}{2}K$, so that we have to take $V_{ab}/V_{2b} = 1/2$.

With the glass choice

- (a) N-SF 5, $n_a = 1.67764$, $V_a = 31.972$
- (b) BK 7, $n_b = 1.51872$, $V_b = 63.957$

we have $V_a/V_b = 0.49997$, good enough.

With our correction algorithm, see the introduction to this section, we obtain the following conditions for the component coefficients:

$$S_{11} = S_{12} = 0,$$

$$-S_{21} = S_{22} = -(S_{31} + S_{32})/2q_2 = -0.03375 \left/ \left(2 \cdot \frac{4}{3} \right) \right. = -0.01266,$$

where we used $H = -10 \cdot 0.15 = -1.5$: field radius is 10 mm, aperture is $u' = 0.15$. See Fig. 6.27.

Note that the second doublet of the Petzval lens has flint in front ($V_a < V_b$).

Kidger's "Petzval lens" looks more like a Lister microscope objective (five times magnified); see [7, p. 187].

When we turn the second doublet around we obtain a Dallmeyer lens [5, p. 259].

We now calculate the form factors of the components using the equations of the thin lens design, (6.11).

The results of the thin lens calculations are

$$(1) \quad B_{1a} = 0.2487 \quad \text{or} \quad (2) \quad B_{1a} = 2.2538, \\ B_{1b} = 1.1309 \quad \quad \quad B_{1b} = -9.7553$$

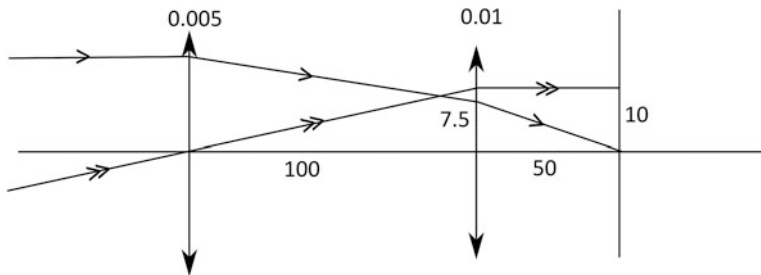


Fig. 6.27 Lay out of the Petzval lens I

With the first solution we obtain

$$r_1 = 83.079$$

$$r_2 = -138.093$$

$$r_3 = -127.200$$

$$r_4 = 2070.078$$

$$(1) \quad B_{2a} = 3.1542 \quad \text{or} \quad (2) \quad B_{2a} = -18.904 \\ B_{2b} = -0.1871 \quad \quad \quad B_{2b} = 3.8759$$

Again from the first solution

$$r_5 = -32.624$$

$$r_6 = -62.913$$

$$r_7 = 63.811$$

$$r_8 = -43.696$$

We show a rough sketch of this design in Fig. 6.28. It looks a bit questionable. The distance d is too large, so that the field diameter is small (20 mm) and the diameter of the second component quite large ($2h_2 + 2\bar{h}_2 = 35$ mm).

Moreover lens 2a is curved the wrong way, leading to large angles of incidence (large values of A) and large values of spherical and coma at surface 5, so that we can expect large higher order aberrations.

The main difference between Kidger's lay-out and the original Petzval design are

- Kidger's design is telecentric, this limits the diameter of the image field,
- the original design, as shown by Berek has a distance between the components d smaller than $\frac{1}{2}f$,
- the second doublet is originally flint-in-front, whereas Kidger has a crown-in-front one,
- the second component is a split doublet in the original design.

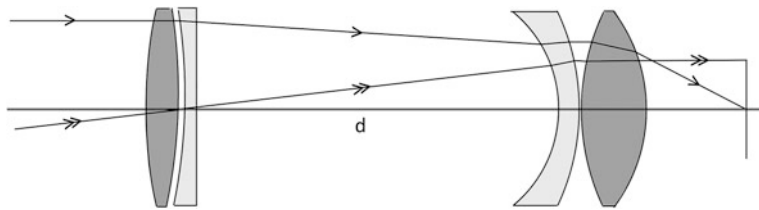


Fig. 6.28 Petzval radii from the thin lens model I

6.3.7 Exercise 12, Aberrations of a Petzval Lens

Berek gives the following data for the thin lens model of a Petzval lens:

$$\begin{aligned} n_{1a} = n_{2b} &= 1.517 \quad V = 60.2 \\ n_{1b} = n_{2a} &= 1.575 \quad V = 41.1 \end{aligned}$$

$$f = 100$$

$$\begin{array}{lll} r_1 = 53 & r_4 = 86 \\ r_2 = -46 & d = 38.7 & r_5 = 35 \\ r_3 = 300 & & r_6 = 41 \\ & & r_7 = -366 \end{array}$$

Calculate the thin-lens aberrations. Give thickness and calculate the third-order coefficients. Compare the result to those with design II.

Petzval Lens, New Lay-out

We try a new lay-out with $d = f/2$.

We take $h_1 K_1 = h_2 K_2$ to make the derivations of the marginal ray equal at both lenses (and as small as possible).

$$\begin{aligned} h_2 &= h_1(1 - dK_1) \\ K_1 &= K_2(1 - dK_1) \\ K &= K_1 + K_2(1 - dK_1) = 2K_1 \end{aligned}$$

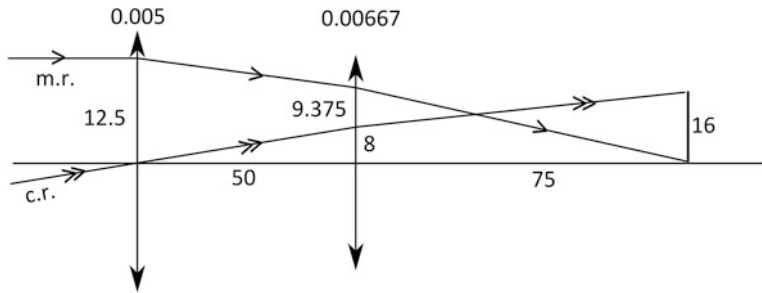
This is valid for all values of d .

With $d = \frac{1}{2}f$ we have $K_1 = 0.005$, $K_2 = \frac{2}{3}K = 0.00666\dots$. We have the back focal length $s_2' = 75$ mm.

$$u_2' = -h_1 \quad K = -2 h_1 K_1.$$

With $h_1 = 12.5$ we have aperture $u_2' = -0.125$.

$$h_2 = \frac{3}{4}h_1 = 9.375 \text{ mm}$$

**Fig. 6.29** Lay-out of Petzval lens II

With the stop in the first surface, $\tan w = \frac{\bar{h}_2}{d} = 0.16$

$$H = -12.5 \times 0.16 = -2$$

$$\bar{h}_{im} = \frac{H}{-u'_2} = 16$$

We keep the stop in the first lens. We now have $q_2 = \frac{8}{9.375} = 0.9532\dots$

The lay-out is shown in Fig. 6.29. The conditions on the component coefficients now become:

$S_{11} = S_{12} = 0$ as before,
with

$$S_{31} = 16 \cdot 0.005 = 0.080, \quad S_{32} = 16 \cdot 0.000667 = 0.107, \\ S_{22} = -S_{21} = -0.187/0.852 = -0.2192,$$

so that $\bar{S}_3 = 0$. S_4 is approximately equal to 0.125, and cannot be corrected any further.

From the thin lens (6.11) we now find the form factors and radii of a thin lens predesign.

Note that the system is no longer telecentric.

$$(1) \quad B_{1a} = 0.6336 \quad \text{or} \quad (2) \quad B_{1a} = 3.0958 \\ B_{1b} = 0.7449 \quad \quad \quad B_{1b} = -12.627$$

The first solution has the following curvatures

$$r_1 = 63.506 \\ r_2 = -283.13 \\ r_3 = -155.34 \\ r_4 = 1062.5$$

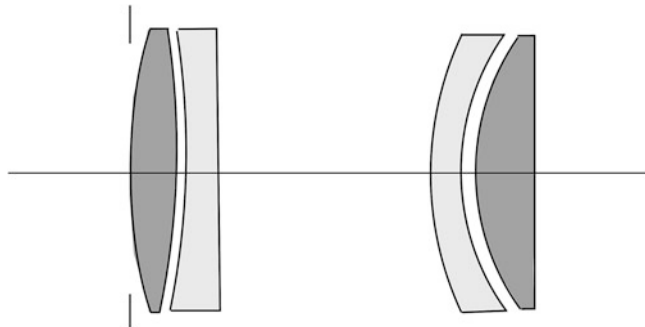


Fig. 6.30 Radii from the Petzval design II

$$(1) \quad B_{2a} = -4.5815 \quad \text{or} \quad (2) \quad B_{2a} = 7.6031 \\ B_{2b} = 0.9227 \quad \quad \quad B_{2b} = -1.3191$$

with the following radii, from the first solution:

$$\begin{aligned} r_5 &= 56.762 \\ r_6 &= 36.422 \\ r_7 &= 40.468 \\ r_8 &= -1006.6 \end{aligned}$$

This solution shows (see sketch in Fig. 6.30) a first doublet “from the book” and the second doublet with positive curvatures c_5 , c_6 and c_7 .

This looks much better than the previous design (Fig. 6.28).

The value of Δ on surface 5 is nearly zero, so that this surface is aplanatic (see Sect. 3.5). After surface 6 the marginal ray is parallel to the axis ($u'_6 \cong 0$). Changing the distance between surfaces 6 and 7 (d_6) does not change h_7 , but it does change \bar{h}_7 . That means that coma and astigmatism can be fine-tuned by little changes of d_6 .

Thus far we have not bothered to correct distortion. This can be done easily by shifting the stop; because we made spherical, coma and astigmatism equal to zero (at least approximately) a shift of the stop influences only distortion.

We have, with given \bar{S}_5 , to apply a correction $\Delta q \cdot S_4 = -\bar{S}_5$.

In Sect. 3.4 (3.24) we gave the following expression connecting Δq and the shift Δt of the entrance pupil:

$$\Delta q = \frac{\bar{h}_0}{h_p} \frac{\Delta t}{t + \Delta t'}$$

where t is the distance from the object to the entrance pupil (in this case $t = -s_1$).

With the object at infinity we must take $\frac{\bar{h}_0}{t} = \tan w$, the field angle, and we have

$$\Delta q = \Delta t \frac{\tan w}{h_p}.$$

Before giving thickness to the thin lens design of p. 127, we checked this design by calculating the third order coefficients according to the surface model.

Because it is a thin lens design we make all distances between surfaces zero for the first and second doublet, respectively. Moreover we take the same ray height for the surfaces 1 to 4, and also for the surfaces 5 to 8.

For the distances d_0 , d_4 and d_8 we use the lay-out values.

Now it turned out that $S_{11} = -0.01974$ and $S_{12} = -0.00010$.

Because the paraxial results (magnification, image distance, telecentricity) were correct, the form factors of the first doublet should be in error.

Going over the thin lens calculation of the first doublet again, we found a small error in the calculation of B_{1a} ; this resulted in a much larger error in B_{1b} .

The values of p. 127 are

$$B_{1a} = 0.6337, \quad B_{1b} = 0.7448$$

After correction we have now

$$B_{1a} = 0.6429, \quad B_{1b} = 0.6947.$$

We calculate the radii of the first doublet again and checked the first doublet in the way described above. Now we found $S_{11} = -0.00009$, $S_{12} = -0.00010$, $S_1 = -0.00001$.

We comment on the propagation of errors below.

On the Propagation of Errors

In the thin lens calculation we use equations of the following form:

$$\begin{aligned} aB_a^2 + bB_a + c &= 0 && \text{(condition on spherical)} \\ B_b &= dB_a + e && \text{(condition on coma)} \end{aligned}$$

to calculate the form factors of a doublet, where a , b , c , d , e are numerical constants. We see that variations of b and c give variations of B_a according to

$$\frac{dB_a}{dc} = \frac{1}{B_a} \frac{dB_a}{db} = \frac{\pm 1}{\sqrt{b^2 - 4ac}}.$$

In the example above we had an error $\Delta c = 0.02$. This gave a variation of B_a equal to 0.00925. Because the value of d was -5.43 , the variation of B_b became -0.0502 , quite substantial.

With $B_a = 0.6337$, $B_{1b} = 0.7448$ (uncorrected values) we have

$$\frac{dB_a}{dc} = 0.0146 \quad \frac{dB_b}{db} = -0.0674$$

If we want the corrected values for the form factors to be correct in the fourth decimal, our calculation must be correct in the fifth decimal (or perhaps sometimes in the sixth).

The new prescription of our Petzval design (version IIc) becomes (in mm)

$$\begin{array}{ll} r_1 = 63.146 & r_5 = 56.762 \\ r_2 = -290.52 & d_4 = 50 \quad r_6 = 36.422 \quad r_4 = 887.83 \\ r_3 = -159.94 & r_7 = 40.468 \\ r_4 = 887.83 & r_8 = -1006.6 \end{array}$$

We give thickness to this design and calculate the third order coefficients. For the prescription of the surface model we find

#	Radius	Thickness	Glass	Diam
0	Plane	Infinity		-
1	66.328	8.403	N-BK 7	25
2	-305.16	2.101		25
3	-168.00	5.252	N-SF 5	25
4	923.57	30.854		25
5	59.529	5.244	N-SF 5	26
6	38.197	2.098		26
7	42.441	10.488	N-BK 7	26
8	1055.67	65.373		26
9	Plane	-		32

The diameters of the second component need to be somewhat larger than 25 if we do not want to have vignetting. It may be that some vignetting will be necessary to cut off rays with large aberrations.

The result of our calculations of the Seidel coefficients was

#	nu	h	n <u>h</u>	<u>h</u>	A	<u>A</u>	hΔ
1	0	12.500	0.16	0	0.1883	0.16	-0.5298
2	-0.09776	11.959	0.16	0.8853	-0.1573	0.15559	-0.9054
3	-0.11809	11.711	0.15850	1.2183	-0.1878	0.15125	1.0881
4	-0.07085	11.489	0.16637	1.7297	-0.0502	0.16648	-0.4288
5	-0.06250	9.561	0.16463	6.8091	0.0981	0.27901	0.0155
6	-0.17133	9.025	0.08712	7.0814	0.2251	0.39814	0.4482
7	-0.01122	9.002	0.21275	7.5277	0.2009	0.39012	-0.3722
8	-0.12123	8.165	0.12075	8.3615	-0.1290	0.10872	-0.5935

#	S ₁	S ₂	S ₃	S ₄	S ₅	C ₁	C ₂
1	0.01878	0.01595	0.01355	0.01558	0.02475	0.01250	0.01062
2	0.02239	-0.02215	0.02190	0.00448	-0.02610	0.00999	-0.00988
3	-0.03838	0.03215	-0.02490	-0.00963	0.02780	-0.02743	0.02209
4	0.00108	-0.00358	0.01188	-0.00173	-0.03365	0.00719	-0.02385
5	-0.00015	-0.00043	-0.00120	0.02713	0.07375	0.01170	0.03326
6	-0.02270	-0.04016	-0.07105	-0.04230	-0.20050	-0.02533	-0.04481
7	0.01502	0.02916	0.05663	0.03220	0.17750	0.00960	0.01865
8	0.00987	-0.00831	0.00703	0.00130	-0.00700	0.00559	-0.00472
Σ	0.00591	0.00264	0.01383	0.02703	0.03655	0.00381	0.00137

We summarize these results as follows:

$$\begin{aligned} S_{11} &= 0.00388 & S_{21} &= 0.02240 & S_{31} &= 0.0224 & S_{41} &= 0.0087 & S_{51} &= -0.00720 \\ S_{12} &= 0.00204 & S_{22} &= -0.01974 & S_{32} &= -0.0086 & S_{42} &= 0.0183 & S_{52} &= 0.04405 \\ S_1 &= 0.00592 & S_2 &= 0.00266 & S_3 &= 0.0138 & S_4 &= 0.0270 & S_5 &= 0.03685 \end{aligned}$$

$$\begin{aligned} C_{11} &= 0.00226 & C_{21} &= -0.00102 \\ C_{12} &= 0.00156 & C_{22} &= 0.00238 \\ C_1 &= 0.00382 & C_2 &= 0.00136 \end{aligned}$$

The coefficients are still larger than those of designs from the literature, but the design has not yet been optimized.

As a first step toward optimization we changed the form of the lenses of the first component. We found that the first lens has nearly minimum spherical aberration; therefore we tried changing the second lens. With radii $r_3 = -150.00$ and $r_4 = 2,905.00$ and thickness $d_3 = 5.8046$, which leaves the paraxial properties unchanged, we found

$$S_{11} = -0.00005, \quad S_{21} = 0.0233, \quad S_{31} = 0.0225$$

so that

$$S_1 = 0.00200, \quad S_2 = 0.00010, \quad S_3 = 0.0139.$$

Spherical has become much better, coma and astigmatism did not change much.

After that we changed the form of the lenses of the second component. The positive lens had again nearly minimum spherical. Therefore we bent the negative lens a bit more. With $r_5 = 57.428$ and $r_6 = 37.269$, and thickness $d_5 = 5.1245$ we found the aberration coefficients

$$S_{12} = 0.00010, \quad S_{12} = 0.00010, \quad S_{32} = -0.0113$$

so that

$$S_1 = 0.00005, \quad S_2 = 0.00020, \quad S_3 = 0.0122, \quad S_4 = 0.0270.$$

For the moment we are content with this result. Kidger's design (in fact a Dallmeyer lens) has

$$S_1 = 0.0282, \quad S_2 = 0.0062, \quad S_3 = -0.0327.$$

This design has F/2.3, where our design has F/4. With F/4 Kidger's design would have

$$S_1 = 0.00308, \quad S_2 = 0.00107, \quad S_3 = -0.0108.$$

We can understand that the Petzval lens was applied originally as a portrait lens.

The correction can be very good in the central part of the image (spherical and coma are quite small).

The "Dallmeyer" design of Kidger has a better correction of the field curvatures. With $S_4 = 0.13244$ meridional curvature is $3S_3 + S_4 = 0.0346$ and the sagittal curvature is $S_3 + S_4 = 0.0997$. Converting to F/4 we get $3S_3 + S_4 = 0.0114$, $S_3 + S_4 = 0.0330$.

The prescription of the optimized design is

	#	Radius	Thickness	Glass	Diameter
OB	0	Plane	Infinity		—
STO	1	66.328	8.403	N-BK 7	25
	2	-305.16	2.101		25
	3	-150.00	5.805	N-SF 5	25
	4	2905.00	30.854		25
	5	57.428	5.125	N-SF 5	26
	6	37.269	2.098		26
	7	42.441	10.488	N-BK 7	26
	8	1055.67	65.373		26
	9	Plane	—		32

6.3.8 Exercise 13, Air Space of the Petzval Lens

We saw, in the preceding pages, that the choice of distance equal to f between the components of a Petzval lens leads to a positive form factor B_{2a} for the first lens of the second doublet. When we take $d = 1/2f$ we obtain a negative value for B_{2a} .

It is plausible that an intermediate value of d , say $0.75f$, could lead to a small value of B_{2a} . Find out which value of d gives a zero value of B_{2a} , using the thin lens algorithm of the beginning of this section, (6.11).

Optimization of the Petzval Lens

The F/4, EFL = 100 mm Petzval lens was optimized for field angles of 0, 7 and 10°, with the surface radii as variables. From the ray fan plot shown in Fig. 6.31b

it can be seen that the correction in the center of the field is satisfactory, with a small defocus.

For the middle field astigmatism shows up; at the field edge also coma is quite visible and astigmatism becomes dominant. Colour correction is sufficient.

In Fig. 6.31 a we give the lay-out of this design.

The prescription follows.

Surface data summary:

Surf	Radius	Thickness	Glass	Diameter
OBJ	Infinity	Infinity		
STO	121.7345	2.557114	BK 7	25
2	-57.1543	2.902504		25.30732
3	-41.2824	10.00	SF 5	25.32251
4	-64.50738	30.854		28.02487
5	173.3332	2.041382	SF 5	32.53365
6	60.74304	2.405679		32.55371
7	-1530.003	3.285918	BK 7	32.59258
8	-48.06819	70.00157		32.72703
IMA	Infinity			35.62443

Comment

We learn the following about the design of two-component systems from our attempts at optimization.

- The positive lenses of the doublets that we designed have a minimum of spherical aberration. This corresponds to a small value of the coma coefficient.
- The negative lenses of the doublets must compensate for the spherical of the positive ones, and generate part of the coma that is necessary to correct astigmatism. These two points make clear that the positive lenses must have a form factor in the neighborhood of 0.8 (minimum spherical for $n = 1.5 n$), whereas the negative lens of the second doublet (with a position factor of 3) will have a larger bending.

With the Petzval IIc design the following form factors resulted

$$\begin{aligned} B_{1a} &= 0.6429, & B_{1b} &= 0.6947 \\ B_{2a} &= -4.5815, & B_{2b} &= 0.9227 \end{aligned}$$

With these form factors (B_{1a} and B_{1b}) for the positive components it is clear that there is some freedom to change the coma coefficient without changing spherical much.

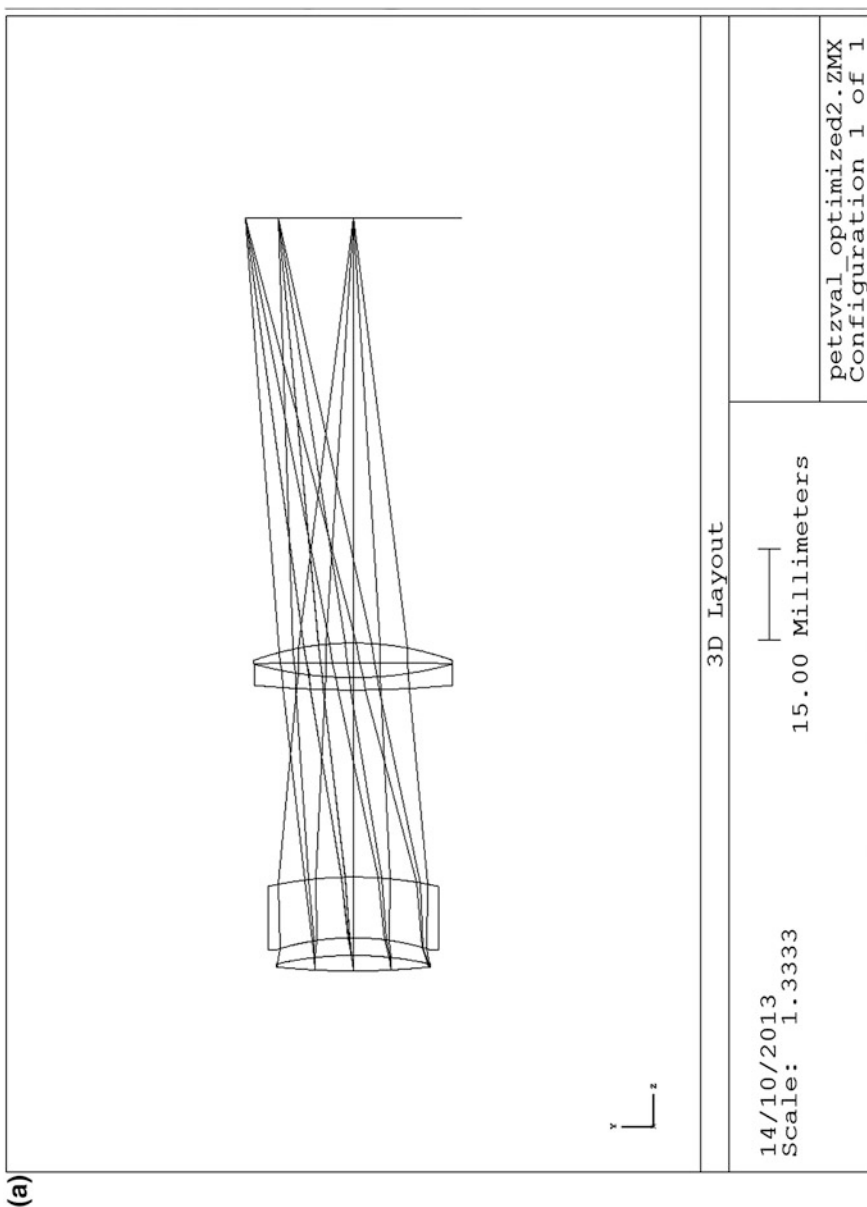


Fig. 6.31 a Petzval lens 2, lay-out. b Petzval lens 2, aberrations

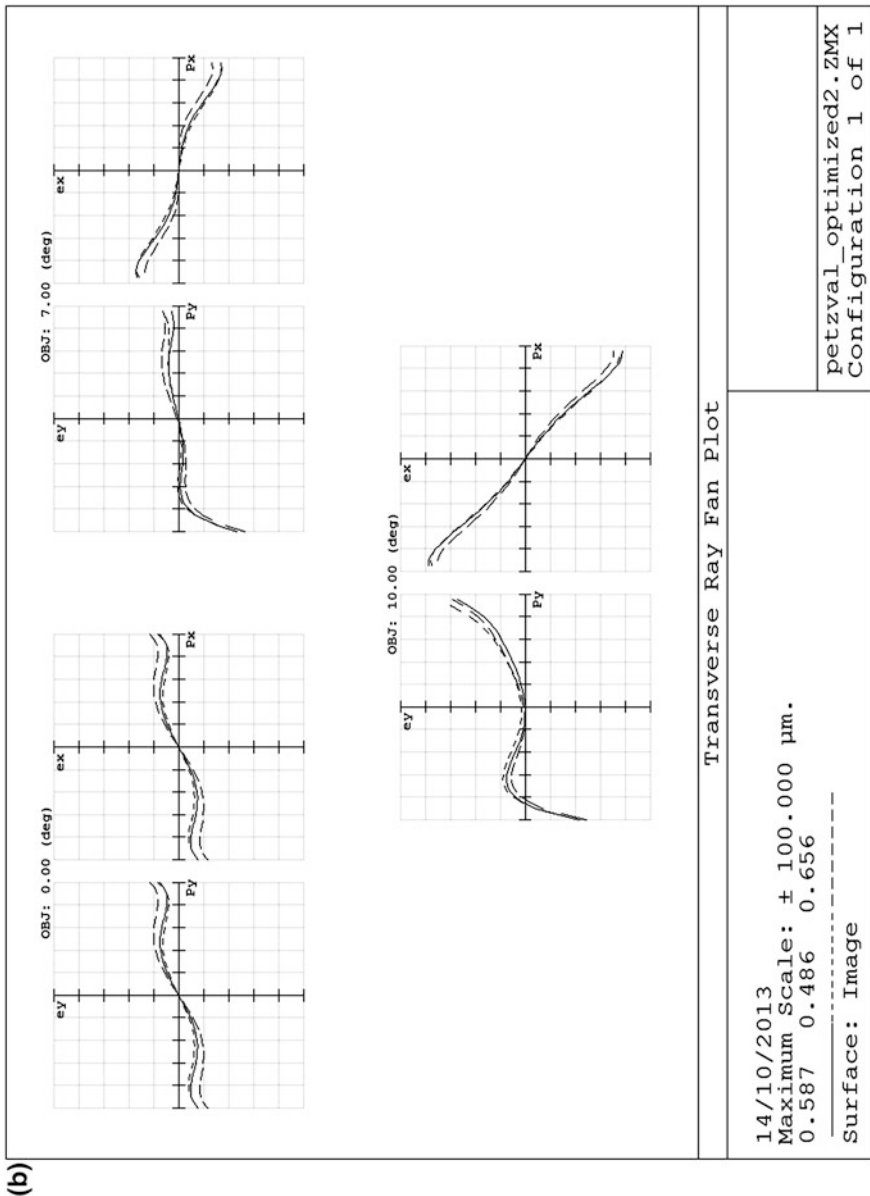


Fig. 6.31 (continued)

6.3.9 Tele-Objectives

A two-component lens with a negative second component is called a tele-objective. From Fig. 6.32 we see directly that such a system has a focal length ($H'F'$ in Fig. 6.32) that is larger than the distance from the first lens to the image (V_1F').

The ratio $R_t = V_1F'/H'F'$ is called the *telephoto ratio*.

With such a system, field curvature and astigmatism can be corrected easier than with the two-component systems treated before, because the sum of powers is smaller. Berek warns [12, Chap. 9f] that distortion cannot be so easily corrected with this type of system.

Lay-out of the Tele-Objective

A simple lay-out follows when we take $K_2 = -K_1$, with K_1 positive.

We then find, using paraxial equations,

$$R_t = 1 - \frac{f_1}{f} + \left(\frac{f_1}{f} \right)^2$$

When R_t is given, f_1/f follows as

$$\frac{f_1}{f} = \frac{1}{2} \left(1 \pm \sqrt{1 - 4(1 - R_t)} \right)$$

For $R_t < 0.75$ there is no solution for f_1/f .

With $R_t = 0.8$ we find the two solutions

$$\frac{f_1}{f} = 0.7236 \text{ or } 0.2764$$

With $f = 100$ we now have

$$\begin{aligned} (\text{Ia}) \quad f_1 &= -f_2 = 72.36, & d &= 52.36, & s'_2 &= 27.64, & \text{or} \\ (\text{Ib}) \quad f_1 &= -f_2 = 27.64, & d &= 7.64, & s'_2 &= 72.36. \end{aligned}$$

We find two types of tele-objectives, that are both present in the literature [7, 8, 17]. The first type mentioned above has the advantage that its powers K_1, K_2 are smallest. For a mirror reflex camera one would prefer the second type, because it has a large back focal length (s'_2).

We give the thin lens aberration equations (6.11) for the case that $q_1 = 0$ (stop at the first component).

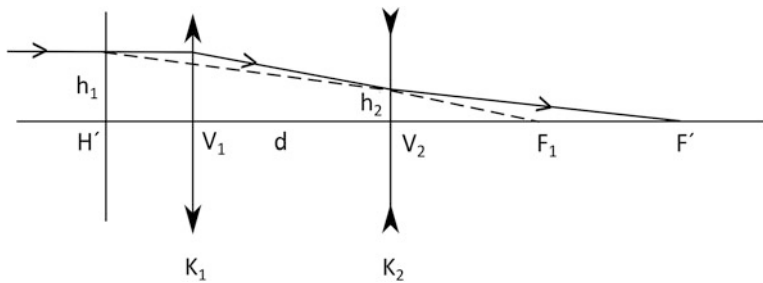


Fig. 6.32 Lay-out of the tele-objective

$$\begin{aligned}
 S_1 &= S_{11} + S_{12} \\
 S_2 &= S_{21} + S_{22} + q_2 S_{12} \\
 S_3 &= S_{31} + S_{32} + 2q_2 S_{22} + q_2^2 S_{22} \\
 S_4 &= S_{41} + S_{42} \\
 S_5 &= S_{51} + S_{52} + q_2(3S_{32} + S_{42}) + 3q_2^2 S_{22} + q_2^3 S_{12}
 \end{aligned} \tag{6.16}$$

With two aplanats, \$S_{11} = S_{12} = 0\$, \$S_{21} = S_{22} = 0\$ we have

$$S_5 = q_2(3S_{32} + S_{42}).$$

This situation arises when \$K_1 = -K_2\$, so that \$S_{31} + S_{32} = 0\$; we assumed that \$S_{51} = S_{52} = 0\$.

When we take the same glasses for both components, also \$S_4\$ becomes zero.

From the aberration equations follows that we can make all third order aberrations zero in our thin lens predesign, except distortion for which we find, for modest performance parameters \$\tan w = 0.1\$ and \$h_p = 15\$ (or \$F = 3.3\$) a value of \$-4.7\%\$, for the lay-out Ia.

We can try to reduce the distortion by giving different powers to the two components.

With \$K_2 = -xK_1\$ we have

$$xR_t = 1 + (x-2)\frac{f_1}{f} + \left(\frac{f_1}{f}\right)^2,$$

so that

$$\frac{f_1}{f} = 1 - \frac{1}{2} \left(x \pm \sqrt{x^2 - yx(1 - R_t)} \right)$$

and

$$\frac{d}{f} = \frac{x-1}{x} \frac{f_1}{f} + \frac{1}{x} \left(\frac{f_1}{f} \right)^2 \quad \frac{s'_2}{f} = \frac{1}{x} \left(1 - \frac{f_1}{f} \right).$$

With $K_2 = -\frac{3}{4}K_1$ we obtain

$$\frac{f_1}{f} = \frac{5}{8} \pm \sqrt{3 \left(R_t - \frac{13}{16} \right)}.$$

with $R_t = \frac{13}{16} = 0.8125$, slightly higher than before, we find

$$\frac{f_1}{f} = 0.625, \quad \frac{f_2}{f} = -0.833, \quad \frac{d}{f} = 0.313, \quad \frac{s'_2}{f} = 0.5.$$

From the lay-out data follows $q_2 = (4.16)\tan w$, and $S_5 = -0.0407$, $S_5/2n'u' = 0.135$ (mm), so that we have a distortion of -1.35% .

With $f = 100$ we have the lay-out $f_1 = 62.5$ mm, $f_2 = -83.33$ mm, $d = 31.25$ mm, $s_2 = 50$ mm

With tele-objectives with components of unequal power ($x \neq 1$) the Petzval curvature S_4 cannot be corrected. We can reduce it by giving the second component a different equivalent index from the first.

In the following table we compare the two lay-outs that we found

	K_1	K_2	d	s'_2	S_4	S_5
I	0.0138	-0.0138	52.36	27.640	0	-0.1415
II	0.0160	-0.0120	31.25	50.00	0.0065	-0.0407

In both lay-outs S_1 , S_2 and S_3 are fully corrected. We see that we can reduce S_5 at the cost of some field curvature.

Thin Lens Predesign of the Tele-objective

With the lay-out I we have $S_{31} + S_{32} = 0$. When we take the same glasses for the two components we also have $S_{41} + S_{42} = S_4 = 0$.

From the lay-out we have, with the glasses

$$\text{N-BK 7, } n = 1.51872, \quad V = 63.957,$$

$$\text{N-SF5, } n = 1.67764, \quad V = 31.972,$$

$$K_{1a} = 0.02764, \quad K_{1b} = -0.01382, \quad G_{1a} = -1, \quad G_{1b} = 3;$$

$$K_{1b} = -0.02764, \quad K_{2b} = 0.01382, \quad G_{2a} = 2.6232, \quad G_{2b} = -4.2512$$

with crown-in-front for both components.

When we take aplanatic doublets: $S_{11} = S_{12} = 0$ and $S_{21} = S_{22} = 0$ we obtain the solution for the bendings

$$B_{1a} = -0.1460, \quad B_{1b} = 2.007,$$

$$\text{or } B_{1a} = 1.7293, \quad B_{1b} = -8.1825,$$

$$B_{2a} = -1.395, \quad B_{2b} = 0.4210,$$

$$\text{or } B_{2a} = -3.060, \quad B_{2b} = -9.4572.$$

Taking the alternatives with the lowest bending values, we obtain the following prescription for the thin lens model I:

$$\begin{array}{ll} r_1 = 44.015 \text{ (mm)} & r_5 = 95.161 \\ r_2 = -32.801 & r_6 = 15.697 \\ r_3 = -32.728 & r_7 = 69.112 \\ r_4 = -98.142 & r_8 = -169.66 \\ d = 52.36 & s'_2 = 50.00 \end{array}$$

Because of the small value of r_6 , the second doublet has a large airgap (see Fig. 6.33a). this will lead to large differences in the aberration values between the thin lens model and the surface model.

We also tried a flint-in-front solution for the second component, with

$$K_{2a} = 0.01382, K_{2b} = -0.02764, G_{2a} = -8.2464, G_{2b} = 3.6198.$$

We obtained the following solutions for the bendings:

$$\begin{array}{ll} B_{2a} = 5.0096, & B_{2b} = -2.2587 \\ \text{or } B_{2a} = 12.7901, & B_{2b} = -3.6918. \end{array}$$

The first solution leads to the prescription

$$\begin{array}{l} r_5 = 16.348 \text{ (mm)} \\ r_6 = 24.499 \\ r_7 = 29.822 \\ r_8 = 11.519 \end{array}$$

The airgap has become quite modest (see Fig. 6.33b) but the last radius is small. We tried a different couple of glasses:

$$\begin{array}{ll} \text{PSK 52} & n = 1.60530, V = 65.137 \\ \text{SF 50} & n = 1.65994, V = 32.628 \end{array}$$

but the results were not much better: a large airgap for the crown-in-front and a small value of r_8 for the flint-in-front.

The thin lens model with two aplanats results in a distortion $S_5 = -0.1415$ corresponding to -4.7% .

We consider the reduction of distortion for lay-out I. From the aberration equations (6.16) we see that astigmatism is corrected ($S_3 = 0$) when $S_{12} = -2S_{22}/q_2$. In that case $S_5 = q_2(3S_{32} + S_{42}) + q_2^2S_{22}$. To correct the negative distortion we must have a positive value of S_{22} . The values of S_{21} and S_{11} follow from the aberration equations.

We tried $S_{12} = -0.0632$, $S_{22} = 0.0397$; this gives $S_5 = -0.1416 + 0.0633 = -0.0828$ or -2.8% distortion.

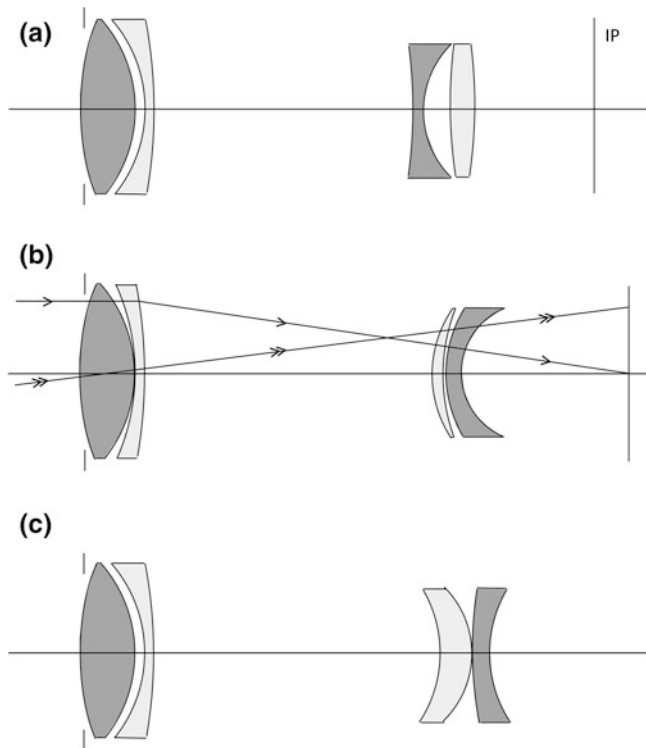


Fig. 6.33 **a** Teleobjective Ic, crown-in-front second doublet. **b** Tele-objective If, flint in front second doublet, **c** Tele-objective Id, reduced distortion

The radii for this case become (with flint-in-front)

$$\begin{aligned}
 r_1 &= 55.818 & r_5 &= -21.482 \\
 r_2 &= -28.277 & r_6 &= -14.936 \\
 r_3 &= -28.370 & r_7 &= 66.769 \\
 r_4 &= 67.322 & r_8 &= 14.650 \\
 d &= 52.36 & \text{bfl} &= 27.64
 \end{aligned}$$

The crown-in-front second doublet with the same value of S_{12} and S_{22} has a smaller value of r_6 . Comparing this result to that with aplanatic doublets, we see that the radius values r_6 and r_8 are small, but the value of r_8 has improved.

We now consider lay-out II.

With the same glasses as before (N-BK 7 and N-SF 5) we have $q_1 = 0$, $q_2 = 0.416$, and

$$\begin{aligned}
 K_{1a} &= 0.0320, & K_{1b} &= -0.0160, & G_{1a} &= -1, & G_{1b} &= 3, \\
 K_{2a} &= -0.0240, & K_{2b} &= 0.0120, & G_{2a} &= \frac{5}{3}, & G_{2b} &= -\frac{7}{3}
 \end{aligned}$$

with flint in front.

We make $S_3 = 0$ taking $S_{11} = S_{12} = 0$, $S_{21} = -S_{22} = 0.01082$. The first doublet gets the radii

$$\begin{aligned}r_1 &= 39.716 \text{ (mm)} \\r_2 &= -27.389 \\r_3 &= -27.330 \\r_4 &= -77.051 \\d &= 31.25\end{aligned}$$

The crown-in-front second doublet has the radii

$$\begin{aligned}r_5 &= -59.923 \\r_6 &= 33.068 \\r_7 &= -67.106 \\r_8 &= -30.666 \\blf &= 50.00\end{aligned}$$

In flint-in-front version has the prescription

$$\begin{aligned}r_5 &= 50.433 \\r_6 &= 471.765 \\r_7 &= 2068.25 \\r_8 &= 21.389\end{aligned}$$

A sketch of both models is given in Fig. 6.34.

The residual aberrations are: $S_4 = 0.00648$ and $S_5 = -0.0474$ (or -1.4%).

A comparison of the results with both lay-outs gives the following conclusion:

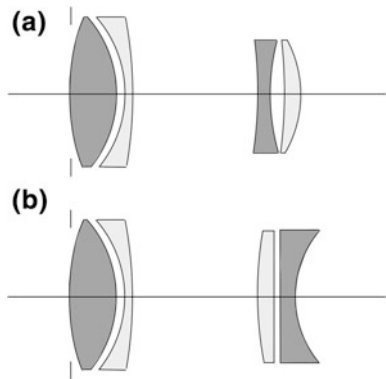
Lay-out II has less distortion, larger radius values and smaller airgaps than lay-out I, lay-out II has a residual field curvature of $S_4 = 0.00648$. This gives an aberration of $21.6 \mu\text{m}$ at the edge of the field (the Airy diameter is about $4 \mu\text{m}$). Lay-out I has a residual barrel distortion larger than 2.8% .

We will use both versions obtained with lay-out II to produce a surface model in order to optimize them.

Surface Models for the Tele-objective II

We start with the crown-in-front predesign. After the usual routine (described in Sect. 4.4 and worked out in detail in Sect. 6.3) we arrive at the following prescription:

Fig. 6.34 **a** Tele-objective II, crown-in-front second doublet. **b** Tele-objective II, flint in front second doublet



Tele-objective IIc

	#	Radius	Distance	Glass	Diameter
ST	1	37.679	6.640	N-BK 7	30
	2	-27.730	0.098	Air	30
	3	-27.450	2.784	N-SF 5	30
	4	-80.423	30.334	Air	30
	5	-52.449	1.804	N-BK 7	22
	6	30.155	2.213	Air	22
	7	-62.135	3.408	N-SF 5	22
	8	-27.705	41.434	Air	22
	9	Plane	-	-	20
IM					

The results of the paraxial calculations and the third order coefficients are given below. We see from these results that the balances in the thin lens predesign have been taken over by the surface model. The coefficients of field curvature and distortion (-2 %) have already acceptable values.

Paraxial results of Tele-objective IIc

#	nu	h	n <u>u</u>	<u>h</u>	A	<u>A</u>	hΔ
1	0	15	0.1	0	0.3981	0.1	-1.343
2	-0.20651	14.097	0.1	0.4372	-0.9786	0.0761	-5.367
3	-0.47021	14.051	0.09182	0.4462	-0.9821	0.0756	5.991
4	-0.12335	13.846	0.10283	0.6168	-0.4135	0.0900	-2.717
5	-0.24002	6.566	0.09763	3.5783	-0.3652	0.0294	1.078
6	-0.17509	6.358	0.13302	3.7363	0.1451	0.3212	0.065
7	-0.06573	6.212	0.19729	4.1729	-0.1657	0.1301	0.413
8	0.00202	6.216	0.24279	4.6662	-0.3784	-0.0398	-0.937

#	S ₁	S ₂	S ₃	S ₄	S ₅	C ₁	C ₂
1	0.2128	0.0535	0.0134	0.02039	0.0085	0.03171	0.00797
2	5.1390	-0.3994	0.0310	0.02772	-0.0045	0.07325	-0.00570
3	-5.7783	0.4445	-0.0342	-0.03309	-0.0052	-0.17208	0.01325
4	0.4644	-0.1010	0.0219	0.01130	0.0072	0.07139	-0.01554
5	-0.1437	0.0115	-0.0009	-0.01465	0.0012	-0.01273	0.00102
6	-0.0014	-0.0030	-0.0067	-0.02363	-0.0671	-0.00490	-0.01084
7	-0.0113	0.0093	-0.0069	-0.01463	-0.0169	-0.01284	0.01008
8	0.1341	0.0141	0.0015	0.03281	0.0036	0.02933	0.00308
Σ	0.0150	0.0295	0.0191	0.00622	-0.0732	0.00313	-0.00284

We see from the paraxial results that surfaces 2 and 3 have high values of A and high, but opposite, values of $h\Delta$. This results in high values of S₁ for these surfaces. Because the radii of surfaces 2 and 3 are about equal, we could cement these surfaces, giving them a common radius of -27.590.

The values of spherical and coma of the resulting surface 2 would be approximately S₁ = -0.64 and S₂ = 0.045, with a small value of astigmatism S₃ ≈ -0.003.

Even then the first doublet has a heavy load; this could be reduced by splitting the first lens. We will come back to that topic in the next subsection.

We now consider the surface model of the predesign with a flint-in-front second doublet (see Fig. 6.34b). We take over the prescription of the first doublet, given above, and obtain the following prescription:

Tele-objective IIIf

	#	Radius	Distance	Glass	Diameter
ST	1	37.679	6.640	N-BK 7	30
	2	-27.730	0.098	Air	30
	3	-27.450	2.784	N-SF 5	30
	4	-80.423	19.484	Air	30
	5	45.780	2.193	N-SF 5	25
	6	428.886	0.091	Air	25
	7	1886.255	2.178	N-BK 7	25
	8	19.618	54.292	Air	25
IM	9	Plane	-	-	20.05

The results of the paraxial calculations and the surface coefficients of the Seidel aberrations are given below. We see that the resulting values of the third order coefficients are of the same order for both systems considered.

Paraxial results of Tele-objective IIIf

#	n_u	h	$n\bar{u}$	\bar{h}	A	\bar{A}	$h\Delta$
1	0	-1.5	0.1	0	0.3981	0.1	-1.3430
2	-0.20651	-1.497	0.1	0.4372	-0.9786	0.0756	-5.3665
3	-0.47021	-1.507	0.09182	0.4462	-0.9821	0.0761	5.9911
4	-0.12335	-1.501	0.10283	0.6168	-0.4135	0.0900	-2.7166
5	-0.24002	-1.500	0.09763	2.5349	-0.03972	0.1526	0.9766
6	-0.37575	-1.500	0.05962	2.6148	-0.3418	0.0699	-1.9833
7	-0.36204	-1.500	0.06375	2.6206	-0.3575	0.0651	1.7641
8	-0.36442	-1.502	0.06303	2.7110	-0.2644	0.2729	0.0681

#	S_1	S_2	S_3	S_4	S_5	C_1	C_2
1	0.2128	0.0535	0.0134	0.02039	0.0213	0.03171	0.00797
2	5.1390	-0.0399	0.0310	0.02772	-0.0045	0.07325	-0.00570
3	-5.7783	0.4445	-0.0342	-0.0331	-0.0052	-0.17208	0.01325
4	0.4644	-0.1010	0.0219	0.0113	0.0072	0.07139	-0.01554
5	-0.0015	0.0154	-0.0227	0.0199	-0.0109	0.00454	0.01745
6	0.2317	-0.0473	0.0097	-0.0021	-0.0015	0.03699	-0.00756
7	-0.2157	0.0411	-0.0075	0.0004	0.0014	-0.01641	0.00299
8	-0.00476	-0.00491	-0.00507	-0.0392	-0.0077	-0.00502	-0.00965
Σ	0.0476	0.00679	0.0116	0.0053	0.0001	0.02437	0.00321

Optimization of a Telephoto Objective

The telephoto objective IIc, with F/4 and EFL = 100, was optimized for the field angles 0, 8.06 and 11.4°.

After an optimization run with only the surface radii it turned out that it was necessary to vary also the air distance between the components and to find new glasses. After this the correction was uniform over the field, with r.m.s. spot radii of 8 μm.

The lay-out is shown in Fig. 6.35a, the ray fan plots in Fig. 6.35b.

The prescription of this design is shown in the table below.

Surface data summary

Surf	Radius	Thickness	Glass	Diameter
OBJ	Infinity	Infinity		
STO	38.25139	6.64	LAK 33	24
2	-66.19386	0.098		24.57753
3	-63.11035	2.784	N-SF 10	24.5591
4	152.0804	12.54019		24.22412

(continued)

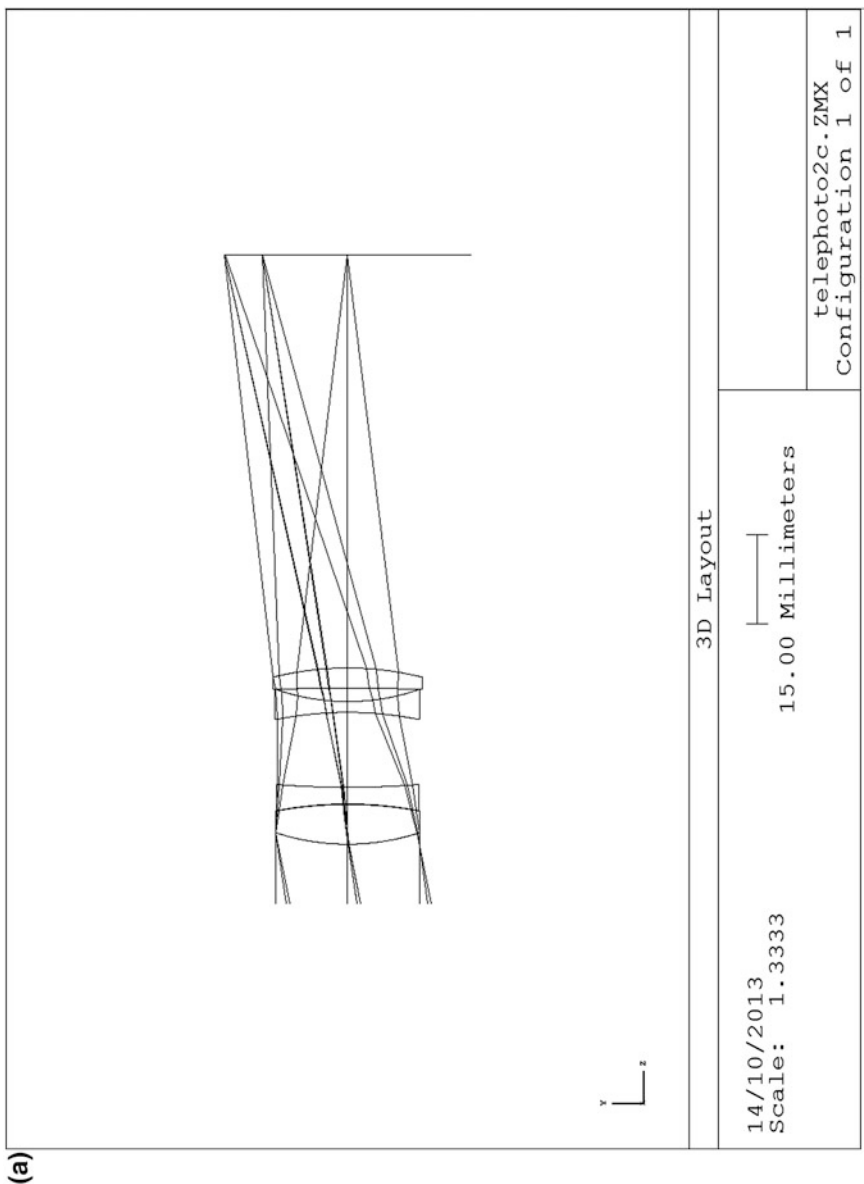


Fig. 6.35 a Telephoto lens 2c, lay-out. b Telephoto lens 2c, aberrations

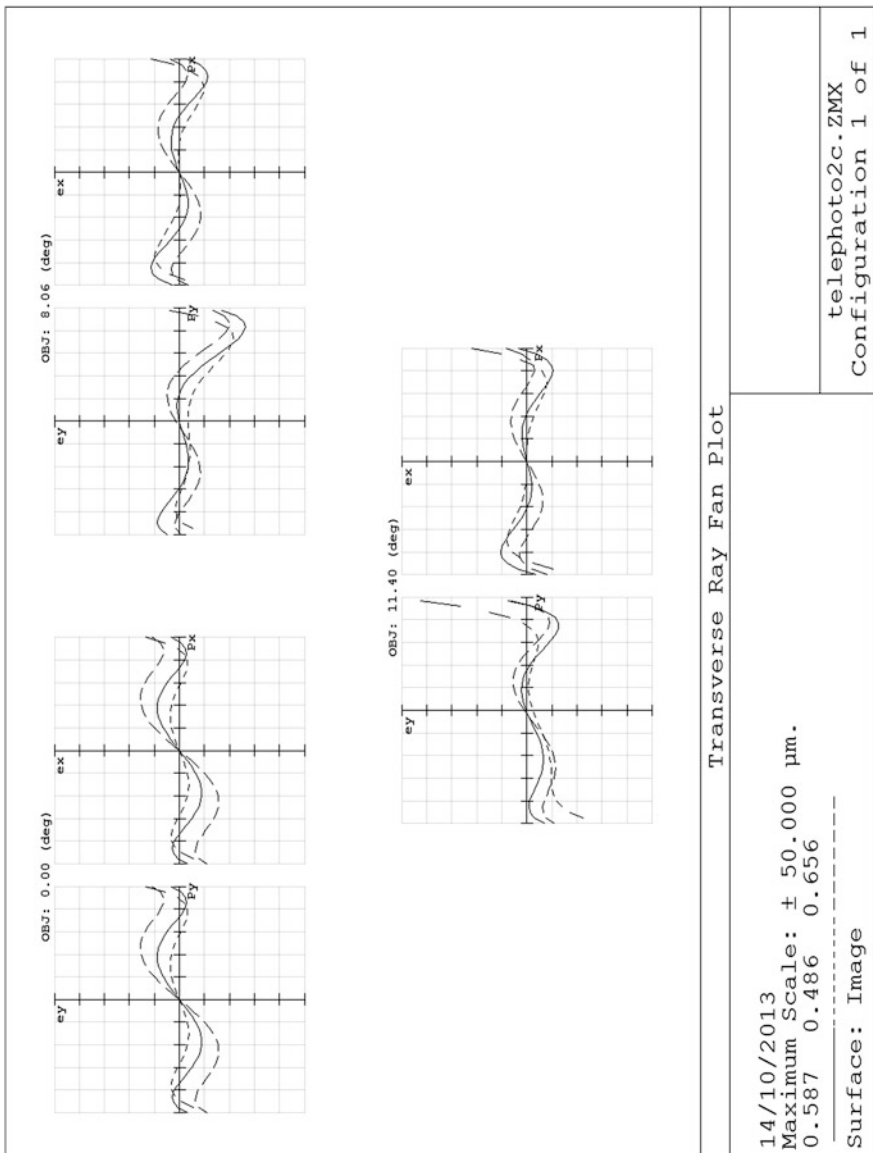


Fig. 6.35 (continued)

(continued)

Surf	Radius	Thickness	Glass	Diameter
5	-59.34959	1.804	KZFN 2	24.07505
6	36.13923	2.213		24.77126
7	-587.5455	3.408	N-LASF 31	24.7024
8	-50.98128	69.17733		25.39134
IMA	Infinity			41.16574

6.3.10 The Split Tele-Objective

In the previous section we saw that the first doublet of our telephoto design (II) is heavily loaded. Its second and third surface have large values of $h\Delta$ as well as of A , and consequently of S_1 .

To reduce the load we split the first lens of this doublet. With the stop at the lens we obtain the aberration equations

$$\begin{aligned} S_{11} &= S_{1a} + S_{1b} + S_{1c} \\ S_{21} &= S_{2a} + S_{2b} + S_{2c}, \end{aligned}$$

where a and b denote positive lenses, and c the negative lens; together the three lenses form a (thin) achromat.

The right-hand-side of the first equation is quadratic in the form factors B_a , B_b and B_c , and the right-hand-side of the second equation is linear. We suppose that the targets S_{11} and S_{21} are given, as is the case in the design examples treated thus far.

To solve these two equations we have three degrees of freedom, so that we can introduce an extra condition. In this case we decide to cement the second and third components (b and c); the cementing condition is given in Sect. 6.1 as

$$B_b = 1 + \frac{K_c n_b - 1}{K_b n_c - 1} (B_c + 1).$$

Substituting B_b in S_{1b} and S_{2b} we obtain two equations for B_a and B_c , of which one is linear and the other quadratic, so that we can proceed as we did before with our thin lens predesign.

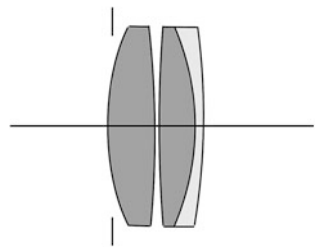
As an example we take the first doublet of Tele-objective II (this is identical in the version IIC and IIf).

With the existing doublet we have

$$K_{1a} = 0.0320, \quad K_{1b} = -0.0160, \quad \frac{1}{S_a} = 0.$$

The glasses used were N-BK7 and N-SF5.

Fig. 6.36 The first doublet of the split tele-focus lens



We split the first lens into two lenses of equal power, so that we obtain

$$K_a = 0.0160, \quad K_b = 0.0160, \quad K_c = -0.0160$$

We have to calculate first the position factors.

With $1/s_a = 0$ we obtain

$$G_a = -1 \quad G_b = -3 \quad G_c = +3$$

Following the procedure outlined above, with the targets $S_{11} = 0$, $S_{21} = 0.01082$ we obtain the solutions

$$\begin{aligned} (1) \quad B_a &= 0.6263, & B_b &= -1.0716, & B_c &= 1.7063 \\ (2) \quad B_a &= 2.275, & B_b &= -44.90, & B_c &= 58.97 \end{aligned}$$

Clearly the second solution is impractical; from the first solution we find the radii

$$\left. \begin{aligned} r_1 &= 39.876 \\ r_2 &= -173.537 \\ r_3 &= -905.738 \\ r_4 &= -31.305 \\ r_5 &= -31.314 \\ r_6 &= -119.927 \end{aligned} \right\} \quad \begin{aligned} &a \\ &b \\ &c \end{aligned}$$

Giving thickness results in the distances

$$d_1 = 4.5, \quad d_2 = 0, \quad d_3 = 4.5, \quad d_4 = 0, \quad d_5 = 2 \text{ (mm).}$$

In Fig. 6.36 we give a sketch of this design.

We show the results of the paraxial calculations and the aberrations per surface. Clearly the spherical aberration is out of balance. Also the power of the component is too small: $K_1 = 0.0155$.

Paraxial results of the tele-objective II, splitted first doublet, surface model

#	nu	h	$n\bar{u}$	\bar{h}	A	\bar{h}	$h\Delta$
1	0	15	0.1	0	0.3762	0.1	-1.269
2	-0.19512	14.422	0.1	0.2963	-0.3213	0.0974	-2.216
3	-0.23823	14.422	0.09911	0.2963	-0.2542	0.0988	1.998
4	-0.22996	13.741	0.09928	0.5905	-0.8965	0.0707	0.587
5	-0.16023	13.540	0.10228	0.7124	-0.3497	0.0923	-2.437

#	S ₁	S ₂	S ₃	S ₄	S ₅	C ₁	C ₂
1	0.1795	0.0477	0.0127	0.0193	0.0085	0.02996	0.00797
2	0.2277	-0.0693	0.0210	0.0044	-0.0077	0.02460	-0.00746
3	-0.1291	0.0509	-0.0198	-0.0009	0.0080	-0.01947	0.00757
4	-0.4717	0.0368	-0.0029	-0.0045	0.0006	-0.08820	0.00696
5	0.2980	-0.0766	0.0205	0.0076	-0.0075	0.05904	-0.01558
Σ	0.1034	-0.0105	0.0315	0.0259	0.0019	0.00593	-0.00054

We tried to improve the design by shifting some power from surface 3 to surface 4, and adapting the power of surface 5 so that we obtain the correct power, $K_1 = 0.0160$.

The prescription of the design becomes

#	Radius	Distance	Glass	Diameter
1	39.876	4.5	N-BK 7	30
2	-173.54	0	Air	30
3	Plane	4.5	N-BK 7	30
4	-28.100	2.0	N-SF 5	30
5	-115.50		Air	30

We show the results of the paraxial calculations and the aberration coefficients below.

We add also the chromatic aberration coefficients, to make sure that the correction of colour is still sufficient.

There is now a marked improvement of spherical aberration, at the cost of some increase of coma.

Paraxial results of tele-objective II, splitted first doublet, revised surface model

	nu	h	$n\bar{u}$	$n\bar{u}$	A	\bar{A}	$h\Delta$
1	0	15	0.1	0	0.3762	0.1	1.269
2	-0.19512	14.422	0.1	0.2963	-0.3206	0.0974	-2.216
3	-0.23823	14.422	0.09911	0.2963	-0.2382	0.0991	1.946
4	-0.23823	13.716	0.09911	0.5900	-0.98527	0.0673	0.6338
5	-0.16065	13.525	0.10245	0.7121	-0.3577	0.0920	-2.501

#	S ₁	S ₂	S ₃	S ₄	S ₅	C ₁	C ₂
1	0.1795	0.0477	0.0127	0.0193	0.0085	0.0301	0.0080
2	0.2277	-0.0693	0.0210	0.0044	-0.0077	0.0246	-0.0075
3	-0.1104	0.0459	-0.0191	0	0.0080	-0.0183	0.0076
4	-0.6153	0.0420	-0.0029	-0.0050	0.0005	-0.0985	0.0067
5	0.3200	-0.0823	0.0211	0.0076	-0.0072	0.0611	-0.0157
Σ	-0.0003	-0.0160	0.0328	0.0263	0.0021	-0.0010	-0.0009

Adding the aberrations of the flint-in -front second component we obtain

$$\begin{array}{lllll} S_{11} = -0.0003 & S_{21} = -0.0160 & S_{31} = 0.0328 & S_{41} = 0.0263 & S_{51} = 0.0021 \\ S_{12} = 0.0126 & S_{22} = 0.0091 & S_{32} = -0.0205 & S_{42} = -0.0210 & S_{52} = -0.0187 \\ S_1 = 0.0123 & S_2 = -0.0069 & S_3 = 0.0123 & S_4 = 0.0053 & S_5 = -0.0166 \end{array}$$

Adding the surface data of the second component of Tele-objective IIIf we obtain the prescription

Tele-objective IIIf with split first component

	#	Radius	Distance	Glass	Diameter
STO	1	39.876	4.5	BK 7	30
	2	-173.54	0	Air	30
	3	Plane	4.5	BK 7	30
	4	-28.100	2	Sf 5	30
	5	-115.50	18.122	Air	30
	6	45.780	2.193	SF 5	25
	7	428.886	0.091	Air	25
	8	1886.26	2.178	BK 7	25
	9	25.672	54.292	Air	25
	10	Plane	-	-	20.05
IM					

Optimization of the Split Telephoto Objective

The split telephoto objective had EFL = 100 mm as before, but F/3.3 instead of F/4. It was optimized for the field angles 0, 3.5, 6.0, 9.0, 11.4°. We used the same variables as with the previous telephoto lens: radii, main air distance and glasses. We obtained again a uniform correction with r.m.s. spot radii of 12.8, 11.0, 9.1, 9.8 and 12.9 μm. The previous lens had r.m.s. spot radii of about 8 μm. When we take the difference in F-number into account and assume that the r.m.s. spot radius is determined mainly by spherical aberration and defocus, we can conclude that the image quality has become slightly better with splitting (r.m.s. spot sizes below 7 μm with F/4).

In Fig. 6.37a the lay-out is shown and in Fig. 6.37b the ray-fan plots.

The prescription of this system follows below.

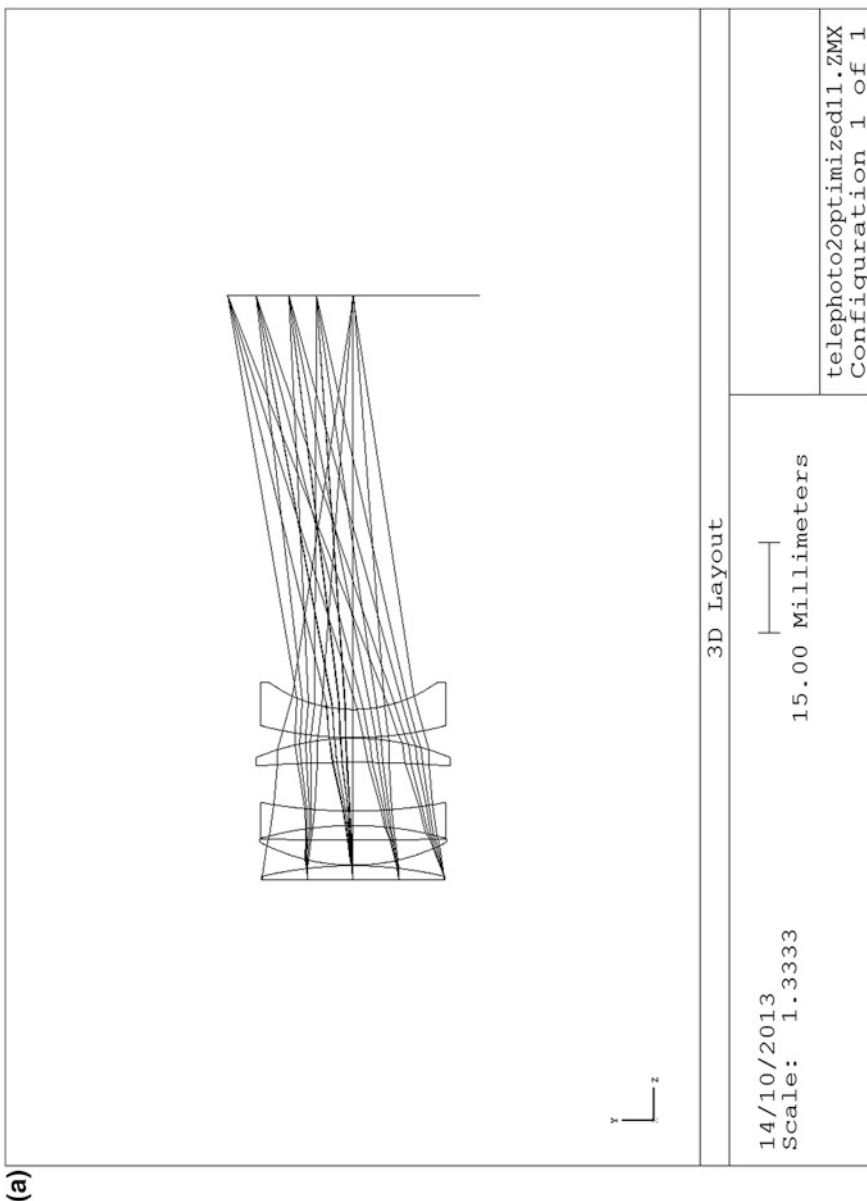


Fig. 6.37 a Split telephoto lens, lay-out. b Split telephoto lens, aberrations

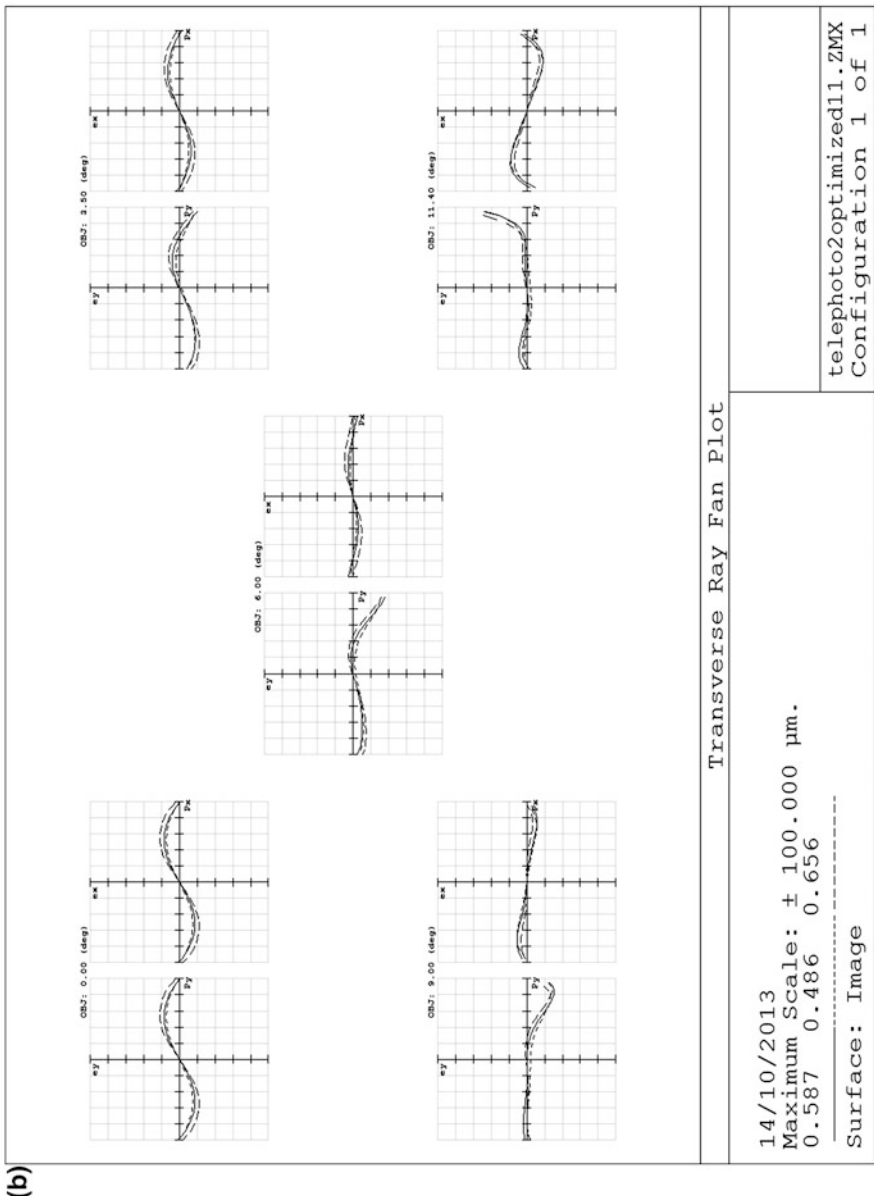


Fig. 6.37 (continued)

Surface data summary

Surf	Radius	Thickness	Glass	Diameter
OBJ	Infinity	Infinity		
STO	11692.45	2.264586	N-PSK 53	30
2	-65.54108	0.09770865		30.12664
3	32.81418	4.130125	N-PSK 58	30.73579
4	615.5602	2.388752		30.58248
5	-56.52253	2.39974	SF 8	30.5378
6	82.78951	8.015268		30.36177
7	-213.4595	3. 966014	N-SF 15	31.64333
8	-41.83557	0.09999978		31.90599
9	59.46838	4.646747	LLF 2	30.4804
10	23.83578	68.10092		27.92158
IMA	Infinity			41.44934

6.3.11 The Reversed Tele-Objective

The original idea of the reversed telephoto lens was to add a negative lens to an existing photographic objective, in its front focal plane. This results in a system with an increased back focal length and a widened field. The back focal length can be used to introduce components like a beam splitter or a mirror (as in a single-lens reflex camera).

Lay-out of the Reversed Telelens

The notation for the lay-out is shown in Fig. 6.38.

Using elementary paraxial equations, we can show that

$$\frac{d}{f} = \frac{f_1}{f} + \frac{f_2}{f} - \frac{f_1 f_2}{f^2}$$

$$\frac{b}{f} = \frac{f_2}{f} \left(1 - \frac{f}{f_1} \right)$$

From the figure we have, with the stop at the second component,

$$\frac{w}{w'} = 1 - \frac{d}{f_1} = \frac{b}{f}$$

Here f_1, f_2 are the focal lengths of the two components, and f is the focal length of the objective. We can express f_1 and f_2 in d, b and f , by

$$f_1 = \frac{df}{f - b}, \quad f_2 = \frac{db}{f - d - b}$$

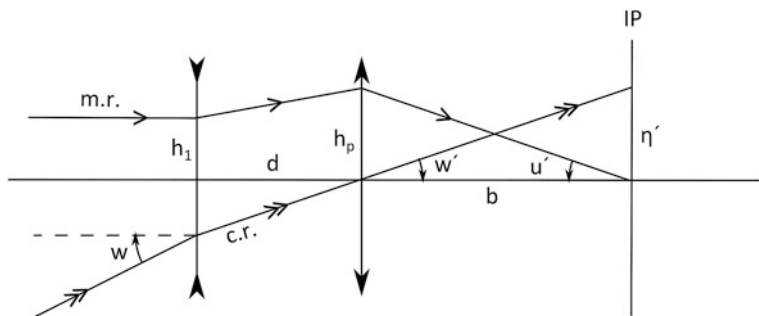


Fig. 6.38 Reversed telephoto lens lay-out

Example

We want to design an objective with a field angle of $w = 0.3$ and image field radius of $\eta' = 21.4$ mm (this is the field radius of the 35 mm camera) and an F-number of about 4.

We choose $b = 100$, so that we have $w' = \frac{\eta'}{b} = 0.214$.

With $\frac{b}{f} = 1.4$ we obtain $w = 0.3$.

This gives $f = \frac{100}{1.4} = 71.429$, $K = 0.0140$.

Because $\frac{d}{f_1} = 1 - \frac{b}{f}$ we have $\frac{d}{f_1} = -0.4$.

When we make $f_1 = -f_2$ we obtain $-f_1 = f_2 = 0.4f = 28.571$, $-K_1 = K_2 = 0.0350$.

Also $d = 0.16f = 11.429$.

We take $h_p = 12.5$, so that $u' = h_b/b = 0.125$ and $F\# = b/2h_p = 4$.

Now $h_1 = h_b f/b = 8.929$, $\bar{h}_1 = -w'd = -2.446$, $\frac{\bar{h}_1}{h_1} = q_1 = -0.274$, $q_2 = 0$ (stop at the second component). Finally we have $H = -w'h_p = -2.675$. This completes the lay-out.

Thin Lens Design of the Reversed Tele-objective

In the design of the ordinary tele-objective we saw that there are three possible strategies.

1. We correct chromatic aberrations, spherical and coma of the two components individually and take the residual aberrations: astigmatism, field curvature and distortion, for granted. By making the powers of the two components equal and opposite astigmatism can be made zero. Field curvature vanishes when we take the same glasses for the two components. The only aberration that remains is distortion, its value depends on certain lay-out parameters.
2. The second strategy is to allow a nonzero sum of powers of the components. Then the two components must be given at least equal and opposite amounts of coma. When the stop is at one of the components, usually the positive one, the

coma of the other component is used to correct astigmatism and/or distortion. A moderate reduction of distortion can be obtained in this way, together with correction of astigmatism.

3. The third strategy is to use the two coefficients of spherical and the two of coma to correct all aberrations except field curvature. The lay-out must be chosen so that field curvature is at an acceptable level. Our results with this strategy were not very encouraging: we obtained designs with too high values of some of the curvatures.

In this case we will apply only the first strategy; the targets are $S_{11} = S_{12} = 0$ and $S_{21} = S_{22} = 0$. The most simple realization is by taking two aplanatic doublets.

We take the powers equal and opposite, and the glasses identical for the two doublets. We discuss the residual distortion; like in the previous section the distortion is determined by the component(s) with a remote stop.

As we will use the lay-out of the above example, this is the first component. With $S_{11} = 0$, $S_{21} = 0$ we have $S_5 = q_1(3S_{31} + S_{41})$.

Using the lay-out equations and introducing the estimate $S_{41} = \frac{5}{8}S_{31}$ we can write this as

$$S_5 = -\frac{29}{8}w^3h_p b(f - b)$$

so that we have

$$\frac{\delta\eta'}{\eta'} = -\frac{29}{8}w^2(f - b)/b.$$

In our lay-out we have $w = 0.3$, $b/f = 1.40$ so that $\delta\eta'/\eta' = 0.0466$; this is 4.66 % of positive distortion.

The rest of the thin lens design we leave to the reader as an exercise. Use the lay-out given in the example above.

6.3.12 Exercise 14, Design of a Reversed Tele-Objective

The thin lens design procedure is identical to that followed in the other cases treated in this section. We summarize the steps of this procedure for convenience.

1. Choose a crown glass with high index (SK) and a flint glass with moderate index (SF).
2. Calculate the powers of the doublet elements (we use the same glasses for each doublet).
3. Calculate all the G-factors.
4. Write the equations for $S_1 = 0$ and $S_2 = 0$ in the thin lens approximation, and solve for the form factors. Do this for both components (take care, the elements have different G-factors).

For each component we find in principle two solutions; usually one of these is not practical (too high curvatures). Note that there are two configurations possible for each component, one with crown in front and one with flint in front. We suggest that you do the exercise only for crown-in-front doublets.

5. Calculate the radii for the solutions found. Discard the solutions with impractically small radii (as a criterium you can use $|r| > 2|h|$).
6. Select the solution that you like most. If you did not find one at this stage, try flint-in-front doublets. Compose a surface model and calculate its Seidel coefficients.
7. Optimize, using the lens software that you have access to, or “use your head as a personal computer”.

6.3.13 The Galilei Telescope

This system resembles very much the tele-objective. It was already introduced in [Sect. 2.4](#).

6.3.14 Exercise 15, Design of a Galilei Telescope

We propose that you design a Galilei telescope, consisting of two doublets, of the following specifications: angular magnification $M = 2$, $K_1 = 0.01$, $q_1 = -2.57$, $h_p = 7$ mm, $\tan w = 0.1$.

With an afocal system such as the Galilei telescope we express the aberrations in the form of angular deviations. Usually the angle aberrations are given in object space, so that we have

$$\delta\alpha = \delta\xi'/f, \delta\beta = \delta\eta'/f,$$

where $\delta\xi'$, $\delta\eta'$ are the aberrations in the focal plane. Thanks to Seidel's theory of aberrations, the aberration coefficients of the objective and the eye lens can be added. For an example design see [Sect. 11.3.3](#) of Kidger [7].

6.4 Three Component Lenses

This is a large category of mainly photographic objectives, among which is most important the Cooke triplet. The Cooke triplet was designed by H. Dennis Taylor (1893). It has eight degrees of freedom: three powers, three form factors and two distances, and therefore the seven primary aberrations (five Seidel and two colour

aberrations) can be corrected at a fixed value of focal length. The Cooke triplet can be used for a variety of applications: wide field and moderate resolution, narrow field and high resolution, and everything in between. It has a large family of offsprings: split triplets, systems with doublet components (one, two or three), among which the famous Tessar invented by Rudolph (1902), and the Sonnar which is a split triplet with doublet components (Bertele 1931). In the following we will discuss three design forms: the simple Cooke triplet, the Tessar and the Heliar.

6.4.1 The Cooke Triplet

The lay-out equations for the Cooke triplet are (see Fig. 6.39 for the notation)

$$\begin{aligned} K &= K_1 + \frac{h_2}{h_1} K_2 + \frac{h_3}{h_1} K_3 : && \text{Power} \\ P &= \frac{K_1}{n_1} + \frac{K_2}{n_2} + \frac{K_3}{n_3} : && \text{Petzval} \\ C_1 &= \frac{h_1^2 K_1}{V_1} + \frac{h_2^2 K_2}{V_2} + \frac{h_3^2 K_3}{V_3} : && \text{LCA} \\ C_2 &= \frac{h_1 \bar{h}_1 K_1}{V_1} + \frac{h_2 \bar{h}_2 K_2}{V_2} + \frac{h_3 \bar{h}_3 K_3}{V_3} : && \text{TCA} \end{aligned} \quad (6.17)$$

In the lay-out we take the stop at the second lens. This ensures a degree of symmetry. In the fourth equation we now have $\bar{h}_2 = 0$. We first attack the fourth equation further. We make the deviation of the chief ray zero by taking $\bar{h}_1 K_1 + \bar{h}_3 K_3 = 0$, so that $d_1 K_1 = d_2 K_3$.

With $C_2 = 0$ we now have $h_1/h_3 = V_1/V_3$. As targets for the remaining equations we have K , P and $C_1 = 0$. With conventional glasses a low value of P will lead to high values of the component powers Berek [12].

A smart choice of glasses can, however, lead to quite small values of P . A good choice of glass will be SK (high n , high V) for the outer lenses, and LF (moderate n , low V) for the inner lens.

The lay-out equations now become

$$\begin{aligned} K &= K_1 + \eta_2 K_2 + \eta_3 K_3 && (\text{a}) \\ P &= \frac{K_1}{n_1} + \frac{K_2}{n_2} + \frac{K_3}{n_3} && (\text{b}) \\ 0 &= \frac{K_1}{V_1} + \frac{\eta_2 K_2}{V_2} + \frac{\eta_3 K_3}{V_1} && (\text{c}) \\ d_1 K_1 &= d_2 K_3 && (\text{d}) \end{aligned} \quad (6.18)$$

with $\eta_2 = h_2/h_1$, $\eta_3 = h_3/h_1 = V_3/V_1$.

Using the transfer equations of Sect. 1.5, in the form $\eta_2 = 1 - d_1 K_1$, $\eta_3 = \eta_2 - d_2(K_1 + \eta_2 K_2)$ we can write the fourth equation as

$$(1 - \eta_2)K_1 + \eta_2(1 - \eta_2)K_2 + (\eta_3 - \eta_2)K_3 = 0$$

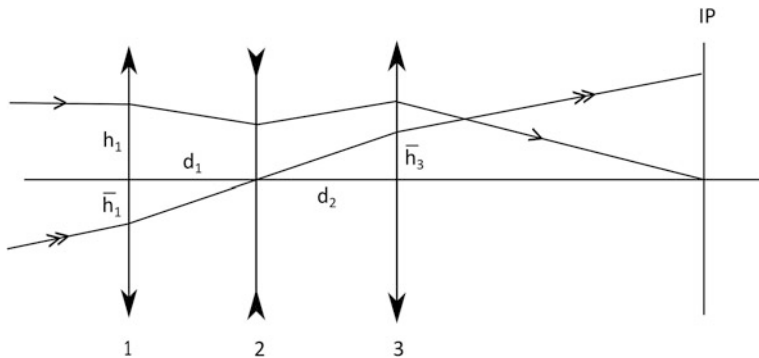


Fig. 6.39 Triplet lay-out

Subtracting (6.18a) we can obtain

$$K = \eta_2 K_1 + \eta_2^2 K_2 + \eta_2 K_3 \quad (6.19)$$

From (6.18a) and (6.18c) we obtain directly

$$K_2 = K / (\eta_2 - \eta_2^2 V_1 / V_2) \quad (6.20)$$

Because we have four equations and three powers to find, we can follow two strategies. We want to reach our targets for K (system power) and LCA anyway. We have the targets for Petzval and TCA left. We choose for the latter; inserting K_2 from (6.20) in (6.18a) and (6.19) we obtain the equations

$$\begin{aligned} K_1 + K_3 V_3 / V_1 &= K - \eta_2 K_2 \\ K_1 + K_3 &= K / \eta_2 - \eta_2 K_2 \end{aligned} \quad (6.21)$$

that are easily solved. From a choice of V_2/V_1 , V_3/V_1 and η_2 the three powers and the Petzval sum follow.

From (6.21) we see that the sum of powers Σ , used in the calculation of S_3 , is given by

$$\Sigma = K / \eta_2 + (1 - \eta_2) K_2 \quad (6.22)$$

As a last step of this algorithm we determine the distances d_1 and d_2 . From $\eta_2 = 1 - d_1 K_1$ and $d_1 K_1 = d_2 K_3$ follows

$$d_1 = (1 - \eta_2) / K_1, \quad d_2 = (1 - \eta_2) / K_3 \quad (6.23)$$

This completes the lay-out.

We used three of the four lay-out equations for the Cooke triplet to find the power distribution. As data we used η_2 and the glass dispersions. The distances d_1 and d_2 followed from the transfer equation and the condition $d_1 K_1 = d_2 K_3$, that led to the fourth lay-out equation.

That means that we can find an infinity of triplet lay-outs in a three-dimensional space (η_2 , V_1/V_2 , V_3/V_1). All of these lay-outs have the property $d_1K_1 = d_2K_3$.

We still have three variables left (the three form factors) to correct spherical, coma and astigmatism. Because the primary achromatic aberrations are corrected in the lay-out, this leaves field curvature and distortion uncorrected. The condition $d_1K_1 = d_2K_3$ corrects distortion approximately, according to Berek [12].

Field curvature is not corrected because we do not use the second lay-out equation in the determination of the powers and distances.

In the optimization phase of the Cooke triplet design the stop position may be used for the fine tuning of distortion.

We intend to make the glass choice more systematic. From the lay-out algorithm we have

$$K_2 = \frac{K}{\eta_2 - \eta_2^2 V_1/V_2}, \quad K_3 = \frac{K(1/\eta_2 - 1)}{1 - V_3/V_1}, \quad \Sigma = K/\eta_2 + (1 - \eta_2)K_2$$

We consider the combinations

$$\begin{aligned} \eta_2 &= 0.8 & \eta_3 &= V_3/V_1 = 0.875 \\ \eta_2 &= 0.7 & \eta_3 &= V_3/V_1 = 0.785 \\ \eta_2 &= 0.9 & \eta_3 &= V_3/V_1 = 0.945 \end{aligned}$$

with $K_3 = 2$ K, $K_2 = -2, -3, -4$ K

because of the following arguments:

- η_2 around 0.8 (Berek's advice),
- K_3 not larger than $-K_2$,
- $\eta_3 > \eta_2$ because of symmetry.

From the above equations we find

η_2	K_2/K	Σ/K	V_1/V_2	K_1/K	V_3/V_1	K_3/K
0.7	-2	0.88	2.45	0.83		
	-3	0.53	2.11	1.53	0.785	2
	-4	0.23	1.94	2.23		
0.8	-2	0.85	2.03	0.85		
	-3	0.65	1.77	1.65	0.875	2
	-4	0.45	1.64	2.45		
0.9	-2	0.91	1.72	0.91		
	-3	0.81	1.52	1.81	0.945	2
	-4	0.71	1.42	2.71		

The glass choice that we made in the example below has moderate values of V_1/V_2 and Σ/K . This choice fits in the table with $\eta_2 = 0.8$ and K_2/K between -3 and -4 .

Example

We chose $\eta_2 = 0.8$, $V_1/V_2 = 1.70$, $\eta_3 = V_3/V_1 = 0.87$.

We use the glasses SK 6: 622601, F 6: 636353 and N-LAK 33: 757522 and find the powers $K_1 = 2.106$ K, $K_2 = -3.47$ K, $K_3 = 1.92$ K, $\Sigma = 0.56$ K and Petzval sum $P = 0.36$ K.

Moreover $d_1 = 9.48$ mm, $d_2 = 10.42$ mm with $K = 0.01$.

Correction of the Triplet

After the lay-out has been found we can try to correct the shape-dependent aberrations by bending the three lenses.

Because $q_2 = 0$ the aberration equations become

$$\begin{aligned} S_1 &= S_{11} + S_{12} + S_{13} \\ S_2 &= S_{21} + S_{22} + S_{23} + q_1 S_{11} + q_3 S_{13} \\ S_3 &= H^2 \Sigma + 2q_1 S_{21} + 2q_3 S_{23} + q_1^2 S_{11} + q_3^2 S_{13} \end{aligned}$$

The component contributions S_{11} and S_{21} are functions of the three variables B_1 , B_2 and B_3 (the position factors G_1 , G_2 , G_3 follow from the lay-out). Because the right-hand-sides are quadratic in the variables, the solution of the aberration equations is not straight forward as with the two-component systems of [Sect. 6.3](#).

To find a starting system for optimization can be done in different ways, dependent on the type of triplet that one wants to design.

For a high-resolution lens with a small field angle we have to make S_1 and S_2 small. We can do this in the following way:

- we take B_1 so that S_{12} has its maximum (negative) value,
- then we take B_1 and B_3 so that S_1 is zero and $S_{21} = -S_{23}$; when q_1 is negative (as in Fig. 4.51) and Σ is positive we must take S_{21} positive,
- then we change B_2 so that $S_{22} = -q_1 S_{11} - q_3 S_{13}$, this makes S_2 zero without changing S_{12} much,
- finally we calculate S_1 , S_3 , S_4 and S_5 from the aberration equations.

When we do not accept the value of S_3 found, we can change the value of H . If that does not help enough, we must consider the lay-out anew, perhaps a different choice of glasses will help. This procedure is worked out in exercise 16 below.

With a lens of moderate resolution, but with a larger field angle, we must take care that the field aberrations, astigmatism and coma, are well corrected. We achieve this goal as follows:

- we make an estimate of the term $q_1^2 S_{11} + q_3^2 S_{13}$ by inserting the minimum values of S_{11} and S_{13} ,
- we introduce the condition $S_{21} = -S_{23}$ and choose a target value for S_3 ; now we can calculate the value of S_{21} and S_{23} , and determine B_1 and B_3 ,
- we calculate S_{11} and S_{13} , find $S_{22} = -q_1 S_{11} - q_3 S_{13}$, and determine B_2 ; S_2 is now equal to zero,
- finally we calculate S_1 and S_3 , S_4 , S_5 .

When we do not accept the value of S_1 , we have to change something in the lay-out, probably the choice of glasses.

We work out the example for the “larger field” triplet.

Example

From the lay-out obtained above follow the position factors

$$G_1 = -1, \quad G_2 = 0.5154, \quad G_3 = -0.1966$$

and the q-factors

$$q_1 = -0.379, \quad q_2 = 0, \quad q_3 = 0.474.$$

With $h_p = 10$, $\tan \omega = 0.32$ so that $H = -3.2$ we find the component aberrations

$$\begin{aligned} S_{11} &= 0.1348 B_1^2 - 0.2425 B_1 + 0.2576 \\ S_{12} &= -0.2350 B_2^2 - 0.2232 B_2 - 0.3310 \\ S_{13} &= 0.0378 B_3^2 - 0.0165 B_3 + 0.0591 \\ S_{21} &= 0.1042 B_1 - 0.1855 \\ S_{22} &= 0.3121 B_2 + 0.1658 \\ S_{23} &= 0.0925 B_3 - 0.0225. \end{aligned}$$

We follow the procedure outlined above. In the aberration equation

$$S_2 = S_{21} + S_{22} + S_{23} + q_1 S_{11} + q_2 S_{12}$$

we take $S_{21} = -S_{23}$. We use this in the equation for S_3 and find a value for B_1 and B_3 for which S_3 is equal to its target value.

With the target $S_3 = -0.014$ we find $B_1 = 1.368$, $B_3 = -0.475$, so that $S_{11} = 0.1780$, $S_{13} = 0.0754$.

This makes that $S_1 = 0.2534 + S_{12}$. Because S_{12} has a maximum value of -0.2779 (for $B_2 = -0.475$) we can have a maximum value of $S_1 = -0.0224$.

With $B_1 = 1.368$, $B_2 = -0.475$, $B_3 = -0.475$ we have the system coefficients

$$S_1 = -0.0224, \quad S_2 = 0.014, \quad S_3 = -0.014.$$

In order to correct spherical further we change n_3 to a lower value, $n_3 = 1.622$. The aberrations of the third component now become

$$\begin{aligned} S_{13} &= 0.0584 B_3^2 - 0.0207 B_3 + 0.0705 \\ S_{23} &= 0.1158 B_3^3 - 0.0229. \end{aligned}$$

Repeating the procedure we obtain

$$B_1 = 1.368, \quad B_2 = -0.450, \quad B_3 = -0.373$$

and the system coefficients

$$S_1 = -0.0137, S_2 = -0.0012, S_3 = -0.0120, S_4 = 0.0370, S_5 = 0.0315.$$

Spherical is the best we can have in this way.

An optimized design of Kidger [7, p. 202] has the coefficients (adapted to $f = 100$)

$$K: S_1 = 0.034, S_2 = -0.010, S_3 = 0.031, S_4 = 0.112, S_5 = 0.0381.$$

The field angle of this design is 22° , against 17.7° for ours, therefore the comparison is a bit misleading. When we correct the field aberrations of our design for the larger field, we obtain

$$V: S_1 = -0.0137, S_2 = -0.0015, S_3 = -0.0185, S_4 = 0.0570, S_5 = 0.0605.$$

Note that the meridional field curvature $3S_3 + S_4$ is well corrected as a consequence of our choice of a negative target for S_3 . The glass that we chose, with $n_3 = 1.622$, $V_3 = 52.2$, does not exist in the Schott catalogue. The glass N-SSK 2 is very near to these values.

In this procedure we create, by the condition $S_{21} = -S_{23}$, an additional aberration equation. This enables us to “solve” the last two aberration equations, so that we obtain B_1 and B_3 as functions of the target S_3 . B_2 is found from the additional equation.

By introducing the augmented condition $S_{21} = \chi S_{23}$ we will find systems with a value of S_1 dependent on χ . The coefficients S_2 and S_3 will not be different: $S_2 = 0$ and S_3 is equal to the target. Also S_5 will depend (rather weakly) on χ .

With the form factors of this design:

$$B_1 = 1.368, B_2 = -0.450, B_3 = -0.373,$$

and giving thickness according to the usual procedure we obtain a surface model with the following specification.

Surface model of the Cooke triplet

#	Radius	Thickness	Glass	Diameter
1	24.742	2.975	SK 16	28
2	159.67	5.970	Air	28
3	-66.663	3.021	F 6	18
4	25.527	8.643	Air	18
5	102.54	2.977	N-SSK 2	28
6	-46.839		Air	28

The results of the paraxial calculations and the third order surface coefficients are given below. We will optimize this design with the targets

$$S_1 = -0.0137, S_2 = 0.005, S_3 = -0.020, S_5 = 0.030.$$

nu	h	$n\bar{u}$	\bar{h}	A	\bar{A}	$h\Delta$
1	0	10	0.3211	-3.9376	0.4042	0.1613
2	-2.513	9.5391	0.4197	-3.1687	-0.1545	0.3872
3	-0.2142	8.2602	0.4070	-0.7386	-0.3381	0.4181
4	-0.1353	8.0101	0.4	0	0.3838	0.4
5	0.06423	8.5646	0.4	3.4572	0.1477	0.4337
6	0.01224	8.5870	0.3790	4.1528	-0.2852	0.2352

	S_1	S_2	S_3	S_4	S_5	C_1	C_2
1	0.1561	0.0622	0.0249	0.1586	0.0732	0.0258	0.0103
2	0.0270	-0.0677	0.1697	-0.0245	-0.3638	0.0094	-0.0132
3	-0.1545	0.1910	-0.2366	-0.0596	0.3663	-0.0307	0.0380
4	-0.1354	-0.1411	-0.1470	-0.1560	-0.3158	-0.0338	-0.0338
5	0.0111	0.0327	0.0958	0.0383	0.3937	0.0093	0.0272
6	0.0743	-0.0613	0.0506	0.0838	-0.1108	0.0179	-0.0149
Σ	-0.0214	0.0158	-0.0427	0.0406	0.0427	-0.0021	0.0136

The distortion coefficient of our triplet design corresponds to about 0.5 % of positive distortion (with the 22° field this becomes 1 %).

This moderate value is in part a consequence of Berek's condition $d_1 K_1 = d_2 K_3$.

This leads to $\bar{h}_1 K = -\bar{h}_3 K_3$ (see Fig. 4.50). When h_1 and h_3 do not differ much, $q_1 K_1 + q_3 K_3$ will be small (in our design it is equal to 0.0011).

The first term of S_5 in the aberration equation is given by

$$q_1(3S_{31} + S_{41}) + q_3(3S_{33} + S_{43}).$$

When the indices n_1 and n_3 are equal (as in our design) this is proportional to $q_1 K_1 + q_3 K_3$.

Berek's condition corrects the leading term of S_5 .

Note: with the target $S_3 = 0$ we obtain, with

$$B_1 = 1.6, B_2 = -0.645, B_3 = -0.0208$$

the system coefficients

$$S_1 = 0.0008, S_2 = 0.0006, S_3 = 0.$$

This can be used as an alternative starting design.

6.4.2 Exercise 16, Design of a High Resolution Triplet

The thin lens formula for coma is (see Sect. 4.3)

$$S_{2i} = -\frac{1}{2} h_i^2 K_i^2 H(\mu_{5i} B_i + \mu_{6i} G_i).$$

Using this formula find a relation between B_1 and B_3 when $S_{21} = -S_{23}$ (The coefficients μ_{5i} and μ_{6i} are defined as $\mu_{5i} = \frac{n_i+1}{n_i(n_i-1)}$, $\mu_{6i} = 2 + \frac{1}{n_i}$).

From the lay-out found above take the data

$$\begin{aligned} h_1 &= 10, & h_3 &= 8.7, & K_1 &= 0.0211, & K_3 &= 0.0192, \\ H &= 2 & \text{(this implies } \tan w = 0.2\text{)}, & n_1 &= 1.622, & n_3 &= 1.757, \\ G_1 &= -1, & G_3 &= -0.314. \end{aligned}$$

Eliminate B_3 from

$$S_1 = S_{11} + S_{12} + S_{13}$$

and with $S_1 = 0$ and S_{12} maximum solve for B_1 .

Choose from the two solutions for B_1 the one that makes S_{21} positive. Calculate S_{21} and $S_{23} = -S_{21}$.

Then complete the procedure for a high-resolution triplet outlined above.

Optimization of the Cooke Triplet

The design goal of the triplet was EFL = 100 mm, F/3 and a field angle of 10°.

In Fig. 6.40a we show the ray fan plots of our surface model. The chromatic aberrations are not well corrected. Moreover there is quite a lot of astigmatism.

Optimization with radii and glasses as variables was necessary to improve the colour correction. The original glasses were SK 16, F 6 and N-SSK 2. The optimized system has N-LAK 14, F 15 and PSK 53A.

The lay-out of the optimized triplet is shown in Fig. 6.40b and the ray fan plots in Fig. 6.40c.

The changes in the Abbe numbers of the glasses have been drastic as is shown in the following table

	V ₁	V ₂	V ₃
Before	60.1	35.1	52.9
After	55.2	37.6	63.2

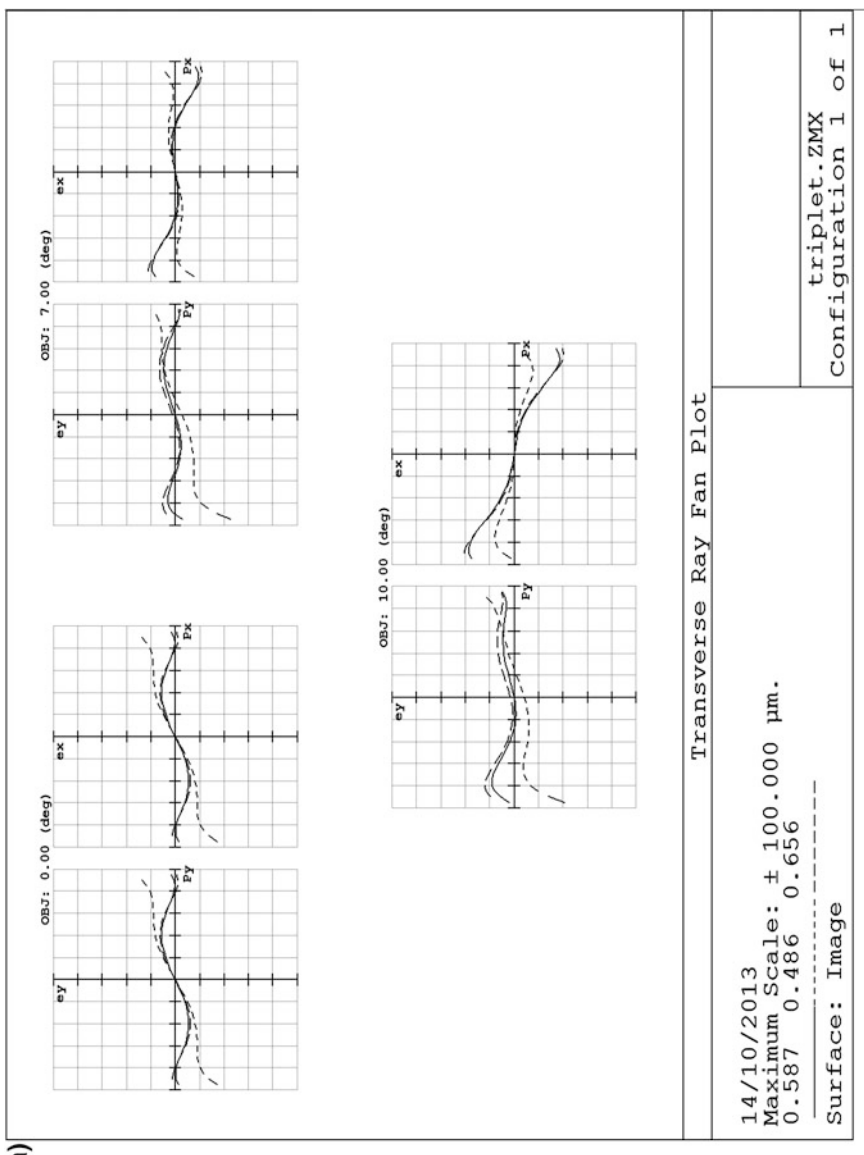


Fig. 6.40 **a** Cooke triplet, surface model. **b** Cooke triplet optimized, lay-out. **c** Cooke triplet optimized, aberrations

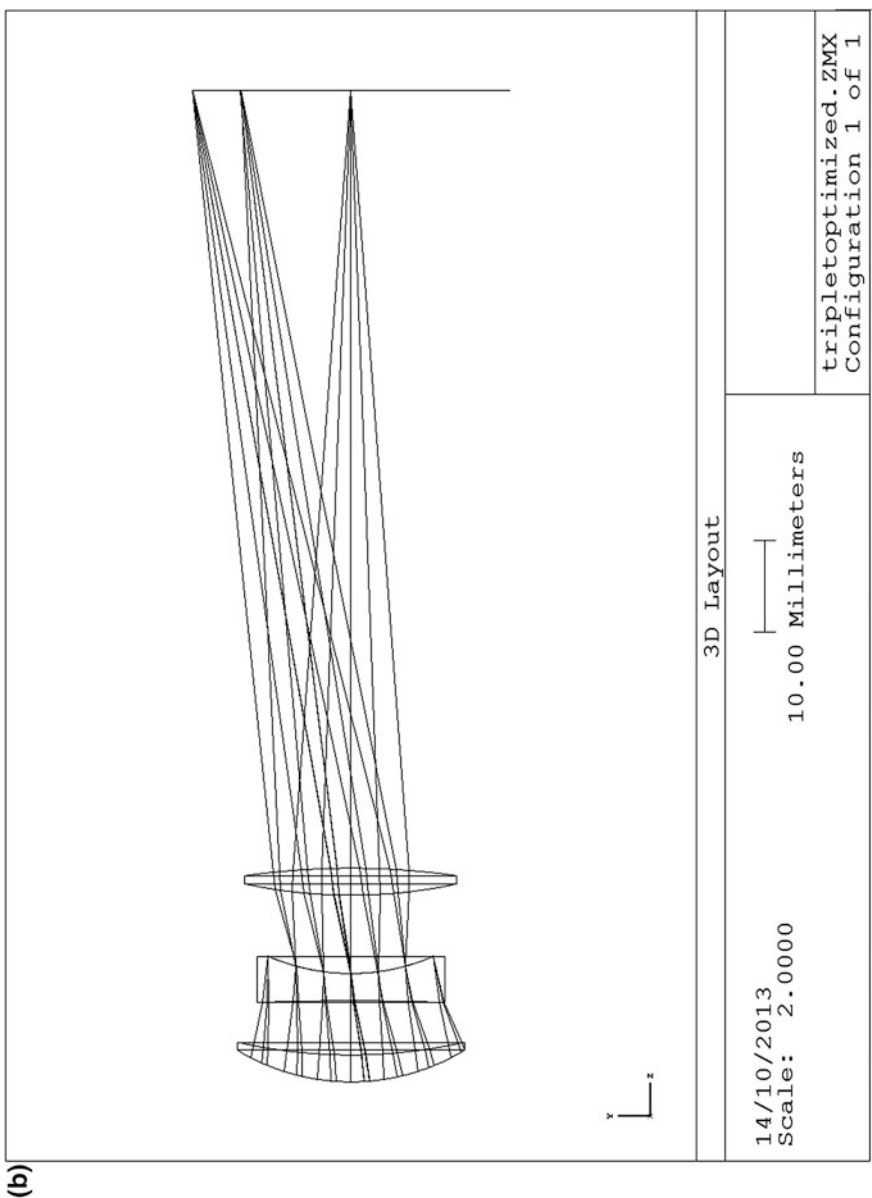


Fig. 6.40 (continued)

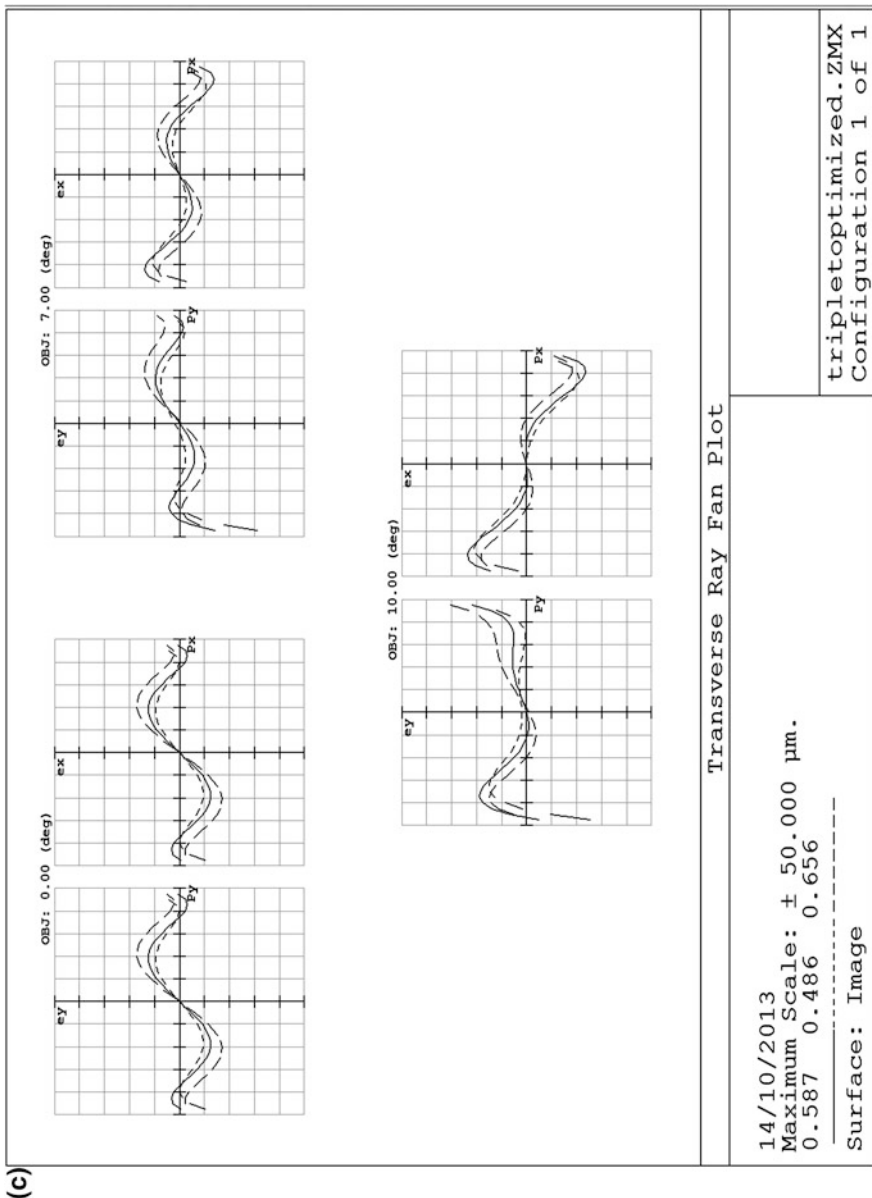


Fig. 6.40 (continued)

The prescription of the optimized triplet is shown below
Surface data summary

Surf	Radius	Thickness	Glass	Diameter
OBJ	Infinity	Infinity		
1	24.09773	2.975	N-LAK 14	25.05175
2	56.2893	5.97		24.49495
3	-299.4603	3.021	F 15	20.65655
STO	22.75093	8.643		18
5	55.23713	2.977	PSK 53A	23.17245
6	-81.86538	85.82917		23.348
IMA	Infinity			34.8933

6.4.3 The Tessar

Although it was not conceived in this way (see Kingslake [5], p. 409) the Tessar looks like a triplet where the last lens is replaced by a doublet. This doublet is not of the achromat type that we used often before, however. It is composed of lenses with approximately the same value of V and widely different values of n; the purpose of this is to obtain a high value of the doublet's equivalent index that brings down the Petzval sum. With

$$\frac{K}{n} = \frac{K_a}{n_a} + \frac{K_b}{n_b},$$

where $K_a + K_b = K > 0$ and $n_b > n_a$ one obtains a value of n higher than n_b by taking K_a negative. This gives a positive doublet where the index n_a of the negative component has the smallest value.

Lay-out of the Tessar

We borrowed a Tessar lay-out from Havlicek [18] with the prescription

#	Power (mm^{-1})	Distance (mm)	Glass
1	0.0196	12.13	1.6230/58.1 (SK 15)
2	-0.0310	14.13	1.6483/33.8 (SF 2)
3a	-0.0280	0	1.5407/47.2 (LLF 2)
3b	0.0451	81.3	1.6700/47.2 (NBAF 10)

This lay-out has $\sum K_i = 0.57$ K ($K = 0.01$), $P = 0.21$ K. The equivalent index of the last component is $n_3 = 1.9360$.

Thin Lens Design of the Tessar

From the prescription follow the component aberration equations

$$S_{11} = 0.10826 B_1^2 - 0.19253 B_1 + 0.20738$$

$$S_{12} = -0.12947 B_2^2 - 0.16274 B_2 - 0.20513$$

$$S_{13} = 0.1720 B_b^2 - 0.2225 B_b + 0.1943$$

$$S_{21} = 0.1490 B_1 - 0.1524$$

$$S_{22} = 0.2074 B_2 + 0.1456$$

$$S_{23} = 0.1750 B_b - 0.0898$$

The aberrations of the system are found from

$$S_1 = \sum_i S_{1i}, \quad S_2 = \sum_i (S_{2i} + q_i S_{1i})$$

$$S_3 = \sum_i (K_i H^2 + 2q_i S_{2i} + q_i^2 S_{1i}), \quad S_4 = \sum_i K_i H^2 / n_i$$

$$S_5 = \sum_i (q_i K_i H^2 (3 + 1/n_i)) + 3q_i^2 S_{2i} + q_i^3 S_{1i}$$

where, from the lay-out, $q_1 = -0.4932$, $q_2 = 0$ (stop at the second lens), $q_3 = 0.6952$. The Lagrange invariant is, with $\tan w = 0.3$ and $h_p = 10$, given by $H = -3$.

With the component aberrations from above we can write

$$S_1 = 0.10826(B_1 - 0.889)^2 + 0.1720(B_b - 0.646)^2 + 0.2444 + S_{12}$$

$$S_2 = -0.05341(B_1 - 2.246)^2 + 0.1196(B_b - 0.0850)^2 + 0.0673 + S_{22}$$

$$S_3 = 0.02634(B_1 - 3.679)^2 + 0.08313(B_b + 0.821)^2 - 0.1914.$$

We use the aberration equations in the following way.

We choose a pair of B_1 and B_b that makes S_3 equal to a target value.

Then we calculate S_{22} so that $S_2 = 0$; this gives us the value of B_2 . We calculate S_1 .

We move the starting point (B_1 , B_b) along the S_3 curve until we find a minimum for S_1 .

The S_3 curve is an ellipse with its centre at $B_1 = 3.679$, $B_b = -0.821$.

We give the results of a search for Havlicek's lay-out. Target value for S_3 is -0.0095 .

B_1	B_b	B_2	S_1
2.428	0.48	-1.09	0.3239
1.848	0.24	-0.995	0.2010
1.493	0	-0.867	0.1943
1.262	-0.24	-0.821	0.2357
1.121	-0.48	-0.867	0.3016

Clearly we have chosen goals ($S_2 = 0$, $S_3 = -0.0095$) that are too ambitious for this lay-out. We considered only a part of the S_3 —ellipse to avoid impractically high curvatures of the component surfaces.

A possible way to change the lay-out, keeping the character of the Tessar design intact, is changing the ratio of K_{3a} and K_{3b} . In Havlicek's lay-out we had $K_{3a} = -0.028$ and $K_{3b} = 0.0451$. We tried $K_{3a} = -0.02$ and $K_{3b} = 0.0371$, and found a minimum $S_1 = 0.0821$, with $S_2 = 0$ and $S_3 = 0$, for the form factors $B_1 = 1.17$, $B_b = -0.1$ and $B_2 = -0.467$.

With $K_{3a} = -0.01$ and $K_{3b} = 0.0271$ we found a minimum of $S_1 = 0.0304$, with $S_2 = 0$ and $S_3 = 0$, for the form factors $B_1 = 1.1$, $B_b = -0.078$ and $B_2 = -0.328$.

The aberration equations for this case are

$$\begin{aligned} S_{11} &= 0.10826 B_1^2 - 0.19253 B_1 + 0.20738 \\ S_{12} &= -0.12947 B_2^2 - 0.16274 B_2 - 0.20513 \\ S_{13} &= 0.0635 B_b^2 - 0.0848 B_b + 0.0632 \\ S_{21} &= 0.1490 B_1 - 0.1524 \\ S_{22} &= 0.2074 B_2 + 0.1456 \\ S_{23} &= 0.1102 B_b - 0.0671 \end{aligned}$$

The equation for the S_3 —curve becomes

$$S_3 = 0.02634 (B_1 - 3.565)^2 + 0.02924 (B_b + 1.919)^2 - 0.2591$$

By moving about in the neighborhood of the minimum S_1 system we find a minimum of S_1 for $B_1 = 1$, $B_2 = -0.3$; $B_a = -1$, $B_b = -0.3$ with coefficients $S_1 = 0.0194$, $S_2 = 0.0057$, $S_3 = 0.0037$. With a stop shift $\Delta q = -0.3$ we obtain $S_2^* = 0$, $S_3^* = 0.0020$.

We use this thin lens design, without the stop shift, to obtain a surface model.

Surface model of the Tessar

The prescription of the surface model becomes

	#	Radius (mm)	Distance (mm)	Glass
STO	1	31.786	1.575	1.6230/58.1 (SK 15)
	2	Plane	10.362	Air
	3	-60.166	2.013	1.6483/33.8 (SF 2)
	4	32.397	13.706	Air
	5	Plane	1.00	1.5407/47.2 (LLF 2)
	6	54.070	2.00	1.6700/47.2 (NBAF 10)
	7	-45.424	82.036	Air
IP	8	Plane	-	-

The results of the paraxial calculations and the surface aberration coefficients are given below.

	nu	h	n <u>u</u>	<u>h</u>	A	<u>A</u>	hΔ
1	0	10	0.3000	-4.987	0.3146	0.1431	-0.7440
2	-0.1960	9.810	0.3978	-4.601	-0.1960	0.3978	-1.1929
3	-0.1960	7.779	0.3978	-0.479	-0.3252	0.4057	1.2037
4	-0.1121	7.641	0.3926	0	0.2766	0.3926	0.6304
5	0.04080	8.200	0.3926	5.381	0.0408	0.3926	-0.1936
6	0.04080	8.226	0.0326	5.636	0.2751	0.5531	-0.0791
7	0.02113	8.251	0.3791	6.090	-0.2822		-0.7673

	S ₁	S ₂	S ₃	S ₄	S ₅	C ₁	C ₂
1	0.0736	0.0335	0.0152	0.1087	0.0563	0.0207	0.0094
2	0.0458	-0.0930	0.1887	0	-0.3779	0.0127	-0.0258
3	-0.1273	0.1588	-0.1981	-0.0589	0.3094	-0.0293	0.0366
4	-0.0482	-0.0684	-0.0972	-0.1093	-0.2965	-0.0245	-0.0348
5	0.0003	0.0031	0.0298	0	0.2868	0.0025	0.0238
6	0.0060	-0.0120	0.0242	0.0084	0.0655	0.0025	0.0050
7	0.0611	-0.0381	0.0185	0.0795	-0.0539	0.0198	-0.0108
Σ	0.0113	0.0124	-0.0189	0.0284	-0.0103	0.0044	0.0034

Optimization of the Tessar

The paraxial parameters of this design were: EFL = 100 mm, F/5.4, object field angle 10°.

We first optimized our surface model with the radii as variables only. This resulted in a well corrected design for the middle wavelength, but a rather poor correction of longitudinal colour. Varying also the glasses resulted in a reduction

of LCA and monochromatic aberrations below 4 μm . According to Havliček [16] a value of F/2.8 can be obtained with this design form.

We show the lay-out of the optimized design in Fig. 6.41a and the ray fan plots in Fig. 6.41b. A comparison with Fig. 6.40 shows the greater potentiality of the Tessar over the Cooke triplet.

The prescription of the optimized Tessar is shown below
Surface data summary

Surf	Radius	Thickness	Glass	Diameter
OBJ	Infinity	Infinity		
1	33.37203	1.575	LAK 21	18.63105
2	-765.8639	10.362		18.54633
3	-47.52372	2.013	F 14	10.73498
STO	27.19289	13.706		10
5	-237.3731	1	KZFS 1	17.63279
6	35.34276	2	N-LAK 34	18.54596
7	-38.10774	82.036		18.4301
IMA	Infinity			33.41615

We compare the aberrations of our surface model with those of a design of Max Berek (1922). We found this design in a book describing Berek's career and his work in the company Leitz (now Leica) [19].

The design shows a stage in the development of the Elmax, the first lens that Berek developed for the celebrated Leica 35 mm camera.

Its prescription, as given in the book, is shown below. We found the following aberration coefficients:

$$S_1 = 0.0253, S_2 = -0.0074, S_3 = -0.0225, S_4 = 0.0560, S_5 = -0.0309 \\ (f = 50).$$

Berek's design has three lenses in the third component. He developed later a version with a doublet, called Elmar. Although we have no data of this lens, we tried to reproduce this development. The prescription of the resulting lens is given below as well. It is clearly a Tessar variant, although it could not be called so for reasons of industrial property.

Its aberration coefficients are

$$S_1 = 0.0206, S_2 = -0.0100, S_3 = -0.0230, S_4 = 0.0549, S_5 = -0.0292 \\ (f = 50).$$

For comparison we show again the values of our Tessar:

$$V : S_1 = 0.0113, S_2 = 0.0124, S_3 = -0.0189, S_4 = 0.0284, S_5 = -0.0103, \\ (f = 100).$$

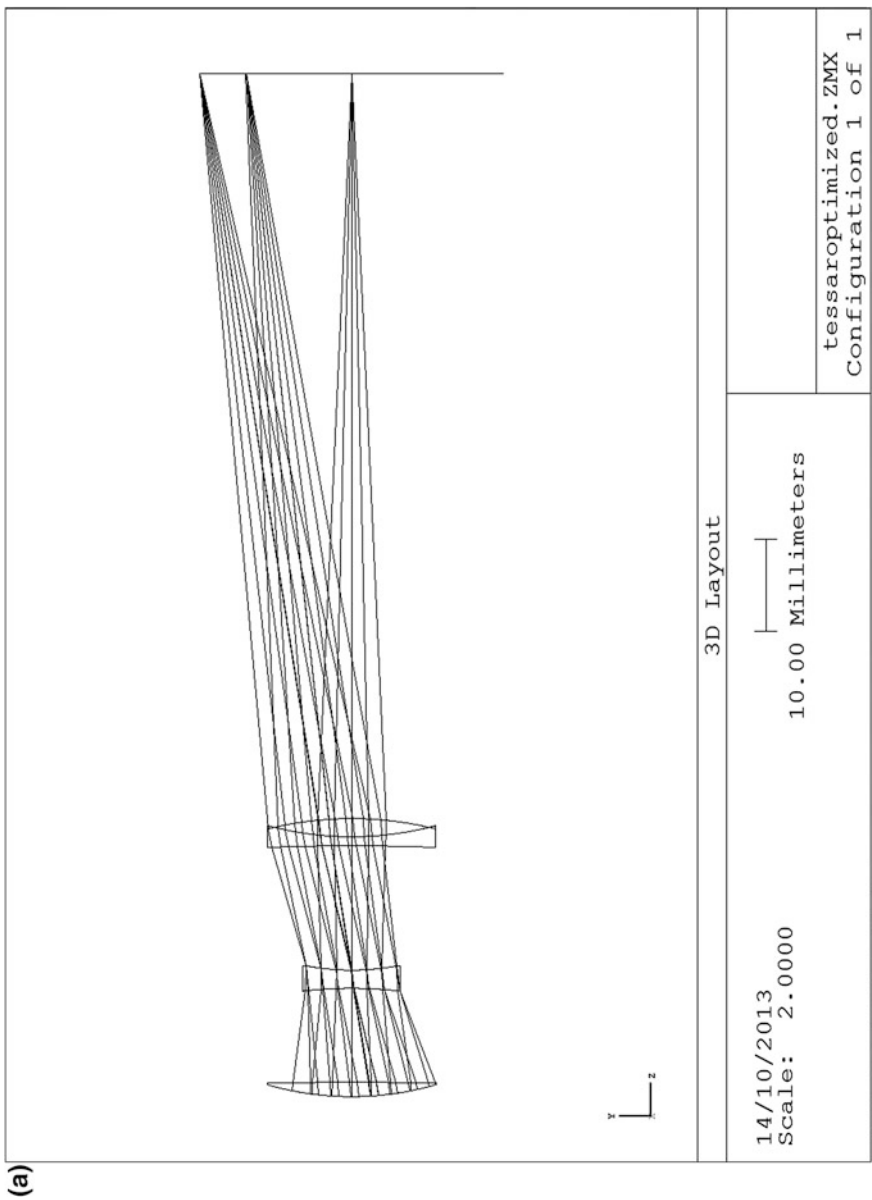


Fig. 6.41 a Tessar, lay-out. b Tessar, aberrations

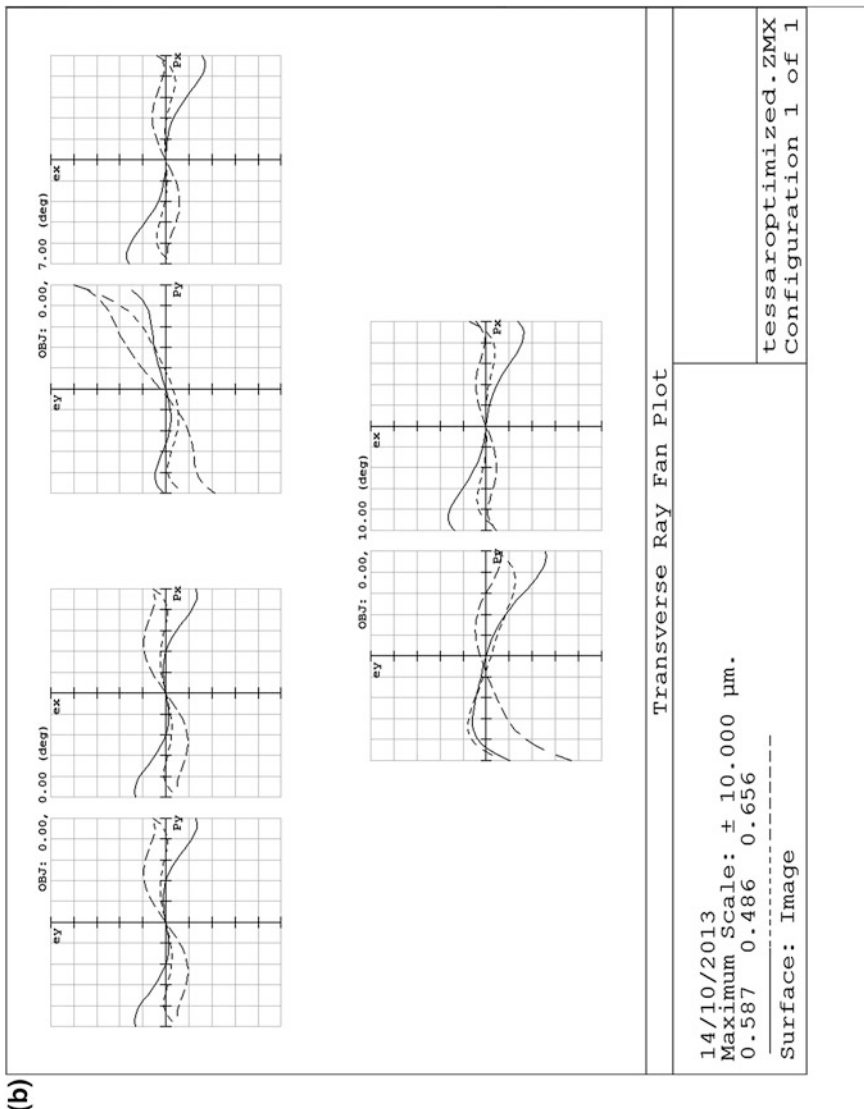


Fig. 6.41 (continued)

Taking account of the difference in focal length, and of a factor 4/3 in field angle, this becomes

$$V : S_1 = 0.0057, S_2 = 0.0083, S_3 = -0.0168, S_4 = 0.0252, S_5 = -0.0122, \\(f = 50).$$

Prescription of Berek's lens "Elmax"

#	Radius	Distance	n_D	V	Diameter
1	15.035	2.692	1.6063	58.5	17
2	Plan	3.868	Air		17
3	-30.018	0.914	1.6031	38.3	13.7
4	13.536	2.794	Air		13.7
5	Plan	1.016	1.5162	64.0	14.7
6	50.000	1.067	1.515	56.6	14.7
7	14.400	3.378	1.6092	58.9	14.7
8	-20.545	40.514	Air		14.7

$f = 50$ mm, $\tan w = 0.4$, $h_p = 6$

STO is 2 mm behind #2

Prescription of pseudo-Elmar

#	Radius	Distance	n_D	V
1	15.035	2.692	1.6063	58.6 (SK 3)
2	Plan	3.868	Air	
3	-30.018	0.914	1.6031	38.3 (F 5)
4	13.536	2.794	Air	
5	Plan	2.083	1.5160	58.7 (K 3)
6	14.400	3.378	1.6062	58.6 (SK 3)
7	-20.545	41.164		

$f = 50$ mm, $\tan w = 0.4$, $h_p = 6$, field radius 21.7 mm

STO is 2 mm behind #2

6.4.4 The Heliar

The Heliar can be considered as a symmetrized version of the Tessar. See Fig. 4.11 for a Heliar from the literature. The return to a more symmetric design should make it easier to correct for the “uneven” aberrations: coma, distortion and transverse chromatic.

Lay-out

For the lay-out of the Heliar we depart from the lay-out of a symmetric triplet.

Starting with $\eta_2 = 0.8$ and $K_2 = -0.03$ we find $K = 0.01$ with $V_1/V_2 = 1.766$.

We take the glasses SF 2, with $n_2 = 1.64769$ and $V_2 = 33.85$, and LAK 21 with $n_1 = 1.64049$ and $V_1 = 60.10$.

For the third glass we choose SSK 5, with $n_3 = 1.65844$ and $V_3 = 50.88$, so that $V_3/V_1 = 0.85$.

From the triplet lay-out equations (Sect. 6.4.1) we find $K_1 = K_3 = 0.0179$. The distances become $d_1 = d_2 = 11.17$ mm.

With the glasses K 7, with $n_{1b} = 1.51112$, $V = 60.41$, and N-KF 9, with $n_{3a} = 1.52346$, $V_{3a} = 51.54$ we can create doublets that have a higher equivalent index than the corresponding lenses in the triplet, and approximately the same V- values.

As starting values for the Heliar lay-out we take $K_{1a} = 0.0279$, $K_{1b} = -0.01$, so that $n_{eq} = 1.722$ for the first component, and $K_{3a} = -0.01$, $K_{3b} = 0.0279$, so that $n_{eq} = 1.744$ for the third component.

We now obtain for the present lay-out $P = 0.00216$ whereas for the triplet we would have $P = 0.00352$.

The prescription for the lay-out is summarized in the table below.

Lay-out of the Heliar

#	Power	Distance	Glass
1 _a	0.0279	0	N-LAK 21
1 _b	-0.0100	11.17	K 7
2	-0.0300	11.07	SF 2
3 _a	-0.0100	0	N-KF 9
3 _b	0.0279		N-SSK 5

Thin Lens Design

Calculation of the position factors gives $G_{1a} = -1$, $G_{1b} = 4.580$, $G_2 = 0.492$, $G_{3a} = -2.406$, $G_{3b} = 0.221$. With the cementing conditions for the first and third components:

$$B_{1b} = -2.226 B_{1a} + 1.226$$

$$B_{3a} = -2.218 B_{3b} - 1.218$$

we eliminate the form factors B_{1b} and B_{1a} from the component aberration equations, and obtain

$$\begin{aligned}
 S_{11} &= 0.1876 B_{1a}^2 - 0.0972 B_{1a} + 0.1210 \\
 S_{12} &= -0.1446 B_2^2 - 0.1311 B_2 - 0.2059 \\
 S_{13} &= 0.0945 B_{3b}^2 - 0.0904 B_{3b} + 0.0809 \\
 S_{21} &= 0.1850 B_{1a} - 0.0619 \\
 S_{22} &= 0.2134 B_2 + 0.1106 \\
 S_{11} &= 0.1321 B_{3b} - 0.0639
 \end{aligned}$$

To obtain the system aberration coefficients we need the q-factors and the Helmholtz invariant. With $h_p = 10$ and $\tan w = 0.32$ we have $H = -3.2$.

With the stop at the second lens we find $q_1 = -0.447$, $q_2 = 0$, $q_3 = 0.520$.

We want to obtain a design of which the field aberrations are well corrected. We will find the form factors in the same way as with the thin lens design of the Tessar that we discussed earlier in this section.

We choose a starting value of B_{1a} and find the value of B_{3b} for which $S_3 = 0$. Then we take B_2 so that $S_2 = 0$ and find the resulting value of S_1 .

In this way we found, beginning with $B_{1a} = 0.5$, $B_{3b} = 0.0389$ and $B_2 = -0.332$ and the system aberrations $S_1 = 0.0228$, $S_2 = 0$, $S_3 = 0$, $S_4 = 0.0221$, $S_5 = 0.0635$.

From this design we found, applying the usual procedure of giving thickness, a surface model with the following prescription.

Heliar, surface model

	#	Radius	Thickness	Glass	Diameter
STO	1	31.335	6.142	N-LAK 21	30
	2	-94.019	3.071	K 7	30
	3	117.987	4.028	Air	30
	4	-65.069	2.014	SF 2	18
	5	32.633	7.187	Air	18
	6	336.853	3.000	N-KF 9	25
	7	44.948	4.499	N-SSK 5	25
	8	-48.586	89.479	Air	25
IMA	9	Plane	-	-	66.838

The results of the paraxial calculations and the surface aberration coefficients are given below.

#	nu	h	$n\bar{u}$	\bar{h}	A	\bar{A}	$h\Delta$
1	0	10	0.3179	-4.495	0.3191	0.1744	-0.7595
2	-0.2044	9.235	0.4098	-2.961	-0.3655	0.4615	-0.1086
3	-0.2171	8.794	0.4139	-2.120	-0.1044	0.3844	-0.7380
4	-0.1790	8.073	0.4048	-0.4892	-0.3013	0.4172	1.1511
5	0.0988	7.952	0.4	0	0.3018	0.4	0.7562
6	0.0587	8.374	0.4	2.875	0.0835	0.4085	-0.3268
7	0.0457	8.465	0.3955	3.645	0.3326	0.5190	-0.1042
8	0.0202	8.519	0.3846	4.677	-0.2706	0.2250	-0.8738

	S ₁	S ₂	S ₃	S ₄	S ₅	C ₁	C ₂
1	0.0773	0.0422	0.0231	0.1276	0.0823	0.02073	0.01133
2	0.0145	-0.0183	0.0231	0.0057	-0.0364	0.00303	-0.00016
3	0.0080	-0.0296	0.1091	-0.0294	-0.2935	0.00514	-0.01893
4	-0.1058	0.1455	-0.2004	-0.0618	0.3609	-0.02846	0.03915
5	-0.0688	-0.0912	-0.1210	-0.1231	-0.3235	-0.02789	-0.03697
6	0.0023	0.0114	0.0545	0.0104	0.3106	0.00466	0.02280
7	0.0115	0.0180	0.0280	0.0122	0.0627	0.00320	0.00500
8	0.0639	-0.0532	0.0442	0.0836	-0.1062	0.01799	-0.01496
Σ	0.0030	0.0248	-0.0393	0.0252	0.0569	-0.00160	0.00726

Optimization of the Heliar

The Heliar has EFL = 100 mm, F/4.7 and object field angle 12.5°.

The optimization algorithm changed the composition of the doublets. The aberrations are larger than with the optimized Tessar, but the invariant is two times as large. Also the ray fan plots, that are shown in Fig. 6.42b are more uniform over the field. In Fig. 6.42a we show the lay-out and in the table below the prescription of the design.

Surface data summary

Surf	Radius	Thickness	Glass	Diameter
OBJ	Infinity	Infinity		
1	33.62252	6.142	N-LAK 14	27.77867
2	-57.19823	3.071	N-K 5	26.80936
3	117.1345	4.028		22.71968
4	-57.52795	2.014	SF 2	19.67523
STO	33.28017	7.187		18
6	496.1916	3	N-LAK 21	22.4736
7	33.10365	4.499	N-LAK 9	24.57235
8	-49.54372	89.479		24.77442
IMA	Infinity			47.80955

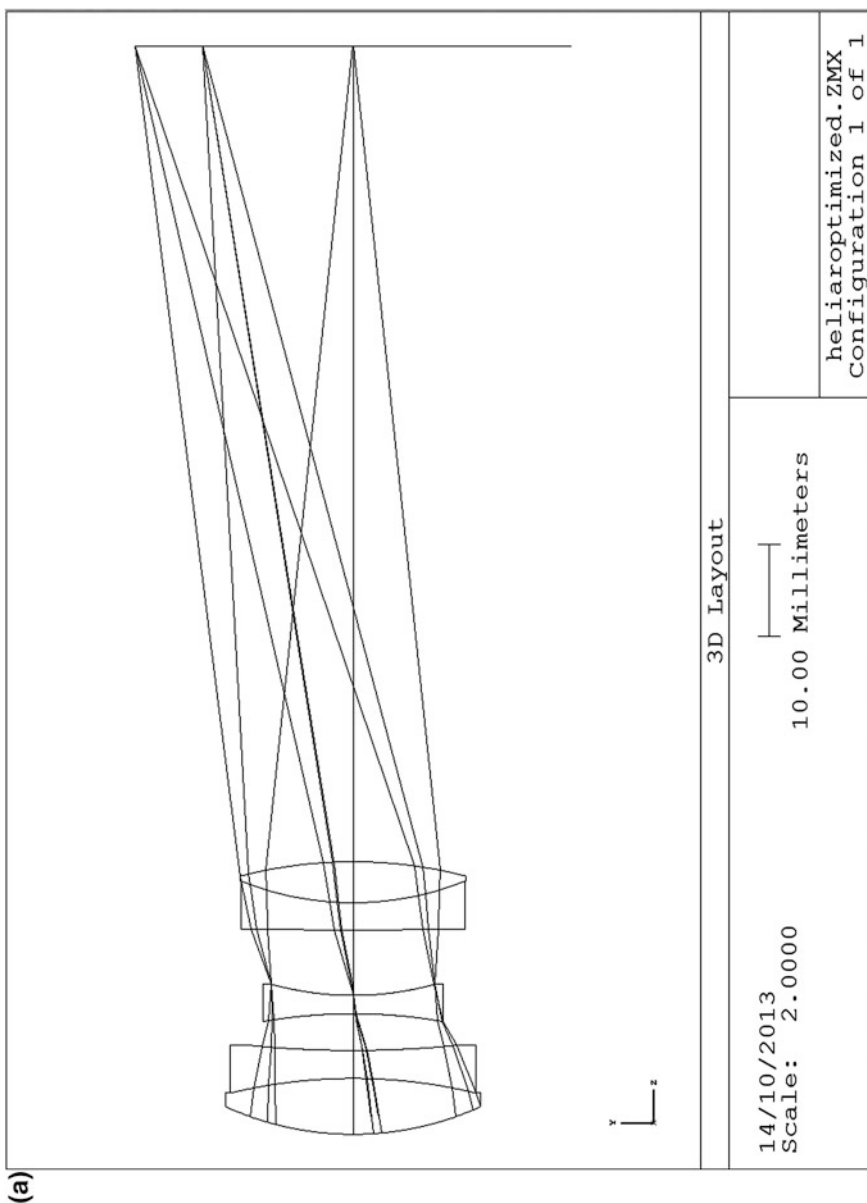


Fig. 6.42 a Heliar, lay-out. b Heliar, aberrations

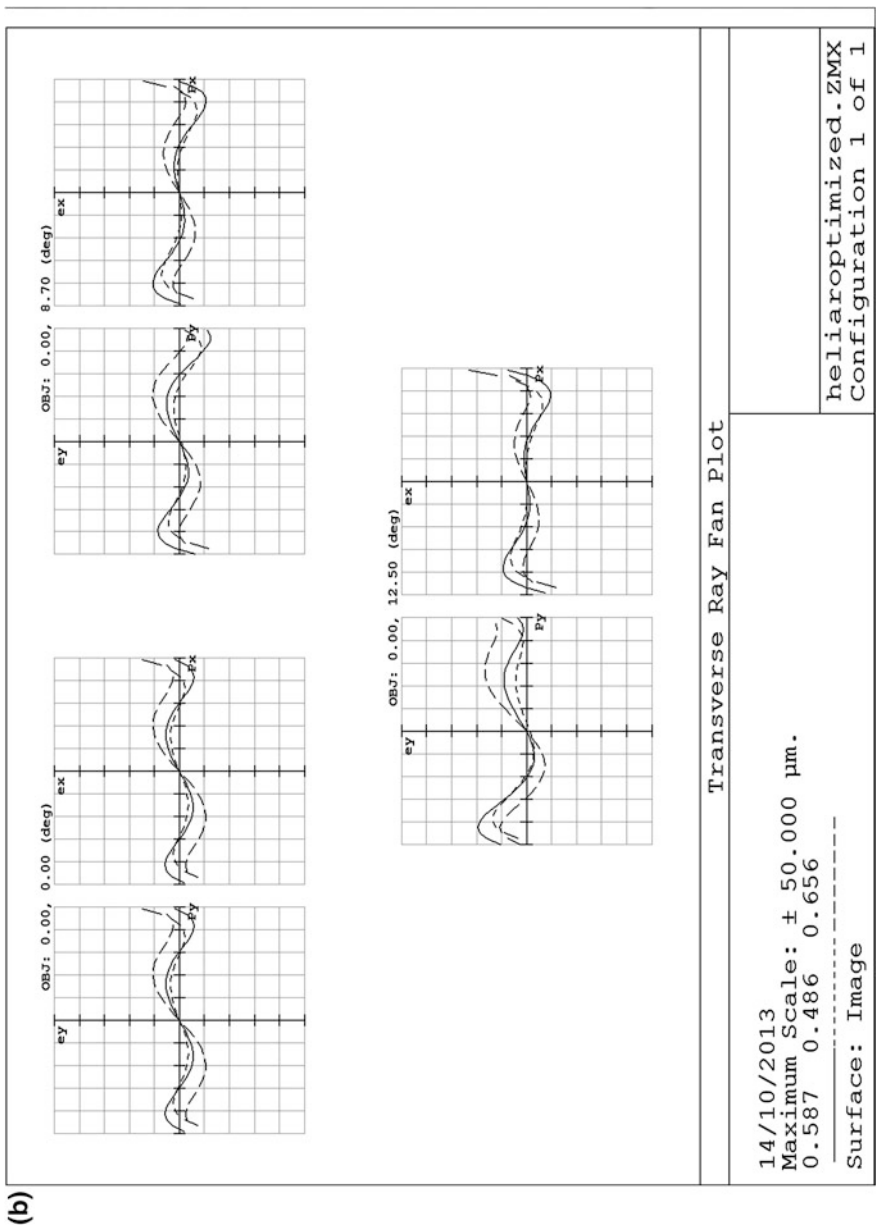


Fig. 6.42 (continued)

6.4.5 Exercise 17, Predesign of a Heliar

From the aberration equations of the thin lens design of the Heliar objective, and with the q-factors of the lay-out, it can be shown that the system coefficient of astigmatism is given by

$$S_3 = 0.03748(B_{1a} - 2.4653)^2 + 0.02506(B_{3b} + 2.2366)^2 - 0.2658.$$

Check this expression (use the stop shift equations of Sect. 4.3).

For $B_{1a} = 0.3$ calculate the value of B_{3b} for which $S_3 = -0.01$.

Calculate S_{11} , S_{13} , S_{21} , S_{23} .

Calculate $R_2 = S_{21} + q_1 S_{11} + S_{23} + q_3 S_{13}$.

Calculate the value of B_2 for which $S_{22} = -R_2$.

Calculate $S_1 = S_{11} + S_{12} + S_{13}$.

Now you have the form factors of a thin lens design with $S_2 = 0$, $S_3 = 0$.

Calculate S_4 and S_5 .

Calculate the radii of the design.

6.5 Symmetric Four-Component Lenses

In this section we discuss a category of photographic objectives with a moderate to large field angle.

That means that correction of field curvature is desirable. With symmetric four-component lenses this means that all designs must belong to the categories PNNP and NPPN (Kross [10]). In words, either two “telephoto” lenses in a symmetric configuration, or two reversed “telephoto” lenses.

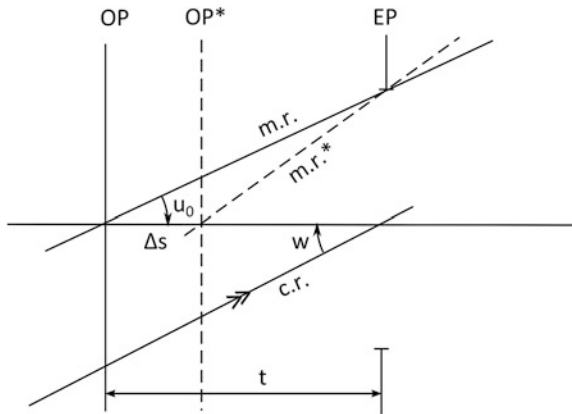
We will discuss the design of three PNNP examples and two NPPN designs.

Before we begin with the design examples we will describe some results from theory. We mentioned already in Sect. 5.3 that for a symmetric system that is used at magnification $M = -1$, the coefficients of coma, distortion and TCA are equal to zero. With a photographic objective the object is usually far away ($-s \gg -f$) and the aberrations become different from the $M = -1$ case.

In the following we will discuss equations that describe the change of the aberration coefficients when the object plane is shifted. These equations, that are companions to the stop shift equations, are called the *conjugate shift equations*.

The theory that we need is described by Welford [9, Sect. 8.7]. In the following we give an outline of that theory and discuss its application to symmetric systems.

Fig. 6.43 Conjugate shift, notation



6.5.1 Conjugate Shift Equations

In Fig. 6.43 we show the change of the marginal ray when the object plane is shifted over a distance Δs (In the case of the stop shift equations the chief ray changed with a shift of the stop. See Fig. 3.17 in Sect. 3.4).

The new marginal ray has parameters

$$h^* = h + \Delta \bar{q} \bar{h}, \quad u^* = u + \Delta \bar{q} \bar{u},$$

where $\Delta \bar{q}$ has to be determined, so that we have also new values of A and $\Delta(\frac{u}{n})$,

$$A^* = A + \Delta \bar{q} \bar{A}, \quad \Delta^*(\frac{u}{n}) = \Delta(\frac{u}{n}) + \Delta \bar{q} \Delta(\frac{\bar{u}}{n}).$$

When we take

$$\Delta \bar{q} = u_0 \Delta s / (t - \Delta s) \tan w$$

the marginal ray height in the EP has the same value as before the shift. This makes that the Lagrange invariant $H = -h_p \tan w$ is conserved. For the notation see Fig. 6.43.

So far it was not necessary to calculate $\Delta(\frac{\bar{u}}{n})$ in the calculation of the Seidel coefficients. Because we have \bar{u} in our calculation scheme, it is easy to obtain $\Delta(\frac{\bar{u}}{n}) = \frac{\bar{u}'}{n'} - \frac{\bar{u}}{n}$.

The Seidel coefficients can now be calculated by inserting the starred values h^* , A^* and $\Delta^*(\frac{u}{n})$ in the equations for the surface coefficients of Sect. 3.3. This gives the Seidel coefficients after the shift of the object plane.

The conjugate shift equations that are derived by Welford connect the starred coefficients (after the shift) to the aberration coefficients before the shift. They can be written in the form

$$\begin{aligned} S_1^* &= S_1 + \Delta\bar{q}(3S_2 + \bar{S}_5) + \Delta\bar{q}^2(3S_3 + 3\bar{S}_3 + 2S_4) + \Delta\bar{q}^3(3\bar{S}_2 + S_5) + \Delta\bar{q}^4\bar{S}_1, \\ S_2^* &= S_2 + \Delta\bar{q}(2S_3 + \bar{S}_3 + S_4) + \Delta\bar{q}^2(S_5 + 3\bar{S}_2) + \Delta\bar{q}^3\bar{S}_1, \\ S_3^* &= S_3 + \Delta\bar{q}(S_5 + \bar{S}_2) + \Delta\bar{q}^2\bar{S}_1, \\ S_4^* &= S_4, \quad S_5^* = S_5 + \Delta\bar{q}\bar{S}_1, \quad S_6^* = \bar{S}_1, \end{aligned} \quad (6.24)$$

where Δq is the increment of $\bar{q} = h/\bar{h}$. Just as Δq with the stop shift equations, $\Delta\bar{q}$ is the same for all surfaces.

In the above formulas figure six new coefficients.

The coefficient S_6 is defined as

$$S_6 = -\bar{A} \bar{h} \Delta \left(\frac{\bar{u}}{n} \right). \quad (6.25)$$

It is equal to \bar{S}_1 and invariant under a conjugate shift. This coefficient is sometimes called the sixth Seidel coefficient. It is linked to the term $b_6 W^2$ in the wavefront error expansion (see Sect. 3.3) so that $b_6 = \frac{1}{8} S_6$.

The coefficients $\bar{S}_1, \bar{S}_2, \bar{S}_3, \bar{S}_4, \bar{S}_5$ represent the so-called *pupil aberrations*. These aberrations are found in the case that object and entrance pupil exchange their positions, so that the marginal ray becomes the chief ray and vice versa. The pupil aberrations are related to the object aberrations by the equations

$$\begin{aligned} \bar{S}_1 &= S_6, \quad \bar{S}_2 = -S_5 - H \Delta(\bar{u}^2), \\ \bar{S}_3 &= S_3 - H \Delta(u \bar{u}), \quad \bar{S}_4 = S_4, \\ \bar{S}_5 &= S_2 - H \Delta(u^2), \end{aligned} \quad (6.26)$$

where $\Delta(u^2) = u'^2 - u^2$, etc.

The sixth Seidel coefficient S_6 is therefore the coefficient of pupil spherical aberration.

Also for the primary chromatic aberrations we can make up conjugate shift equations, that can be written

$$\begin{aligned} C_1^* &= C_1 + \Delta\bar{q}(\bar{C}_2 + C_1) + \Delta\bar{q}^2\bar{C}_1, \\ C_2^* &= C_2 + \Delta\bar{q}C_1, \\ C_3^* &= \bar{C}_1, \end{aligned} \quad (6.27)$$

where \bar{C}_1 and \bar{C}_2 are chromatic aberrations of the pupil. When we define a third chromatic aberration by

$$C_3 = -\bar{A} \bar{h} \Delta \left(\frac{\delta n}{n} \right) = \bar{C}_1 \quad (6.28)$$

we see that we can interpret it as pupil LCA. Then \bar{C}_2 is pupil TCA, and

$$\bar{C}_2 = C_2 - H \Delta \left(\frac{\delta n}{n} \right). \quad (6.29)$$

The new coefficient $C_3 = \bar{C}_1$ is invariant under a conjugate shift. From the shift equations we see that for stable correction of chromatic aberrations all three coefficients C_1 , C_2 and C_3 must be zero (see Velzel [20]).

Application to Symmetric Systems

We apply the conjugate shift equations to the design of symmetric systems. This subject was also treated by Kross [21]. With a symmetric system that is used at magnification $M = -1$, the “uneven” aberrations coma, distortion and TCA become zero, for the object as well as the pupil. Also $\Delta(u^2)$ and $\Delta(\bar{u}^2)$ are zero in this case. With the notation

$$H \Delta(\bar{u}^2) = H_2, \quad H \Delta(u\bar{u}) = H_3, \quad H \Delta(u^2) = H_5$$

the conjugate shift equations for this case become

$$\begin{aligned} S_1^* &= S_1 + \Delta q^2 (6S_3 + 2S_4 - 3H_3) + \Delta \bar{q}^4 S_6, \\ S_2^* &= \Delta \bar{q} (3S_3 + S_4 - H_3) + \Delta q^3 S_6, \\ S_3^* &= S_3 + \Delta \bar{q}^2 S_6, \quad S_4^* = S_4 \\ S_5^* &= \Delta \bar{q} S_6, \quad S_6^* = S_6, \\ C_1^* &= C_1 + \Delta \bar{q}^2 C_3, \\ C_2^* &= \Delta \bar{q} C_3, \quad C_3^* = C_3, \end{aligned}$$

where $\Delta \bar{q} = -u_0 / \tan w$.

Different strategies of correction can be derived from these equations

- (1) When we correct coma, so that

$$3S_3 + S_4 - H_3 = -\Delta\bar{q}^2 S_6$$

we have

$$\begin{aligned} S_1^* &= S_1 - \Delta\bar{q}^2 H_3 - \Delta\bar{q}^4 S_6, \\ S_3^* &= -\frac{1}{3}(S_4 - H_3 + \Delta\bar{q}^2 S_6), \\ S_5^* &= -(3S_3 + S_4 - H_3)/\Delta\bar{q}. \end{aligned}$$

Now correction of meridional field curvature, for which

$$S_3^* + \frac{1}{3}S_4 = 0,$$

is obtained for $H_3 = \Delta\bar{q}^2 S_6$ and we have finally

$$S_1^* = S_1 - 2H_3\Delta\bar{q}^2, \quad S_5^* = H_3/\Delta\bar{q}.$$

It can be shown that $H_3 = -HK$.

With typical values $H = 3$, $K = 0.01$, $\Delta\bar{q} = 0.3$ we have $S_5^* = 0.1$. This distortion cannot be corrected.

The second term in S_1^* is equal to -0.0162 with these data; it can be corrected by bending.

- (2) When we correct astigmatism first we must have

$S_3 = -\Delta\bar{q}^2 S_6$. Now we have left

$$\begin{aligned} S_1^* &= S_1 + \Delta\bar{q}^2(5S_3 + 2S_4 - H_3), \\ S_2^* &= 2\Delta\bar{q}(2S_3 + S_4 - H_3). \\ S_5^* &= -S_3/\Delta\bar{q}. \end{aligned}$$

Correcting field curvature ($S_4 = 0$) and coma ($2S_3 = H_3$) we end up with

$$S_1^* = S_1 + \frac{3}{4}\Delta\bar{q}^2 H_3, \quad S_5^* = -\frac{1}{2}H_3/\Delta\bar{q}.$$

There is a still smaller correction of S_1 , and the rest of distortion is halved as compared to the first strategy.

- (3) When we start with the correction of distortion we must have $S_6 = 0$. Because S_6 is an “even” aberration coefficient, each half of the system must be corrected for it.

Now the correction of coma requires that $3S_3 + S_4 = H_3$ so that we end up with

$$S_1^* = S_1 - \Delta\bar{q}^2 H_3, \quad S_3^* = S_3.$$

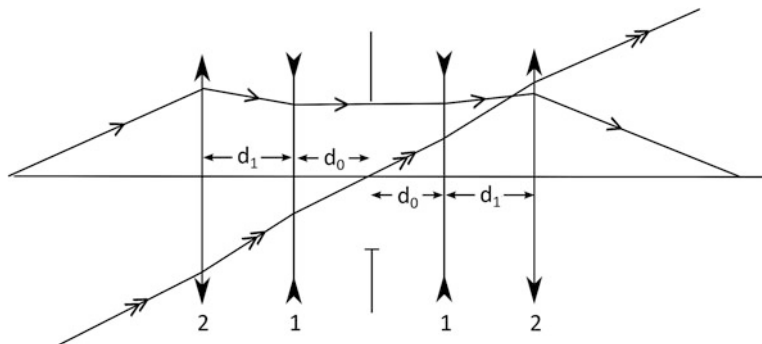


Fig. 6.44 Lay-out of the Celor ($M = 1$)

With a flat field, $S_4 = 0$, we have zero coma for $S_3 = \frac{1}{3}H_3$. Now astigmatism cannot be corrected; a typical value would be 0.03.

(4) For the correction of chromatic aberrations we need sufficiently small values of C_1 as well as C_3 .

6.5.2 The Celor

The Celor (von Hoegh 1898) or Dogmar is a symmetric quadruplet where the components are single lenses. It was used as a general purpose photographic objective and also as an enlarger lens. One can think of the design as a symmetric triplet of which the middle lens has been split. In this way a PNNP-type symmetric anastigmat results.

Lay-out of the Celor

Because the marginal ray at the stop (see Fig. 6.44) is parallel to the axis, we consider only the right half of the system. Its power is given by

$$K_R = K_1 + K_2 - d K_1 K_2$$

We take $K_1 + K_2 = 0$, as in a telephoto lens, so that $K_R = d_1 K_2^2$. The position of the object-side principal plane is given by

$$e_R = V_1 H_R = d_1 K_2 / K_R = 1 / K_2.$$

The power of the complete system is given by

$$K = 2K_R - (2d_0 + 2e_R)K_R^2.$$

With $d_1 K_2 = 0.25$, $2d_0 = d_1$ we obtain

$$K = 0.3593 K_2.$$

With $K = 0.00835$ we obtain $K_2 = 0.0232$, $f_2 = 43.10$ mm, $d_1 = 10.75$ mm.

Thin Lens Design of Celor

From the lay-out we have, for the right half at $M = -1$,

$$G_1 = -1, G_2 = 0.600, q_1 = 0.1613, q_2 = 0.4194$$

and, with $n = 1.65$ for both components

$$\begin{aligned} S_{11} &= -0.1635 B_1^2 + 0.3084 B_1 - 0.3304, \\ S_{12} &= 0.3994 B_2^2 + 0.4520 B_2 + 0.6066, \\ S_{21} &= 0.1994 B_1 - 0.2107, \\ S_{22} &= 0.3116 B_2 + 0.1980, \end{aligned}$$

where we have used the performance parameters

$$h_p = 15, \tan w = 0.2, H = -3.$$

We choose B_2 so that S_{12} is at a minimum. With $B_2 = -0.5625$ we have $S_{12} = 0.4787$, $S_{22} = 0.0227$. With $B_1 = -0.4$ we have $S_{11} = -0.4819$, $S_{21} = -0.2905$ so that for the right half $S_{1R} = -0.0032$, $S_{2R} = -0.1488$, $S_{3R} = -0.0030$ and $S_{4R} = 0$, $S_{5R} = 0.2168$.

For the whole objective at $M = -1$ we will have $S_1 = -0.0064$, $S_2 = 0$, $S_3 = -0.0060$, $S_4 = 0$, $S_5 = 0$.

Surface Model of Celor

The prescription of the surface model, after giving thickness and applying scaling corrections, becomes

	#	Radius	Thickness	Glass	Diameter
STO	1	35.506	3.96	N-LAK 21	30
	2	-126.810	8.58	Air	30
	3	-40.177	2.01	SF 2	25
	4	92.446	4.54	Air	25
	5	Plane	4.53	Air	20
	6	-92.446	2.01	SF 2	20
	7	40.177	8.58	Air	20
	8	126.810	3.96	N-SSK 5	25
	9	-35.506	94.04	Air	25
IMA	10	Plane	-		51.2

We have chosen the glasses N-LAK 21 ($n_D = 1.64049$, $V = 60.1$), SF 2 ($n_D = 1.64679$, $V = 33.8$) and N-SSK 5 ($n_D = 1.65844$, $V = 50.9$). The glass in the last lens has a smaller value of V than its counterpart in the first lens. From our triplet experience we know that this facilitates the correction of TCA.

The results of the paraxial calculations and the Seidel coefficients per surface are shown below.

From these we calculate $\Delta\bar{q} = -0.417$, $H_3 = -0.0812$, $S_6 = 0.2110$. Using these values and the coefficients of the thin lens design at $M = -1$ in the conjugate shift equations for $M^* = 0$ we find $S_1^* = -0.0486$, $S_2^* = 0.0260$, $S_3^* = 0.0306$, $S_4^* = 0$, $S_5^* = -0.511$. The values found for the surface model (at $M = 0$) are

$$S_1 = -0.0959, S_2 = 0.0870, S_3 = -0.0143, S_4 = 0, S_5 = -0.1375.$$

Because of the differences in refractive index and the differences in ray height from the thin lens design these differences between the two sets of coefficients are to be expected.

Paraxial results for the Celor

#	nu	h	$\bar{n}\bar{u}$	\bar{h}	A	\bar{A}	$h\Delta$
1	0	15	0.2150	-5.384	0.4225	0.0648	-1.5285
2	-0.2745	14.337	0.3136	-4.635	-0.4600	0.3730	-3.5269
3	-0.3479	11.352	0.3374	-1.740	-0.6304	0.3809	3.2592
4	-0.1651	11.150	0.3094	-1.362	0.0335	0.2853	-0.3011
5	-0.0878	10.353	0.3	1.362	-0.1998	0.2854	0.8479
6	-0.0161	10.333	0.3094	1.740	0.4074	0.3810	1.6140
7	0.1503	11.622	0.3373	4.635	0.2419	0.3736	-1.3633
8	0.0330	11.839	0.3136	5.384	-0.4622	0.0646	-1.8812

	S_1	S_2	S_3	S_4	S_5	S_6	C_1	C_2
1	0.2728	0.0418	0.0064	0.1165	0.0188	-0.0022	0.0411	0.0063
2	0.7463	-0.6051	0.4907	0.0322	-0.4240	0.1424	0.0428	-0.0347
3	-1.2952	0.7826	-0.4728	-0.1019	0.3472	-0.0564	-0.0464	0.0502
4	0.0003	0.0029	0.0245	-0.0437	-0.1635	0.0206	-0.0043	-0.0370
5	-0.0338	0.0483	-0.0069	-0.0437	0.0722	0.0206	-0.0240	0.0343
6	-0.2679	-0.2505	-0.2343	-0.1019	-0.3144	-0.0564	-0.0489	-0.0457
7	0.0797	0.1232	0.1903	0.0322	0.3436	0.1445	0.0219	0.0338
8	0.4019	-0.0562	0.0078	0.1165	-0.0174	-0.0023	0.0427	-0.0060
Σ	-0.0959	0.0870	-0.0143	0.0062	-0.1375	0.2110	0.0259	0.0012

We also show the coefficients of the primary chromatic aberrations. The correction of LCA is not yet good enough; the correction of TCA is nearly perfect in both cases. The chief ray is not changed by a shift of conjugate.

The surface model that we used thus far was symmetric. In a symmetric design the possibilities for the correction of the “even” aberrations: spherical, astigmatism, axial color and pupil spherical (S_6) are limited. The more so because we had only two degrees of freedom (B_1 and B_2) in our thin lens design.

Therefore we tried to improve the design by releasing the condition of (mirror) symmetry. We increased, as an experiment, the power of the right half of the objective by a factor of 1.1. In this way we obtained what is called a hemisymmetric system.

The prescription of the surface model becomes now

	#	Radius	Thickness	Glass	Diameter
STO	1	35.506	3.96	N-LAK 21	30
	2	-126.810	8.58	Air	30
	3	-40.177	2.01	SF 2	25
	4	92.446	4.54	Air	25
	5	Plane	4.53	Air	22
	6	-84.042	1.83	SF 2	25
	7	36.525	7.80	Air	25
	8	115.282	3.60	N-SSK 5	32
	9	-32.278	-	Air	35
IMA	10	Plane	-	-	51.2

We show the results of the paraxial calculations and the third order coefficients below.

#	nu	h	n <u>u</u>	<u>h</u>	A	<u>A</u>	hΔ
5	-0.0878	10.353	0.3	1.362	-0.2110	0.2040	0.0845
6	-0.0089	10.343	0.3103	1.706	0.4574	0.3872	1.8369
7	0.1743	11.702	0.3405	4.362	0.2758	0.3783	-1.5785
8	0.1984	11.937	0.3149	5.048	-0.5049	0.0565	-2.0449

	S_1	S_2	S_3	S_4	S_5	S_6	C_1	C_2
5	-0.0038	0.0051	-0.0068	-0.0478	0.0734	0.0201	-0.0253	0.0341
6	-0.3843	-0.3253	-0.2753	-0.1123	-0.3281	-0.0578	-0.0548	-0.0464
7	0.1201	0.1647	0.2259	0.0353	0.3582	0.1408	0.0251	0.0345
8	0.5213	-0.0583	0.0065	0.1279	-0.0150	-0.0016	0.0470	-0.0052
Σ	-0.0225	0.0084	-0.0009	0.0061	-0.1330	0.2059	0.0202	0.0018

Note that the Σ -values relate to the complete lens. The left half of this design is identical to that of the previous design. A comparison between the two designs gives.

We compare the coefficients of the symmetric and hemi-symmetric versions in the following table.

	S_1	S_2	S_3	S_4	S_5	S_6	C_1	C_2
Sy	-0.0959	0.0870	-0.0143	0.0062	-0.1375	0.2110	0.0259	0.0012
He	-0.0225	0.0084	-0.0009	0.0061	-0.1330	0.2059	0.0202	0.0018

The hemi-symmetric Celor design has a focal length of 113.72 mm. To compare with systems from the literature (Smith [18]) we have to reduce the focal length to 50 mm.

We apply a scale reduction by a factor of 2.2744 and obtain the prescription

	#	Radius	Thickness	Glass	Diameter
STO	1	15.611	1.741	N-LAK 21	18
	2	-55.755	3.772	Air	18
	3	-17.662	0.883	SF 2	15
	4	40.446	1.994	Air	15
	5	Plane	1.994	Air	12
	6	-36.951	0.803	SF 2	15
	7	16.059	3.429	Air	15
	8	50.686	1.583	N-SSK 5	18
	9	-14.192	39.791	Air	18
IMA	10	Plane	-		22.51

The aberration coefficients of this design are

$$S_1 = 0.0099, \quad S_2 = 0.0037, \quad S_3 = -0.0004, \quad S_4 = 0.0027, \quad S_5 = -0.0584, \\ C_1 = 0.0089, \quad C_2 = 0.0008.$$

This is a good starting point for optimization.

Optimization of the Celor

The paraxial data of this design are: EFL = 100 mm, F = 4.7, object field angle 12.5° .

We show first the lay-out and the ray fan plots of the symmetric Celor. See Fig. 6.45a and b.

The prominent aberrations are coma and field curvature. The coma is expected because we use the lens with the object at infinity; the distortion remains small because the chief ray heights remain the same in a change of object position.

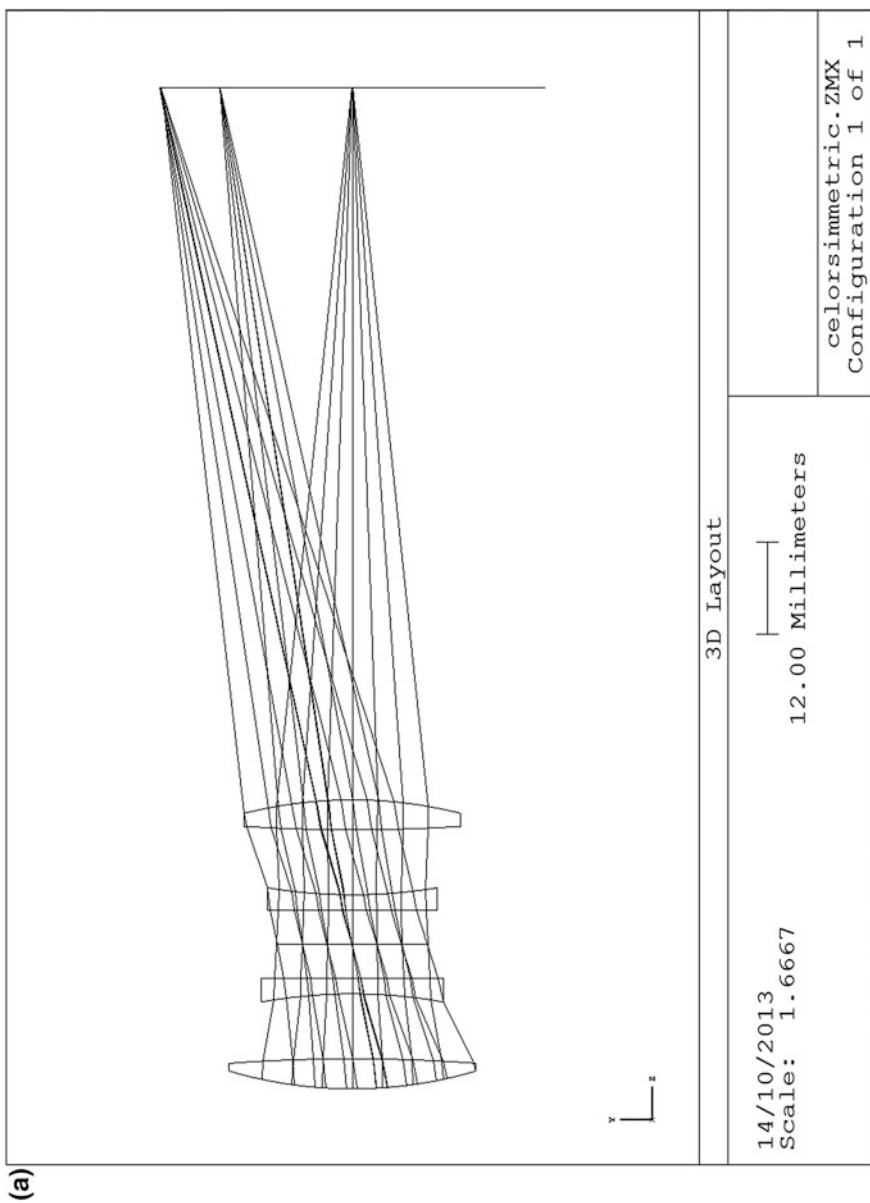


Fig. 6.45 a Celor I, lay-out. b Celor I, aberrations

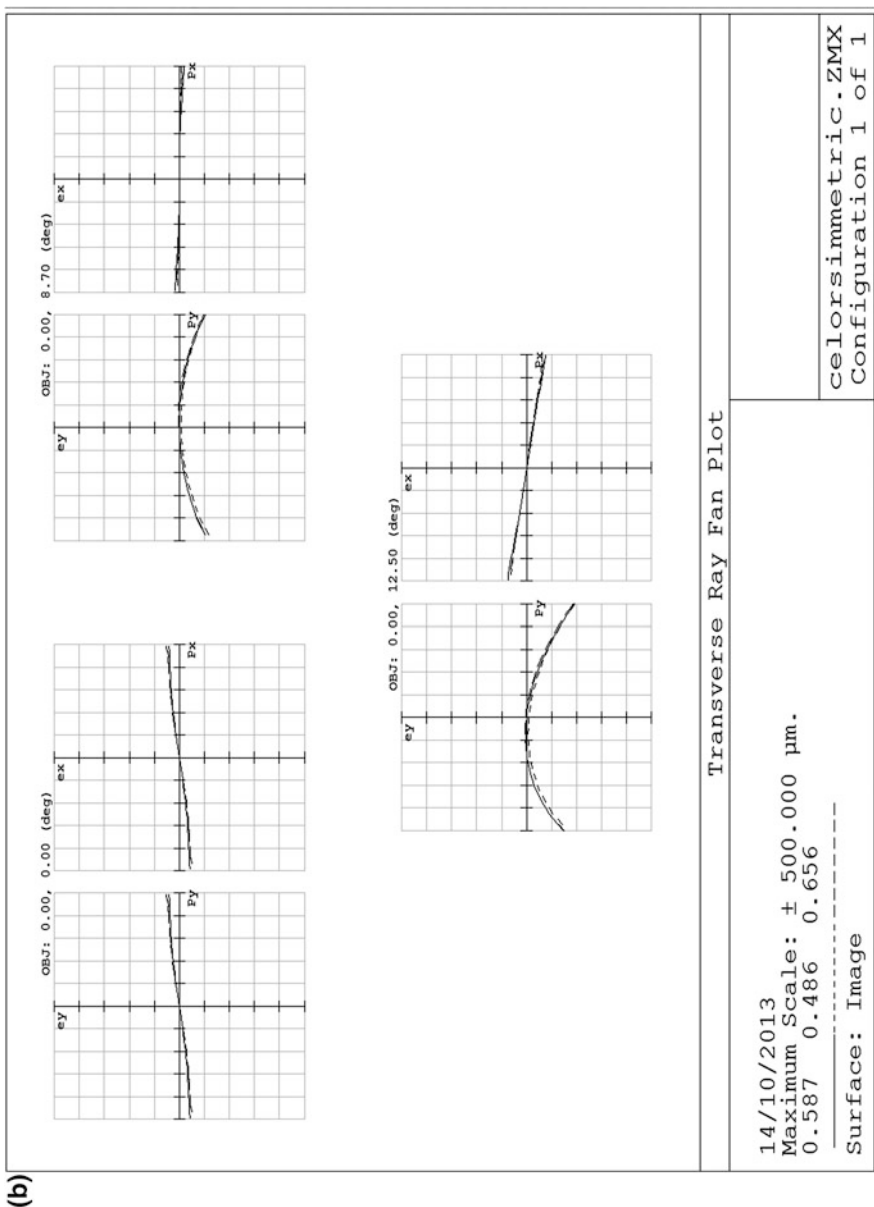


Fig. 6.45 (continued)

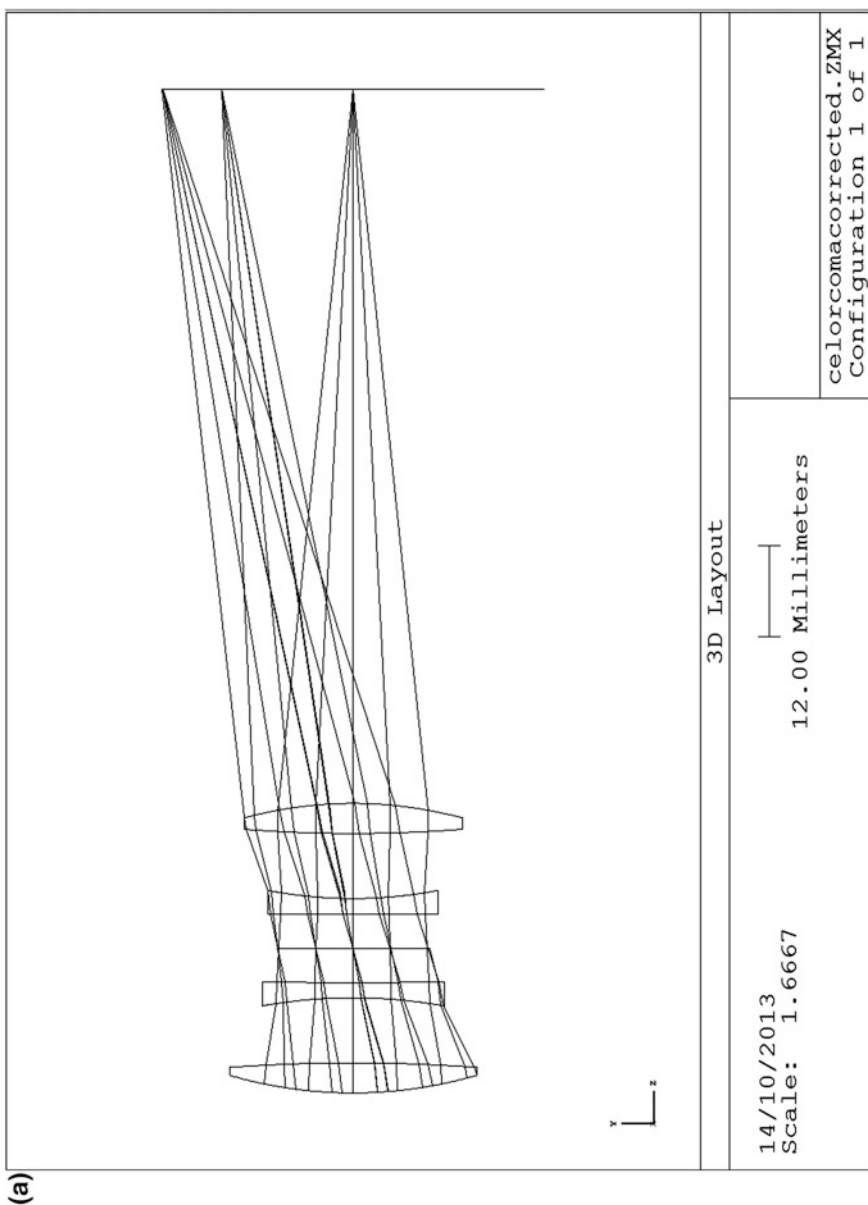


Fig. 6.46 a Celor II, lay-out. b Celor II, aberrations

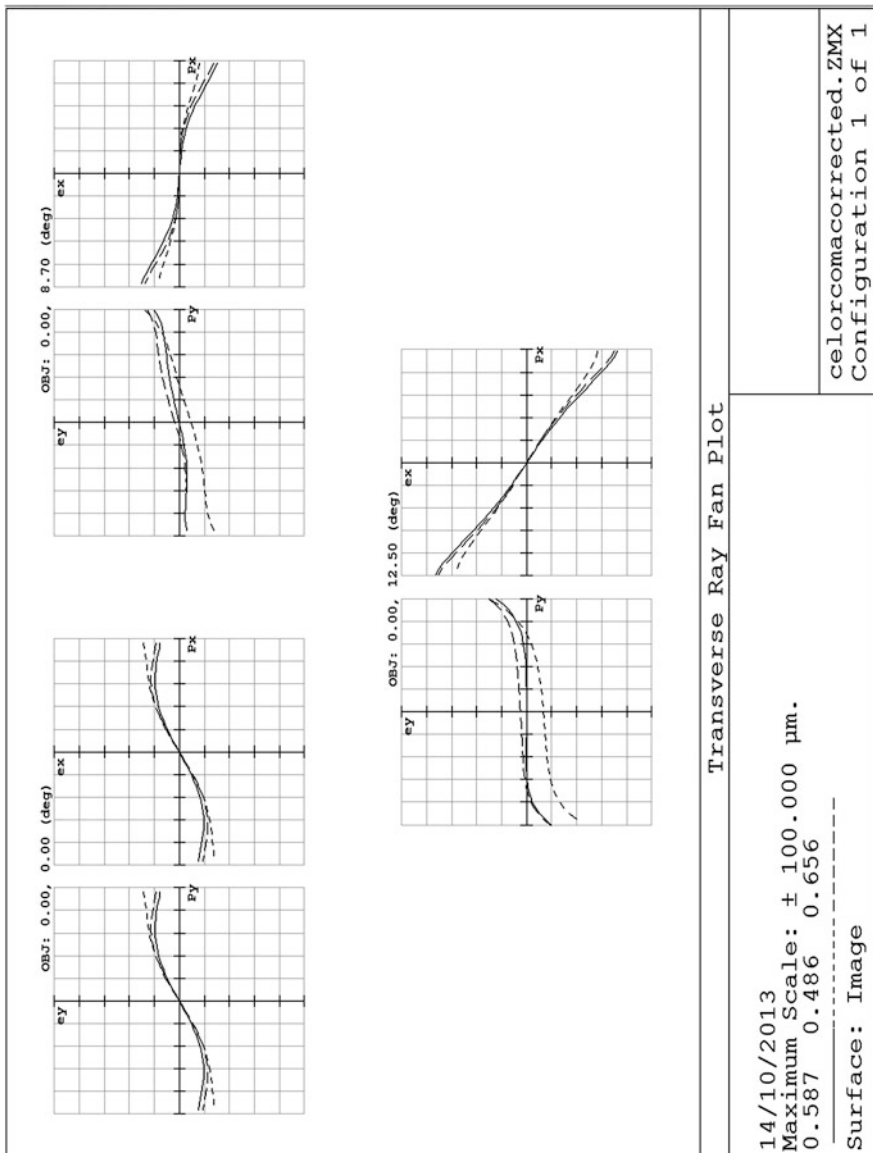


Fig. 6.46 (continued)

We used only the radii as variables in optimization. With the hemi-symmetric design, of which the lay-out is shown in Fig. 6.46a and the ray fan plots in Fig. 6.46b, we can correct coma better.

Now some TCA becomes visible (the scale of the plots has gone from 500 μm in Fig. 6.45b to 100 μm in Fig. 6.46b) and also some astigmatism.

Further optimization, including air distances and glasses, can improve this design.

The prescription of the hemi-symmetric Celor is given below.

Surface data summary

Surf	Radius	Thickness	Glass	Diameter
OBJ	Infinity	Infinity		
1	57.88458	3.96	LAK 21	32.5835
2	-222.7546	8.58		32.06378
3	-67.69269	2.01	SF 2	24.00383
4	907.7381	4.54		22.76258
STO	Infinity	4.53		20
6	-1103.566	2.01	SF 2	21.64604
7	59.23975	8.58		22.42687
8	189.185	3.96	N-SSK 5	28.20414
9	-54.80799	94.04		28.73548
IMA	Infinity			50.25546

6.5.3 The Planar

Like the Celor, the Planar (Rudolph 1907) is one of the prototypes of an extensive generation of symmetric and hemi-symmetric photographic objectives. The principle of the Planar is that a flat field can be obtained by using thick lenses with curvatures of equal sign at the front and the back surface (Fig. 6.47).

Lay-out of the Planar

We start with a simple model, consisting of two thick lenses in a symmetric configuration. At first we do not consider chromatic errors. For a diagram of the lay-out see Fig. 6.47b.

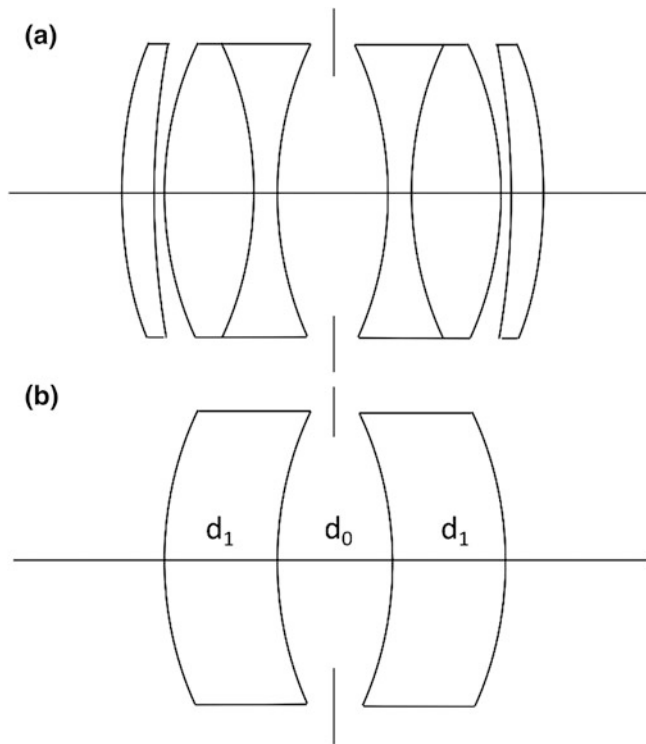


Fig. 6.47 Rudolph's Planar (a) and lay-out (b)

With

$$K_R = K_L = \frac{d_1}{n} K_1^2, \quad e_R = 1/K_1, \quad K = 2K_R - (d_0 + 2e_R) K_R^2$$

we find

$$K = 2 \frac{d_1}{n} K_1^2 - 2 \left(\frac{d_1}{n} \right)^2 K_1^3 - d_0 \left(\frac{d_1}{n} \right)^2 K_1^4.$$

with $K = 0.01$, $\frac{d_1}{n} K_1 = 0.2$, $d_0 K_1 = 0.2$ we find $K_1 = 0.03205$, $\frac{d_1}{n} = 6.24$, $d_0 = 6.24$.

As a glass we take N-LAK 33A ($n_D = 1.75500/V = 52.30$) so that we have $d_1 = 10.925$ and $r_1 = r_2 = -r_3 = -r_4 = 23.557$ mm.

With the lay-out completed, we have directly a surface model. This is the first design example where we will not do a thin lens predesign.

Surface Model of the Planar

The prescription of the surface model is

	#	Radius	Thickness	Glass	Diameter
STO	1	23.557	10.925	N-LAK 33A	36
	2	23.557	3.12	Air	36
	3	Plane	3.12	Air	24
	4	-23.557	10.925	N-LAK 33A	32
	5	-23.557	87.20	Air	32
IMA	6	Plane	-	-	46.80

We show the results of the paraxial calculations and the surface coefficients below.

#	nu	h	n <u>u</u>	<u>h</u>	A	<u>A</u>	hΔ
1	0	15	0.2340	-2.995	0.6410	0.1060	-2.341
2	-0.4808	12.000	0.3300	-0.936	0.4192	0.2598	0.7193
3 STO	-0.0962	11.700	0.3	0	-0.962	0.3	0
4	-0.0962	11.400	0.3	0.936	-0.5832	0.3400	2.0926
5	0.2692	13.080	0.3300	2.995	-0.7118	0.5546	-3.1053

#	S ₁	S ₂	S ₃	S ₄	S ₅
1	0.9618	0.1590	0.0263	0.2255	0.0416
2	-0.1264	-0.0783	-0.0485	-0.2255	-0.1698
3	0	0	0	0	0
4	-0.7117	-0.4149	-0.2419	-0.2255	0.2724
5	1.5733	1.22580	0.9551	0.2255	-0.9198
Σ	1.6970	-0.7303	0.6883	0	-0.7757

We do not show coefficients for the chromatic aberrations because we have only one glass in this design.

Apart from S₄ the four Seidel coefficients of this system are quite large. Especially the last surface has a very heavy load.

We decided to add extra lenses at the front and the back of our system. Adding lenses of power $\frac{1}{2}K_1$ with planar inner surfaces, the prescription becomes

	#	Radius	Thickness	Glass	Diameter
STO	1	47.114	2	N-LAK 33A	32.5
	2	Plane	0	Air	32.5
	3	47.114	10.925	N-LAK 33A	32
	4	23.557	3.12	Air	32
	5	Plane	3.12	Air	22
	6	-23.557	10.925	N-LAK 33A	30

(continued)

(continued)

	#	Radius	Thickness	Glass	Diameter
	7	-47.114	0	Air	30
	8	Plane	2	N-LAK 33A	30
	9	-47.114	85.02	Air	30
IMA	10	Plane	-	-	60.448

The results of the paraxial calculations and the surface coefficients of the split version are shown below.

#	nu	h	n <u>u</u>	<u>h</u>	A	<u>A</u>	hΔ
1	0	12	0.3053	-4.233	0.2544	0.2157	-0.7480
2	-0.1920	11.871	0.3761	-3.994	-0.1920	0.3761	-1.5280
3	-0.1920	11.781	0.3761	-3.994	0.0581	0.2913	0.8070
4	-0.3805	9.407	0.4400	-1.248	0.3205	0.3470	0.4186
5	-0.0790	8.914	0.4	1.248	-0.4574	0.3470	1.3023
6	0.2067	10.203	0.4400	3.994	-0.1733	0.2913	-0.2418
7	0.0434	10.203	0.3761	3.994	0.0434	0.3761	-0.2989
8	0.0141	10.253	0.3761	4.233	-0.3382	0.2157	-1.3811

#	S ₁	S ₂	S ₃	S ₄	S ₅	C ₁	C ₂
1	0.0451	0.0410	0.0348	0.1128	0.1251	0.0251	0.0202
2	0.0563	-0.1103	0.2161	0	-0.4233	0.0186	-0.0364
3	-0.0027	-0.0136	-0.0684	0.1127	0.2068	0.0056	0.0282
4	-0.0429	-0.0466	-0.0504	-0.2255	-0.2987	-0.0248	-0.0268
5	-0.2664	0.2076	-0.1568	-0.2255	0.2900	-0.0335	-0.0254
6	0.0073	-0.0122	0.0205	0.1127	-0.2238	0.0145	-0.0244
7	0.0056	0.0049	0.0422	0	0.3657	0.0036	0.0316
8	0.1580	-0.1021	0.0661	0.1128	-0.1156	0.0285	-0.0184
Σ	-0.0397	-0.0322	0.1041	0	-0.0838	0.0376	-0.0006

To our surprise the state of correction is quite decent, with less than 1 % of distortion.

We still have to take care of the chromatic aberrations. Therefore we will install buried surfaces between the surfaces 3 and 4 and between 5 and 6, so that we obtain two thick doublets.

For the glass of the negative component (on the side of the stop) we have the choice between

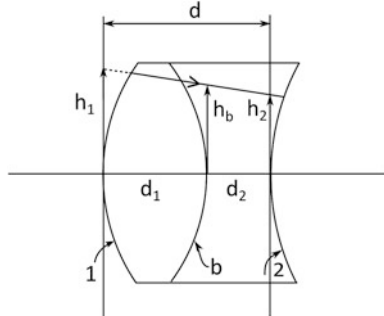
SF 4($n = 1.75513, V = 27.38$)

LAF 7($n = 1.74950, V = 34.82$)

LAF 7($n = 1.75550, V = 45.66$)

from the Schott catalogue. The radii of the buried surfaces will be found from the following algorithm.

Fig. 6.48 Notation for buried surface



Algorithm for Adding a Buried Surface

When we want to correct the primary chromatic aberrations without disturbing the correction of the third order aberrations, we can divide a thick lens in two parts by a buried surface. This means that the refractive index of the two parts is identical but the dispersion is different. Suppose that we have a lens with radii r_1 and r_2 , thickness d , refractive index n_D and V-number V_1 . We want to change this lens into a thick doublet with the same equivalent index and the same outer radii r_1 , r_2 and an inner (buried) radius r_b by a glass with the same index and V-number V_2 . This does not disturb the correction of the third order aberrations. See Fig. 6.48.

The surface coefficient of LCA is given by

$$C_{li} = A_i h_i \Delta \left(\frac{\delta n}{n} \right)_i$$

We know A and h for the outer surfaces from our previous paraxial calculations.

The value of h of the buried surface can be calculated when we fix its axial position. From Fig. 6.48 we see that

$$h_b = \frac{d_2 h_1 + d_1 h_2}{d}$$

For A_b we have the formula

$$A_b = \frac{n h_b}{r} + n u_2$$

Also $n u_2$ follows from the paraxial calculations. Because of the change of glass in the part of the lens occupied by the negative component the coefficient C_1 is changed by an amount

$$\Delta C_1 = (A_b h_b - A_2 h_2) \Delta C$$

where Δ_C is the difference in value of $\Delta(\frac{\partial n}{n})$ of the glasses on the right side and the left side of the buried surface. We have in this case

$$\Delta_C = \left(\frac{1}{V_2} - \frac{1}{V_1} \right) \frac{n_D - 1}{n_D}.$$

For the change in C_2 we find

$$\Delta C_2 = (\bar{A}_b h_b - \bar{A}_2 h_2) \Delta C$$

where $\bar{A}_b = \frac{n \bar{h}_b}{r} + n \bar{u}_2$, $\bar{h}_b = (d_2 \bar{h}_1 + d_1 \bar{h}_2)/d$.

As before we assume that we know \bar{h}_1 , \bar{h}_2 and \bar{U}_2 from previous paraxial calculations.

Application to the Design of the Planar

From the paraxial results for the split Planar we have, with $d_1 = d_2 = \frac{1}{2}d$,

$$\begin{aligned} h_b A_b &= 197.0 c - 4.03, \\ -h_2 A_2 &= -3.02. \end{aligned}$$

Using the glass LAF 37 we find

$$\Delta_C = 0.4302 \left(\frac{1}{45.66} - \frac{1}{52.30} \right) = 0.001196$$

so that we obtain

$$\Delta C_1 = 0.2356 c - 0.00843.$$

We want to have $\Delta C_1 = -0.0190$ for both buried surfaces. This leads to a curvature

$$c = -0.04486, r = -22.292$$

for the curvature in the left side component and its opposite in the right side.

The specification of the design that we have obtained now is given below.

The third order coefficients of this design will not be different from those of its predecessor. The coefficient of LCA will become small enough ($C_1 \approx 0.0004$) and the coefficient of TCA will remain unchanged.

Prescription of the Split Planar with Colour Correction

	#	Radius	Distance	Glass	Diameter
STO	1	47.114	2	N-LAK 33A	33
	2	Plan	0	Air	33
	3	47.114	5.447	N-LAK 33A	32
	4	-22.292	5.477	N-LAF 3	27
	5	23.557	3.12	Air	22
	6	Plan	3.12	Air	19
	7	-23.557	5.447	N-LAF 3	22
	8	22.292	5.477	N-LAK 33A	27
	9	-47.114	0	Air	32
	10	Plan	2	N-LAK 33A	33
	11	-47.114	85.016	Air	33

We changed the outer lenses of this design slightly. The new radii were

$$\begin{aligned} r_1 &= 42.230, \quad r_2 = 401.606 \\ r_{10} &= -401.606, \quad r_{11} = -42.230. \end{aligned}$$

The resulting design has the following aberration coefficients

$$\begin{aligned} S_1 &= -0.0095, \quad S_2 = -0.0076, \quad S_3 = 0.0402, \quad S_4 = 0.0012, \quad S_5 = 0.0168, \\ C_1 &= -0.0002, \quad C_2 = 0.004. \end{aligned}$$

Now we are ready for the optimization phase. A sketch of the Planar that we designed is shown in Fig. 6.49.

Optimization of the Planar

The paraxial parameters of the Planar are EFL = 100 mm, F/4, object field angle 15°.

We show first the optimization results of the split Planar, without colour correction. We optimized the surface model with the radii, air distances and glass thicknesses as parameters. We let the design become asymmetric.

As a result we obtain a decent correction of the center and 10° field, with aberrations smaller than 10 μm. At 15° we see some fifth order spherical (TO-BSA); this is the dominating aberration of this design form.

The lay-out of the monochromatic Planar is shown in Fig. 6.50a and the ray fan plots in Fig. 6.50b.

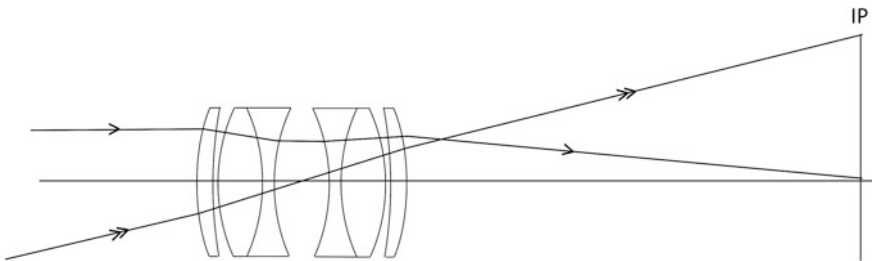


Fig. 6.49 Split Planar design

Below we show the prescription of this design.
Surface data summary

Surf	Radius	Thickness	Glass	Diameter
OBJ	Infinity	Infinity		
1	147.533	1.998384	LAK 33	33.59667
2	Infinity	0		33.17957
3	32.23472	10.18639	LAK 33	30.38138
4	26.3162	5.943907		22.57775
STO	Infinity	12.40423		20
6	-29.85287	16.90571	LAK 33	25.04325
7	-42.30028	0		36.25775
8	Infinity	3.04992	LAK 33	38.53051
9	-78.06779	87.66569		38.71969
IMA	Infinity			53.12012

Next we optimized the surface model of the split Planar with colour correction, where the glass P-LAF 37 was used as a flint glass.

With radii and glass thicknesses as variables we optimized this design. The resulting lay-out is shown in Fig. 6.51a and the ray fan plots in Fig. 6.51b. It is seen from the ray-fan plots that there is still a considerable amount of longitudinal colour. The aberrations of the middle wavelength are larger than with the monochromatic version.

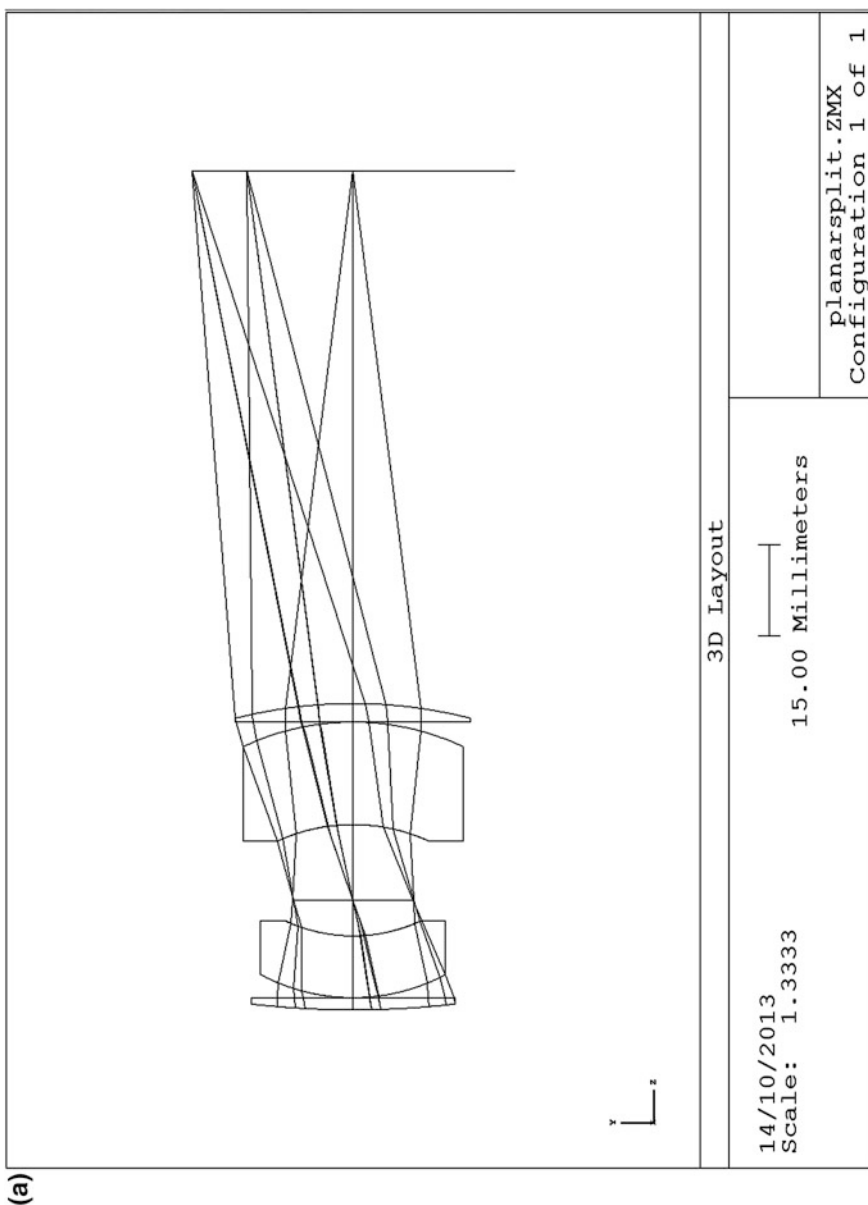


Fig. 6.50 **a** Planar I, lay-out. **b** Planar I, aberrations

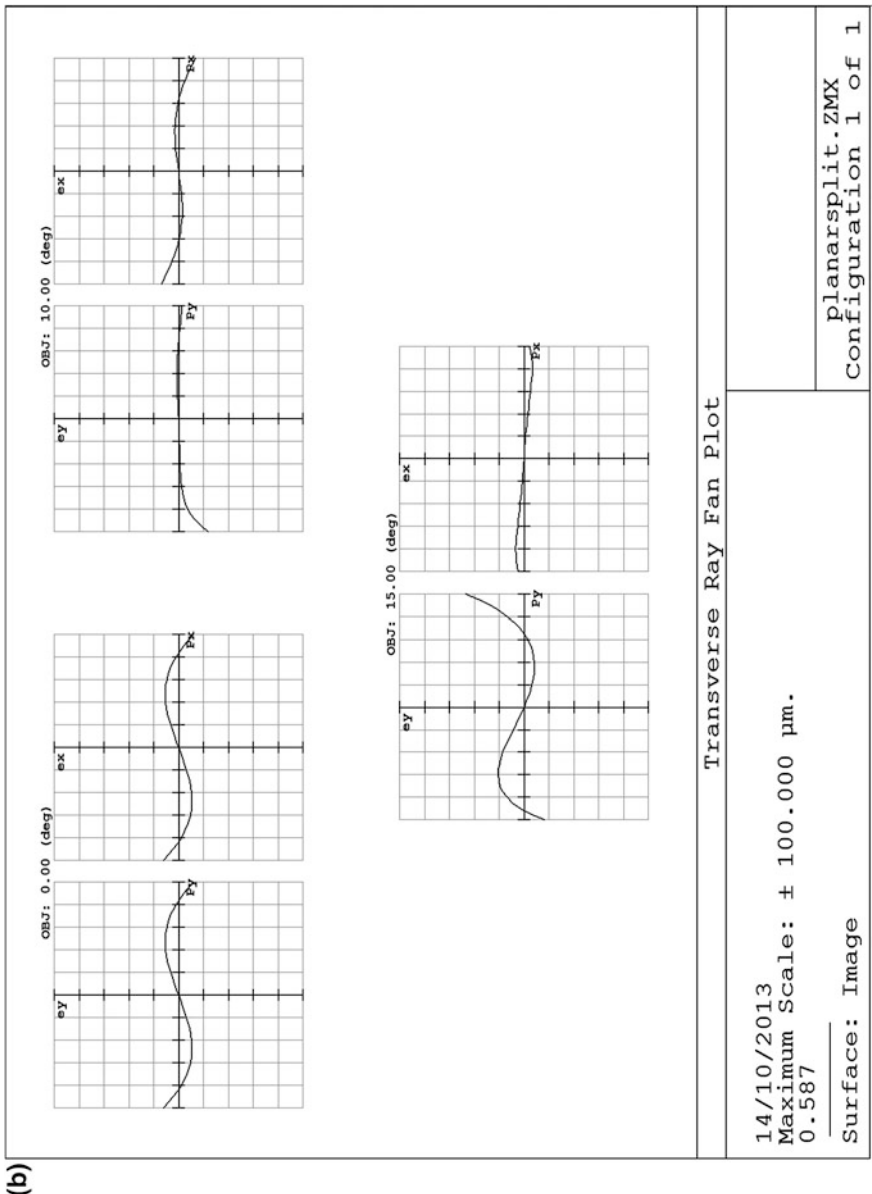


Fig. 6.50 (continued)

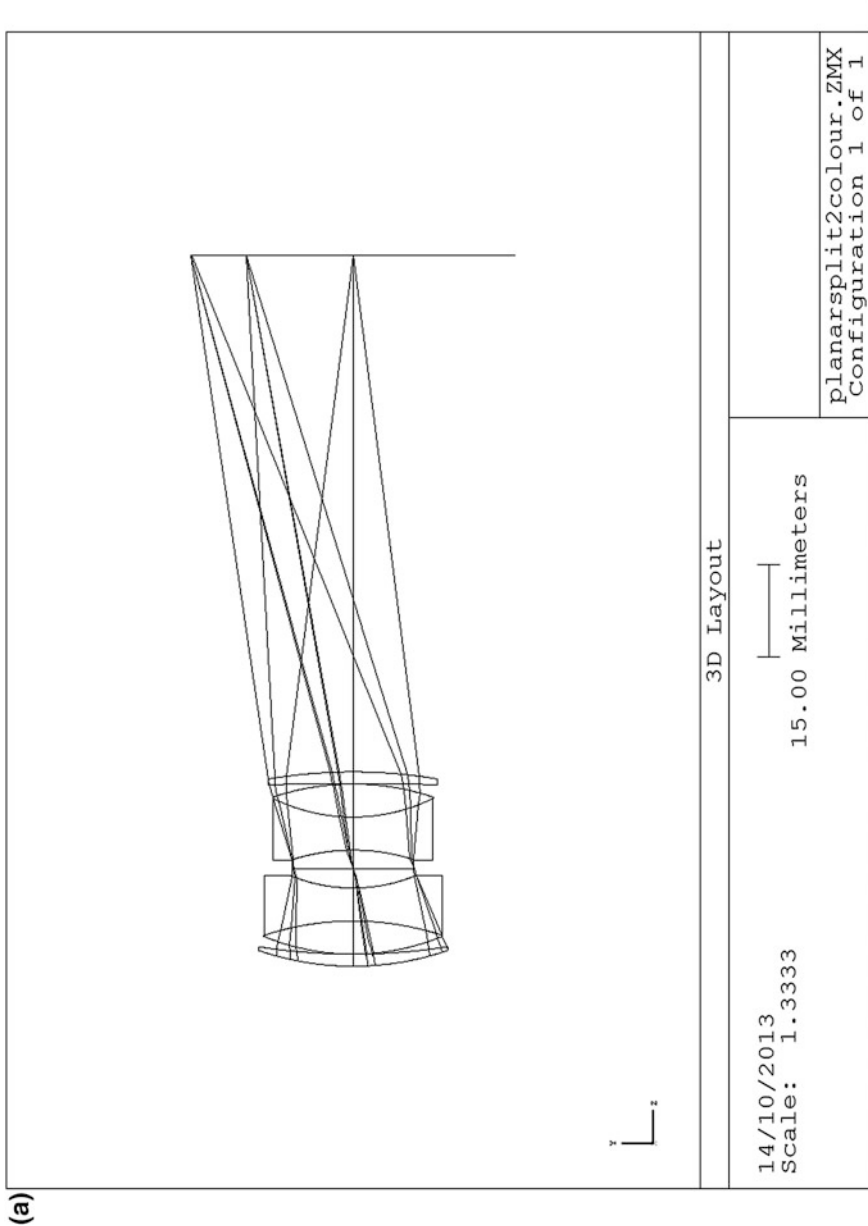


Fig. 6.51 a Planar II, lay-out. b Planar II, aberrations

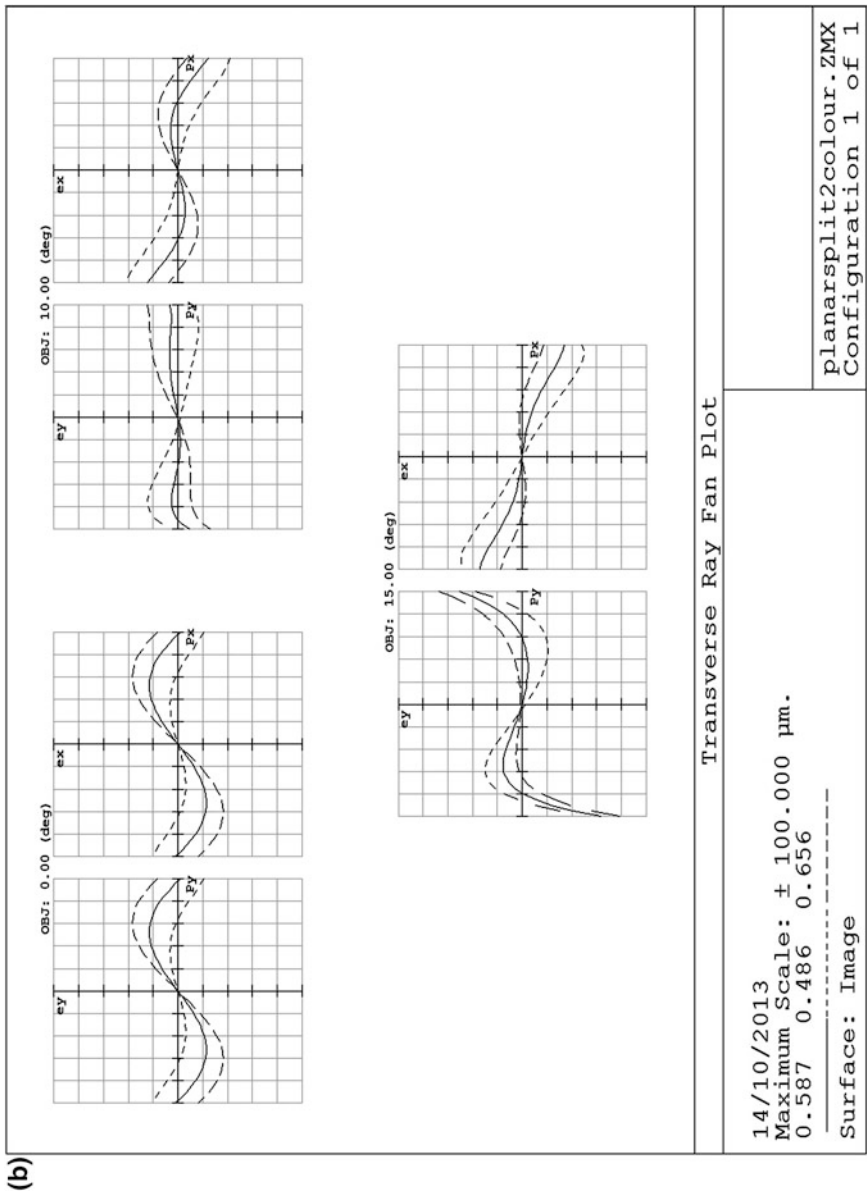


Fig. 6.51 (continued)

The prescription of this design is given in the table below.

Surface data summary

Surf	Radius	Thickness	Glass	Diameter
OBJ	Infinity	Infinity		
1	47.69438	2	LAK 33	31.19074
2	100.3909	0		30.84753
3	38.38463	5.447	LAK 33	29.39227
4	-46.68872	5.447	P-LAF 37	29.24791
5	27.1158	3.12		20.98375
STO	Infinity	3.12		20
7	-32.64411	5.447	P-LAF 37	20.20498
8	29.64522	5.447	LAK 33	26.28164
9	-41.142	0		26.40196
10	-1135.899	2	LAK 33	27.54291
11	-83.06259	85.016		27.82961
IMA	Infinity			53.40524

We did a second optimization run with the colour corrected split Planar, letting the glasses be substituted. This improved the colour correction and the aberrations of the middle wavelength, as can be seen from the ray fan plot in Fig. 6.52b (note the scale). The optimization program introduced 6 glasses in this design, that can be found in the literature [22], but are no longer produced by Schott. In practice one must be careful and work with up-to-date software.

The lay-out of this design is shown in Fig. 6.52a and its prescription in the table below.

Surface data summary

Surf	Radius	Thickness	Glass	Diameter
OBJ	Infinity	Infinity		
1	42.59144	1.999302	LAK 28	33.4734
2	66.24503	0.09924913		33.02938
3	28.39424	6.50361	LAK 31	30.98026
4	-1398.613	3.582688	LAFN 24	29.17565
5	21.77426	6.000221		22.70705
STO	Infinity	5.81829		20
7	-38.25297	6.999983	LAFN 8	21.35979
8	28.63201	7.000444	LAK 33	29.22751
9	-46.12812	2.608152		29.56252
10	107.1459	2.000037	LAKN 14	33
11	-310.1351	84.64342		33.05413
IMA	Infinity			52.5507

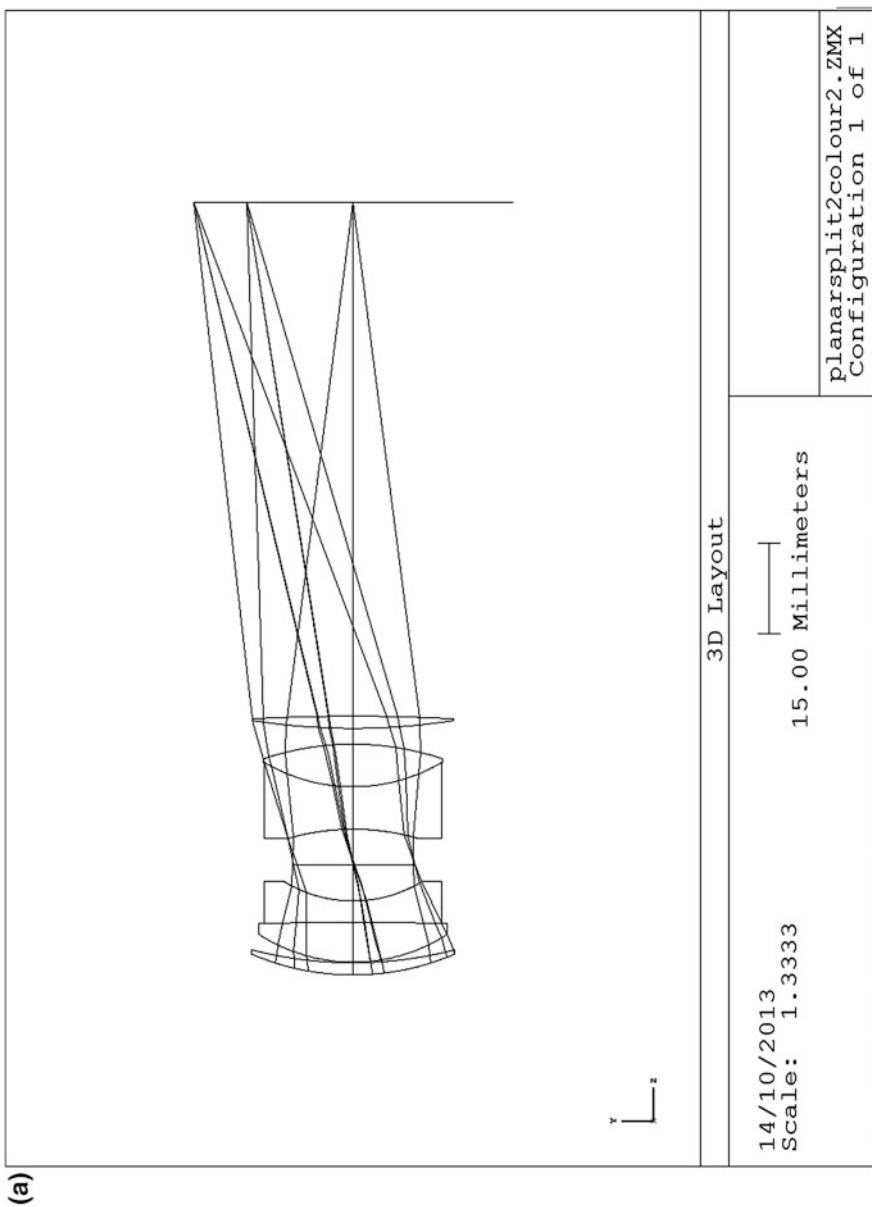


Fig. 6.52 a Planar III, lay-out. b Planar III, aberrations

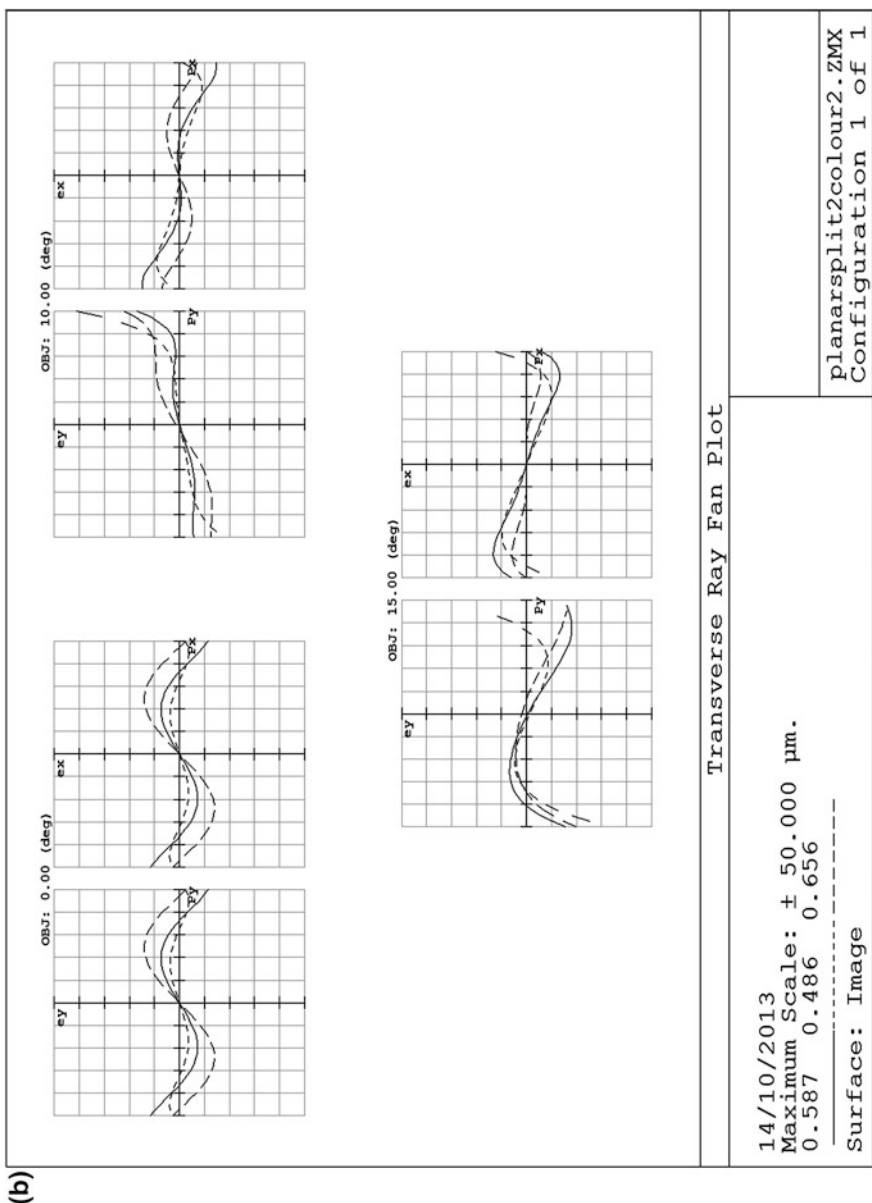


Fig. 6.52 (continued)

6.5.4 The Double Gauss

Above we designed a Planar with the glasses LAK 33 and LAF 37. When we take for the flint glass NSF_4 ($n = 1.75513$, $V = 27.38$) we obtain for the buried surfaces (in the same position as before) the radii

$$r_4 = 43.663, r_8 = -43.663.$$

Inserting these radii in the prescription of the Planar, we obtain the prescription

	#	Radius	Distance	Glass	Diameter
STO	1	42.230	2	N-LAK 33A	33
	2	401.606	0	Air	33
	3	47.114	5.447	N-LAK 33A	32
	4	43.663	5.477	SF 4	27
	5	23.557	3.120	Air	22
	6	Plan	3.120	Air	19
	7	-23.557	5.447	SF 4	22
	8	-43.663	5.477	N-LAK 33A	27
	9	-47.114	0	Air	32
	10	401.606	2	N-LAK 33A	33
	11	-42.230	83.480	Air	33

We give a sketch of this design in Fig. 6.53.

An objective as shown in the figure belongs to the type Double Gauss; it is a frequently used photographic objective that can be used at a field angle of 22° and with an aperture of F/1. Thus far we produced a starting design with F/4 and 17.7° field angle. We should try to optimize in both directions.

The results of the paraxial calculations are found below.

Paraxial results for Double Gauss

	#	$n\bar{u}$	h	$n\bar{u}$	\bar{h}	A	\bar{A}	$h\Delta$
STO	1	0	10	0.3042	-4.431	0.2368	0.1993	-0.5800
	2	-0.1788	9.796	0.3835	-3.994	-0.1360	0.3660	-1.0029
	3	-0.1604	9.796	0.3760	-3.994	0.0475	0.2912	0.5617
	4	-0.3174	8.806	0.4400	-2.621	0.0366	0.3346	0
	5	-0.3174	7.815	0.4400	-1.248	0.2649	0.3470	0.2831
	6	-0.0668	7.606	0.4	0	-0.0668	0.4	0
	7	-0.0668	7.397	0.4	1.248	-0.3808	0.3470	0.9030
	8	0.1703	7.929	0.4400	2.621	-0.1484	0.3346	0
	9	0.1703	8.461	0.4400	3.994	-0.1448	0.2912	-0.1739
	10	0.3474	8.461	0.3760	3.994	0.0137	0.3661	-0.1548
	11	0.0507	8.519	0.3835	4.431	-0.3034	0.1994	-1.0060

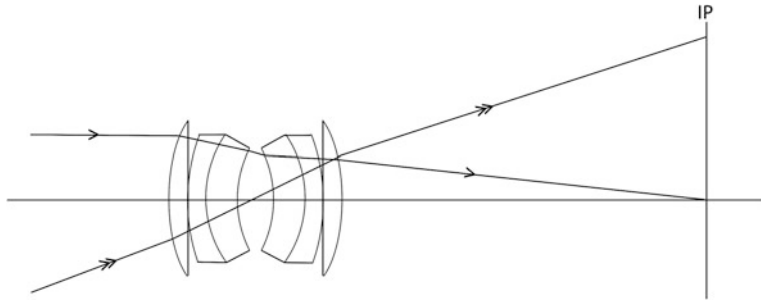


Fig. 6.53 Double Gauss design

#	S ₁	S ₂	S ₃	S ₄	S ₅	C ₁	C ₂
1	0.0325	0.0273	0.0230	0.0942	0.0986	0.0196	0.0164
2	0.0186	-0.0499	0.1343	-0.0099	-0.3347	0.0110	-0.0296
3	-0.0013	-0.0077	-0.0473	0.0845	0.2281	0.0038	0.0235
4	0	0	0	0	0	0.0024	0.0222
5	-0.0199	-0.0337	-0.0340	-0.1690	-0.2902	-0.0327	-0.0428
STO	6	0	0	0	0	0	0
	7	-0.1508	0.1193	-0.1087	-0.1690	0.2530	-0.0445
	8	0	0	0	0	0.0157	-0.0200
	9	0.0036	-0.0073	0.0147	0.0845	-0.1994	0.0101
	10	0	0.0077	0.0207	-0.0099	0.2886	-0.0009
	11	0.0926	-0.0608	0.0400	0.0942	-0.0881	0.0213
	Σ	-0.0247	-0.0051	0.0427	-0.0004	-0.0441	0.0058
							0.0014

Optimization of the Double Gauss

The Double Gauss design has paraxial parameters EFL = 100 mm, F/3.9, object field 15°.

It was optimized using the radii as variables only. The colour correction is good enough, with some remaining field curvature balanced by field dependent spherical (TOBSA).

We show the lay-out in Fig. 6.54a and the ray fan plots in Fig. 6.54b. The image field diameter of this design is 53.6 mm; with an EFL of 50 mm and a field angle of 24° it will be a nice objective for a 35 mm camera. The prescription is given in the table below.

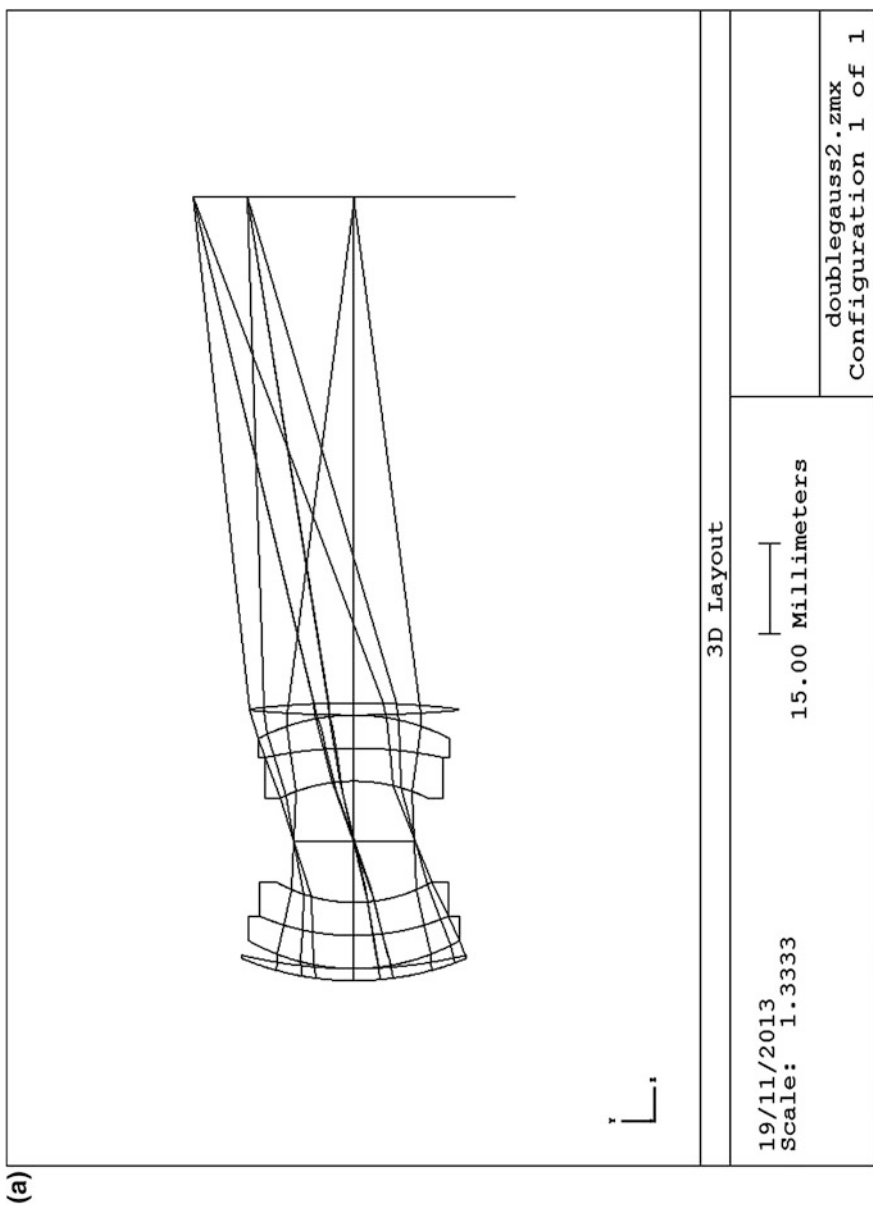


Fig. 6.54 a Double Gauss, lay-out. b Double Gauss, aberrations

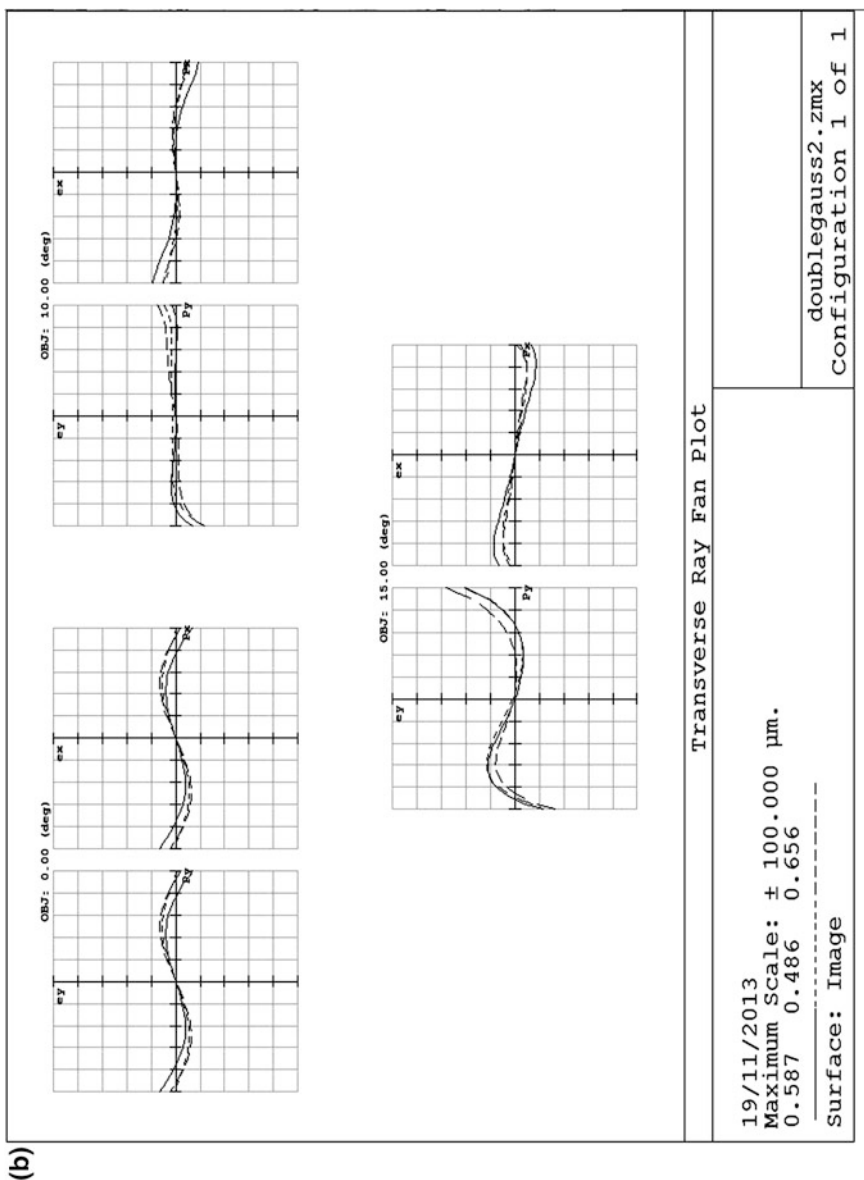


Fig. 6.54 (continued)

Surface data summary

Surf	Radius	Thickness	Glass	Diameter
OBJ	Infinity	Infinity		
1	48.66467	2	LAK 33	37.03454
2	78.75136	0		36.7017
3	35.05049	5.447	LAK 33	34.75705
4	39.69197	5.447	N-SF 4	31.0117
5	25.96831	10.00034		25.67176
OBJ	Infinity	10.00034		20
7	-27.879	5.447	N-SF 4	24.19968
8	-69.62807	5.447	LAK 33	29.27356
9	-33.9342	0		31.63001
10	184.1517	2	LAK 33	34.29148
11	-147.7727	83.48		34.33652
IMA	Infinity			52.9391

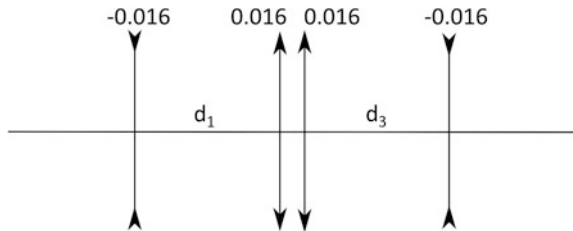
6.5.5 Exercise 18, Matsui's Double Gauss

In the book of Matsui and Nariai [15] we find (p. 20) the following prescription of a Double Gauss objective designed by Matsui (Nikon) himself. The glasses in this design are not available in the Schott catalogue and are not included in our glass list in [Sect. 5.1](#).

#	Radius	Distance	Glass	
			n_d	V
1	70.819	7.60	1.66608	40.0
2	277.443	0.30	Air	
3	35.975	8.997	1.67732	55.8
4	78.458	2.8	Air	
5	87.426	3.0	1.70570	29.8
6	25.561	21.622	Air	
7	-27.840	2.0	1.56535	43.1
8	253.485	7.696	1.67660	55.5
9	-41.076	0.3	Air	
10	-550.037	6.40	1.67660	55.5
11	-57.233		Air	

These data result in a focal length (EFL) of 100 mm. The book does not give a pupil radius or a field angle; also the stop position is not given.

Fig. 6.55 Lay-out for wide-angle SQ



This exercise contains the following assignments

- With the stop 10 mm behind surface 6, $h_1 = 14$, $\tan w = 0.45$, calculate the Seidel coefficients of this design and the chromatic aberration coefficients.
- Using the stop shift equations (Sect. 2.4) determine the value of Δq for which the coma coefficient is zero. Calculate the new stop position.
- Find also Δq for zero distortion.
- With the stop position from (b), optimize the design for $F\# = 2.8$, by bending all lenses.

6.5.6 The Symmetric Wide-Angle Quadruplet

Of this type of four-component symmetric objective, that has negative outer components, there are many different realizations. See Glatzel [23] or Kross [10].

Like the reversed tele-objective, the wide-angle SQ can be designed for field angles of up to 60° .

The symmetry helps to hold distortion in check.

We begin our study of this type of lenses with a lay-out given by Glatzel (see Fig. 5.7). The data of this lay-out are $K_1 = -0.0160$, $K_2 = K_3 = 0.0160$, $K_4 = -0.0160$, $d_1 = d_3 = 15.625$ mm.

The distance d_2 between the positive lenses is at the moment undetermined. We begin taking $d_2 = 0$, as in Glatzel's lay-out.

When we use this system at magnification $M = -1$, we will have $S_2 = S_5 = C_2 = 0$. With identical indices for all lenses we will have also a flat field, $S_4 = 0$, because the power sum is zero.

Thin Lens Design of the Wide-Angle SQ

With the lay-out of Fig. 6.55 we obtain $G_1 = -1$, $G_2 = 0.6$, $G_3 = -1.4$, $G_4 = 2.429$.

With $h_1 = 8$ we have $h_2 = 10 = h_3$, $h_4 = 7$.

With $\bar{h}_1 = -6.25$ and $\bar{u}_1 = 0.5$ we have $\bar{h}_2 = \bar{h}_3 = 0$, $\bar{h}_4 = 6.25$ and $H = 4$.

Now $q_1 = -0.781$, $q_2 = q_3 = 0$, $q_4 = 0.893$.

The component aberration equations become

$$\begin{aligned} S_{11} &= -0.0220 B_1^2 + 0.0414 B_1 - 0.0447 \\ S_{12} &= 0.0537 B_2^2 + 0.0607 B_2 + 0.0815 \\ S_{13} &= 0.0537 B_3^2 - 0.1416 B_3 + 0.1504 \\ S_{14} &= -0.0128 B_4^2 - 0.0590 B_4 - 0.0769 \\ S_{21} &= 0.0809 B_1 - 0.0855 \\ S_{22} &= 0.1265 B_1 + 0.0803 \\ S_{23} &= 0.1265 B_1 - 0.1869 \\ S_{24} &= 0.0619 B_1 + 0.1591 \end{aligned}$$

With a symmetric design we have $B_2 = -B_3$ and $B_4 = -B_1$, and

$$\begin{aligned} S_1 &= 0.1074 B_2^2 + 0.2023 B_2 + 0.2319 - 0.0348 B_1^2 + 0.1004 B_1 - 0.1216 \\ S_2 &= 0.0058 B_1^2 + 0.0394 B_1 - 0.0668 \\ S_3 &= -0.0237 B_1^2 - 0.1644 B_1 + 0.3289 \end{aligned}$$

We have not enough degrees of freedom to correct these three aberrations. $S_4 = 0$ because of the lay-out, and we can expect that distortion will be moderate because of the symmetry of the design.

With $B_2 = -0.941$, $S_{12} + S_{13}$ has a minimum value of 0.1308 and we obtain

$$S_1 = -0.0348 B_1^2 + 0.1004 B_1 + 0.0092$$

Solutions for $S_1 = 0$ are $B_1 = 2.974$ or $B_1 = -0.089$.

Solutions for $S_3 = 0$ are $B_1 = 1.62$ or $B_1 = -8.56$.

With $B_1 = 1.8$ we have $S_1 = 0.0772$, $S_2 = 0.0229$, $S_3 = -0.0438$.

A sketch of this design is given in Fig. 6.56. It does not look quite right!

We would like to have lenses that are curved toward the stop, so that the ideal of a concentric system is approached.

With this design spherical and astigmatism, both “even” aberrations, are difficult to correct simultaneously. Therefore we will construct a different lay-out.

From the paper of Glatzel [23] we see that we can do two things to improve the design: we can move the inner lenses away from the stop, and we can use thick lenses. In the following we will explore both strategies.

Wide-Angle Lens, New Lay-out II

The new lay-out is shown in Fig. 6.57. The component powers are $K_1 = -0.015 = K_4$, $K_2 = 0.015 = K_3$; the distances are $d_1 = 22.222$, $d_2 = 44.444$, $d_3 = 22.222$.

The stop is in the middle between lens 2 and 3. With this lay-out the EFL is 81.96 mm and the back focal length 51.542 mm.

The q-factors have the values $q_1 = -2.469$, $q_2 = -1.111$, $q_4 = 1.332$, $q_5 = 3.921$.

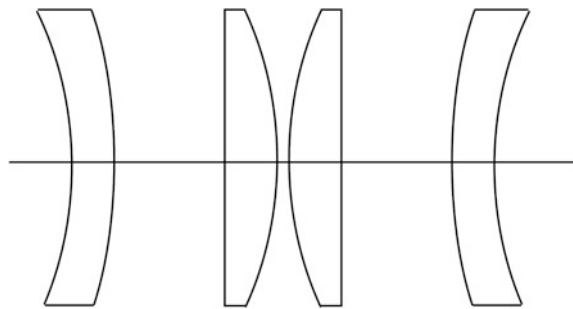


Fig. 6.56 A first design of a symmetric wide-angle lens

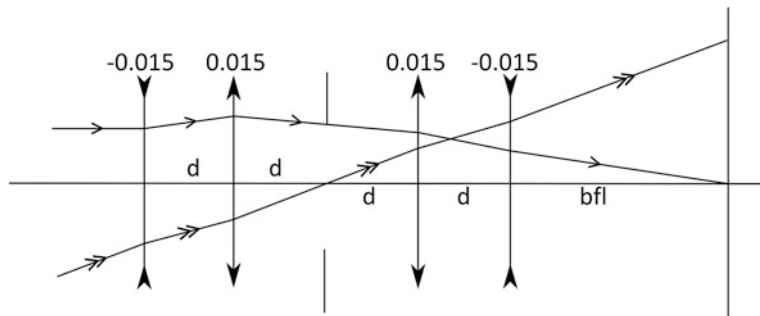


Fig. 6.57 Layout of wide angle lens II, $d = 22.222$, $bfl = 51.542$

With $h_1 = 6$ and $\tan w = 0.4888$ the invariant is $H = -2.933$, $h_2 = 8$, $h_3 = 6.666$, $h_4 = 3.778$.

Thin Lens Design II

From the lay-out, the position factors are given by $G_1 = -1$, $G_2 = 0.5$, $G_4 = -1.6$, $G_5 = 3.586$.

With $n = 1.65$ for all lenses, we have the component aberrations:

$$\begin{aligned} S_{11} &= -0.00109 \{5.24 B_1^2 - 9.88 B_1 + 10.65\} \\ S_{12} &= 0.00346 \{5.24 B_2^2 + 4.94 B_2 + 7.49\} \\ S_{13} &= 0.00166 \{5.24 B_3^2 - 15.81 B_3 + 17.22\} \\ S_{14} &= -0.000172 \{5.24 B_4^2 + 35.43 B_4 + 60.58\} \\ S_{21} &= 0.0118(2.47 B_1 - 2.61) \\ S_{22} &= 0.0215(2.47 B_2 + 1.31) \\ S_{23} &= 0.0146(2.47 B_3 - 4.176) \\ S_{24} &= 0.0047(2.47 B_4 + 9.359). \end{aligned}$$

With $B_1 = -1.5$, $B_2 = +1$, $B_3 = -1$, $B_4 = 1.5$ we obtain

$$S_1 = 0.0625, S_2 = 0.0037, S_3 = 0.0207, S_4 = 0.$$

In order to diminish S_1 , without changing S_3 too much, we bend the outer lenses somewhat more and increase the refractive index of the inner lenses to 1.7.

With $B_1 = -2$, $B_2 = -1$, $B_3 = -1$, $B_4 = 2$ we obtain

$$S_1 = 0.0318, S_2 = -0.0197, S_3 = 0.0287, S_4 = -0.0092, S_5 = 0.0111.$$

Surface Model II

The prescription of the surface model becomes

	#	Radius	Distance	Glass	Diameter
STO	1	84.829	3.915	KZFS 5	44
	2	28.275	21.005	Air	40
	3	46.667	4.500	N-LAK 14	33
	4	Plane	18.433	Air	30
	5	Plane	18.433	Air	15
	6	Plane	4.500	N-LAK 14	30
	7	-46.667	21.005	Air	30
	8	-28.275	3.915	KZFS 5	36
	9	-84.829	62.705	Air	40

with $EFL = 95.192$ mm, $\tan w = 0.4817$, field radius $\bar{h}_{10} = 45.835$ mm.

The glass data are:

NLAK 14, $n = 1.69680$, $V = 55.41$,

KZFS 5, $n = 1.65412$, $V = 39.70$.

The results of the paraxial calculations are shown below.

Wide-angle lens II, paraxial calculations

	#	nu	h	n <u>h̄</u>	<u>h̄</u>	A	<u>A</u>	hΔ
STO	1	0	6	0.4817	-15.630	0.0707	0.2974	-0.1015
	2	-0.0463	5.889	0.6023	-14.191	0.2982	-0.2279	0.6290
	3	0.0899	7.779	0.2741	-8.434	0.2566	0.0933	-0.7701
	4	-0.0262	7.709	0.4	-7.373	-0.0262	0.4	-0.1319
	5	-0.0262	7.226	0.4	0	-0.0262	0.4	0
	6	-0.0262	6.743	0.4	7.373	-0.0262	0.4	0.1153
	7	-0.0262	6.674	0.4	8.434	-0.2689	0.0933	-0.7788
	8	-0.1258	4.030	0.2741	14.191	-0.2683	-0.2277	0.4590
	9	-0.0326	3.952	0.6023	15.630	-0.1096	0.2975	-0.2021
IMA	10	-0.0630	0	0.4817	45.835	-0.0630	0.4817	-

#	S ₁	S ₂	S ₃	S ₄	S ₅	C ₁	C ₂
STO	1	0.0005	0.0021	0.0089	0.0389	0.2011	0.00427
	2	-0.0559	0.0427	-0.0327	-0.1169	0.1143	-0.01768
	3	0.0507	0.0184	0.0067	0.0735	0.0292	0.01489
	4	0.0001	-0.0013	0.0211	0	-0.3221	0.00151
	5	0	0	0	0	0	0
	6	-0.0001	0.0012	-0.0184	0	0.2809	-0.00132
	7	0.0563	-0.0195	0.0068	0.0735	-0.0279	0.01338
	8	-0.0330	-0.0280	-0.0237	-0.1169	-0.1193	-0.01089
	9	0.0024	-0.0066	0.0178	0.0389	-0.1539	0.00436
Σ		0.0210	0.0079	-0.0135	-0.0090	0.0033	0.00852
							0.00914

The aberration coefficients of this design are:

$$S_1 = 0.0210, S_2 = 0.0079, S_3 = -0.0135, S_4 = -0.0090, S_5 = 0.0033, \\ C_1 = 0.0085, C_2 = 0.0091.$$

We can correct the chromatic aberrations better by introducing one or two achromatizing doublets. For a thin doublet the chromatic aberrations are given by:

$$C_1 = \frac{h^2 K_a}{V_a} + \frac{h^2 K_b}{V_b}, \\ C_2 = \frac{h \bar{h} K_a}{V_a} + \frac{h \bar{h} K_b}{V_b}.$$

In this case we have to correct roughly equal amounts of LCA and TCA. That means that we must look for a position where h and \bar{h} are about equal; this is the case with the third lens. When we take the glasses N-LAK 14 and N-SF 15 with the data

$$\text{N-LAK 14: } n = 1.69680, V = 55.41$$

$$\text{N-SF 15: } n = 1.69892, V = 30.20$$

we can correct LCA without changing the monochromatic aberration coefficients.

We have

$$K_a + K_b = 0.01493$$

and, with $h = 7.779$, and crown in front

$$1.092 K_a + 2.003 K_b = -0.0085.$$

The solution is $K_a = 0.0423$, $K_b = -0.0273$. We make the first surface of our doublet plane, as before, and obtain for the second and third surface the radii

$$r_2 = -16.512, \\ r_3 = -46.453.$$

A sketch of this doublet is given in Fig. 6.58a.

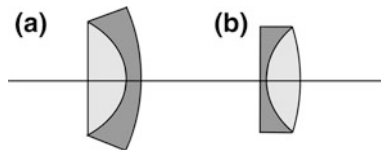


Fig. 6.58 Achromatizing doublets for the wide-angle lens II. **a** Crown-in front. **b** Flint-in-front.
Scale 1:1

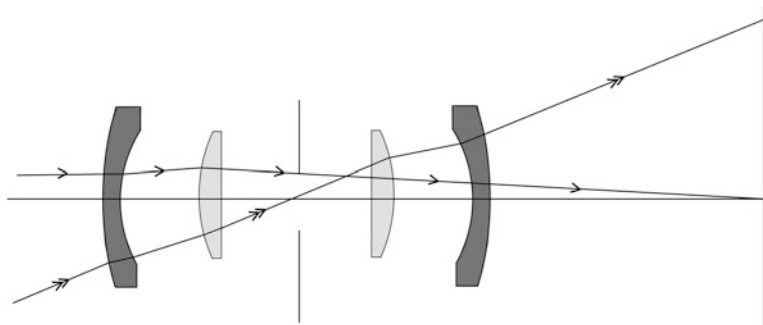


Fig. 6.59 Wide-angle lens II

Instead of the crown-in-front solution we can also find a flint-in-front one with the radii

$$\begin{aligned} r_2 &= 25.735, \\ r_3 &= -46.453. \end{aligned}$$

See Fig. 6.58b.

In Figs. 6.59 and 6.60 we show our design and a comparable lens, Bertele's Angulon.

The description of the Angulon can be found in Smith [18, p. 573], it shows a delicate interplay of glass choices and thicknesses, combined with the introduction of asymmetry.

We will optimize our design, using bendings, thicknesses and asymmetries as variables.

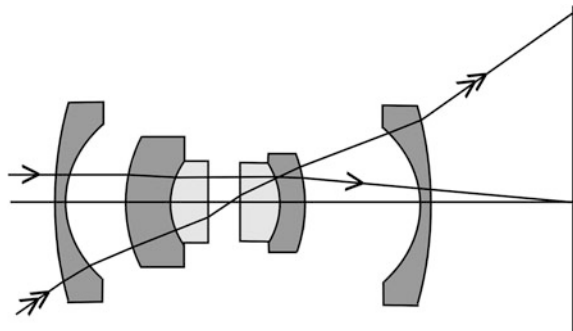
Optimization of the Wide-Angle Lens

This lens has parameters $\text{EFL} = 100$, F/7.25 and a modest field angle of 15° .

We optimized the start system with radii, glass thicknesses and air distances as variables.

The resulting lay-out is shown in Fig. 6.61a. From the ray fan plots in Fig. 6.61b it is seen that colour correction still can be improved. The r.m.s. spot sizes are below $8 \mu\text{m}$. The field curvature is balanced by TOBSA, as with the Double Gauss.

Fig. 6.60 Angulon, after Smith [18]



The resulting design, that has much thicker inner lenses than the starting design, is related to the Angulon (Fig. 6.60).

Its prescription is given in the table below.

Surface data summary

Surf	Radius	Thickness	Glass	Diameter
OBJ	Infinity	Infinity		
1	51.62237	3.915	N-KZFS 5	30.96142
2	27.43952	19.53856		27.9004
3	46.63675	3.124607	SF 15	24.38961
4	58.47854	10.29781	LAKN 14	23.46916
5	183.7281	10.68841		20.2623
STO	Infinity	4.809082		15
7	599.5928	9.451029	LAKN 14	16.87058
8	-25.02741	11.89139	SF1 5	18.72906
9	-49.5598	20.99521		21.79261
10	-27.40122	3.915	N-KZFS 5	23.83668
11	-61.0432	62.705		26.0998
IMA	Infinity			53.62433

6.5.7 The Hologon

We study the effects of thickening by paraxial analysis of the Hologon, a design of Glatzel [23]. A picture of this design is given in Fig. 6.62. The prescription is as follows

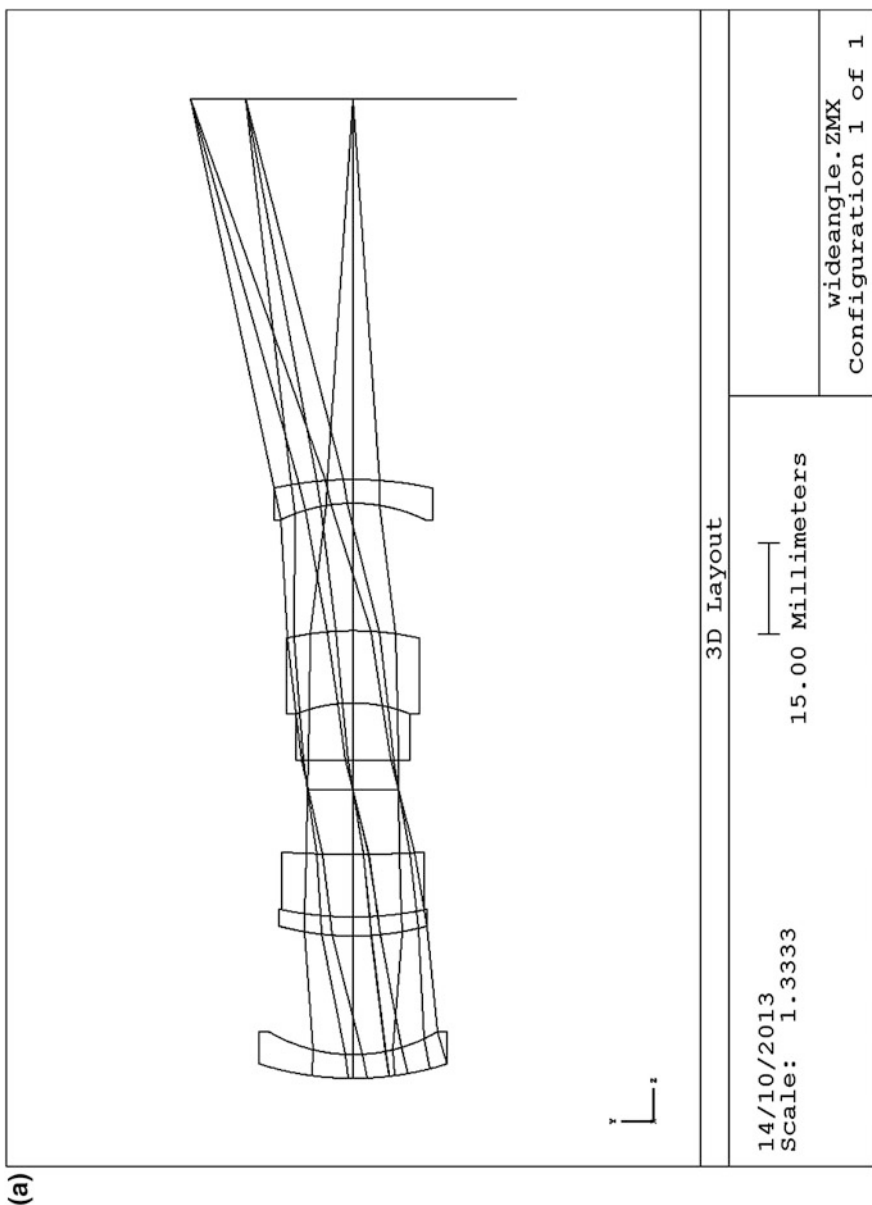


Fig. 6.61 a Wide-angle lens, lay-out. b Wide-angle lens, aberrations

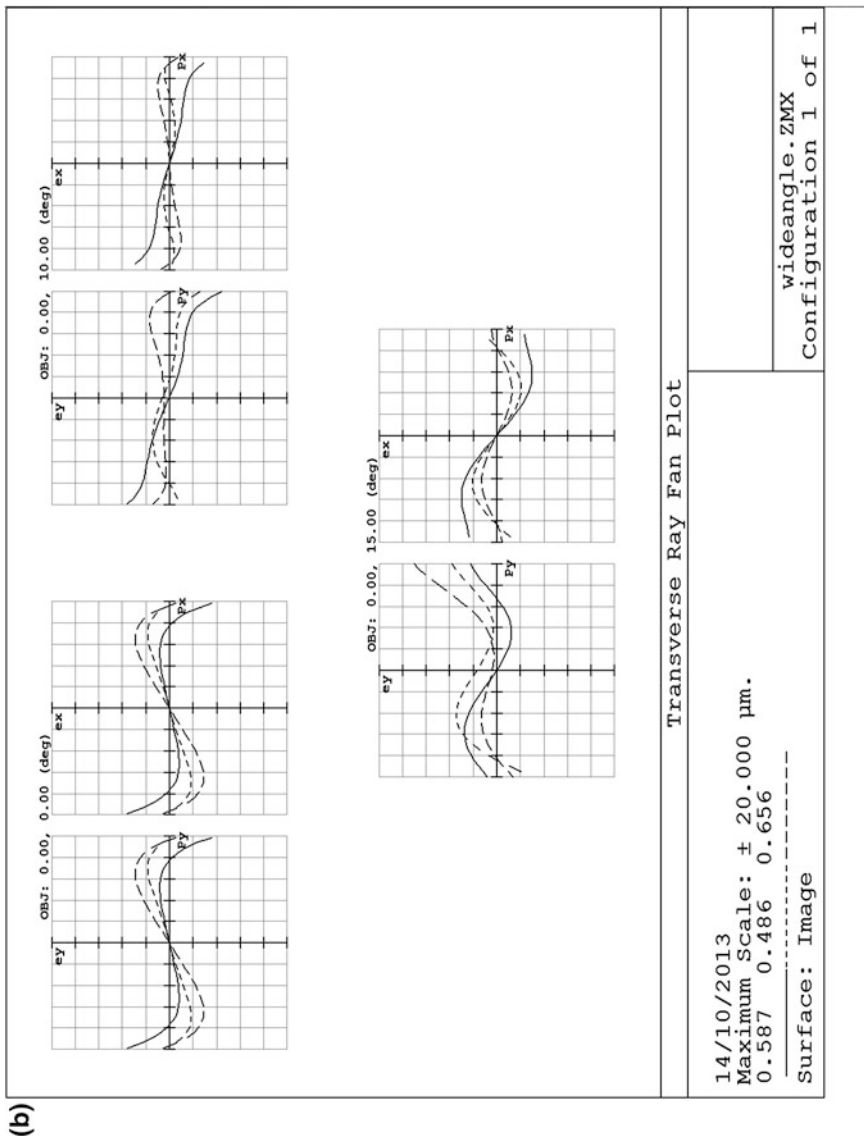


Fig. 6.61 (continued)

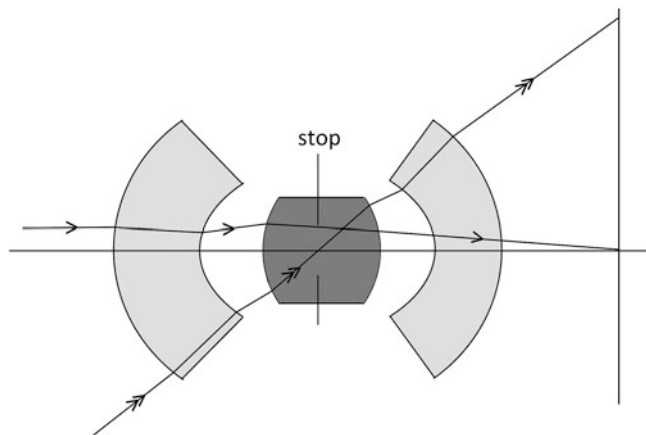


Fig. 6.62 Glatzel's Hologon, $f = 100$, scale 1:1

#	Radius	Distance	Glass	Semidiameter
1	47.41	26.42	SF 4	45.3
2	20.98	18.63	Air	21.0
3	29.72	17.20	N-BK 7	17.7
STO	-	18.23	N-BK 7	5.67
4	-28.38	15.41	Air	17.7
5	-19.78	21.13	SF 4	19.7
6	-42.52	51.27	Air	39.1

Focal length $f' = 100$ mm, aperture angle 0.0625 rad, $\tan w = 0.49$, invariant $H = -2.847$.

We show the results of the paraxial calculations below.

Paraxial results of the Hologon

#	n_u	h	$n\bar{u}$	\bar{h}	A	\bar{A}	$h\Delta$
1	0	6.250	0.4911	-28.366	0.1318	-0.1072	-0.2038
2	-0.0996	4.751	0.9429	-14.174	0.2446	-0.2429	0.4931
3	0.0715	6.083	0.4327	-6.112	0.2762	0.2270	-0.5254
4 STO	-0.0343	5.493	0.5390	0	-0.0343	0.5390	0
5	-0.0343	5.282	0.5390	6.478	-0.3166	0.1927	-0.6104
6	-0.1305	3.271	0.4210	12.966	-0.2959	-0.2345	0.4208
7	-0.0056	3.204	0.9160	23.994	-0.1378	-0.0746	-0.1944

#	S ₁	S ₂	S ₃	S ₄	S ₅	C ₁	C ₂
1	0.0325	-0.0029	0.0023	0.0736	-0.0617	0.0125	-0.0106
2	-0.0295	0.0293	-0.0268	-0.1662	0.1916	-0.0184	0.0182
3	0.0400	0.0329	0.0270	0.0929	0.0985	0.0089	0.0073
4 STO	0	0	0	0	0	0	0
5	0.0611	-0.0372	0.0227	0.0973	-0.0730	0.0089	-0.0054
6	-0.0368	-0.0291	-0.0231	-0.1762	-0.1579	-0.0177	-0.0121
7	0.0037	0.0020	0.0025	0.0820	0.0449	0.0070	0.0038
Σ	0.0420	-0.0050	0.0034	0.0034	0.0424	0.0012	0.0012

In comparison to our wide angle lens II the Hologon has much thicker lenses.

The outer lenses have negative power and near-concentric surfaces. The concentric form helps to correct higher order field dependent spherical aberration, whereas the higher thickness makes the inner surfaces stronger so that their contribution to spherical and field curvature is better matched to that of the inner lenses.

The thickness of the inner lenses helps to correct astigmatism, because the surfaces are further from the stop.

The colour correction of the Hologon is very good; there is a balance between the two halves for LCA and enough symmetry for TCA.

6.6 Microscope Objectives

With a microscope objective high resolution is pursued in a small field. When we assume that the image field has a diameter of 20 mm, the object field of a 20× objective has a diameter of 1 mm.

An objective with magnification $M = 5$ can be designed as an achromatic doublet. With an image distance of 200 mm its focal length will be 33.3 mm. We discussed achromatic doublets in Sect. 6.1 so that it is not necessary to repeat the design here. Note that the field diameter is 4 mm in this case, so that the field angle is about 3° which is suitable for an achromatic doublet. With a pupil diameter of 8 mm the axial resolution is of order of 5 μm. At the edge of the field we will be limited in resolution by astigmatism; the transverse aberration is of the order of 25 μm.

Objectives with magnification $M = 10$ are usually composed of two achromatic doublets. The amateur optician J. J. Lister (1786–1869), a well-to-do wine merchant, achieved an improvement of the resolution of this type of objectives. He noted that an achromatic doublet has two object positions for which spherical aberration is corrected. It is possible to arrange two doublets in such a way that not only spherical is minimized, but also coma is corrected so that an aplanatic objective results [24, p. 408].

The Italian astronomer G. B. Amici (1786–1863) further improved the microscope objective by adding aplanatic lenses to the Lister objective. In this way magnifications up to $40\times$ can be obtained, at numerical apertures of 0.68. The numerical aperture can be further enlarged by immersion; this is also an invention of Amici [24].

Modern developments in the field of objective design are connected with chromatic correction and image field flattening. The step from achromatic correction to apochromatic correction can be made by the introduction of new materials, such as fluorite (CAF_2) and fluorite crown (FK) glasses. Field flattening can be obtained by the use of negative components, as in a telephoto objective. The development of flat field microscope objectives was incited by the use of solid state image sensors (CCD's). From the design of the Zeiss S-Planar objective its designer Glatzel proceeded to optolithographic projection lenses, that are used in the production of solid-state electronic circuits [25]. With such a “stepper lens” diffraction limited imaging is possible at a wavelength of $248\text{ }\mu\text{m}$ and a numerical aperture of 0.7 over a field of 30 mm diameter. This leads to a resolution of about $0.2\text{ }\mu\text{m}$ [26].

In this section we will treat the design of Lister and Amici objectives, with magnifications of $10\times$ and $40\times$. The design of an apochromatic $40\times$ objective using fluor-crown doublets is given as an exercise.

Designing a flat-field $40\times$ objective will be the next subject. It will be seen that the design strategies that we used up to now in this course must be stretched to the limit to obtain a useful result. This is still more so with the design of stepper lenses; in that case we would have to extend the scope of our course by far.

6.6.1 The Lister Type

We start from the lay-out of a two-component system given in Sect. 5.2. We design the objective with the long conjugate on the left side.

With magnification $M = 0.1$ and tube length $t = 170$ we have a free working distance $t' = 9.35$. With this lay-out we have the stop at the first lens and telecentricity on the image side. When the deviation of the marginal ray is equal at both components we find $K_1 = 0.03235$, $d_1 = 17$, $K_2 = K = 0.05882$, $f' = 17$. The optical throw, this is the distance between object and image plane, is 196.35 mm. We show the lay-out in Fig. 6.63.

As a field angle we take $\bar{u}_1 = 0.05882$; the aperture angle chosen was $u_1 = 0.02$. This gives a value of the invariant $H = -0.2$.

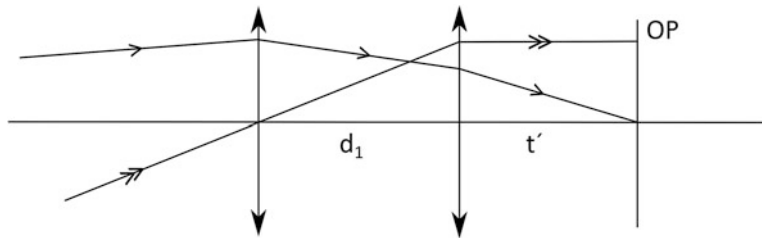


Fig. 6.63 Lay-out of the Lister objective

Thin Lens Design

We choose the glasses

N-SK 5, $n = 1.59142$, $V = 61.0$

F 5, $n = 1.60718$, $V = 37.2$

With crown-in-front doublet components, we obtain

$$K_{1a} = 0.08506, \quad K_{1b} = -0.05271, \quad h_1 = 3.4$$

$$K_{2b} = 0.15466, \quad K_{2b} = -0.09584, \quad h_2 = 1.87.$$

From the aberration equations for two-component systems (with $q_1 = 0$, stop at the first component) given in Sect. 6.3 we obtain the following equations that express the coefficients of spherical and coma (at the stop) for the components in terms of the lay-out data:

$$S_{22} = \frac{1}{q_2^2} \bar{S}_5 - \frac{1}{q_2} (\bar{S}_3 - S_{31} + 2S_{32} + S_{42}),$$

$$S_{12} = -S_{11} = -\frac{1}{q_2^3} \bar{S}_5 + \frac{1}{q_2^2} (3\bar{S}_3 - 3S_{31} + 3S_{32} + 2S_{42}),$$

$$S_{21} = -\frac{1}{q_2} (2\bar{S}_3 - 2S_{31} + S_{32} + S_{42}),$$

where \bar{S}_3 and \bar{S}_5 are the targets for the system astigmatism and distortion, respectively (see also Hopkins and Rao [11]).

With

$$H = -0.2, \quad K_1 = 0.03235, \quad K_2 = 0.05882$$

we have

$$S_{31} = H^2 K_1 = 0.001294, \quad S_{32} = 0.002353, \quad S_{42} = 0.001470.$$

With $q_2 = 0.8565$ and the targets $\bar{S}_3 = S_{31} - S_{32} = -0.001059$, $\bar{S}_5 = 0$ we now find

$$S_{22} = -0.004464, \quad S_{21} = -0.001031, \quad S_{12} = -S_{11} = 0.004008.$$

Using the thin lens aberration expressions from Sect. 4.3 we find the following solutions for the component form factors

$$B_{1a} = -0.4543, B_{1b} = 1.4287 \text{ or } B_{1a} = 1.7429, B_{1b} = 4.4675$$

$$B_{2a} = 0.1340, B_{2b} = 0.4437 \text{ or } B_{2a} = 2.242, B_{2b} = -5.214.$$

There are four solutions for the system; Kingslake [5, p. 181] also finds four solutions from an ingenious graphical method originated by Conrady [27, p. 662].

We adopt the solution with the smallest values of the form factors. The thin lens model now becomes

	#	Radius	Distance	Glass	Diameter
STO	1	25.483	0	N-SK 5	7
	2	-9.562	0	Air	
	3	-9.486	0	F 5	
	4	-53.740	17	Air	
	5	6.744	0	N-SK 5	6
	6	-8.831	0	Air	
	7	-8.877	0	F 5	
	8	22.776	9.35	Air	
IM	9	Plane	-	-	2

We construct a surface model, using the procedure outlined in Sect. 4.4 and described in detail in Sect. 6.2 and obtain the following prescription

#	Radius	Distance	Glass	Diameter
1	25.090	1.969	N-SK 5	7
2	-9.415	0	Air	7
3	-9.340	1.476	F 5	7
4	-52.911	16.649	Air	7
5	7.446	2.761	N-SK 5	6
6	-9.751	0	Air	6
7	-9.692	1.656	F 5	6
8	25.150	5.669	Air	6
9	Plane	-	-	2

We give the results of the paraxial calculations and the Seidel coefficients of this system in the following tables.

	#	h	n u	\bar{h}	$n \bar{u}$	A	\bar{A}	$h\Delta$
STO	1	3.400	0.0200	0	0.06	0.1555	0.06	-0.1965
	2	3.326	-0.0601	0.0743	0.06	-0.6222	0.0474	-0.7690
	3	3.326	-0.2691	0.0743	0.0553	-0.6251	0.0453	0.7854
	4	3.277	-0.0529	0.1295	0.0601	-0.1524	0.0562	-0.1887
	5	1.771	-0.0905	1.1054	0.0586	0.1473	0.2071	-0.0006
	6	1.371	-0.2306	1.0547	-0.0292	-0.4543	-0.2013	-0.3052
	7	1.371	-0.3138	1.0547	-0.0932	-0.4552	-0.2013	0.3091
	8	1.136	-0.2279	1.0267	-0.0271	-0.1553	-0.0385	-0.1275
IM	9	0	-0.2004	1.0129	-0.0023	-	-	

#	S ₁	S ₂	S ₃	S ₄	S ₅	C ₁	C ₂
1	0.00475	0.00183	0.00070	0.00059	0.00050	0.00322	0.00124
2	0.2977	-0.02268	0.00173	0.00158	-0.00025	0.01260	-0.00096
3	-0.3068	0.02322	-0.00175	-0.00161	0.00023	-0.02077	0.00150
4	0.00438	-0.00162	0.00060	0.00029	-0.00032	0.00499	-0.00183
5	0.00001	0.00002	0.00003	0.00200	0.00285	0.00158	0.00223
6	0.06299	0.02791	0.01237	0.00152	0.00615	0.00379	0.00168
7	-0.06405	-0.02842	-0.01261	-0.00155	-0.00628	-0.00623	-0.00276
8	0.00307	-0.00076	0.00018	-0.00060	0.00010	0.00176	-0.00044
I	0.00030	-0.00023	0.00142	0.00085	0.00016	0.00004	-0.00005
II	0.00202	-0.00125	-0.00003	0.00137	0.00282	0.00090	0.00071
Σ	0.00232	-0.00050	0.00126	0.00222	0.00298	0.00094	0.00066

The Airy radius for this design is 3.58 μm . The aberrations of our surface model are of the same order of magnitude. We will see in how far optimization can improve this result.

The design has an unfavorable property, however. From the paraxial ray data it is seen that the back focal length, given by $h_8/-u_9$, is equal to 5.67 mm. This is sufficient as a free working distance for a 10 \times objective, but it does not provide enough space for the introduction of more than one aplanatic lens. Therefore we can obtain a magnification of 25 \times , as we will see, but 40 \times is out of reach.

The first surface of an aplanatic lens for this design will have an object distance s_9 , smaller than the back focal length given above, of $s_9 = 5.5$ mm. Its radius is given by

$$r_9 = s_9 / (1 + n),$$

with an index of 1.6 we have $r_9 = 2.115$ mm. This gives a magnification $M = 25.6$ at a numerical aperture NA = 0.51.

Optimization of the 10× Microscope Objective

This system has an EFL of 20.6 mm, an object space NA of 0.15 and an object field diameter of 2 mm.

The Airy radius for $\lambda = 0.587 \mu\text{m}$ is given by $r_a = 2.39 \mu\text{m}$. The lay-out is given in Fig. 6.64a.

From the ray fan plots, given in Fig. 6.64b it is seen that the aberrations stay inside the Airy radius in the center of the field. Only for the blue wavelength the aberrations exceed the Airy radius at the edge of the field.

The optimization only concerned the surface radii in order to keep the paraxial lay-out intact.

Its prescription is given in the table below.

Surface data summary

Surf	Radius	Thickness	Glass	Diameter
OBJ	Infinity	170		20
STO	12.24537	1.969	SK 5	7
2	-12.47089	0.2		6.965594
3	-11.51953	1.476	F 5	6.86506
4	52.41402	16.649		5.8
5	7.483203	2.761	SK 5	5.210541
6	-28.66499	0.2		4.494752
7	-13.13166	1.656	F 5	4.431675
8	15.54435	5.669		3.953656
IMA	Infinity			2.662777

6.6.2 A 40× Apochromatic Objective

Avoiding problems with a too small back focal length, we begin this design with what is called a duplex front. This consists of two aplanatic lenses in tandem (see Sect. 4.1). The first of these lenses has an aplanatic front surface and a concentric back surface. The radius of the first surface is given by

$$r_1(1 + n_2) = s_1,$$

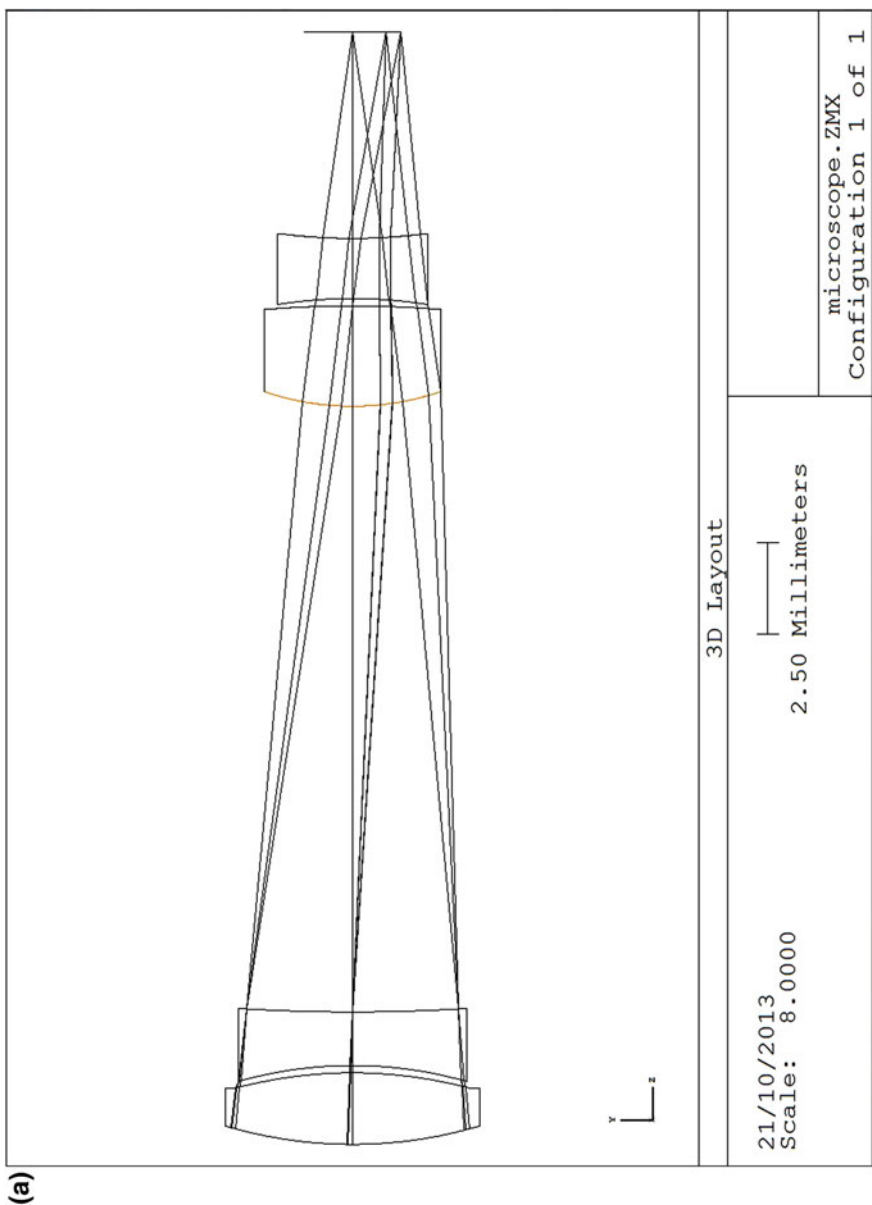
where s_1 is the object distance. From the previous design we learned that the free working distance of the first part of the objective determines the value of s_1 .

We assume here $s_1 = 12 \text{ mm}$; with $n_2 = 1.6$ we have $r_1 = 4.615 \text{ mm}$. For the image distance follows

$$s_1' = r_1(1 + 1/n_2),$$

so that $s_1' = 7.500 \text{ mm}$.

Taking $d_1 = 1.5$, not too small because this reduces field curvature, we have $r_2 = 6.000 \text{ mm}$.



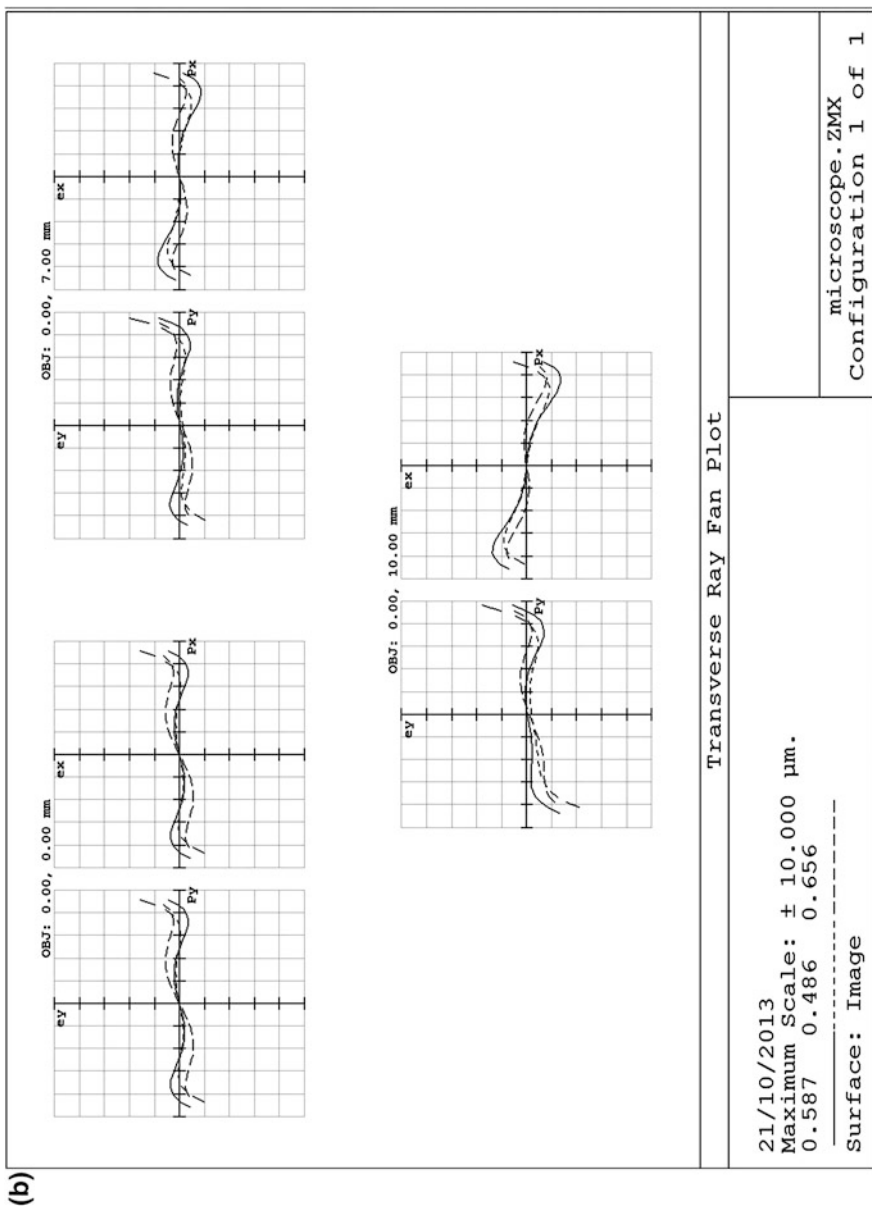


Fig. 6.64 (continued)

With $d_2 = 0.5$ the next aplanatic surface has abject distance $s_3 = r_2 - d_2 = 5.500$ mm. With

$$r_3(1 + n_4) = s_3$$

as in (1) and $n_4 = 1.6$ again, the radius becomes $r_3 = 2.115$ mm. The thickness of this aplanat must be

$$d_3 = r_3(1 + 1/n_4)$$

so that $d_3 = 3.437$ mm. The next surface is the object plane, $h_4 = 0$. We design the objective from the image plane, therefore also the duplex front has the object plane in its last surface.

With a numerical aperture of the duplex front of $n_4 u_4 = 0.72$ and a magnification of $(1.6)^3 \approx 4$ we must have an entrance height $h_1 = -s_1/u_1 = 2.16$ mm. With these data we find the lay-out of the rest of the objective. The construction parameters of the duplex front are as follows.

	#	Radius	Distance	Glass	Diameter
	1	4.615	1.5	N-SK 14	5
	2	6.000	0.5	Air	5
	3	2.115	3.437	N-SK 14	4.23
OBJ	4	Plane	—	Air	0.5

With one lens to converge the rays from the duplex front at a distance of 3 mm the ray height of the chief ray becomes $h = h_1 + u_1 d = 2.16 + 0.54 = 2.70$. With $u = 0.018$, $u' = -0.18$ we find $K = 0.073333$ and $s = -150$ for this lens.

In order to conform to a standard tube length of 180 mm we have to scale up the dimensions of the lay-out by a factor $p = 180/150 = 1.2$.

For the duplex front this gives the parameters

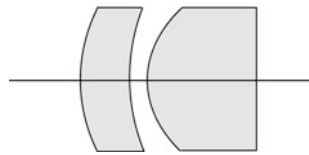
#	Radius	Distance	Diameter
1	5.538	1.8	6
2	7.200	0.6	6
3	2.538	4.124	5.076

and the entrance height 2.592. See Fig. 6.65.

For the convergence lens we have $h = 3.24$, $d = 3.6$ and $s = -180$, $K = 0.061111$, $f' = 16.364$.

For a simple doublet the ratio $F = f'/2 h = 2.525$ is quite low, therefore we will take two doublets in tandem. A triplet could be used also, as in the paper of Sharma [28].

With two cemented doublets we have two degrees of freedom for the correction of spherical and coma. Because we want to design an apochromatic objective we choose the glasses N-FK 51A and N-KzFS 2, recommended in Sect. 5.1.

Fig. 6.65 Duplex front

The field angle is $\tan w = -10/180 = -0.0555$, this gives $H = 0.18$ for the invariant.

We will take the stop at the first doublet on the long conjugate side.

Thin Lens Design of the 40× Apochromat

The familiar procedure is followed, of which we give here an outline.

The component powers of the doublets are calculated, the component aberration equations are set-up, using the position factors (G-factors) calculated from the layout data.

The position factors B_{1b} and B_{2b} are eliminated using the cementing condition [see (6.1) of Sect. 6.1 (doublets)]. S_{11} and S_{12} are expressed as functions of B_{1a} and B_{2a} .

Using the coma condition $S_2 = S_{21} + S_{22} = 0$ gives a linear relation between B_{1a} and B_{2a} , by which B_{2a} is eliminated so that $S_1 = S_{11} + S_{12}$ becomes a function of B_{1a} only.

Setting $S_1 = 0$ (or another convenient value) leads to two solutions for B_{1a} .

Finally B_{2a} is calculated from the coma condition and B_{1b} , B_{2b} from the cementing conditions.

The following two solutions, cemented doublets with $S_1 = 0$ and $S_2 = 0$, were found:

- (1) $B_{1a} = 0.1140$, $B_{1b} = -0.5933$, $B_{2a} = -0.3652$, $B_{2b} = 2.0486$
- (2) $B_{1a} = -0.7702$, $B_{1b} = 2.1835$, $B_{2a} = 0.5190$, $B_{2b} = -0.1350$

The radii of these solutions are:

$$(1) \quad \begin{array}{ll} r_1 = 10.309 & r_4 = 18.092 \\ r_2 = -12.920 & r_5 = -8.391 \\ r_3 = 50.452 & r_6 = -45.446 \end{array}$$

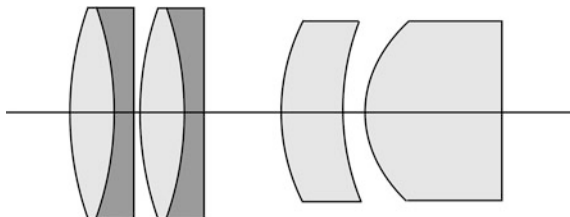
$$(2) \quad \begin{array}{ll} r_1 = 49.976 & r_4 = 7.561 \\ r_2 = -6.466 & r_5 = -23.798 \\ r_3 = -16.336 & r_6 = 18.078 \end{array}$$

Both solutions have strongly curved inner surfaces. We prefer the first solution because it has the smaller curvatures.

We have set up a predesign that is totally aplanatic ($S_1 = 0$, $S_2 = 0$). The rest aberrations are

$$S_3 = 0.00279, \quad S_4 = 0.00637$$

Fig. 6.66 Thin lens design of $40\times$ apochromat with duplex front. Scale 10:1



and a small amount of distortion. We give a sketch of the predesign, with fictive thicknesses for the doublets, in Fig. 6.66.

We invite the reader to complete this design in the following exercise.

6.6.3 Exercise 19, Aberrations of the $40\times$ Apochromat

Give thickness to the doublets of the thin lens design. Add the duplex front as designed above. Take N-SK 14 as glass, this will make small corrections of the radii and distances necessary.

For the paraxial calculations we start from the image plane of the objective; the surface numbers of the duplex front now become 7–10 (instead of 1–4).

Calculate the Seidel coefficients of the surface model. Because the duplex front cannot be made achromatic there will be a remainder of longitudinal chromatic error. When the system is optimized this can be corrected by varying the component powers of the doublets and correcting the achromatic aberrations by bending.

An objective with a planar aplanat front lens can be geared to different applications.

In Fig. 6.67a we show the application to immersion microscopy. An immersion oil must be used that has a refractive index near to that of the front lens. See [29] for immersion oils.

In our design we took the planar surface as object plane, which is not possible in practical use. With immersion one has to make the front lens shorter with about half a millimeter.

In Fig. 6.67b we show the configuration of a “dry” objective, meant to observe planar, reflecting objects. The illumination will be done through the lens in this case. To obtain a free working distance of $d_{10} = 0.5$ mm the front lens must be made 0.8 mm shorter. It is clear that this surface will induce aberrations that must be compensated by the rest of the system. Usually this is done by changing one of the doublets. See also the discussion of Tudorovsky’s objective in this section.

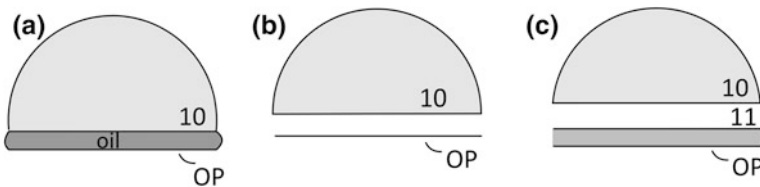


Fig. 6.67 The front lens in three applications of the objective: **a** with immersion, $d_{10} = 0.5$ mm, **b** dry, $d_{10} = 0.8$ mm, **c** cover glass, $d_{10} = 0.8$ mm, $d_{11} = 0.17$ mm

In Fig. 6.67c the objective will be applied to “wet” objects, for which a cover glass is necessary. The object plane is now at the underside of the cover glass. The front lens must be shortened by $0.8 + 0.17 = 0.97$ mm.

The standard thickness of cover glasses is 0.170 mm. Some companies use other values, care should be taken to use cover glasses that have the right thickness for the objective in use.

6.6.4 Tudorovsky’s Objective

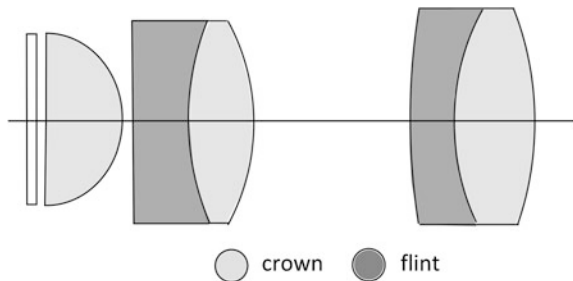
As a benchmark for our objective designs we take an objective of Tudorovsky (1948), of which the prescription is given by Havliček [14]. A cross section is shown in Fig. 6.68.

A $40\times$, $NA = 0.65$ Objective by Tudorovsky

	#	Radius	Distance	Glass
IMA	0	Plane	168.22	Air
STO	1	7.98	1.80	1.5100/63.4 [K 7 or BK 7]
	2	-5.59	1.00	1.6169/36.5 [F 2]
	3	-26.53	3.47	Air
	4	4.60	1.50	1.5100/63.4
	5	-4.17	1.30	1.6725/32.2 [SF 5]
	6	Plane	0.22	Air
	7	1.85	1.72	1.5100/63.4
	8	Plane	0.60	Air
	9	Plane	0.17	1.5100/63.4
OBJ	10	Plane	-	-

Note that there is a cover glass, $d_9 = 0.17$, $n' = 1.51$ on the object side. We take the stop at the first surface, with $(nu)_1 = 0.018$ and $(\bar{n}\bar{u})_1 = 0.04$.

Fig. 6.68 Tudorovsky's objective, scale 10:1



The index data of the glass are slightly different from the corresponding glasses in the Schott catalogue. In case the reader wants to use this design for own purpose (recommended as an exercise) we have given the nearest Schott glasses between brackets. The Soviet Union at that time produced its own optical glass (in Smolensk, now Belarus).

We calculate again beginning from the image plane. The results of the paraxial calculations are shown in the following tables.

Tudorovsky objective, paraxial calculations

	#	nu	h	A	nū	h̄	Ā	hΔ
IMA	–	–	0	–	–	–6.721	–	–
STO	1	0.01625	2.734	0.3589	0.04	0	0.04	–0.2344
	2	–0.15845	2.545	–0.8459	0.04	0.0477	0.0271	0.0699
	3	–0.10978	2.477	–0.2608	0.0409	0.0730	0.0365	–0.3149
	4	–0.16738	1.896	0.2448	0.0392	0.2090	0.0846	0.00337
	5	–0.37760	1.521	–0.9284	0.0160	0.2249	–0.0654	0.0807
	6	–0.31468	1.276	–0.3147	0.0253	0.2446	0.0253	–0.2580
	7	–0.31468	1.207	0.3324	0.0253	0.2502	0.1597	–0.03713
	8	–0.64735	0.3494	–0.6474	–0.0437	0.1923	–0.0437	–0.1270
	9	–0.64735	0.1683	–0.6474	–0.0437	0.1801	–0.0437	0.03070
	OBJ	10	–0.64735	0.0002	–	–0.0437	0.1687	–

#	S ₁	S ₂	S ₃	S ₄	S ₅	C ₁	C ₂
1	0.03019	0.00337	0.000375	0.000506	0.000098	0.00520	0.00087
2	–0.05002	0.00160	–0.000051	–0.000093	–0.000005	–0.01119	0.00062
3	0.02142	–0.00300	0.000420	0.000184	–0.000084	0.01098	–0.00153
4	–0.00020	–0.00007	–0.000024	0.000878	0.000295	0.00371	0.00128
5	–0.06956	–0.00489	–0.000345	–0.000184	–0.000037	–0.01836	–0.00129
6	0.02555	–0.00205	0.000165	0	–0.000013	0.00843	–0.00068
7	0.00410	0.00197	0.000964	0.002183	0.001512	0.00321	0.00154
8	0.05323	0.00359	0.000242	0	0.000016	0.00154	0.00012
9	–0.01287	–0.00087	0.000059	0	–0.000004	0.00180	–0.00006
Σ	0.00184	–0.00035	0.001687	0.003474	0.001778	–0.00291	0.00087

From the aberration coefficient table we see that the first doublet (surfaces 1–3) is well corrected for spherical; the second doublet has an excess of negative spherical that balances the aberrations of the cover glass. This objective cannot be used without a cover glass (of 170 µm thickness).

The inner surfaces (2 and 5) of the doublets have high values of A, that is the angle of incidence. This helps in the balancing of higher order spherical.

Coma is balanced neatly by the second doublet.

The highest contribution of astigmatism and field curvature, and nearly all of the distortion, comes from surface 7, that has a curvature of 0.54 mm⁻¹. Because of the low field angle (0.04 rad on both sides of the system) the distortion is below 1 %.

Surface 7 is by no means aplanatic, its value of $h\Delta$ is small, but because the incident angles of both the marginal and the chief ray (A and \bar{A}) are not small, the aberrations are not negligible. The contribution of surface 7 to the Petzval curvature coefficient S_4 is the highest of all surfaces, about two-thirds of the system value. In this type of objective there is little compensation for field curvature.

The first surface (4) of the second doublet is more nearly an aplanat; it has very small aberration coefficients (except S_4). In comparison to the previous design it is seen that the second doublet takes the function of the concentric aplanat. This makes that the correction of chromatic aberrations is easier.

The system value of spherical is quite high, $S_1 = 0.00184$. From the book of Havliček [14], where this design is discussed and optimized in [Chap. 3](#), it can be seen that a measure of spherical is necessary to balance higher order spherical. Havliček also discusses the correction of spherochromatism. This is the dependence of spherical aberration on the wavelength, a topic that is left aside in this book. Havliček remarks that the higher index of the flint in the second doublet helps to reduce spherochromatism.

6.6.5 Centring Tolerance Calculations

The centring tolerance Δy is calculated for the surfaces of the Tudorovsky objective. The marginal ray is followed through the system and the linear part and the third order part of the sensitivity factor $n'M' - nM$ are calculated, using (4.42) and (4.47) of [Sect. 4.6](#), and the results of the paraxial calculations.

The tolerance value for Δy is found from the condition

$$\left| \text{OPD}_y^{(3)} \right| = |\Delta y| \cdot |M'n' - nM|^{(3)} < \lambda/4$$

The transverse shift of the object is given by

$$\sigma = \text{OPD}^{(1)} / n'u' = \Delta y (M'n' - nM)^{(1)} / n'u'$$

In the following table we show the values of $(M'n' - nM)^{(1)}$ and $(M'n' - nM)^{(3)}$, the tolerance value $|\Delta y/\lambda|$ and the value of $|\sigma/r_a|$, where r_a is the Airy radius, given by $r_a = \lambda \cdot 0.6/n'u'$, so that

$$\sigma/r_a = \Delta y(n'M' - nM)^{(1)}/0.6\lambda.$$

In the table we use the tolerance value $|\Delta y/\lambda|$ to calculate $|\sigma/r_a|$.

#	$(M'n' - nM)^{(1)}$	$(M'n' - nM)^{(3)}$	$ \Delta y/\lambda $	$ \sigma/r_a $
1	0.17470	0.01775	14.0	4.00
2	-0.04867	0.00800	31.2	2.48
3	0.5760	0.00146	171.2	16.16
4	0.21022	0.02780	9.0	3.10
5	-0.06292	-0.01627	15.4	1.58
6	0	0	-	-
7	0.33267	0.08333	3.0	0.86
8	0	0	-	-
9	0	0	-	-

6.6.6 Exercise 20, Centring Tolerances of the 40× Apochromat

This exercise is dependent on the result of exercise 19.

When you have completed the paraxial calculations on the surface model of the apochromat objective, calculate the centring tolerances as shown above for the Tudorovsky objective. The supporting theory is found in [Sect. 4.6](#); see also the text above.

6.6.7 A Flat Field Objective

For this design we use a modular approach.

We begin with a duplex front that we want to make achromatic as far as possible. For that purpose we replace the concentric aplanat by a doublet with an aplanatic surface. See Fig. 6.69.

To minimize field curvature, the planar surface of the front lens is replaced by a curved surface, with a radius equal to that of the aplanatic surface.

The modified duplex front is followed by a doublet that collimates the axial beam. The resulting system has positive field curvature. To compensate we add a positive component and a stronger negative one at a distance, as was suggested in [Sect. 5.5](#) (Fig. 5.10). Both components are doublets, to make a precise colour correction possible.

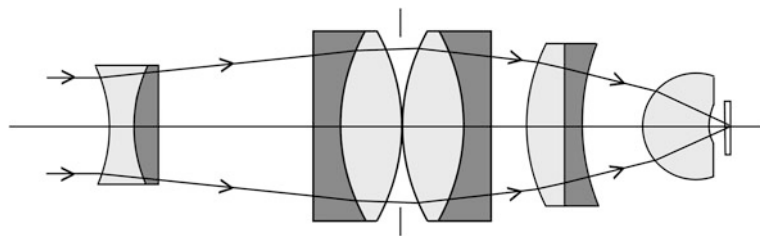


Fig. 6.69 Flat field microscope objective

The positive doublet will have an equal form as the collimating doublet, but opposite orientation. The two doublets form a symmetric pair; also the stop is placed between them.

The pair of doublets is corrected for coma when used at a magnification $M = -1$, as is the case here. Small corrections of coma and distortion can be made by making the pair slightly asymmetric.

Finally at the object side a cover glass is added.

The prescription of the surface model is given below. We have four doublets that we use to make the Seidel coefficients small enough. As glasses we chose N-PK 51 and F 5 for the doublets and N-SK 14 for the front lens.

	#	Radius	Distance	Glass	Diameter
IMA	0	Plane	Infinite	Air	-
	1	-5.533	1	N-PK 51	5
	2	5.059	0	Air	5
	3	5.663	1	F 5	5
	4	98.263	6.725	Air	5
	5	39.576	1.482	F 5	8
	6	9.240	2.446	N-PK 51	8
	7	-12.032	0	Air	8
STO	8	12.032	2.446	N-PK 51	8
	9	-9.240	1.482	F 5	8
	10	-39.576	1.434	Air	8
	11	7.421	1.5	N-PK 51	7
	12	Plane	1	F 5	7
	13	23.495	2.334	Air	7
	14	2.305	2.935	N-SK 14	4.5
	15	2.305	0.445	Air	1.4
OBJ	16	Plane	0.170	N-BK 7	0.7
	17	Plane	-	-	0.0516

The results of the paraxial calculations are given in the following table.

#	nu	h	A	$\bar{n}\bar{u}$	\bar{h}	\bar{A}	$h\Delta$
1	0	2	-0.3614	0.09002	-0.4696	0.1749	0.1635
2	0.19104	2.1250	0.8330	0.04510	-0.4401	-0.0879	0.7040
3	0.41304	2.1250	0.7882	-0.00082	-0.4401	-0.0785	-0.7237
4	0.18621	2.2411	0.2228	0.04609	-0.4113	0.0393	0.2860
5	0.20004	3.5865	0.2907	0.04362	-0.1179	0.0406	-0.5148
6	0.14527	3.7193	0.7910	0.04542	-0.0764	0.0322	0.0696
7	0.17577	4.0010	-0.3324	0.04479	-0.00473	0.0454	-0.2311
STO 8	0.00003	4.0010	0.3324	0.04500	-0.00473	0.0454	-0.2311
9	-0.17571	3.7194	-0.7910	0.04479	0.0669	0.0337	0.0696
10	-0.14521	3.5867	-0.2906	0.04534	0.1083	0.0410	-0.5148
11	-0.20000	3.3000	0.2447	0.04368	0.1709	0.0667	0.0456
12	-0.43503	2.8732	-0.4350	0.03150	0.2018	0.0315	0.0493
13	-0.31852	2.6018	-0.1257	0.03150	0.2215	0.0578	-0.3890
14	-0.80477	1.8583	0.4877	0.04142	0.3182	0.1794	0.0054
15	-0.70241	0.3912	-0.3658	-0.04184	0.2419	0.1264	-0.2079
16	-0.70241	0.0787	-0.7024	0.02877	0.2550	0.0288	0.0337
IMA 17	-0.70241	0	-	0.02877	0.2582	-	-
	S ₁	S ₂	S ₃	S ₄	S ₅	C ₁	C ₂
1	-0.02135	0.01033	-0.00500	-0.00200	0.00521	-0.00325	0.00157
2	-0.48850	0.05155	-0.00543	-0.00221	0.00080	-0.01120	0.00084
3	0.44060	-0.04483	0.00446	0.00215	-0.00065	0.01658	-0.00165
4	-0.01412	-0.00250	-0.00044	-0.00012	-0.00010	-0.00494	-0.00087
5	0.04350	0.00607	0.00058	0.00031	0.00016	0.01032	0.00144
6	-0.04355	-0.00177	-0.00007	-0.00010	0	-0.01589	-0.00065
7	0.02550	-0.00348	0.00048	0.00093	-0.00019	0.00597	-0.00081
8	0.02550	0.00348	0.00048	0.00093	0.00019	0.00597	0.00081
9	-0.04355	0.00180	-0.00008	-0.00010	0	-0.01589	0.00065
10	0.04350	-0.00613	0.00087	0.00031	-0.00016	0.01032	-0.00144
11	-0.00237	-0.00074	-0.00095	0.00150	0.00014	0.00363	0.00099
12	-0.00933	0.00067	-0.00005	0	0	-0.00675	0.00049
13	0.00615	-0.00282	0.00130	-0.00085	-0.00020	0.00323	-0.00148
14	-0.00127	0.00047	-0.00017	0.00529	0.00188	0.00562	0.00207
15	-0.02781	-0.00961	0.00332	-0.00529	0.00182	0.00088	-0.00031
16	-0.01660	0.00068	-0.00003	0	0	-0.00029	0.00001

The correction of the flat field objective is summarized in the following table that shows the aberration coefficients in four subsystems: the front lens, the (quasi) aplanat, the central doublets and the field flattener.

Component Surfaces	Front lens 16–14	Aplanat 13–11	Doublets 10–5	Field flattener 4–1	All (Σ)
S ₁	0.02489	0.00045	0.05090	-0.07463	0.00161
S ₂	-0.00846	-0.00289	-0.00003	0.01455	0.00317
S ₃	0.00312	0.00030	0.00252	-0.00641	-0.00047
S ₄	0	0.00065	0.00228	-0.00218	0.00075
S ₅	0.00370	-0.00006	0	0.00526	0.00890
C ₁	0.00621	0.00011	0.00080	-0.00281	0.00431
C ₂	0.00177	0	0	-0.00011	0.00166

It is seen from the table that the field flattener has an important function in the correction of spherical, coma, astigmatism and field curvature. Coma is slightly overcorrected and distortion pushed in the wrong direction.

This picture must be slightly corrected, because with a $40\times$ magnification the tube length will be only 114 mm. We can bring this to 170 mm by scaling up the design by a factor of $170/114 = 1.49$. This makes the field too large, dividing the field angle by the same factor will result in an image field of 20 mm again. The system aberration coefficient now become

$$S_1 = 0.00285, \quad S_2 = 0.00317, \quad S_3 = -0.00032, \quad S_4 = 0.00050, \quad S_5 = 0.00401 \\ C_1 = 0.00642, \quad C_2 = 0.00166.$$

In the optimization LCA and coma must be further corrected.

Optimization of the 40 \times , Flat Field Microscope Objective

To prevent the transformations that were necessary to give the surface model the required magnification, we optimized an objective with a finite image distance of 170 mm. As a starting image we took the surface model described above.

In the first optimization runs the radii of surfaces 1–4 and the distance d_4 were not used as variables. In later runs all radii, the main air distance and the glasses were varied, except the glasses of the front lens and the cover glass.

We optimized for image fields of 0, 2.5, 5, 7.5 and 10 mm height, with a numerical aperture of 0.56 on the object side. The center fields had wavefront errors smaller than a quarter of the 587 nm wavelength. For the 7.5 mm field the 656 nm wavelength exceeded this limit; at the edge of the field all wavelengths had ptv values larger than a quarter wavelength.

In Fig. 6.70a we give the lay-out of the optimized system, in Fig. 6.70b the OPD plots are shown and in Fig. 6.70c we show the MTF. Note that for the 7.5 and 10 mm fields the MTF value at high spatial frequencies is larger than the value of the aberration-free MTF.

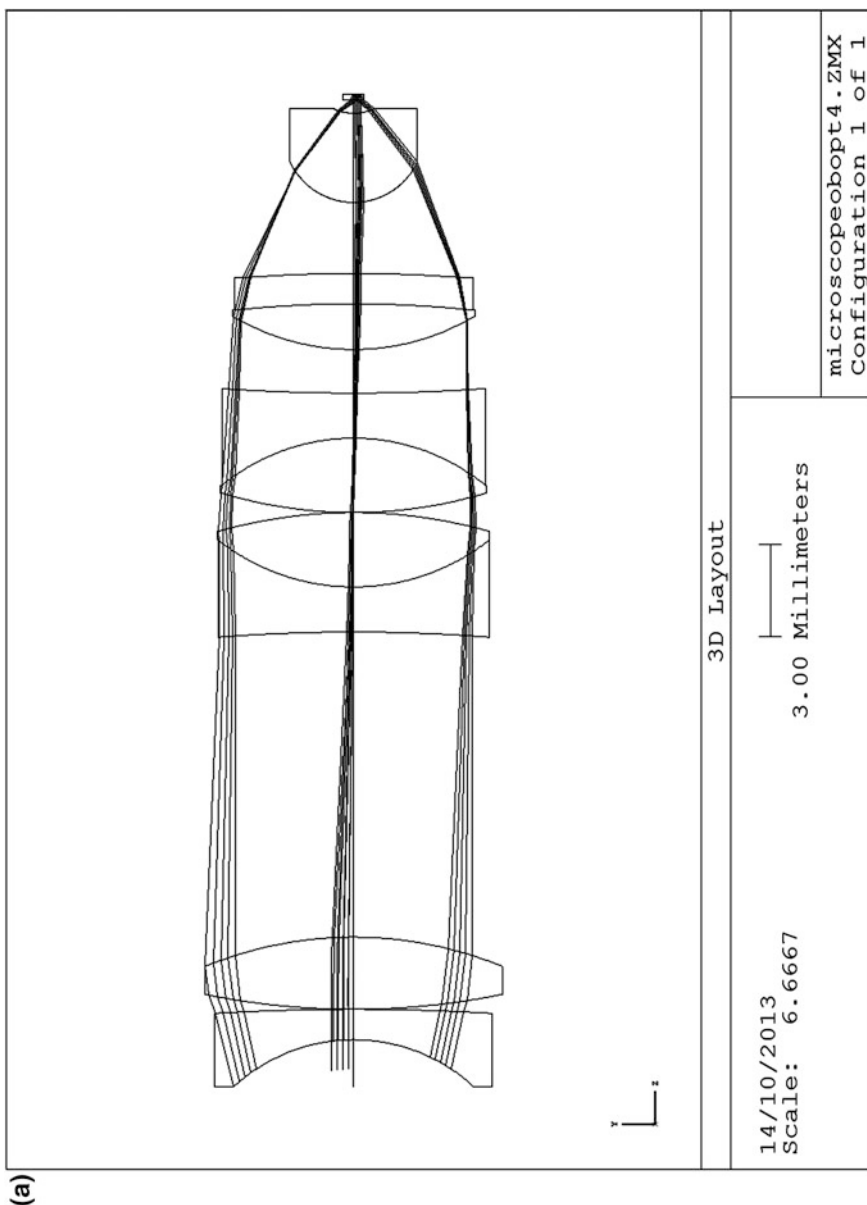


Fig. 6.70 a 40 \times microscope objective, lay-out. b 40 \times microscope objective, wave front errors. c 40 \times microscope objective, MTF

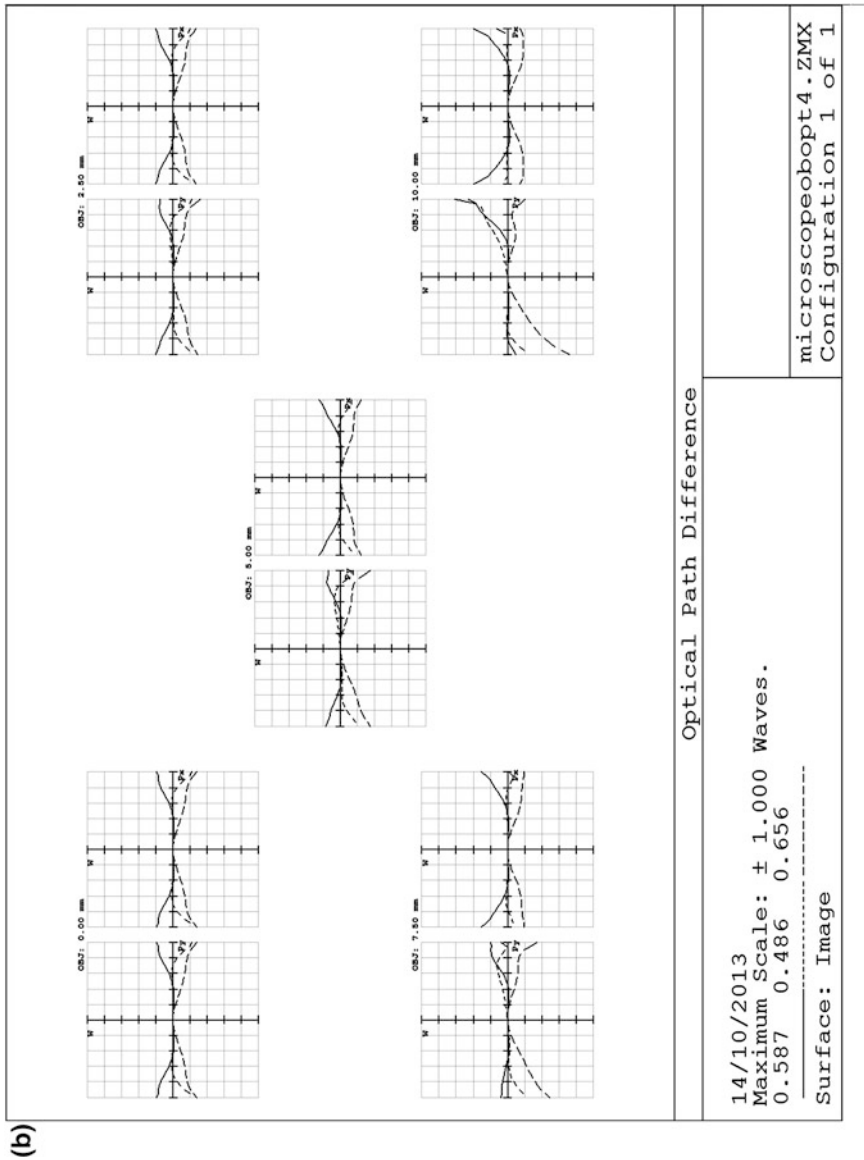


Fig. 6.70 (continued)

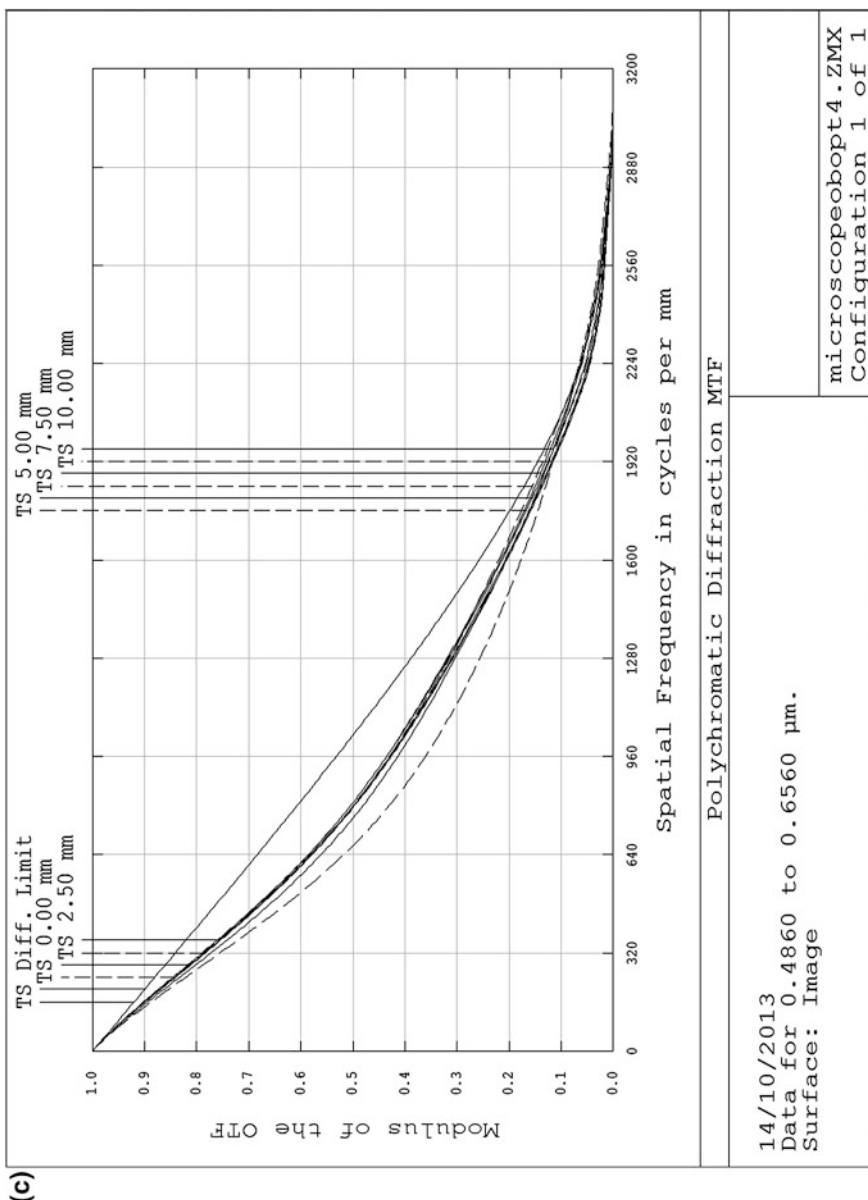


Fig. 6.70 (continued)

The prescription of the system is given in the table below.

Surface data summary

Surf	Radius	Thickness	Glass	Diameter
OBJ	Infinity	170		20
1	-5.809143	1	N-FK 51A	7.875166
2	-77.59481	0		9.118406
3	24.40756	2.373248	F 13	9.562355
4	-12.86208	10.03366		9.800145
5	-58.10399	1.482	N-F 2	8.883833
6	7.2021	2.446	N-PK 51	8.906022
7	-16.29874	0		8.934269
STO	15.04247	2.446	N-PK 51	8.746683
9	-6.81821	1.482	N-BASF 2	8.674168
10	63.20894	1.434		8.258721
11	7.767751	1.5	N-PSK 57	7.94577
12	-37.24243	1	N-SSK 8	7.844867
13	-46.29371	2.334		7.321447
14	2.305	2.935	N-SK 14	4.181269
15	1.592716	0.445		1.345931
16	Infinity	0.17	BK 7	0.6923412
IMA	Infinity			0.5100512

6.7 Applications of Aspheric Surfaces

The tools for this section were prepared in [Sect. 5.2](#), under the heading “aspherics”. Here we will show, with some simple examples, how aspheric surfaces can be used to improve a design. The treatment is limited to third order considerations; to optimize the design one needs lens design software that offers the opportunity to introduce higher orders of aspheric deformations.

6.7.1 Design of a CD Objective

The objective in a CD player focuses a laser beam on the back side of an optical disk. A number of factors important for the lay-out are:

- to make fast focusing and tracking possible, the weight of the lens must be small;
- the numerical aperture must be chosen so that crosstalk between tracks of the disk is minimal;
- not only spherical aberration must be corrected, but also coma, since this makes the system of disk and lens more insensitive against deviations from symmetry.

Because of the first point we make the focal length small, 8 mm.

With a standard distance between tracks of 1.6 μm and a refractive index of 1.6 of the disk material we obtain a numerical aperture of 0.16 with a laser wavelength of 0.7 μm .

A convex-plane lens is chosen to make the initial spherical aberration and coma small. As material of the lens we take polystyrene, index 1.59, $V = 30.8$, density 1.4. Half a sphere of this material with a radius of 5 mm weighs 336 mg.

The dispersion of polystyrene is not small, but changes of the laser wavelength are of the order of 1 nm per 10°K ; this does not change the aberration coefficients greatly and the focus is controlled.

The prescription of the system is as follows (a comparable system was shown in Fig. 4.24)

#	Radius	Thickness	Material	Diameter
0	—	Infinite	Air	—
1	4.72	4.72	Polystyrene	1.5
2	Plane	4.25	Air	1.5
3	Plane	1.20	Polystyrene	—
4	Plane	—	—	—

The paraxial calculation, with $\mu_1 = 0$, $h_1 = 0.64 \text{ mm}$, $\bar{u}_1 = 0.02$, $\bar{h}_1 = 0$ (stop at the first surface, field radius 160 μm) gives the result $S_1 = 0.00762$, $S_2 = 0.000230$.

We will correct both aberrations by making both surfaces of the lens aspherical. For the correction we must have (see Sect. 5.2).

$$\begin{aligned} (\kappa_1 h_1^4 - \kappa_2 h_2^4)(n - 1) &= -S_1 \\ -\kappa_2 h_2^3 \bar{h}_2(n - 1) &= -S_2 \end{aligned} \quad (6.30)$$

where κ_1 , κ_2 are the fourth order coefficients defined in Sect. 5.2, (5.16).

This gives, with h_1 and h_2 from the paraxial calculation, $\kappa_1 = 0.002075$, $\kappa_2 = 0.0229$.

The aspherical deformations become

$$z_1 = \frac{1}{8} h_1^4 \kappa_1 = 0.0007 \text{ mm}, \quad z_2 = 0.00048 \text{ mm}.$$

A tilt of the disk will cause axial coma (see Sect. 4.6). To make that the wavefront error is smaller than $\lambda/4$ the tilt must be smaller than 15.6 mrad, about 1° .

6.7.2 Mirror Objectives

We make a third order analysis of a class of two-mirror objectives, used primarily in astronomical telescopes. An extensive treatment of this subject is given in the book of Rutten and Van Venrooy [13].

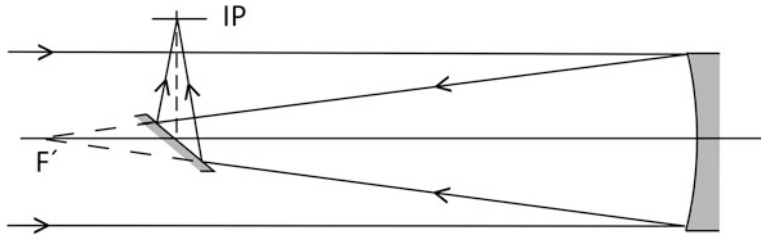


Fig. 6.71 Newton objective

The formulas for paraxial raytracing must be reconsidered when mirrors are used. Considering the imaging equation of a concave mirror [(1.8) of [Sect. 1.2](#)]:

$$-\frac{1}{s'} = \frac{1}{s} + K$$

it is clear that the paraxial raytracing equations of (1.21) of [Sect. 1.4](#) can be used in their original form:

$$\begin{aligned}(nu)_{i+1} &= (nu)_i - h_i K_i \\ h_{i+1} &= h_i + (nu)_{i+1} \cdot (d/n')_i\end{aligned}$$

when we take n negative after an uneven number of reflections and positive after an even number. In the following examples $n_1 = -n_2 = n_3 = 1$. Note that $(d/n')_i$ is always positive.

The power of a mirror is then $K = -2c$, where c is the curvature.

The aberrations coefficients of a spherical mirror become, because $\Delta(u/n) = -hK = 2hc$,

$$\begin{aligned}S_1 &= -2A^2 h^2 c, \quad S_2 = -2A \bar{A} h^2 c, \quad S_3 = -2\bar{A}^2 h^2 c, \\ S_4 &= 2H^2 c, \quad S_5 = (S_3 + S_4) \bar{A}/A.\end{aligned}\tag{6.31}$$

6.7.3 Newton's Objective

The first system that we consider is Newton's objective (1668), that consists of a paraboloid primary mirror and a flat secondary, with the stop at the primary, see Fig. 6.71.

We give the coefficients of spherical and coma first for a spherical mirror. When the object is at infinity, $u = 0$ and $h = -Ac$; with $\bar{A} = \tan w$ we obtain

$$\begin{aligned}S_1 &= -2h^4 c^3 \\ S_2 &= -2 \tan w h^3 c^2\end{aligned}\tag{6.32}$$

Spherical can be corrected by introducing an asphericity so that

$$-2\kappa h^4 = -S_1 \quad (6.33)$$

With $\kappa = c^3(e - 1)$ we find from (6.32) and (6.33) that $\kappa = -c^3$, $e = 0$. This means that with a paraboloid surface we can correct spherical aberration (not only the third order, but all orders).

The field aberrations will not be influenced by this change of the form of the primary, because we have the stop at the primary ($\bar{h} = 0$).

We calculate the coma of a spherical surface, with $h = 50$ and $c = -0.001$ we have

$$S_2 = -0.25 \tan w$$

The size of the coma tail is given by (Sect. 3.3)

$$\delta\eta' = 3S_2/2n'u'$$

we find $\delta\eta' = -3.75 \tan w$.

The required resolution in a visual telescope is given approximately by

$$\delta\eta' = f_{oc}'/2,000$$

With a $10\times$ ocular, $f_{oc}' = 25$ we have $\Delta\eta' = 0.0125$ mm. Because the coma tail has a relatively small intensity at its end, we take as a representative size for the coma spot 1/3 of its tail length [13].

From the resolution required and the tail length calculated we find that the field angle must be limited by $\tan w < 0.01$. The full image field has a diameter

$$2\bar{h}_{im} = 2 \tan w \cdot f_{ob}' \#$$

With $f_{ob}' = 500$ we find $2\bar{h}_{im} = 10$ mm.

Astigmatism and field curvature are equal but opposite, $S_3 = -S_4 = 0.0005$. These aberrations are smaller than 10 μm at the edge of the field. Distortion is zero, $S_3 + S_4 = 0$.

With one degree of freedom, the form of the primary, we can correct only spherical aberration. In the following we discuss systems with two degrees of freedom.

6.7.4 Cassegrain-Type Objectives

The analysis will follow the same pattern as with the Newtonian objective. First we will consider a lay-out with two spherical objectives; then we will correct spherical and coma by aspherizing both surfaces.

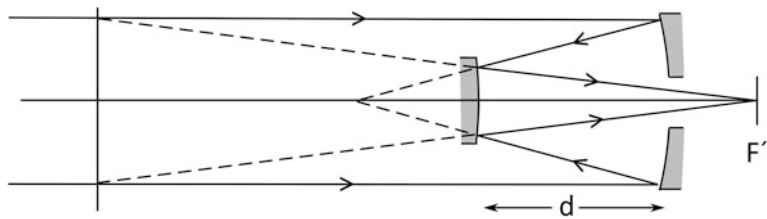


Fig. 6.72 Cassegrain objective

The paraxial lay-out is found in the following way: (see Fig. 6.72 for the notation). According to the scale equation (4.5) we have

$$h_1 K_1 + h_2 K_2 = h_1 K$$

where K is the system power.

Mirror 2 obstructs the beam to the primary mirror, the obstruction rate is $(h_2/h_1)^2$. With $h_2 = \frac{1}{2}h_1$ the obstruction rate becomes 25 %.

We take the factor $M = K_1/K$ equal to 2; M is called the *secondary magnification*. We find that we must take $K_2 = -K_1$.

With $K_1 = -2c_1$ and $K_2 = 2c_2$ we have $c_1 = c_2$. The curvatures are chosen as $c_1 = c_2 = -0.001$. This makes the system power equal to $K = 0.001$.

The value of d is found from:

$$h_2 = h_1(1 + 2c_1d)$$

this gives, with $h_2 = \frac{1}{2}h_1$ and $c_1 = -0.001$, $d = 250$ mm.

The lay-out results directly in a surface model. The paraxial calculations have the input values $u_1 = 0$, $h_1 = 50$, $\tan w = 0.02$, $\bar{h}_1 = 0$.

The results are shown in the following tables.

#	nu	h	$n\bar{u}$	\bar{h}	A	\bar{A}	$h\Delta$
1	0	50	0.02	0	-0.05	0.02	-5
2	-0.1	25	0.02	-5	-0.075	0.015	1.25
3	-0.05	0					

#	S_1	S_2	S_3	S_4	S_5
1	0.01250	-0.00500	0.00200	-0.00200	0
2	-0.00703	0.00140	-0.00028	-0.00200	-0.00034
Σ	0.00547	-0.00360	0.00172	-0.00400	-0.00034

Several methods have been used to correct the aberrations of objectives of this type. This resulted in a great variety of Cassegrain-type systems [13].

We limit ourselves here to correction by aspherizing the two surfaces. The design goals are to correct spherical and coma; astigmatism and distortion are not very strong, field curvature cannot be corrected in this lay-out.

The classical Cassegrain has a paraboloid primary and a hyperboloid secondary mirror, that images the primary focus in the Cassegrain focus. The coma of the combination limits the image field diameter to about 20 mm, twice as much as with the Newtonian.

We use the equation (6.30) that become, with $n_1' - n_1 = -2$, $n_2' - n_2 = 2$,

$$\begin{aligned} -2\kappa_1 h_1^4 + 2\kappa_2 h_2^4 &= -S_1 \\ 2\kappa_2 h_2^3 \bar{h}_2 &= -S_2 \end{aligned}$$

With S_1 and S_2 from the table we obtain

$$\begin{aligned} \kappa_1 &= 1.8776 \cdot 10^{-9}, & e_1 &= -0.8776, & z_1 &= \frac{1}{8} h_1^4 \kappa_1 = 0.00146 \\ \kappa_2 &= 2.3040 \cdot 10^{-8}, & e_2 &= -22.04, & z_2 &= \frac{1}{8} h_2^4 \kappa_2 = 0.00113 \end{aligned}$$

about 3 waves for z_1 and 2 for z_2 .

The secondary mirror gives an additional contribution to S_3 of -0.00072 .

The system that we have designed has two hyperboloid surfaces, it is called a Ritchey-Chrétien objective in the literature. It has zero spherical and coma, small astigmatism and distortion, but a considerable negative field curvature.

With a positive lens as a field flattener, with power 0.002, we can obtain equal curvatures of the meridional and sagittal image surfaces: $3S_3 + S_4 = 0.001$, $S_3 + S_4 = -0.001$. This gives symmetrical spots in the focal plane, which makes this objective useful for photography.

6.7.5 The Schmidt Camera

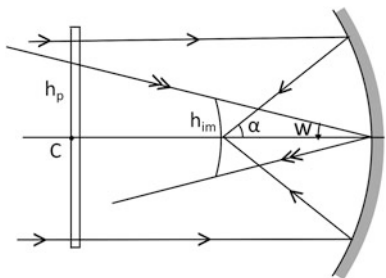
The lay-out of the Schmidt camera is very simple: a spherical mirror with the stop in its centre of curvature and the concentric image surface half way in between. See Fig. 6.73.

Because this system is concentric, the only aberration is spherical, as was already explained in Sect. 5.3. To correct this aberration Schmidt placed a corrector plate at the stop. When the corrector has a fourth order wavefront error $W = bh^4$, and

$$bh_p^4 = -S_1/8$$

spherical is corrected. The factor 1/8 must be used because the wavefront error of spherical aberration is 1/8 times its Seidel coefficient. See (3.18) of Sect. 3.3.

Fig. 6.73 Lay-out of the Schmidt camera



Because the corrector is a refracting component, chromatic errors will be caused by it. The error in question is spherochromatism, with a value of $E(h_p)/V$ at the edge of the stop, where V is the Abbe number of the corrector material. To minimize the effects of dispersion some power is given to the corrector, so that its wavefront error becomes

$$E(h) = ah^2 + bh^4$$

Note that the deformation of the corrector is given by $\Delta z = E(h)/(n - 1)$. We choose the ratio of a and b in such a way that the variance of $E(h)$ over the pupil, defined as $\text{Var}(E)$ in Sect. 4.7, is minimal. It turns out that, with $E(h)$ from (6.15) this is the case when

$$ah_p^2 = -bh_p^4$$

so that $E(h) = 0$ at the edge of the pupil. The value of $\text{Var}(E)$ then becomes

$$\text{Var}(E) = \left(bh_p^4 \right)^2 / 180$$

With bh_p^4 from (6.14) this becomes

$$\text{Var}(E) = S_1^2 / 11520$$

The RMS wavefront error, defined as the square root of $\text{Var}(E)$, for spherochromatism now becomes

$$\sigma = |S_1| / 107.3V$$

From (6.31) we have $S_1 = -2h_p^4 c^3 = 0.0125$ with $h_p = 50$ and $c = -0.001$, so that $bh^4 = -ah^2 = -0.00156$. With $V = 64.06$ for N-BK 7 we obtain $\sigma = 1.8 \cdot 10^{-6}$. This is about 0.1 % of the corrected spherical aberration; spherochromatism is suppressed sufficiently.

With our modest aperture of F/5 we have to correct 3 waves of spherical aberration. The peak value of Δz becomes 0.00078 mm or about 3/2 wave.

The field angle of a Schmidt camera is related to the aperture angle by (see Fig. 6.73)

$$\tan w = \tan \alpha \overline{h_{im}} / h_p$$

In the case of the Schmidt camera $(\overline{h_{im}}/h_p)^2$ is the obstruction ratio. This means that with an obstruction ratio of 0.25 a camera with an aperture F/5 or $\tan \alpha = 0.1$ the field angle is $\tan w = 0.05$, in practice somewhat smaller.

6.7.6 Exercise 21, Aspherization of a Double Gauss Objective

Simons [30] described the design of a Double-Gauss reproduction objective, used at a magnification $M = -1$. The system has the following prescription:

#	Radius	Distance	Glass	Diameter
1	68.297	8.084	N-LAF 21	24
2	461.625	1.882	Air	24
3	42.100	9.966	N-SK 15	20
4	101.002	3.986	SF 50	20
5	29.126	9.413	Air	15
6	Plane	9.413	Air	11
7	-29.126	3.986	SF 50 ^a	15
8	-101.002	9.966	N-SK 15	20
9	-42.100	1.882	Air	20
10	-461.625	8.084	N-LAF 21	24
11	-68.297		Air	24

^a The glass SF 50 is no longer found in the Schott catalogue, its data are $n = 1.65944$, $V = 32.63$, $P_d = 0.525$ [31]

Calculate the aberration coefficients (profit from symmetry). The designer was not content with the astigmatism and changed the radii of surfaces 4 and 8 to -153.846 and 153.846 , respectively. Check the aberration coefficients of the resulting system.

Note the change of sign of the two radii. The system now looks more like our split Planar design of Sect. 6.5. The designer wanted to correct the remaining spherical aberration by aspherizing the inner surfaces (5 and 7). Because of symmetry with respect to the stop, the changes in the field-dependent aberrations will be small.

Calculate the necessary surface deformation for this correction.

6.7.7 Diffractive Optics

An alternative to aspherizing surfaces (which is expensive, except when used in mass production of plastic lenses) can be found in the use of diffractive optics.

Diffractive optics uses gratings (periodic structures) to deflect rays. The deflection by a linear grating is given by the *grating equation*

$$n' \sin u' = n \sin u + m\lambda/p \quad (6.34)$$

where λ is the wavelength and p is the period of the grating. The integer m is called the order number, it can take a number of values limited by the condition

$$-1 < n' \sin u' < 1$$

The rest of (6.34) is just Snell's law. When we take a circular grating and we make p dependent on the distance from the center, so that in a meridional plane we can write

$$m\lambda/p = hK$$

we have, with $p = ap_0/h$, a lens with power K ,

$$K = m\lambda/ap_0 \quad (6.35)$$

where a is the semi-diameter of this *diffractive lens*.

First note that this lens has multiple foci, as many as there are possible values of m . The foci of a planar diffractive lens with 7 orders are shown in Fig. 6.74. The zero order focus is infinitely far away.

Secondly, we see from (6.33) that K depends linearly on the wavelength. That means that a planar diffractive lens has an effective Abbe number

$$V = \frac{\lambda_d}{\lambda_F - \lambda_C} = -3.45$$

meaning that it has a very strong negative dispersion. It follows that a diffractive lens on its own can be used for imaging by monochromatic light (from a laser) or that it can be used as a part of a hybrid lens, to correct chromatic errors. Such a hybrid lens can be a plane-convex singlet, with the grating on the planar side.

By adding a third order term to p also spherical aberration can be corrected.

The m th order efficiency of a diffraction grating, defined as the power in the m th order diffracted wave divided by the power in the incoming wave, depends on the structure of the grating period.

In the use of diffraction optics for imaging applications, as described above, an efficiency of 100 % is pursued. It is clear that this can only be tried by using phase gratings.

With a *binary phase grating*, with phase differences 0 and π in structural elements of equal area, two diffraction orders can be produced ($m = 1, -1$) with an efficiency of 40.5 % each [32, Chap. 13]. The period structure is shown in Fig. 6.75a.

With a *quaternary grating* we have four equal phase steps of $\pi/2$ per period, as shown in Fig. 6.75b.

The efficiency is now 81 % in one order.

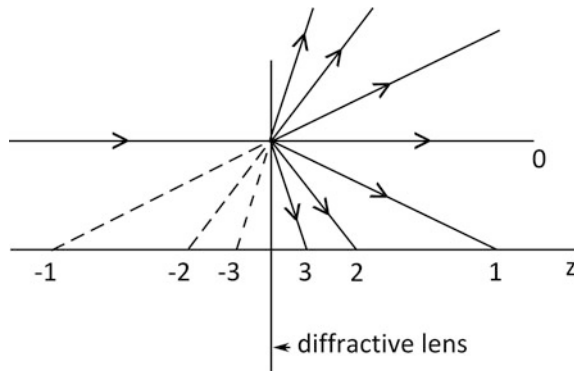


Fig. 6.74 Orders of a diffractive lens

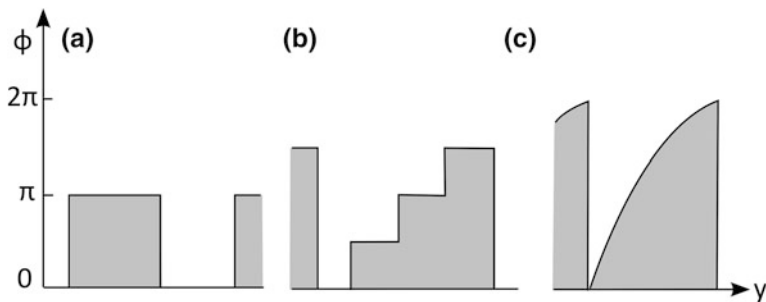


Fig. 6.75 Phase profiles of diffractive gratings, **a** binary, **b** quaternary, **c** kinoform

Binary and quaternary gratings can be produced by masked exposure and etching, techniques familiar from the production of integrated circuits.

An efficiency of 100 % in one order can be approached by the *kinoform*, a grating with a continuous, quadratic phase profile in each period. See Fig. 6.75c. The profiles of all periods of a diffractive lens of this type can be combined to form the profile of a classical lens, in the same way as a Fresnel lens.

Such gratings can be produced by single point diamond turning, when the period is not too small. Because of the small value of V , the power of a diffractive corrector in a hybrid lens is about 20 times smaller than of the lens to be corrected (for BK 7 glass $V = 64$).

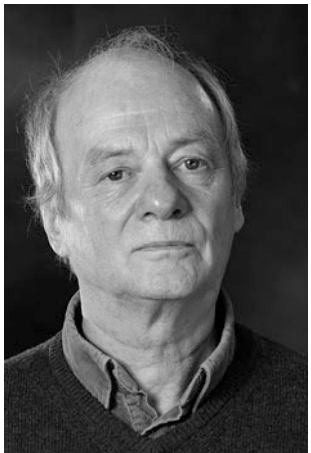
A first order diffractive lens with a power of 0.01 and a semi-diameter of 10 mm has, according to (6.35) a smallest period of 10λ . For the correction of colour of a BK 7 lens of the same power a smallest period of 185λ or $93 \mu\text{m}$ is required.

Mass production techniques for this application could be injection moulding of hot pressing.

References

1. K. Schwarzschild, *Untersuchungen zur geometrischen Optik* (Weidmannsche Buchhandlung, 1905)
2. A.C.S. van Heel, *Inleiding in de Optica* (M. Nijhoff, Leiden, 1950)
3. P. Mouroulis, J. McDonald, *Geometrical Optics and Optical Design* (Oxford University Press, Oxford, 1997)
4. J. McDonald, *Syllabus of SIRA Course in Optical Engineering III* (London, 1987)
5. R. Kingslake, R.B. Johnson, *Lens Design Fundamentals*, 2nd edn. (SPIE Press/Academic Press, USA, 2010)
6. R.I. Mercado, Design of Apochromats and Superachromats, in *Lens Design*, ed. by W.J. Smith (SPIE CR41, USA, 1992), p. 270
7. M. Kidger, *Fundamental Optical Design* (SPIE Press, USA, 2001)
8. C. Shannon, W. Weaver, *The Mathematical Theory of Communication* (University of Illinois Press, Illinois, 1964)
9. W.T. Welford, *Aberrations of Optical Systems* (Taylor and Francis, United Kingdom, 1986)
10. J. Kross, Typenkunde optischer Systeme, Thesis, Technische Universität Berlin (1970)
11. H.H. Hopkins, V.V. Rao, The systematic design of two-component objectives. *Opt. Acta* **17**, 497 (1970)
12. M. Berek, *Grundlagen der praktischen Optik* (W. de Gruyter, Verlag, 1970)
13. H. Rutten, M. van Venrooy, *Telescope Optics* (Willmann-Bell Inc., Virginia, 2002)
14. F.I. Havlicek, J. Opt. Soc. Amer. **41**, 1958 (1954)
15. Y. Matsui, K. Nariai, *Fundamentals of Practical Aberration Theory* (World Scientific, Singapore, 1993)
16. F.I. Havlicek, *Einführung in das korrigieren optischer Systeme* (Wissenschaftlicher Verlagsgesellschaft, 1960)
17. M. Kidger, *Intermediate Optical Design* (SPIE Press, USA, 2004)
18. W. Smith, *Modern Optical Engineering*, 2nd edn. (SPIE Press, USA, 2008)
19. K. Kühn-Leitz (ed.), Max Berek, Schöpfer der ersten Leica Objektive Pionier der (Mikroskopie, Lindemann's Verlag 2009)
20. C.H.F. Velzel, Chromatic aberrations in lens design, vol. 3190. *SPIE Proceedings*, p. 65 (1997)
21. J. Kross, Untersuchung ueber die Ortsabhaengigkeit der Abbildungsfehler, *Optik* **20**, 497–505, (1963)
22. M. Laikin, *Lens Design*, 1st edn. (Marcel Dekker, New York, 1990)
23. E. Glatzel, New lenses for microlithography, vol. 1780. *SPIE Proceedings*, p. 439 (1992)
24. R.S. Longhurst, *Geometrical and Physical Optics*, 2nd edn. (Longman, Harlow, 1973)
25. D.M. Williamson, The monochromatic quartet explained, in *Lens Design*, ed. by W.J. Smith (SPIE CR41, USA, 1992)
26. J.R. Sheats, B.W. Smith, *Microlithography, Science and Technology* (Marcel Dekker, New York, 1998)
27. A.E. Conrad, *Applied Optics and Optical Design, Parts I and II* (Dover Books, Mineola, 1985)
28. K.D. Sharma, High power micro-objective, a new design. *Appl. Opt.* **24**, 2577 (1985)
29. H. Beyer, H. Riesenbeck, *Handbuch der Mikroskopie*, 3rd edn. (VEB Verlag Technik, Berlin, 1988), p. 212
30. C.A.J. Simons, The Application of Eikonal Functions in the Practice of Optical Design, Doctoral thesis, Delft Technical University (1969)
31. M. Laikin, *Lens Design*, 1st edn. (Marcel Dekker, New York, 1990)
32. R. Fischer, B. Tadic-Galeb, P.R. Yoder, *Optical System Design*, 2nd edn. (SPIE Press, USA, 2008)

About the Author



The author studied Technical Physics at the Technical University of Delft, The Netherlands. He obtained a master's degree in 1965 with a thesis on the fabrication of lasers. After military service he found a position with Philips Electronics of Eindhoven, where he joined projects in holography, spectroscopy, optical recording, and semiconductor laser research. He obtained a doctor's degree from the University of Utrecht with a thesis on Fourier spectroscopy (1974).

In the second half of his Philips career (1982–1997) he was a consultant in industrial metrology.

Dr. Velzel left Philips in 1997 to join the company Nano Focus (Oberhausen, Germany), of which he is a co-founder. After 7 years with Nano Focus, where he assisted in the development of confocal microscopes for surface characterisation, he started a new career as a teacher and consultant in optics, which he follows until the present day.

Dr. Velzel is co-author of the book “What Is Light,” with his teacher Prof. A. C. S. van Heel and of many other publications and patents. He served on the International Commission for Optics as a Vice-President (for industry) from 1986–1992.

Index

A

- Abbe, Ernst, 36
- Abbe's number, 79
- Abbe's sine rule, 31
- Aberration(s), 39–57
 - balancing, 96
 - coefficients, 49, 53
 - chromatic, 47–49
 - fifth order, 97–100
 - plots, 103
- Achromat, 79
- Airspace (doublet), 136
- Airy radius, 118
- Amici, G. B., 298
- Angle
 - aperture, 20
 - field, 20
 - of incidence, 2
 - of reflection, 2
 - of refraction, 2
 - solve, 93
- Angulon, 69, 292
- Aperture
 - angle, 20
 - numerical, 30, 116
- Aplanatic
 - doublet, 154–158
 - surface, 56, 140, 304
- Apochromat, 79, 130
- Apochromatic
 - microscope objective, 304, 307
 - triplet, 66
 - thin systems, 129
- Aspheric surfaces, 137, 318–325
- Astigmatism
 - correction of, 146
 - of eye, 30
 - of third order, 46
- Axial colour, 78–79

B

- Back focal length, 12
- Beam expander, 35
- Berek, Max, 244
- Binary phase grating, 326
- Buried surface, 131, 271–272

C

- Camera, 25
 - lenses, 63–68
 - obscura, 26
- Cassegrain objective, 321–323
- CD objective, 318–319
- Celor, 66, 258–267
- Centering errors, 106, 109–112
- Channel capacity, 37
- Chevalier lens, 64
- Chromatic aberration, 47–48, 50–51
 - longitudinal, 47, 84
 - transverse, 48, 84
- Colour correction, 128–130
- Coma
 - third order, 43
 - fifth order, 97
 - elliptic, 98
- Conjugate shift equations, 254–258
- Constraints, 94
- Convention
 - for distances, 6
 - for angles, 7
- Cooke triplet, 229–237
- Cornea, 27
- Correction
 - of axial colour, 79
 - of astigmatism, 145
 - of distortion, 78, 146–147
 - of (thin) doublets, 154–156
 - of field curvature, 77, 142–145

Correction (*cont.*)
 of lateral colour, 80
 of two-component systems, 130, 132,
 175–179

D

Damped least squares (DLS), 101
 Defocussing error, 41
 Degrees of freedom, 80, 134–138
 Diffraction theory, 114–122
 Diffractive lens, 326
 Diffractive optics, 325–327
 Dispersion, 47, 126
 Distortion, 47, 78
 Double Gauss objective, 66, 282–284
 Doublet achromat
 aplanatic, 154–159
 cemented, 158–161
 Fraunhofer, 69
 Gauss, 66
 Steinheil, 69
 Dupin, C, 1

E

Ektar, 64
 Elmar, 247
 Elmax, 244
 Equivalent
 index, 177
 Abbe number, 177
 Euclid, 3
 Eye, 27–29
 model, 28

F

Fabrication errors, 113
 Farsightedness, 29
 Fermat, Pierre de, 2
 Field angle, 21
 Field curvature, 45, 49, 142–144
 Field flattener, 313
 Field lens, 33
 Flat field microscope objective,
 312–314
 Flint glass (F), 127
 Front focal length (FFL), 13

G

Glass chart, 127
 Glass selection, 132

in triplets, 231
 Grating equation, 326
 Grubb lens, 64

H

Height solve, 93
 Heliar, 247–253
 Hologon, 293–297
 Huygens, Christiaen, 3
 Huygens construction, 57
 Huygens ocular, 74, 131, 146

I

Ideal system, 92
 Illumination, 35–38
 Image, 5
 equation, 129
 Immersion oil, 307
 Incoherent, 119
 Induced aberrations, 113
 Invariant
 Abbe's, 8
 optical, 16
 Lagrange's, 50
 skew, 46
 Inversion, 167
 Inverting prism, 168

K

Kellner ocular, 164–167
 Kinoform, 327
 Kron glass (K), 127

L

Lay-out, paraxial, 76–84
 Leeuwenhoek, Anthoni van, 30
 Lens
 Chevalier, 64, 161
 field, 34
 Grubb, 64
 landscape, 64–65, 150–152, 161
 Petzval, 195–205
 single, 12
 tele, 68, 208–228
 thin, 19
 Lens types, 63–76
 Linear variation, 101
 Lister, J. J., 297
 Lister type microscope objective,
 298–304

M

- Magnification, 7, 10, 12
 - angular, 30, 32
 - linear, 32
- Magnification error, 42
- Magnifier, 31
- Malus, Etienne, 1
- Maximum magnification, 31
- Meridional
 - coma, 45
 - field curvature, 47, 55
 - image surface, 52
 - plane, 46
 - rays, 46, 109
 - ray tracing, 109
- Merit function(s), 93, 96–97
 - variable of, 97
 - weight factors in, 94

Micro-objectives, 71–74**Microscope, 30–32**

- Microscope objective(s), 297–298
 - apoachromatic, 302–307
 - flat field, 311–314
 - Lister type, 298–301
 - Tudorovsky, 308–310

Microscopy

- dry, 308
- immersion, 31, 308
- wet, 307

Mirror

- concave, 6
- convex, 7

Mirror objectives, 319–327**Modulation depth, 94****Modulation transfer function (MTF), 105, 117–120****MTF plots, 106, 190, 315****N**

- Nearsightedness, 29
- Newton objective, 320–323
- Nodal points, 29

O

- Object, 5
- Oculars, 76
 - Huygens, 131, 146
 - Kellner, 166–167
 - Plössl, 174–175
 - Ramsden, 131, 163–166
- Optical instruments, 25–38
- Optical invariant, 16–18
- Optical materials, 126–128

Optical path length, 2

- Optical transfer function (OTF), 121
- Optimization, 92–106

P

- Paraxial
 - approximation, 5
 - optics, 5–22
 - ray tracing, 14–23
- Partial dispersion, 79, 126
- Perspective, 26
- Petzval
 - curvature, 51
 - lens, 65, 176, 195–205
 - sum, 143
- Phase function, 121
- Pick-up solve, 93
- Planar, 268–281
- Plate(s), 9
 - aberrations of, 170
- Point spread function (PSF), 106, 116–118
- Position factor, 134
- Power
 - of lens, 13
 - of mirror, 6
 - of thin lens, 13
 - of thin lens system, 14
 - of surface, 7
- Principal planes (points), 10
- Prism(s), 8–9
 - of Porro, 168
- Pupil(s), 19–21
 - entrance, 20
 - exit, 20

Q

- Quaternary phase grating, 326
- q-factor, 54

R

- Radiance, 36
- Rapid rectilinear, 65
- Ray
 - chief, 21
 - finite, 109
 - marginal, 20
 - skew, 46
- Ray-tracing
 - paraxial, 14
 - meridional, 109
 - thin lenses, 18
- Ray vectors, 24

- Reflection law, 3
 Refraction equation, 15
 Refraction law, 3
 Refractive index, 2
 Relative coordinates, 39, 41
 Retina, 27
 Retinoscope
 lay-out of, 180
 eye lens of, 179
 objective of, 180–191
 Reversed tele-objective, 225–227
- S**
 Sagittal
 coma, 43
 focus, 42
 field curvature, 49, 154
 oblique spherical aberration (SOBSA), 98
 plane, 46
 rays, 46
 Scale factor, 76
 Scale equation, 77
 Schmidt camera, 323–324
 Seidel coefficients, 50–52
 Seidel, L. von, 50
 Shape factor, 85
 Skew rays, 46
 Snell's law, 3
 Snell, Willebrord, 3
 Solves, 93
 Spatial frequency, 105
 Spherical aberration
 of third order, 43
 of fifth order, 98
 oblique, 98–100
 Spherochromatism, 48
 Stigmatic imaging, 92
 Spot diagrams, 103
 Stop(s), 19–24
 aperture, 20
 field, 21
 Stop position, 141
 Stop shift equations, 54, 86
 Strain, 112
 Strehl number, 106, 118–120
 Surface
 refractive, 7
 spherical, 7
 aspheric, 137
 buried, 131
 Symmetry, 138
 mirror, 138, 261–319
 concentric, 138, 323
- T**
 Tangential, *see* Meridional
 Tangential oblique spherical aberration (TOBSA), 98–100
 Telecentricity, 22
 Telecentric perspective, 26
 Tele-objectives, 68, 208–228
 Telescope(s)
 Kepler's, 32
 Dutch or Galilei's, 34
 design of, 163–174
 Tessar, 68, 240–247
 Thickness, 90, 91
 Thin lens, 14
 Thin lens predesign, 84–90
 Throughput, 36
 Tolerancing, 106–116, 311
 Total internal reflection (TIR), 8
 Transfer equation, 12, 15
 Transmission of lenses, 63
 Triplet, 229–238
 Tudorovsky objective, 308–311
 Tunnel diagram, 9
- V**
 Variables (in optimization), 95
 Variables (in lay-out and predesign),
 see Degrees of freedom
 Vertex (V), 5
 Vignetting, 20, 32, 142
- W**
 Wavefront, 1–3, 39–47
 Wavefront coefficients, 39
 and Seidel coefficients, 50
 Wavefront error, 94
 plots, 105, 314
 Weight factors, 93
 Wide-angle lens, 68, 288–294
 Window(s)
 entrance, 20
 exit, 20
- Z**
 Zonal aberration, 136
 Zonal image, 41
 Zoom lens, lay-out of, 82